A STUDY OF THE VALIDITY OF THE WEINREICH RELATIONSHIP FOR CADMIUM SULPHIDE

A THESIS SUBMITTED FOR THE DEGREE OF
DOCTOR OF PHILOSOPHY
IN THE UNIVERSITY OF ASTON IN BIRMINGHAM

DAVID JAMES LARNER, B.Sc.

Physics Department

March, 1970.

ABSTRACT

The validity of the Weinreich relationship was studied under both linear and non-linear conditions using an acoustic amplifier comprising a piece of single crystal, photoconducting, cadmium sulphide sandwiched between two coaxially plated, Y - cut quartz transducers of 15 MHz. fundamental frequency.

Careful attention was paid to the choice of crystal, and also to amplifier fabrication. The experimental arrangement adopted incorporated facilities for varying the crystal conductivity from 10^{-9} (ohm cm)$^{-1}$ to 10^{-4} (ohm cm)$^{-1}$, applying a d.c. voltage from zero to 1 kV, and varying the duration, amplitude and frequency of the input acoustic signal. An essential feature of this arrangement was the simultaneous oscilloscope display of the acoustic echo train, applied d.c. voltage, and acoustoelectric voltage.

Appropriate techniques were devised to enable an accurate determination of the acoustic attenuation coefficient, the input acoustic intensity, and the acoustoelectric voltage. An analysis of the Weinreich relationship consistent with these techniques was presented which allowed a quantitative comparison of theory and experiment to be made under both amplifying and attenuating conditions.

The quantitative validity of the Weinreich relationship was established for linear acoustoelectric behaviour at 45 MHz. and 75 MHz. The results obtained at 15 MHz. indicated the Weinreich relationship to be qualitatively valid under attenuating conditions, but suggested a quantitative validity under amplifying conditions.

The apparent disagreement between theory and experiment noted under certain non-linear conditions was attributed to the non-linear generation of harmonics, and subsequent investigation showed the Weinreich relationship to be valid for each harmonic

generated.

A means of establishing, quantitatively, the validity of the prominent carrier trapping theories was indicated, and it was concluded that these theories describe consistently the effects of carrier trapping on the acoustic attenuation and acoustoelectric voltage variation with applied d.c. voltage.

Finally, some general observations relating to the amplification of broad band acoustic flux were given.

INDEX

CHAPTER 1.

The background to the present research

1.1 Introduction

In 1953 Parmenter [1] predicted that an acoustic wave, propagating through a medium containing mobile charges, would result in a d.c. electric field along the direction of propagation of the wave. He named this the acoustoelectric effect.

Many theoretical papers were subsequently published discussing the acoustoelectric effect in both metals and semiconductors. Implicit in some of the theories presented was the assumption that the mean free path of the carriers was greater than the acoustic wavelength [2.3.4.] Whilst this assumption is satisfied in metals and certain semimetals at liquid helium temperatures for an angular acoustic frequency of 10^8 sec.$^{-1}$, it is not valid for semiconductors. Weinreich [5] and Holstein [6] have treated the acoustoelectric effect from a macroscopic point of view, where they considered the carrier mean free path to be less than the acoustic wavelength. This approach is considered to be the most practical way of discussing the acoustoelectric effect in semiconductors. The discussion of published theoretical work on the acoustoelectric interaction will therefore be restricted to such macroscopic theories, and the various quantum mechanical approaches will not be considered.

The macroscopic theories are concerned mathematically with the interaction between charge carriers and acoustic waves. Consequently the term "acoustic wave" will be used, rather than "phonon", since the latter is conventionally assigned particle properties. This interaction will be described as the acoustoelectric interaction. Furthermore, the phrase "acoustoelectric effect" will imply solely the prediction of Parmenter [1]; that is, the generation of a d.c. electric

field, which will be referred to as the acoustoelectric field. The term "acoustoelectric effects" will, however, be used to describe collectively, all the phenomena resulting from the acoustoelectric interaction.

This literature survey reviews some of the work carried out on acoustoelectric effects, with particular emphasis on the piezoelectric semiconductor cadmium sulphide. It will be established that such effects are small in non-piezoelectric semiconductors, and that few experimental results are available. The work carried out using such materials is thus only briefly reviewed. The realisation that much larger effects could be achieved using piezoelectric semiconductors will be shown to have developed logically from the earlier work. .The more abundant theoretical and experimental investigations which have appeared in the literature describing the acoustoelectric interaction due to piezoelectric coupling are then reviewed in greater detail.

1.2. Acoustoelectric effects in non-piezoelectric semiconductors

In non piezoelectric semiconductors the dominant mechanism whereby the acoustic wave interacts with the charge carriers is deformation potential coupling.[7] This arises because an acoustic wave propagating through a solid causes the atoms of the solid to be displaced from their equilibrium positions, resulting in a change in the crystal potential and a consequent change in the energy of the charge carriers. The deformation potential tensor relates the change in carrier energy to the strain of the crystal lattice.

$$\delta E = \left(\frac{\partial}{\partial x_i}\right) C_{ij}\, \xi_j = jk\, C_{ij}\, \xi_j \qquad \text{---------(1.1)}$$

C_{ij} is the deformation potential tensor and $\frac{\partial \xi_j}{\partial x_i}$ is the lattice strain. $\xi_j = \xi_0 \exp.j(kx - \omega t)$ is the displacement and is periodic in space and time. δE is the change in carrier energy. Since the change in carrier energy is spatially dependent,

a net force is exerted on the carriers which may be written as

$$F_i = -\frac{\partial}{\partial x_i}(\delta E) = k^2 C_{ij} \xi_j \quad \text{-----} \quad (1.2)$$

This shows the coupling to be proportional to the square of the wavenumber, and also to the magnitude of the deformation potential constant. The materials in which this type of coupling dominates are the semimetals Bi, As, Sb, etc., and the non-piezoelectric semiconductors Ge, Si, etc.

As a result of the coupling, the charge carriers are subjected to acoustically induced forces. The carriers in responding to these forces induce new electromagnetic fields, which tend to screen out the acoustically induced forces. Physically, the non-uniform charge distributions resulting from the interaction are opposed by electrostatic repulsion and diffusion. The space charge restricts the bunching density of the carriers, and sets an upper limit on the carrier density taking part in the interaction. The significance of carrier bunching will be considered in chapter 2. Weinreich [5] has discussed the problem of space charge repulsion and has suggested that the presence of both signs of current carriers in a semiconductor allows appreciable spatial bunching without concomitant space charge. Holstein, as quoted in Weinreich and White [8], has pointed out that the screening of the deformation potential forces could also be negligible in a simple multivalley semiconductor such as n-type germanium.

Magnetoresistance, piezoresistance and cyclotron resonance experiments indicate that the minimum energy of the conduction band in germanium occurs at four equivalent points near the surface of the first Brillouin zone. These points lie along [111] directions. An acoustically induced strain lowers the band edge of one group of ellipsoidal energy surfaces, and raises the band edge of another group of ellipsoids. This leads to an increase in electron density in one valley, which is counterbalanced by a decrease in another

valley. Blatt[9] has indicated that the redistribution of the carriers will take place by intervalley scattering, and will depend significantly on the intervalley scattering time.

This was also realised by Weinreich and White[8] who measured the acoustoelectric field in n-type germanium. In a subsequent paper Weinreich, Sanders and White[10] considered theoretically the interaction in n-type germanium, and expressed the acoustoelectric field in terms of the total relaxation time of the electron distribution. The relaxation was shown to proceed by intervalley scattering and diffusion. An essentially similar expression for the acoustoelectric field has also been derived by Mikoshiba[11]. The experimental results of Weinreich et al[8] enabled the dependence of the intervalley scattering rate on temperature and sample doping to be determined. As far as is known, this is the only paper to usefully employ the acoustoelectric effect in non piezoelectric semiconductors.

The acoustoelectric field, produced by a transverse acoustic wave travelling in the [100] direction and polarised in the [010] direction, was measured. For an acoustic frequency of approximately 60 MHz, the acoustoelectric field was determined to be only ten microvolts $cm.^{-1}$. The measurement was carried out at liquid nitrogen temperatures and the acoustic power was estimated to be 0.9 $watt.cm.^{-2}$. In order to avoid complications due to the thermoelectric voltage also developed, the input acoustic wave was modulated at various audio frequencies, and the acoustoelectric effect detected as a voltage at the audio frequency. The modulation of the acoustic power resulted in temperature fluctuations and consequent a.c. thermoelectric voltages. The a.c. temperature component was found to depend strongly on the modulation frequency, which was so chosen to minimise the thermoelectric voltages developed.

The experimental results obtained by Weinreich and White[8] were in reasonable agreement with their theory. It is interesting

to record that they were unable to detect an acoustoelectric voltage for a shear wave propagating in the [110] direction and polarised in the [1$\bar{1}$0] direction. This null result was expected, and in agreement with the established orientation of the valleys.

The problem of the attendant thermoelectric voltage, which is shown by Weinreich and White [8] to be of the same order of magnitude as the acoustoelectric voltage has resulted in several unsuccessful attempts to measure the acoustoelectric field. Thus there are very few published measurements, obtained using non piezoelectric semiconductors. A thermoelectric voltage will arise as a result of a temperature gradient in the material. A contribution to the thermoelectric power is due to thermal phonons which move down the thermal gradient, and transfer momentum to the carriers. This is known as the "phonon-drag" effect, and is qualitatively similar to the acoustoelectric effect. The only other reported acoustoelectric field measurement in non-piezoelectric semiconductors is that of Sasaki and Yoshida [12] also using n-type germanium. Their results suggested that the acoustoelectric field E_{ae} was given by

$$E_{ae} = 1{\cdot}3 \cdot 10^{-7} Q_o \text{ volts. cm}^{-1}$$

where Q_o is the input acoustic power density in watts. cm^{-2}.

In a paper which reviewed the main theoretical treatments of the acoustoelectric effect Parmenter [13] modified the phenomenological approach of Weinreich [5] and Holstein [6], and derived results valid for both semiconductors and metals. Unlike Weinreich and White [8] however, Parmenter [13] did not expressly consider the case of a multivalley semiconductor. He estimated that the acoustoelectric field in n-type germanium should be given by

$$E_{ae} = 1{\cdot}85 \cdot 10^{-9} Q_o \text{ volt.cm}^{-1}$$

Although his treatment was later criticised by Blount [14] and Mikoshiba [15],

who each considered theoretically the acoustoelectric effect in metals, Parmenter's results led him to suggest that the measurements reported by Sasaki and Yoshida [12] were really thermoelectric in origin. He further estimated that for an input acoustic power density of 1 watt.cm^{-2}, a temperature gradient of only 5.10^{-4} °C. cm.$^{-1}$ would be sufficient to produce the reported measurements. It later transpired that his suspicions were well founded [16].

It was pointed out by Blatt [9] that an acoustic wave propagating through n-type germanium and interacting with the electrons would be attenuated. Weinreich [17] has shown that the attenuation due to the acoustoelectric interaction is closely related to the acoustoelectric field thereby generated. Moreover, this relationship was realised to be independent of detailed mechanism. This was a significant conclusion. Weinreich argued that the attenuation, or loss of energy of the acoustic wave due to coupling with the charge carriers, resulted in these carriers gaining momentum. This results in an average d.c. force acting on the carriers which is observed experimentally as the acoustoelectric field. Since the energy and momentum flux of the acoustic wave are linearly related, the attenuation coefficient and the acoustoelectric field are also linearly related. This relationship is known as the Weinreich relationship and is simply expressed.

$$\alpha = \frac{1}{2} \frac{n_o q v_s E_{ae}}{Q} \qquad \text{---------(1.3)}$$

α is the amplitude attenuation coefficient of the acoustic wave, (nepers cm^{-1}).

n_o is the density of conduction electrons (cm^{-3})

q is the electronic charge (coulombs)

v_s is the acoustic velocity (cm sec^{-1})

E_{ae} is the acoustoelectric field (volts cm^{-1})

Q is the local acoustic power density (watts.cm^{-2})

A detailed analysis of this relationship appears in Chapter 2.

The work of Mikoshiba [15] indicated that the Weinreich relationship was valid for both $k\ell > 1$ and $k\ell < 1$ (k is the acoustic wavenumber, and ℓ the mean free path of the electrons), and that it held for both longitudinal and transverse acoustic waves.

Weinreich, Sanders and White [10] have used the Weinreich relationship to predict the electronic attenuation of an input acoustic wave from their acoustoelectric field measurements in n-type germanium. The attenuation was predicted to be very small; about 10^{-3} db.cm^{-1} at an acoustic frequency of 60 MHz. This has discouraged any experimental investigation of the Weinreich relationship using non-piezoelectric materials.

The confusion resulting from the contradictory conclusions of the many theoretical papers discussing the acoustoelectric effect in simple non-piezoelectric semiconductors remains unresolved. Whether the semi-classical theories of Blount [14] and Mikoshiba [15] successfully describe the acoustoelectric effect in metals is still questionable. Their results indicate a small effect and no measurements have been made. The experimental results of Weinreich and White [8] credit their specific theoretical treatment for a multivalley semiconductor such as n-type germanium. In recent years both theoretical and experimental emphasis has been placed on the acoustoelectric interaction in piezoelectric semiconductors.

1.3. Acoustoelectric effects in piezoelectric semiconductors; with emphasis on cadmium sulphide.

1.3.1. The identification of piezoelectric coupling

A temperature gradient in a solid will result in an accompanying thermoelectric voltage. The presence of this effect has resulted in several unsuccessful attempts to measure the acoustoelectric field in non-piezoelectric semiconductors, and an experimental technique concerned with minimising this effect has been

briefly described in the previous section. The total thermoelectric power may be ascribed to two separate contributions, an electronic contribution and the phonon drag contribution. The electronic contribution arises to oppose the diffusion of electrons in the temperature gradient and the phonon drag contribution is a measure of the electric field necessary to halt electron drift down the temperature gradient due to momentum gain from thermal phonons.

Whilst investigating the electronic properties of single crystal n-type zinc oxide, (ZnO), Hutson [18] encountered a large contribution to the thermoelectric power, due to the phonon drag effect, over a wide temperature range. He was able to determine the phonon drag contribution by subtracting a computed value for the electronic contribution from the experimentally determined total thermoelectric power. A subsequent investigation [19] revealed that the magnitude of the phonon-drag effect was too large to be accounted for in terms of deformation potential coupling.

At about the same time the observation of conductivity sensitive acoustic attenuation in single crystal hexagonal cadmium sulphide (CdS) was reported by Nine [20]. This observation was of great importance since it suggested a strong acoustoelectric interaction. The piezoelectric nature of cadmium sulphide was demonstrated shortly afterwards by Hutson [21] who sought the reason for the large phonon drag effect observed in ZnO in his previous work. He measured the piezoelectric moduli for zinc oxide and CdS and compared the known electromechanical coupling factor for an X-cut quartz plate, with that due to comparably oriented CdS and ZnO plates. His results indicated an electromechanical coupling factor of approximately 0.4 for ZnO and 0.2 for CdS compared with only 0.095 for quartz. The electromechanical coupling factor serves to indicate the strength of the coupling, and is discussed in more detail in appendix 1. The piezoelectric nature of the semiconductors was disclosed by ensuring screening effects to be

negligible. Hutson achieved this by compensating the n-type ZnO crystals with lithium acceptors and by annealing the CdS in a sulphur atmosphere, thus quenching the conductivity of the two materials. He concluded that the strongly piezoelectric nature of ZnO was sufficient to account for the large phonon drag effect previously observed.

The piezoelectric nature of CdS was further established by Nine and Truell[22] who used a pulse echo technique to measure the acoustoelectric attenuation in photosensitive CdS. Both shear and longitudinal acoustic waves generated by quartz transducers were propagated through the samples in different crystallographic directions at frequencies between 10 MHz and 200 MHz. They observed that the attenuation of longitudinal waves propagating along the hexagonal, or "C" axis, was affected by illumination, whereas the attenuation of shear waves propagated in this direction was unaffected. However, propagation in the plane perpendicular to the C - axis, resulted in those shear waves producing particle motion along the hexagonal axis, being affected by illumination, whilst the longitudinal waves were unaffected. A comparison of their observations with the piezoelectric polarisations expected for acoustic waves propagated in various directions in CdS, if it were piezoelectric, indicated excellent correlation with the presence or absence of attenuation changes.

The successful identification of the coupling mechanism giving rise to the strong acoustoelectric effects in piezoelectric semiconductors stimulated much experimental and theoretical work. Prior to reviewing this work, the main features of acoustic wave propagation in piezoelectric semiconductors will be considered.

1.3.2. Acoustic wave propagation in piezoelectric materials

An elastic solid may be defined as one in which the strain S is proportional to the stress T and the proportionality constant is a real number. The relationship between the stress and

the strain may then be written in tensor form.

$$T_{ij} = c_{ijkl} \; S_{kl} \qquad \text{---------} \quad (1.4)$$

c_{ijkl} is called the elastic stiffness. The reciprocal of c_{ijkl} is denoted s_{ijkl} and termed the compliance. Equation (1.4) describes Hooke's law. Note that T_{ij} and S_{kl} are both second order tensors, and c_{ijkl} and s_{ijkl} are accordingly fourth order tensors. In an infinite, perfectly elastic solid, a plane wave will propagate without any change in energy. Since the elastic constants are real, the velocity v_s and angular frequency ω of the acoustic wave may be expressed as follows:

$$\omega = k_s v_s$$

$$v_s = \left(\frac{c}{\rho}\right)^{\frac{1}{2}} \qquad \text{---------} \quad (1.5)$$

where k_s is the acoustic wavenumber

c is the appropriate combination of elastic constants

ρ is the mass density of the medium

If however, the medium deviates from elasticity, then a change in wave energy will occur during propagation. The acoustoelectric interaction in solids results in additional contributions to the stress tensor, which, for a linearised theory, are also linear in strain. These additional contributions depend on the electron variables. Equation (1.4) may thus be restated.

$$T_{ij} = c'_{ijkl} \; S_{kl} \qquad \text{---------} \quad (1.6)$$

where c'_{ijkl} are the complex elastic constants, and include the electronic contribution to the elastic properties. Since c'_{ijkl} is complex, the acoustic wave velocity will be complex also and will have real and imaginary parts.

$$v_s' = v_{sr}' + j v_{sj}'$$

The absorption coefficient of the medium is related to the imaginary part of the wave velocity in the following way.

$$\alpha = -k_s \left(\frac{v_{sj}'}{|v_s'|} \right) \quad \text{- - - - - - - - - - (1.7)}$$

Further, the change in wave velocity due to the acoustoelectric interaction may be expressed as

$$\Delta v = v_s' - v_s \quad \text{- - - - - - - - - - (1.8)}$$

In general, $\Delta v \ll v_s'$ and it is usual to replace $|v_s'|$ by v_s in equation (1.7).

The basic equations of state for a piezoelectric crystal may be obtained from thermodynamic consideration of the elastic and electrical properties of the material. These may be shown to be

$$T_{ij} = c_{ijkl} S_{kl} - e_{lij} E_l \quad \text{- - - - - - (1.9)}$$

$$D_k = e_{klm} S_{lm} + \varepsilon_{ik} E_i \quad \text{- - - - - - (1.10)}$$

where D_k is the electric displacement

E_l is the piezoelectric field

c_{ijkl} are the elastic stiffnesses for constant electric field

ε_{ik} are the dielectric permittivities at constant strain

e_{lij} are the piezoelectric constants

T_{ij} and S_{kl} have been previously defined.

The derivation of equations (1.9) and (1.10) demonstrates some important features of the linear theory of acoustic propagation in piezoelectric semiconductors. These equations are thus derived in appendix 1. A short discussion of the electromechanical coupling factor is also given.

Kyame [23] has studied the contribution of internal electric

fields to the elastic stiffness of a piezoelectric medium. The condition that the electromagnetic field quantities satisfied both the piezoelectric equations of state and Maxwell's field equations led to a secular determinant coupling the transverse electromagnetic waves to three acoustic waves. The piezoelectric nature of the medium may result in the electric field of the electromagnetic wave producing an acoustic wave which is forced to travel at the electromagnetic phase velocity. Depending on the piezoelectric tensor and the direction and mode of propagation each acoustic wave may create an electric field with transverse and longitudinal components. The only significant effect in piezoelectric materials is due to the electrostatic nature of the longitudinal component of the electric field travelling at the acoustic phase velocity. Hutson and White [24] have shown that the acoustic wave dispersion caused by coupling to the electromagnetic waves is about 10^{-5} times smaller than that caused by coupling to the electrostatic fields.

For plane waves, the only electrostatic fields of consequence will be longitudinal. The acoustic wavelength may be considered to be much less than the dimensions of the sample through which the acoustic wave propagates. The transverse components of piezoelectric polarisation will only result in boundary charges as shown in figure 1(a). The longitudinal component of piezoelectric polarisation produces charges which are separated by only half a wavelength as shown in figure 1 (b). In order that effective electric fields are generated, the direction of acoustic propagation and particle motion must produce such a longitudinal component of polarisation. Acoustic waves accompanied by strong longitudinal piezoelectric fields are known as piezoelectrically active waves.

Detailed analysis of wave propagation in anistropic solids indicates that acoustic waves may be propagated in any direction in an extended solid. In order to simplify the analysis of experimental results, pure modes of propagation are studied whenever possible.

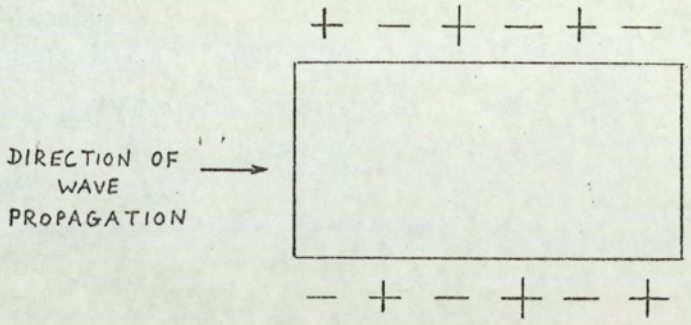

(a) TRANSVERSE ELECTROSTATIC FIELD.

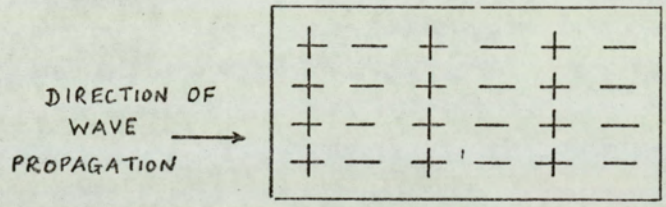

(b) LONGITUDINAL ELECTROSTATIC FIELD.

FIG. 1. ELECTROSTATIC CHARGE CONFIGURATION ACCOMPANYING PLANE WAVES IN A PIEZOELECTRIC MEDIUM. (AFTER McFEE[39]).

Cadmium sulphide is hexagonal at room temperature, and has a point group symmetry of 6 mm. The structure of CdS, illustrated in figure 2 is known as the Wurtzite structure.

This structure consists of two interpenetrating close packed hexagonal lattices, one of which comprises cadmium (Cd) atoms and the other, sulphur (S) atoms. The unit cell contains four atoms: two Cd atoms at (0,0,0.) and (⅓,⅔,½.) and two S atoms at (0,0,⅜.) and (⅓,⅔,⅞.) [25]. The lack of a centre of symmetry - a necessary condition for piezoelectric properties - may be concluded from figure 2.

Waterman [26] has shown that there are five distinct pure modes which may be propagated in a hexagonal crystal. He describes these as follows:

(a) A longitudinal wave along the hexagonal axis.

(b) A transverse wave along the hexagonal axis with arbitrary polarisation of the elastic displacement vector.

(c) A longitudinal wave in any direction in the basal plane.

(d) A transverse wave in any direction in the basal plane with polarisation in the basal plane, and

(e) normal to the basal plane.

A fortunate aspect of pure mode propagation in a hexagonal crystal may be discerned. Namely, that the appropriate propagation directions are those of high crystallographic symmetry. This is experimentally useful since such directions are more easily identified, using simple X-ray techniques.

The piezoelectric moduli of a piezoelectric material form a third order tensor. In general these comprise twenty seven coefficients. However, for a given crystal class these coefficients are reduced in

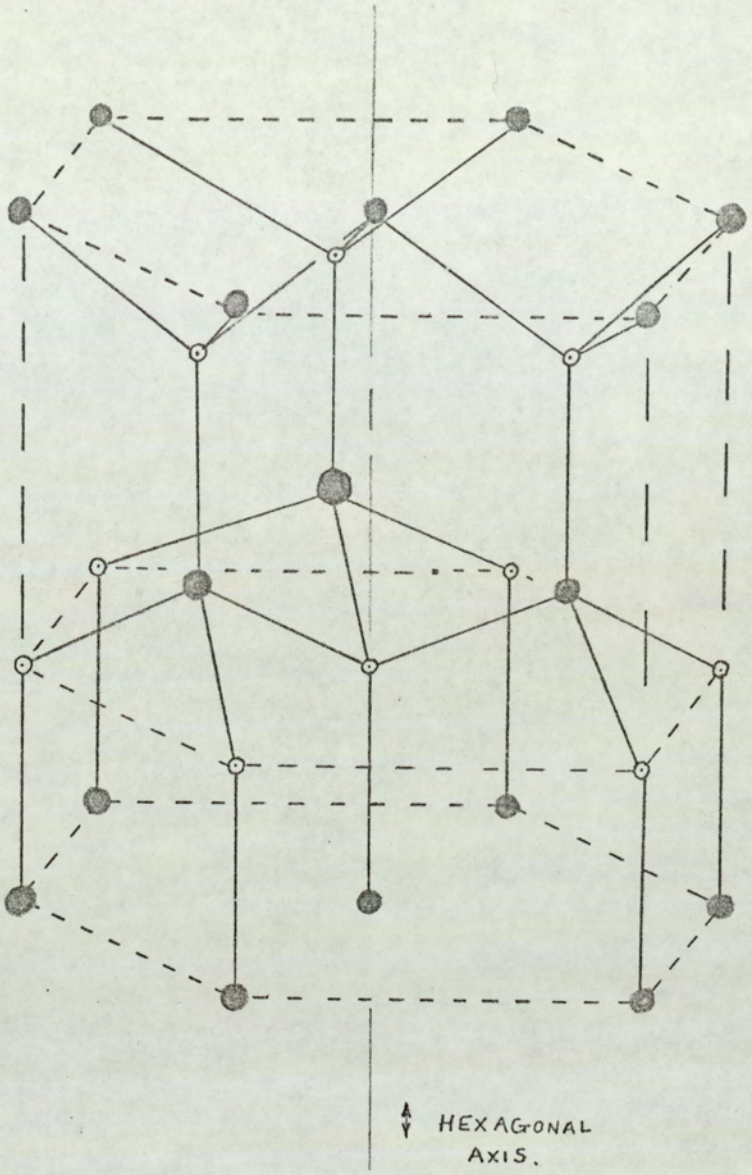

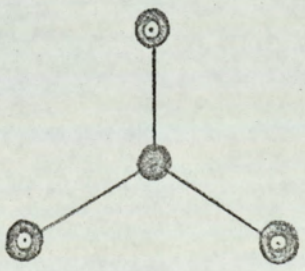

LOOKING ALONG THE HEXAGONAL AXIS.

FIG. 2 THE WURTZITE STRUCTURE.

number by symmetry considerations. For CdS, the piezoelectric constant matrix may be shown, using the matrix notation, to be:

$$\begin{pmatrix} 0 & 0 & 0 & 0 & e_{15} & 0 \\ 0 & 0 & 0 & e_{15} & 0 & 0 \\ e_{31} & e_{31} & e_{33} & 0 & 0 & 0 \end{pmatrix}$$

This leads to the following components of piezoelectric polarisation, (in tensor notation).

$$P_1 = e_{113} S_{13} = e_{131} S_{31} \quad \text{---------} (1.11)$$

$$P_2 = e_{113} S_{23} = e_{131} S_{32} \quad \text{---------} (1.12)$$

$$P_3 = e_{311} S_{11} + e_{311} S_{22} + e_{333} S_{33} \quad \text{---------} (1.13)$$

Conventionally the axes designated 1 and 2 are any two orthogonal directions in the basal plane perpendicular to the hexagonal axis, which is designated the 3 axis.

In order that a given acoustic wave is piezoelectrically active, it must be accompanied by a longitudinal piezoelectric field. The shear strain S_{13} appearing in equation (1.11) is produced by a plane shear wave propagating along the hexagonal axis with particle motion in the basal plane. The shear strain S_{31} which also produces polarisation along the 1 direction is produced by a plane shear wave propagating along the 1 direction with particle motion in the 3 direction. Since the piezoelectric polarisation is transverse in the former case, and longitudinal in the latter case, only the latter case is indicative of a piezoelectrically active acoustic wave. Equation (1.12) may be considered similarly, and shows that a shear wave propagating along the 2 direction with particle motion along the hexagonal axis will also be piezoelectrically active. Equation (1.13) shows that a longitudinal acoustic wave propagating down the hexagonal axis will

be piezoelectrically active but that longitudinal acoustic wave propagation along directions 1 or 2 produces transverse piezoelectric polarisation indicating piezoelectrically inactive acoustic wave propagation. The piezoelectrically active waves correspond to cases (a) and (e) of Waterman [26].

1.3.3. Acoustic amplification in piezoelectric semiconductors

Soon after the observation of strong photosensitive attenuation of piezoelectrically active waves in CdS, Hutson and White [24] presented a linear one-dimensional theory of acoustic wave propagation in piezoelectric semiconductors. A complex elastic constant was derived which included the electrical effects. An expression for the attenuation coefficient in terms of the electron parameters, as outlined on page 11 of this thesis was described.

White [27] realised that the acoustoelectric interaction could lead to amplification of the acoustic wave if the electron drift velocity in the direction of acoustic propagation exceeded the acoustic velocity. This possibility had previously been pointed out by Weinreich [5]. The effect of applying an external d.c. electric field to the crystal was considered theoretically by White [27] and the acoustic attenuation coefficient was determined to be given by the following expression.

$$\alpha = \frac{K^2}{2 v_s}\left[\frac{\omega_c \gamma}{\gamma^2 + \left(\frac{\omega_c}{\omega} + \frac{\omega}{\omega_D}\right)^2}\right] \quad ----(1.14)$$

where α = attenuation coefficient in nepers.cm^{-1}

K = electromechanical coupling factor

ω_c = dielectric relaxation frequency

ω = angular acoustic frequency

ω_D = diffusion frequency

v_s = acoustic velocity.

$\gamma = 1 - \frac{v_d}{v_s}$

v_d = drift velocity of electrons.

$\omega_c = \frac{\sigma}{\varepsilon}$

σ = crystal conductivity.

ε = dielectric permittivity.

$\omega_D = \frac{v_s^2}{f D_n}$

f = trapping factor (see below for explanation).

D_n = Einstein diffusion constant.

The sign of α is controlled by the drift factor γ. When the electron drift velocity becomes greater than the acoustic velocity, then γ becomes negative. This results in negative attenuation or amplification of the acoustic wave. An outline of White's theory is given in chapter 2. The trapping factor f requires explanation here for future discussion.

White expressed the density of electrons in the conduction band as

$$n_c = n_o + f n_s \qquad \text{(1.15)}$$

n_o is the equilibrium number of electrons producing electrical neutrality in the absence of an acoustic wave. The deviation from equilibrium produced by the acoustic disturbance is given by the space charge $q n_s$, where q is the electronic charge. Some of the electrons producing this space charge may be trapped however. Thus only a fraction f of the space charge $q n_s$ was considered to participate in conduction. In the absence of trapping f becomes unity.

Whilst the effects of an external d.c. electric field were being considered theoretically, Hutson, McFee, and White [28] studied experimentally the photosensitive acoustic attenuation in the presence of an applied drift field. Their experimental arrangement

is shown in figure (3).

Shear waves generated by a Y-cut quartz transducer of 15 MHz fundamental, were propagated through the amplifier system, detected by a similar transducer on the output side, and displayed on an oscilloscope. The two fused silica buffers insulated the r.f. equipment from the high voltage generator, and also provided a useful time delay between the generation of the r.f. packet and its entry into the CdS.

Electrons were generated within the photoconductive crystal by illuminating it with weakly absorbed light. Acoustic gains of 26 $db.cm^{-1}$ at 15 MHz and 54 $db.cm^{-1}$ at 45 MHz were reported. Their overall results describing the drift field dependence of the attenuation coefficient for various crystal conductivities were in reasonable qualitative agreement with the predicted behaviour, although the magnitude of the predicted gain was not realised. The existence of acoustic gain was further demonstrated by observing the build up of broadband acoustic flux using an applied drift field having a time duration corresponding to many acoustic transits in the CdS.

The success and novelty of their experiment stimulated much research into acoustoelectric effects in piezoelectric semiconductors. Primarily it seemed that here was the strong possibility of developing a practical solid state acoustic amplifier. Unhappily, reported values of acoustic gain were generally much smaller than those predicted. Hickernell and Sakiotis [29] have investigated the basic limitations of the device and have concluded, in agreement with R.M. White [30], that continuous d.c. operation results in gain reduction due to Joule heating, and possible plane wavefront distortion. This restricts any application of the amplifier to pulsed drift field operation. McFee [31] showed that the amplification of broadband, thermally originating, acoustic flux within the crystal resulted in gain reduction of an input acoustic signal. Wang and Pua [32] later

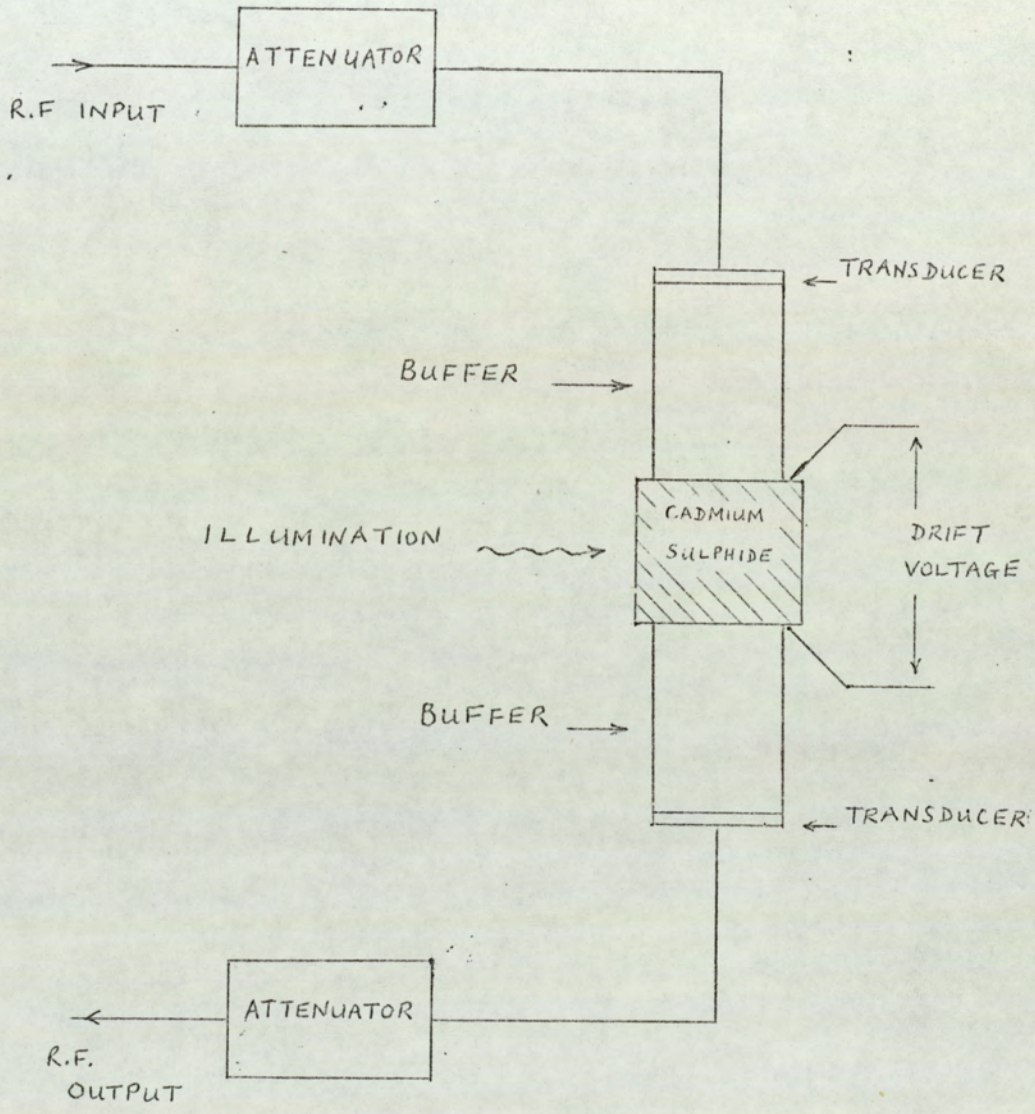

FIG. 3. ACOUSTIC AMPLIFIER ARRANGEMENT (AFTER HUTSON ET AL.)

showed that the interaction between the input acoustic signal and the amplified acoustic flux also led to a reduction in the magnitude of the acoustoelectric field generated by the input acoustic signal. Hickernell et al [29] indicated that gain saturation, due to the build up of random acoustic flux, occurred at gains of about 75 dbs/cm. in a 1 cm. long crystal. This was further investigated by Hanlon [33] who showed that the maximum possible ultrasonic gain was limited to about 80 dbs. Deviations from theory were also attributed to sample inhomogeneity, and carrier trapping.

White, Handelman and Hanlon [34] obtained experimental results over a certain range of operating conditions which did agree closely with those predicted theoretically. They prepared high resistivity samples of CdS by sulphur doping high purity material. Their amplifiers exhibited a low noise figure, and no trapping effects. At large gains however, deviation between experiment and theory did occur, and gain saturation was noted. The design of a practical ultrasonic amplifier has also been investigated comprehensively by May [35].

The realisation that achievable gain magnitude was in part dependent on the quality of the material used, resulted in a more insistant demand for improved stoichiometry. This demand has not been met to date, and interest in the acoustic amplifier from a device point of view has somewhat waned.

Research is now mainly directed at understanding and possibly exploiting the strong non-linear acoustoelectric behaviour observed under certain conditions.

1.3.4. The Acoustoelectric effect

In 1962 Wang [36] showed that the acoustoelectric effect in CdS was some six orders of magnitude larger than had previously been observed via deformation potential coupling in germanium. His experimental arrangement was similar to that of Hutson et al [28]. With no drift field applied to the crystal and for a given crystal

conductivity, the acoustoelectric field was shown to be linearly related to the input acoustic power, as predicted by the Weinreich relationship. Wang also presented results indicating that the variation of acoustoelectric field with conductivity for a given input acoustic power was in dubious agreement with theory. Of greater significance was his observation that the acoustoelectric field and the attenuation coefficient did not change sign at the same applied drift field.

His published experimental results indicating this violation of the Weinreich relationship were somewhat scant. The variation of acoustoelectric field and attenuation coefficient with applied drift field was given only for one crystal conductivity and one input acoustic power. In view of the importance of this observation, a more detailed experimental investigation might have been expected to follow. Instead, however several theoretical papers were then presented showing the Weinreich relationship to be valid in the presence of applied electric and magnetic fields[37, 38]. In his investigation Wang [36] used input acoustic pulses of 10 μ sec. duration, compared to the acoustic transit time in his crystal of less than 2 μ sec. Consequently, many acoustic reflections would have occurred in the CdS giving rise to an unduly complicated measured acoustoelectric field. In chapter 2 an analysis of the Weinreich relationship is presented which is specifically relevant to an input acoustic signal of duration less than the crystal transit time. In later chapters experimental results are described which support the analysis.

McFee [39] has repeated Wang's measurements using acoustic signals of only 1.5 μ sec. duration. No mention was made of further results to sustain the previously observed violation of Weinreich's relationship. McFee also pointed out that the propagation of such a short duration acoustic packet through the crystal would lead to an acoustoelectric current which would reflect any changes in the attenuation of the acoustic signal. Hence, he suggested, the

acoustoelectric field could be used to determine local conditions in the crystal. Further discussion of this aspect of acoustoelectric field measurement is given in chapter 5.

Greebe [40] has suggested that the acoustoelectric effect might be used to study impurity centres in piezoelectric crystals. He was the first to suggest that the trapping factor "f" appearing in White's theory, which expresses the fraction of bunched space charge present as free carriers, should be considered as a complex quantity, in order to account for the phase relationship between the trapped and free space charge. He argued that the frequency dependence of the acoustoelectric field was entirely due to the frequency dependence of the real part of "f". In a later paper [41], Greebe gave experimental results demonstrating frequency dependence, and used these results to calculate trapping parameters which were in agreement with published values. Very recently, Henrich and Weinreich [42] have measured an acoustoelectric voltage in the absence of any external electric field, and thereby investigated ultrasonic attenuation and electron trapping. They considered Greebe's approach to the frequency dependence of the acoustoelectric effect and noted that trapping effects would modify the magnitude of the measured acoustoelectric voltage. Acoustoelectric voltage waveforms very similar to those shown in chapter 5 of this thesis were observed, and a further discussion of their work will be given appropriately. A measure of the magnitude of the acoustoelectric voltage for different crystal conductivities yielded trapping parameters in close agreement with those obtained by Greebe. The next section describes further work which has been carried out to investigate the effect of carrier trapping on the acoustoelectric interaction.

Apart from the work of Henrich and Weinreich [42] the acoustoelectric effect has been largely ignored experimentally. It is reasonably well established that the acoustoelectric field is proportional to the input acoustic intensity [36, 43, 44]. No

comprehensive investigation of the Weinreich relationship has appeared in the literature however. The results of the few published papers dealing experimentally with the acoustoelectric effect have mostly been obtained with no drift field applied to the crystal. Moreover, no attempt at a quantitative assessment of the validity of the Weinreich relationship has been made. In chapter 5 results are presented which show that non-linear effects such as harmonic generation, and also the effects of carrier trapping, may be identified and investigated more thoroughly if the acoustoelectric field, as well as the attentuation coefficient, is measured.

1.3.5. The effects of Carrier trapping

In order to account for the fraction of space charge which is trapped and therefore not available for mobile carrier bunching, White [27] included a trapping factor "f" in his small signal linearised theory. Greebe [40] suggested that the trapped space charge will in general, be out of phase with the mobile space charge and proposed that a complex trapping factor was required. Uchida et al [45, 46] subsequently considered "f" to be complex and have investigated both theoretically and experimentally the effect of carrier trapping on the acoustic amplification coefficient. They studied the attenuation - d.c. field characteristics of several photoconducting CdS crystals, for acoustic frequencies ranging from 15 - 195 MHz., and showed that their experimental results were better described by their trapping theory than by White's theory. Trapping was shown to reduce the maximum gain considerably. Results more in accord with White's theory were obtained at higher acoustic frequencies and greater crystal conductivities.

The effect of trapping on the acoustoelectric field was later discussed by Southgate and Spector [47]. Adopting the approach of Uchida et al they derived a modified Weinreich relationship, and showed that if trapping effects were present the acoustoelectric field would change sign at a lower applied drift voltage than that required to make the acoustic attenuation change sign. Thus the

anomalous results of Wang's investigation were ascribed to carrier trapping. The effects of carrier trapping on the Weinreich relationship are discussed in more detail in chapter 2.

Moore and Smith [48] have investigated the effect of traps on the acoustoelectric current saturation using semiconducting CdS. The term semiconducting will be used to denote bulk resistivity less than 100 ohm.cm. and the term photoconducting to describe illumination dependent, high resistivity CdS crystals. A single level trap theory which accounted for the relaxation time of electrons in the traps was developed. Measurements were made, over a wide temperature range, of the trap independent Hall mobility, and the trap dependent drift mobility, obtained by noting the required drift field, for the onset of current saturation. The Hall and drift mobilities were observed to be approximately equal at 300 ^{o}K. As the temperature was reduced to 77^{o} K however the drift mobility was found to become much smaller than the Hall mobility. The observed variation of drift mobility with temperature enabled the determination of various trapping parameters. A similar investigation has been carried out by Rannestad [49] who considered a model describing two trapping levels. The angular frequency spectrum of the broadband acoustic flux accompanying the current saturation was determined by Moore and Smith [48] from their trapping results to be in the range 10^{8} - 10^{9} sec $^{-1}$. This value was in agreement with McFee's [31] estimation using transducers, and Blotekjaer and Quate's [50] results derived from the observation of the r.f. crystal current; both of which were obtained using photoconducting crystals.

The experimental results presented in chapter 5 clearly indicate that the amplification coefficient can be reduced significantly, and the threshold field for acoustic crossover affected by non-linear effects resulting initially from too large an input acoustic power density. It is, therefore, important to ensure that no high power

effects are present when investigating the effects of carrier trapping.

1.3.6. Current saturation and oscillation

Shortly after the initial experiment of Hutson, McFee and White, Smith [51] observed a saturation of the drift current in semiconducting CdS. Current saturation was observed for current both parallel and perpendicular to the hexagonal axis, and was shown to be a bulk effect. In both cases Smith reported the current saturated at approximately the same threshold drift field. For smaller drift fields, ohmic behaviour was noted. A typical value for the electron mobility was chosen, and the electron drift velocity at the threshold - drift field was determined to be nearly equal to the longitudinal acoustic velocity. Smith proposed that the saturation was due to the amplification of broad band acoustic waves, referred to as acoustic flux. No build up of flux was observed however.

A related effect observed in bismuth at $2^{o}K$ was described by Esaki [52], at about the same time. Crossed electric and magnetic fields were used to produce both cyclotron motion and a net linear drift of carriers having a drift velocity v_x in a direction perpendicular to both the applied magnetic and electric field directions. The acoustoelectric interaction produces a current parallel to the electric field. Esaki noted a dramatic increase in this current when the drift velocity v_x was approximately equal to the acoustic velocity.

The knowledge that McFee [31] had identified acoustic flux build up as the cause of the current saturation, lead to an explanation of both Esaki's and Smith's results by Hutson [53]. The non-linear terms which had been ignored in the linear theory of White, were shown by Hutson to describe the acoustoelectric current. For a single acoustic frequency, the acoustoelectric current and the attenuation coefficient were noted to have the same sign. Thus it was argued that when the acoustic waves were being attenuated the acoustoelectric component of the current added to the d.c. component

of the current. During amplification however, both the attenuation coefficient and the acoustoelectric current change sign. The acoustoelectric current accordingly subtracts from the ohmic current giving the observed current - voltage (I - V) saturation. A basically similar explanation, but taking into account the applied magnetic field, was suggested for Esaki's results. Moore [54] has demonstrated both types of saturation in the same CdS sample; that is, the current saturation observed by Smith, and that observed by Esaki. This provided further evidence to support Hutson's argument that each was due to a basically similar mechanism. Hutson [53] further suggested that the steady state flux level was determined by a balance between linear acoustic amplification and a non-linear loss resulting from parametric interaction of a given component of the flux spectrum with all the other components. The strong coupling proposed, was ascribed to an interaction between the piezoelectric field of one wave and the space charge bunches of another wave.

McFee [31] investigated the drift field dependence of both shear and longitudinal acoustic wave amplitude in photoconducting CdS and semiconducting ZnO. He noted that the presence of acoustic flux notably reduced the amplification of an input acoustic signal. The applied drift field producing maximum gain of the input acoustic signal was also reduced. McFee emphasised the striking correspondence between the flux build up and the current decay. The observed critical or threshold field for the onset of non ohmic behaviour for shear wave propagation in both materials was in agreement with values predicted from the known Hall mobility and shear acoustic velocity. However, the observed threshold fields for longitudinal waves were found to be approximately one half the expected values, calculated from the longitudinal acoustic velocity. This observation was in disagreement with the results of Smith [51], who reported current saturation occurring at the same applied drift field for both shear and longitudinal

waves.

McFee tentatively suggested that this discrepancy was due to the amplification of "off-axis" shear waves. This suggestion has since received experimental confirmation by Rannestad [49], Zucker and Zemon [55], and recently by Moore [56]. Off-axis propagation has been theoretically investigated by Klein [57], and unpublished results by Moore [57] lend support to Klein's conclusion that the off axis angle for maximum acoustic gain varies with applied drift field.

McFee [31] also reported that the current oscillated as the random acoustic flux became amplified. The oscillations were seen to decay as the flux saturated and for the photoconducting CdS samples the current decay was determined to occur over many transits of the flux, back and forth through the samples. For the semiconducting ZnO samples, however, the current decay to the steady state saturated value was observed to occur in a time short compared to the acoustic transit time in the samples. Smith [51] also observed rapid decay times in high conductivity CdS. Both Smith and McFee proposed that the current oscillation was due to the acoustoelectric field associated with the round trip gain of acoustic flux which was shock excited at the cathode by the fast application of the applied d.c. field.

Later work indicates that the frequency and amplitude of the oscillations depend on the magnitude and polarity of the applied voltage, [58,59]. the intensity and uniformity of illumination and temperature [60].

Kroger et al [61] have reported current oscillations of period much less than the acoustic round trip time. They also demonstrated that these oscillations were not affected by the rise time of the applied voltage contrary to the observation of Smith [51] and McFee [31]. Haydl and Quate [62], whilst investigating microwave emission from semiconducting CdS, measured the electric field distribution in their samples. The results suggested that a high electric field region,

or domain, forms near the cathode and travels to the anode. They considered the formation of the high field domain to be due to the build up of acoustic flux. The origin of the domain was further discussed by Haydl [63] who proposed that the amplification of thermally originating acoustic noise near the cathode was sufficient to lead to domain formation. Thus the assumption of shock excited flux was shown to be unnecessary.

The electric field distribution in CdS has been investigated in a number of ways. Maines [64], and Fossum [65] have used the electro-optic effect to obtain evidence of an increase in electric field near the anode during saturation. This conclusion has also been verified by voltage probe measurement. The most detailed measurements have been made by McFee and Tien [66], who measured the electric field distribution in photoconducting CdS. after the current had reached its saturated value. Their measurements indicated that the steady state electric field distribution became highly non-uniform, near the anode, for applied fields greater than the threshold for current saturation. In a second paper [67] they described their measurement of the spatial electric field distribution during the transient current decay to a steady state value. The initial saturation of the current and subsequent damped oscillation were found to be caused by high field domains moving through the crystal at the acoustic wave velocity. Haydl, Harker and Quate [68] have observed current oscillation to commence when the increase in acoustoelectric field produces a negative differential conductivity in the sample. Some theoretical work by Ridley [69] has shown that this can lead to the formation of a high field domain. The effect of the acoustoelectric field on the drift velocity of the carriers was included in a theoretical model proposed by Haydl et al [68], and the conditions necessary for the onset of negative differential conductivity were established. Reasonable agreement between theory and experiment was noted.

Evidence of acoustic energy associated with the high field domain has been obtained by Maines and Paige [70] who removed the drift field whilst the domain was in transit to the anode. The acoustoelectric current was observed to persist for some time afterwards, while the acoustic energy accompanying the high field domain was attenuated. This has been termed the acoustoelectric after-effect.

The published work relating to current oscillation and saturation, and domain formation and propagation is extensive and has been only briefly reviewed. Current saturation and oscillation due to the amplification of acoustic flux has been observed by the author and is described in chapter 5. Some of the experimental results to be presented in chapter 5 describe strong non-linear behaviour and gain saturation produced by a large input acoustic intensity. Harmonic generation has also been observed, and the effect of harmonic generation on the Weinreich relationship has been investigated. This literature survey concludes with a brief discussion of these aspects of non-linear acoustoelectric behaviour.

1.3.7. Further Non-linear acoustoelectric behaviour

The particular linear solution to the complex wave equation derived by White [27], was consequent of certain assumptions.

Although CdS is vigorously piezoelectric, its electromechanical coupling factor is small, in the absolute sense, thus the change in wave amplitude per acoustic wavelength is also small. Moreover the acoustic phase velocity in the crystal varies by no more than a few percent. Thus it was possible to determine a single solution of an essentially fourth order equation. The neglected solutions describe acoustic waves of strongly decaying amplitudes [71].

In order to ensure a linear solution to the wave equation a second order term describing the product of bunched space charge and piezoelectric field was assumed negligible. This assumption is justified for small acoustic strain since the bunched electron

density is then small compared to the equilibrium electron density. The small signal solution for acoustic attenuation was determined to be independent of strain amplitude. As the acoustic power density is increased however, the bunched electron density becomes an appreciable fraction of the equilibrium electron density. Under these conditions the non-linear term is no longer negligible and non-linear effects become significant. The d.c. character of the non-linear current term is discussed in section 2.2. A discussion will be given here of its harmonic implications.

If the non-linear term may not be neglected, then physically a pure harmonic wave cannot propagate through the medium without distortion. Lord and Chick [72] have observed appreciable acoustic waveform distortion in CdS under certain conditions of illumination and applied drift field. An initially sinusoidal acoustic wave was seen to be distorted to a repeated sawtooth wave.

A successful theoretical description of non-linear effects will depend to a certain extent on the description of the bunched space charge and piezoelectric field, and also the strain and particle displacement of the medium. It is now not sufficient to describe these as sinusoidal quantities of a single frequency and wavenumber. Hutson [53] has shown that appreciable harmonic generation and parametric interaction of acoustic waves will occur when non-linear behaviour is significant.

Harmonic generation has been observed by Kroger [73], Elbaum and Truell [74], and others [46]. A theory of harmonic generation has been given by Tell [75], who expressed the piezoelectric field and the strain as a Fourier series. He assumed that the second harmonic was small compared to the fundamental and that higher harmonics could be considered negligible. Using White's [27] approach the acoustic intensity of the second harmonic was predicted to be proportional to the square of the fundamental intensity. This has been verified experimentally by Tell [75] and others.

The realisation that non-linearity of the acoustoelectric interaction is of great importance in any acceptable explanation of current saturation and oscillation, harmonic generation, and other anharmonic effects have resulted in many non-linear theories appearing in the literature. Some of these theories establish expressions for acoustic gain and acoustoelectric field by using the small signal results of White's theory. Since non-linear behaviour involves large amplitude waves such theories are invalid.

A comprehensive approach to the non-linear consequences of the acoustoelectric interaction has been described by Tien [71]. He has shown by a complicated numerical comparison of two possible models, that the harmonic nature of the elastic wave may be ignored without losing any of the essential features descriptive of non-linear behaviour, providing the harmonic nature of the piezoelectric field and bunched carriers is retained. Of greater significance to the experimental work presented in chapter 5 is his conclusion that the Weinreich relationship may be written for each harmonic independently. This conclusion has also received support from Butcher and Ogg [76, 77], who indicate that the Weinreich relationship is valid for acoustic waves of arbitrary amplitude and harmonic content. Their analysis shows that under such non-linear conditions the power gain of the total acoustic flux is related to the total acoustoelectric current contribution of all the individual harmonics.

Many and Balberg [78] have proposed two simplified models as being descriptive of acoustic gain under large signal conditions. Essentially they question whether the acoustic gain of a narrow domain of acoustic flux propagating though the crystal depends on the local field inside the domain (model A) or the drift current through the crystal (model B). Their experimental work using semiconducting CdS suggested model A to be applicable. Maines and Paige [79] using photoconducting CdS have given support to model B. Since both models

are oversimplified and based on the assumption that the linear White theory may be extended to large signal conditions neither is expected to be valid under large signal conditions. The numerical analysis of Tien [71] presents results which do not conform to either model, but lie in between the saturation limits suggested by each. This controversy is not yet resolved. A recent paper by Ganguly and Conwell [80] extends the theory to include third order acoustic amplitude effects, without any significant conclusions other than to present results in disagreement with those theories already discussed.

1.4. Concluding Remarks.

The experimental observation of acoustic amplification in CdS in 1961 suggested a promising field of research with considerable device potential. This stimulated much investigation into the acoustoelectric interaction in piezoelectric semiconductors. As more experimental results were obtained, it was realised that generally available material was not sufficiently stoichiometric to fulfill that promise. The consequent demand for better quality crystals has not been satisfied to date. Furthermore, the attendant amplification of thermally originating broadband acoustic flux was seen to result in non-linear behaviour and acoustoelectric instability, giving rise to considerably reduced acoustic gain performance.

Small amplitude acoustic input has been shown to be amplified somewhat according to the small signal theory of White. Non-linear behaviour, which may occur as a result of sample inhomogeneity, non-uniform illumination or an excessive acoustic input results in harmonic generation, current saturation and oscillation and also gain saturation.

Recently much attention has been paid to the non-linear instabilities which lead to acoustoelectric oscillation and theories have been proposed to describe the non-linear behaviour of the crystal. Such attempts to describe the acoustic gain and current instability take

into account the local acoustoelectric field generated by the acoustic waves. The acoustoelectric field is related to the local power density of the acoustic wave and also to the electronic attenuation coefficient as described by the Weinreich relationship. A survey of the literature indicates that the Weinreich relationship has lacked any comprehensive experimental test. This thesis describes a study of the validity of the Weinreich relationship under a wide range of experimental conditions. Disagreement between experiment and theory is examined carefully, and an attempt is made to interpret this disagreement using the trapping, and non-linear theories which have been proposed.

The following chapter presents the relevant theoretical work necessary for a discussion of the experimental results. Chapter 3 describes the construction of the acoustic amplifier used in the experiments. The experimental arrangement and a description of the techniques used to determine the experimental parameters is given in chapter 4. The main body of the results are described in chapter 5. A discussion of these results is given in chapter 6, and chapter 7 reviews the work and suggestions are made for future study.

CHAPTER 2

Theory

2.1. Introduction

This chapter reviews some theoretical aspects of the acoustoelectric interaction, and details that theory relevant to a discussion of the experimental results presented in chapter 5. Section 2.2. of this chapter reviews White's [27] linear theory of acoustic attenuation. Rather than present a review essentially similar to many which have already appeared in the literature, an attempt has been made to discuss the important aspects of this theory by considering the relative amplitudes and phases of the various alternating parameters appearing in the theory.

The Weinreich relationship is then considered in detail and an original analysis is given which allows a quantitative investigation of this relationship to be made.

Lastly, the effects of carrier trapping are discussed. A means of determining whether the published trapping theories consistently describe the observed asymmetry and change in crossover d.c. field of both the attenuation coefficient and the acoustoelectric effect is indicated.

2.2. The linear theory of White

The small signal theory of White [27] is well known and only an outline of his treatment is considered necessary. A single acoustic plane wave was described to travel in the x-direction through a piezoelectric material. Gauss' equation, the charge continuity equation, and an expression for the current density in an n-type semiconductor, were combined with the piezoelectric equations of state (see appendix 1), to obtain an equation relating the piezoelectric field to the strain. This expression was substituted into the wave

equation describing the acoustic propagation. It was necessary to consider negligible a second order term describing the product of the bunched space charge and piezoelectric field, since such a product yielded a d.c. term and harmonic terms, the inclusion of which denied a linear solution of the wave equation. This omission is justified for small acoustically induced strains, since the bunched electron density n_{so} is small compared to the equilibrium density n_o. The stress and the strain were thus determined to be related by a complex elastic constant which described the electrical and mechanical contribution to the elastic properties of the medium.

The complex elastic constant was used to determine the resulting acoustic attenuation and dispersion in the manner outlined on page 10. The wave vector k_s' of an acoustic wave travelling with loss and dispersion is given as

$$j k_s' = \alpha + j \frac{\omega}{v_s'} \qquad \text{---------} (2.1)$$

where α is the attenuation coefficient.

ω is the angular acoustic frequency

v_s' is the phase velocity of the wave.

In order to avoid a fourth order solution of k_s' the simplifying assumption that $\alpha << \frac{\omega}{v_s'}$ was made. This is equivalent to assuming that the acoustic loss per wavelength is small. Since the electromechanical coupling factor is only of the order of 10^{-2}, this assumption is justified. Further, the phase velocity of the wave may be considered to be effectively unchanged, and so the wave vector may be written as

$$k_s' \simeq k_s = \frac{\omega}{v_s} \qquad \text{------} (2.2)$$

where v_s is the phase velocity of the wave when no piezoelectric effects are present.

The attenuation coefficient α and the acoustic phase

velocity v_s' were thus determined to be

$$\alpha = \frac{K^2}{2 v_s} \omega_c \left[\frac{\gamma}{\gamma^2 + \left(\frac{\omega_c}{\omega} + \frac{\omega}{\omega_D} \right)^2} \right] \quad ----- (2.3)$$

$$v_s' = v_s \left[1 + \frac{K^2}{2} \left(\frac{\gamma^2 + \frac{\omega_c}{\omega_D} + \left(\frac{\omega}{\omega_D} \right)^2}{\gamma^2 + \left(\frac{\omega_c}{\omega} + \frac{\omega}{\omega_D} \right)^2} \right) \right] \quad --- (2.4)$$

where K = the electromechanical coupling factor (see appendix 1).

$\omega_c = \frac{\sigma}{\varepsilon}$ = angular dielectric relaxation frequency.

σ = crystal conductivity.

ε = dielectric permittivity at constant strain.

ω = angular acoustic frequency.

$\omega_D = \frac{v_s^2}{f D_n}$ = angular diffusion frequency.

f = trapping factor.

D_n = electron diffusion constant.

v_s = acoustic phase velocity for a passive material.

$\gamma = 1 - \frac{v_d}{v_s}$

v_d = drift velocity of electrons

Note that the linear approximation leads to expressions for dispersion and attenuation which do not depend on strain amplitude. White also derived the following equations relating the strain $\tilde{S}$, piezoelectric field $\tilde{E}_1$, alternating current density $\tilde{J}$, and alternating space charge $\tilde{n}_s$.

$$\tilde{J} = \frac{\sigma \tilde{E}_1}{\gamma + j \frac{\omega}{\omega_D}} = - \frac{\sigma e}{\varepsilon} \frac{\tilde{S}}{\gamma + j \left(\frac{\omega_c}{\omega} + \frac{\omega}{\omega_D} \right)} \quad - (2.5)$$

$$\tilde{n}_s = \frac{- \sigma \tilde{E}_1}{q v_s \left(\gamma + j \frac{\omega}{\omega_D} \right)} = \frac{e \omega_c}{q v_s} \frac{\tilde{S}}{\gamma + j \left(\frac{\omega_c}{\omega} + \frac{\omega}{\omega_D} \right)} \quad (2.6)$$

Implicit in these equations is a description of the relative phases of the alternating quantities. The phase relationships are of importance in understanding the process of acoustic attenuation and amplification. They may also be used to derive the Weinreich relationship. Apart from a treatment in terms of rotating vector diagrams by McFee [39], the phase relationships do not appear to have been described very fully in the literature, and a more comprehensive description will now be presented.

Consider the strain to be the reference vector and to be described by

$$\tilde{S} = S_o \exp j(k_s x - \omega t) \quad ----(2.7)$$

where S_o is the strain amplitude. The alternating space charge, current density and piezoelectric field may then be described as follows;

$$\tilde{n}_s = n_{so} \exp j(k_s x - \omega t + \phi) \quad ----(2.8)$$

$$\tilde{E}_1 = E_{1o} \exp j(k_s x - \omega t + \psi) \quad ----(2.9)$$

$$\tilde{J} = J_o \exp j(k_s x - \omega t + \phi') \quad ----(2.10)$$

where ϕ, ψ and ϕ' are the phase angles between the particular alternating vector and the strain vector. n_{so}, E_{1O} and J_o are the amplitudes of the alternating quantities, and are related to the strain amplitude as follows:

$$J_o \exp j\phi' = -\frac{\sigma e}{\varepsilon} \frac{S_o}{\gamma + j\left(\frac{\omega_c}{\omega} + \frac{\omega}{\omega_D}\right)} \quad --(2.11)$$

$$n_{so} \exp j\phi = \frac{e\omega_c}{q v_s} \frac{S_o}{\gamma + j\left(\frac{\omega_c}{\omega} + \frac{\omega}{\omega_D}\right)} \quad --(2.12)$$

$$E_{1o} \exp j\psi = -\frac{e}{\varepsilon} S_o \left[\frac{\left(\gamma + j\frac{\omega}{\omega_D}\right)}{\gamma + j\left(\frac{\omega_c}{\omega} + \frac{\omega}{\omega_D}\right)}\right] \quad --(2.13)$$

Combining equation (2.12) and (2.13) gives the relationship between n_{so} and E_{10}. This is also given in equation (2.6)

$$n_{so} \exp j\theta = \frac{-\sigma}{q v_s} \frac{E_{10}}{\left(\gamma + j\frac{\omega}{\omega_D}\right)} \quad ----(2.14)$$

where $\theta = (\psi - \phi)$ and is the phase angle between $\tilde{n}_s$ and $\tilde{E}_1$. Immediately obvious from equations (2.11) and (2.12) is the relationship

$$J_o = -n_{so} q v_s \quad ------(2.15)$$

The absence of an imaginary factor in this relationship, together with the negative sign indicates that under all conditions the phase angle between $\tilde{J}$ and $\tilde{n}_s$ is 180^o. Thus in equations (2.8) and (2.10) $\phi = (\phi' + 180)$.

Expressions for the sine, cosine, and tangent of each phase angle may be derived using equations (2.11) to (2.14), and their variation with electron drift velocity v_d is shown in figures (4),(5) and (6). The magnitudes n_{so} and E_{10} may also be determined in terms of the strain amplitude S_o, and are plotted as a function of v_d in figure 8(a) and 8(b). In order to calculate the values plotted, $\frac{\omega_c}{\omega}$ was considered to be unity and ω_D typically 0.05 at room temperature, for an acoustic frequency of 45 Mhz., and the following discussion applies particularly to this choice of values, unless otherwise stated. Those results of the analysis which enable the essential features of the acoustic attenuation and amplification process to be discussed are given below.

$$E_{10} = \frac{e}{\varepsilon} \left| \left\{ \frac{\gamma^2 + \left(\frac{\omega}{\omega_D}\right)^2}{\gamma^2 + \left(\frac{\omega_c}{\omega} + \frac{\omega}{\omega_D}\right)^2} \right\}^{\frac{1}{2}} \right| S_o \quad ---(2.16)$$

$$\tan\phi = \frac{-\left(\frac{\omega_c}{\omega} + \frac{\omega}{\omega_D}\right)}{\gamma} \quad ----(2.17)$$

$$n_{so} = \frac{e\omega_c}{q v_s} \left| \left\{ \frac{1}{\gamma^2 + \left(\frac{\omega_c}{\omega} + \frac{\omega}{\omega_D}\right)^2} \right\}^{\frac{1}{2}} \right| S_o \quad ---(2.18)$$

where ϕ is the phase angle between $\tilde{n}_s$ and $\tilde{S}$.

$$\tan\theta = -\frac{\left(\frac{\omega}{\omega_D}\right)}{\gamma} \quad ------- (2.19)$$

$$\cos\theta = -\left[\frac{\gamma^2}{\gamma^2 + \left(\frac{\omega}{\omega_D}\right)^2}\right]^{\frac{1}{2}} \quad ------ (2.20)$$

where θ is the phase angle between $\tilde{n}_s$ and $\tilde{E}_1$.

The complete set of equations used to obtain figures (4) to (8) are given in appendix 2.

Equation (2.16) shows that for an insulating material where ω_c is zero, the piezoelectric field has a maximum value given by

$$E_{1o\,(MAX)} = \frac{e}{\varepsilon} S_o \quad ------ (2.21)$$

and equation (2.18) indicates, as expected, the bunched electron density n_{so} to be zero. If γ is very large, the piezoelectric field also tends to this maximum value for a given crystal conductivity, because negligible electron bunching occurs. When γ is zero, the electron drift velocity is equal to the acoustic velocity. The piezoelectric field is almost zero, and the bunched space charge qn_{so} tends to a value of

$$q n_{so} = \frac{e\omega S_o}{v_s} \quad ---- (2.22)$$

This conclusion is valid for the values of ω and ω_D used in the calculations. A more general discussion of the dependence of n_{so} on ω, ω_c and ω_D is given later. The shorting of the piezoelectric field by the bunched space charge is never fully

accomplished because of the diffusion effects incorporated in the equations as $\frac{\omega}{\omega_D}$.

Figure 4 shows the variation with electron drift velocity v_d of ψ , the phase angle between $\tilde{E}_1$ and $\tilde{S}$, and the corresponding variation of its trigonometrical functions. This variation is seen to be most marked for electron drift velocity near the acoustic velocity. The magnitude of the dramatic change in ψ , shown in figure 4 (d) as v_d changes from 0.75 v_s to 1.25 v_s depends largely on ω_c . A greater change in ψ would occur if the crystal conductivity were increased.

Figure 5 (d), on the other hand, shows that the change in phase angle ϕ , between $\tilde{n}_s$ and $\tilde{S}$ does not occur rapidly over a small electron drift velocity range, as does the change in ψ . Figure 6(d) indicates θ the phase angle between $\tilde{n}_s$ and $\tilde{E}_1$ to change by almost 180° over a small electron velocity variation about v_s. Equations (2.19) and (2.20) show also that the variation of θ and its trigonometrical functions, with electron drift velocity are independent of crystal conductivity. Further comment will be made regarding this conclusion towards the end of this section.

Differentiation of α (equation 2.3)) with respect to γ indicates maximum attenuation and amplification to occur when

$$\gamma = \pm \left(\frac{\omega_c}{\omega} + \frac{\omega}{\omega_D} \right)$$

Substitution of these values of γ into equation (2.17) reveals that maximum attenuation occurs when the phase angle ϕ between $\tilde{n}_s$ and $\tilde{S}$ is 315°, and that maximum amplification occurs when ϕ is 225 °, irrespective of crystal conductivity or electron diffusion.

The relative orientation of the alternating vectors $\tilde{n}_s$, $\tilde{E}_1$, $\tilde{J}$, and $\tilde{S}$, at maximum attenuation, acoustic crossover, and maximum amplification, together with an indication of their relative movement

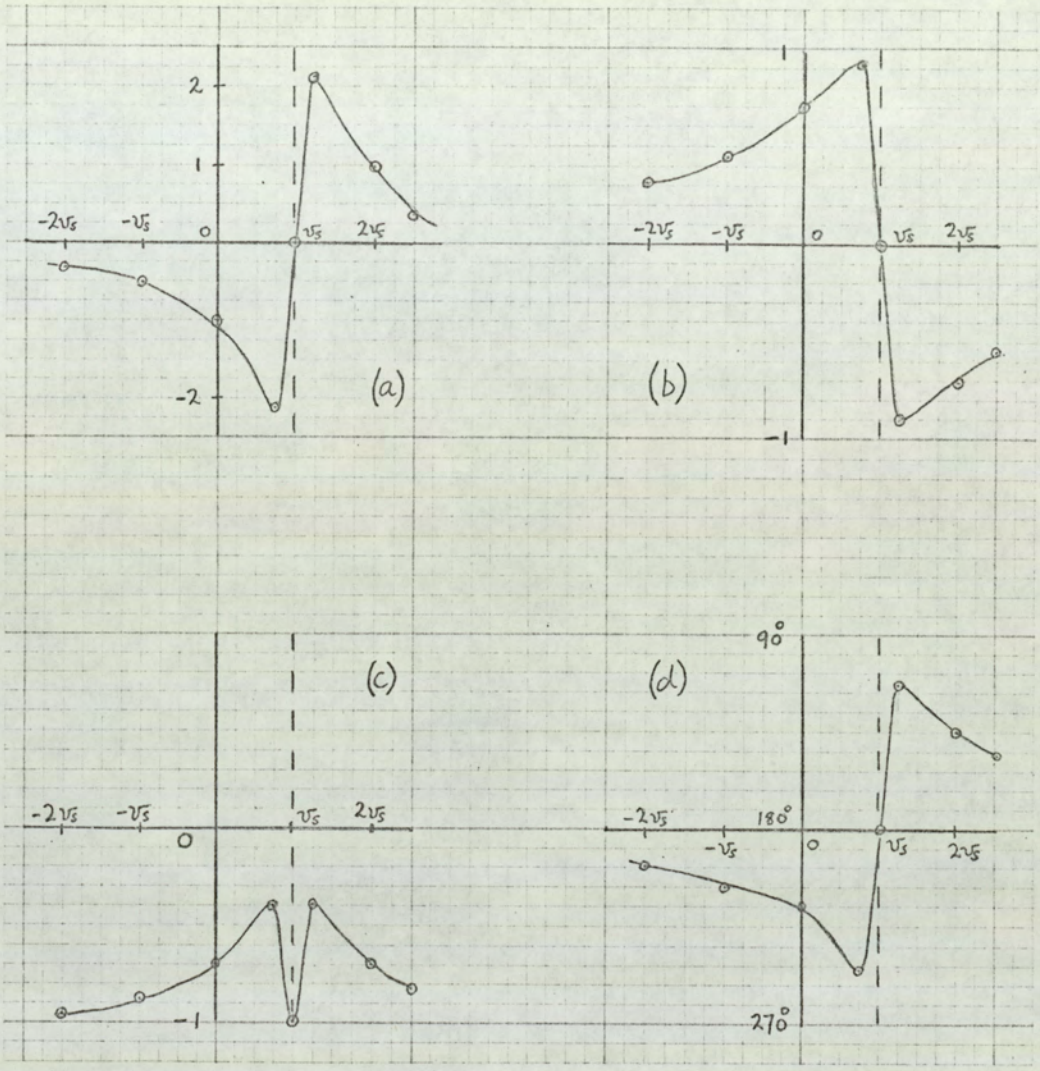

FIG. 4. VARIATION OF a) $-\tan\psi$ b) $-\sin\psi$ (c) $\cos\psi$ (d) ψ

WITH ELECTRON DRIFT VELOCITY.

ψ is the phase angle between $\tilde{E}_1$ and $\tilde{S}$.

$\frac{\omega_c}{\omega} = 1$; $\frac{\omega}{\omega_D} = 0.05$.

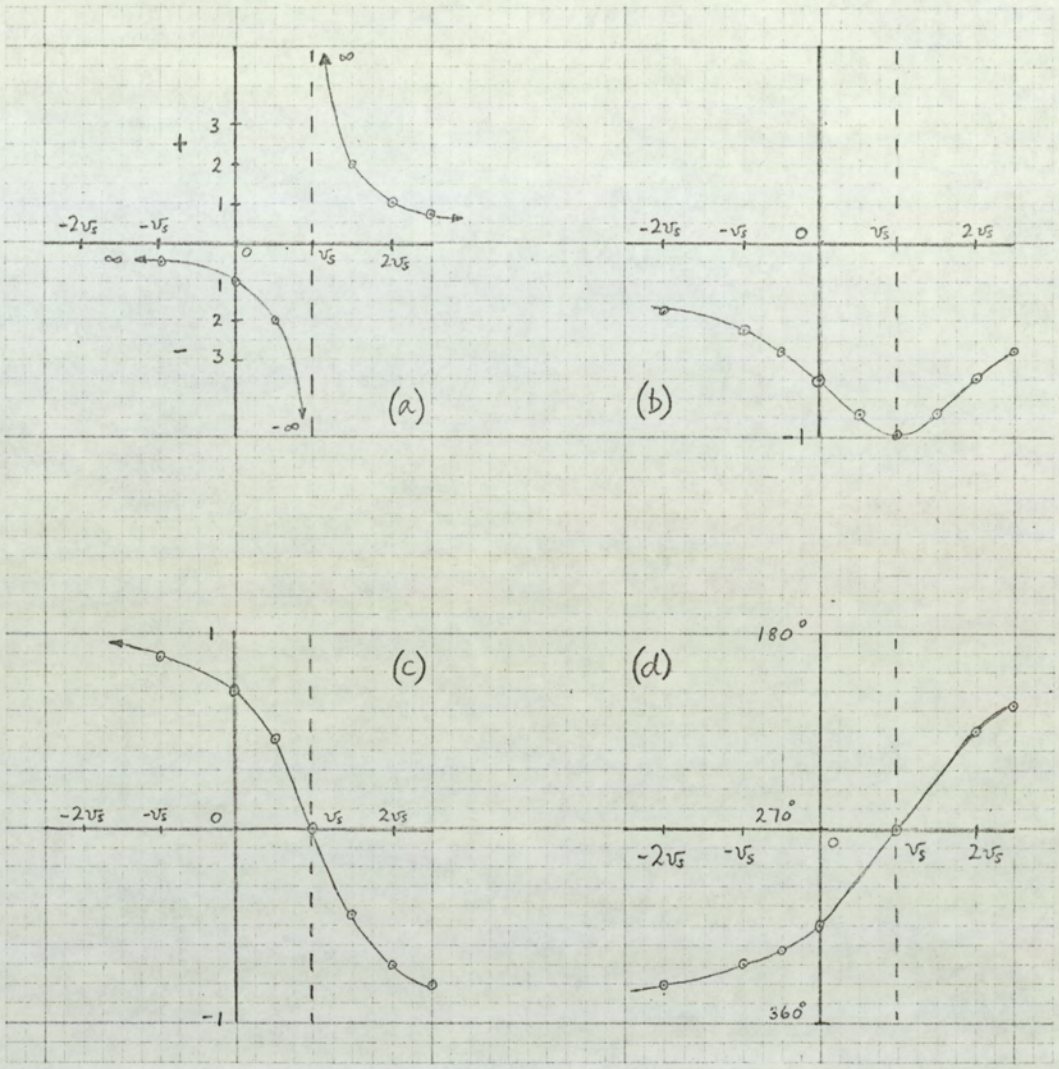

FIG. 5. VARIATION OF a) $\tan \phi$ b) $\sin \phi$ c) $\cos \phi$ d) ϕ

WITH ELECTRON DRIFT VELOCITY.

ϕ is the phase angle between $\tilde{n}_s$ and $\tilde{S}$.

$\frac{\omega_c}{\omega} = 1$; $\frac{\omega}{\omega_D} = 0.05$.

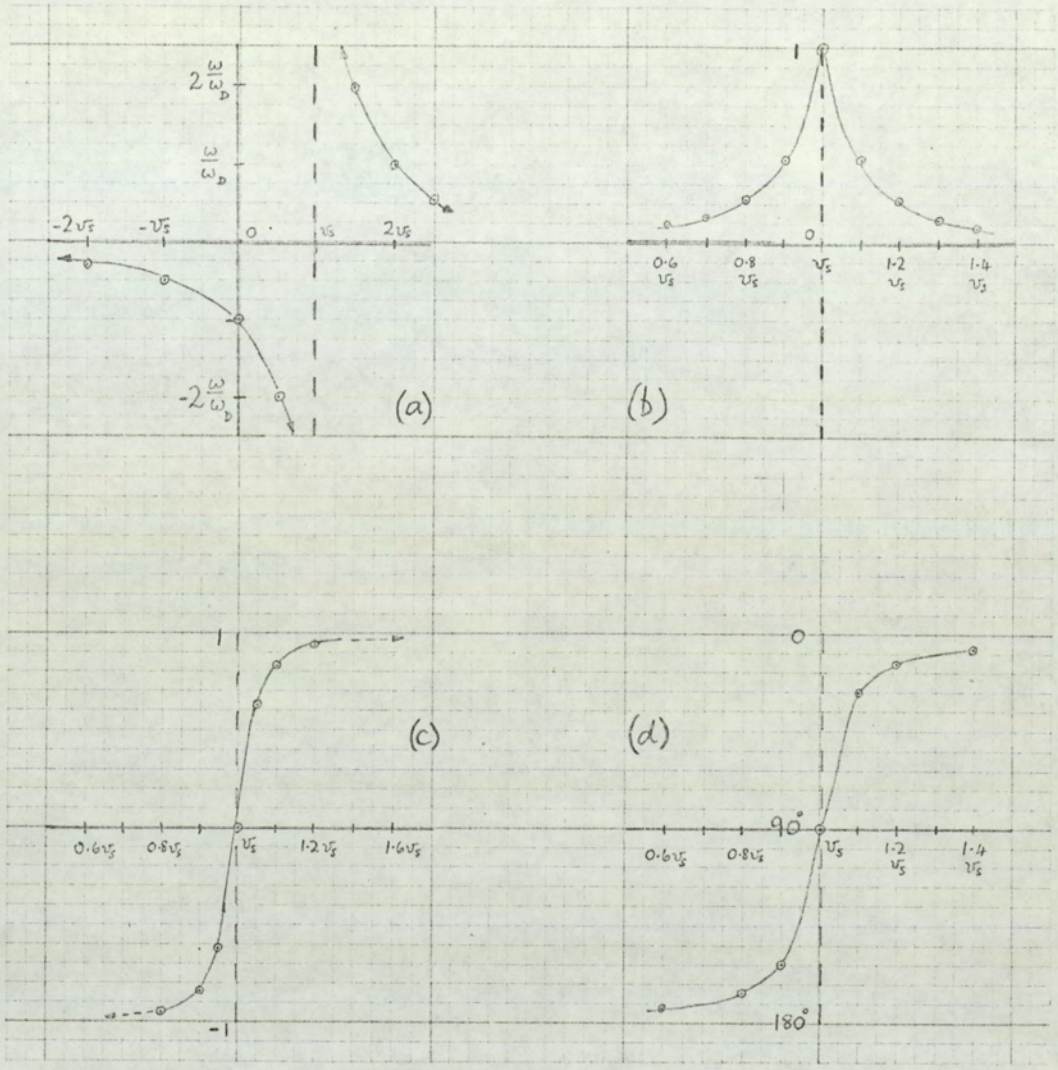

FIG. 6. VARIATION OF a) tan θ
b) sin θ
c) cos θ
d) θ

WITH ELECTRON DRIFT VELOCITY.

θ is the phase angle between $\tilde{n}_s$ and $\tilde{E}_1$, measured from $\tilde{E}_1$.

$\frac{\omega_c}{\omega} = 1$; $\frac{\omega}{\omega_D} = 0.05$.

as γ is varied, is shown in figures 7(a), (b) and (c) respectively. The small phase angle shown between $\tilde{J}$ and $\tilde{E}_1$ in figure 7(a) and $\tilde{n}_s$ and $\tilde{E}_1$ in figure 7(c) is due to electron diffusion. Figure 7(d) presents the variation, of both magnitude and phase of $\tilde{n}_s$ and $\tilde{E}_1$ relative to $\tilde{S}$ as a function of electron drift velocity. Here n_{so} and E_{10} have been normalised to the strain amplitude S_o.

It has previously been noted, that when γ takes a very large positive value, the piezoelectric field E_{10} has virtually the maximum value given by equation (2.21). A large positive value of γ corresponds to a high electron drift velocity in an opposite direction to acoustic propagation. The piezoelectric field for such a value of γ is represented by the vector $\overline{OA}$ of figure 7(d). Under the same conditions, the bunched electron density is virtually zero, and is represented by a point at O on figure 7(d). As γ is reduced from a high positive value to a low positive value, the electron drift velocity becomes smaller and figure 8(b) shows the piezoelectric field to decrease. The bunched electron density is seen in figure 8(a) to increase.

Since the value of $\frac{\omega_c}{\omega}$ was chosen to be unity in the calculation of the values shown in the various figures, maximum attenuation occurs for γ approximately equal to unity. This corresponds to v_d equal to zero, and no external electric field applied to the crystal. A lower crystal conductivity would result in maximum attenuation occurring for $1 > \gamma > 0$. The magnitude and phase of $\tilde{E}_1$, and $\tilde{n}_s$ relative to the reference vector $\tilde{S}$ at maximum attenuation is shown in figure 7(d) by vectors $\overline{OB}$ and $\overline{OX}$ respectively. It has already been noted, figure 7(a), that the effect of electron diffusion results in the vectors $\overline{OB}$ and $\overline{OX}$ not being antiparallel at maximum attenuation. Since the current density $\tilde{J}$, and $\tilde{n}_s$ are always antiparallel (equation 2.15), the effect of diffusion may be seen generally to increase the acute angle between

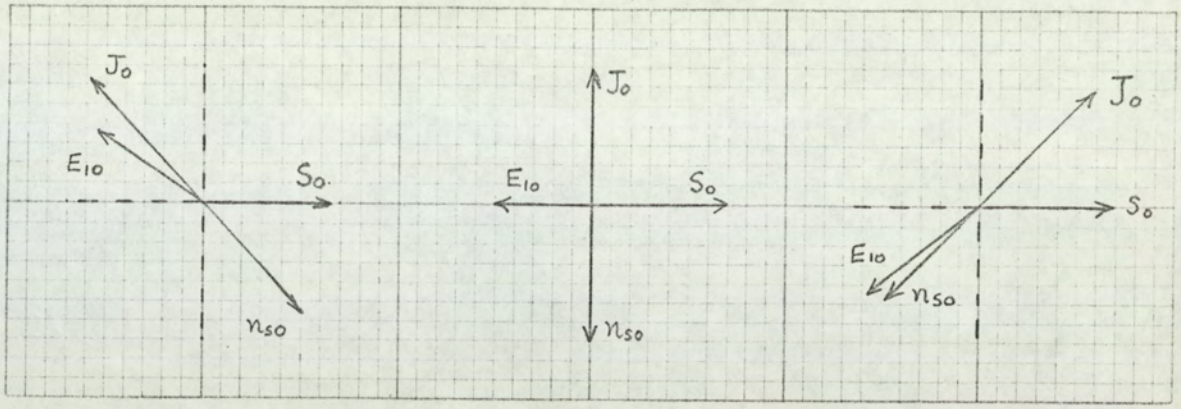

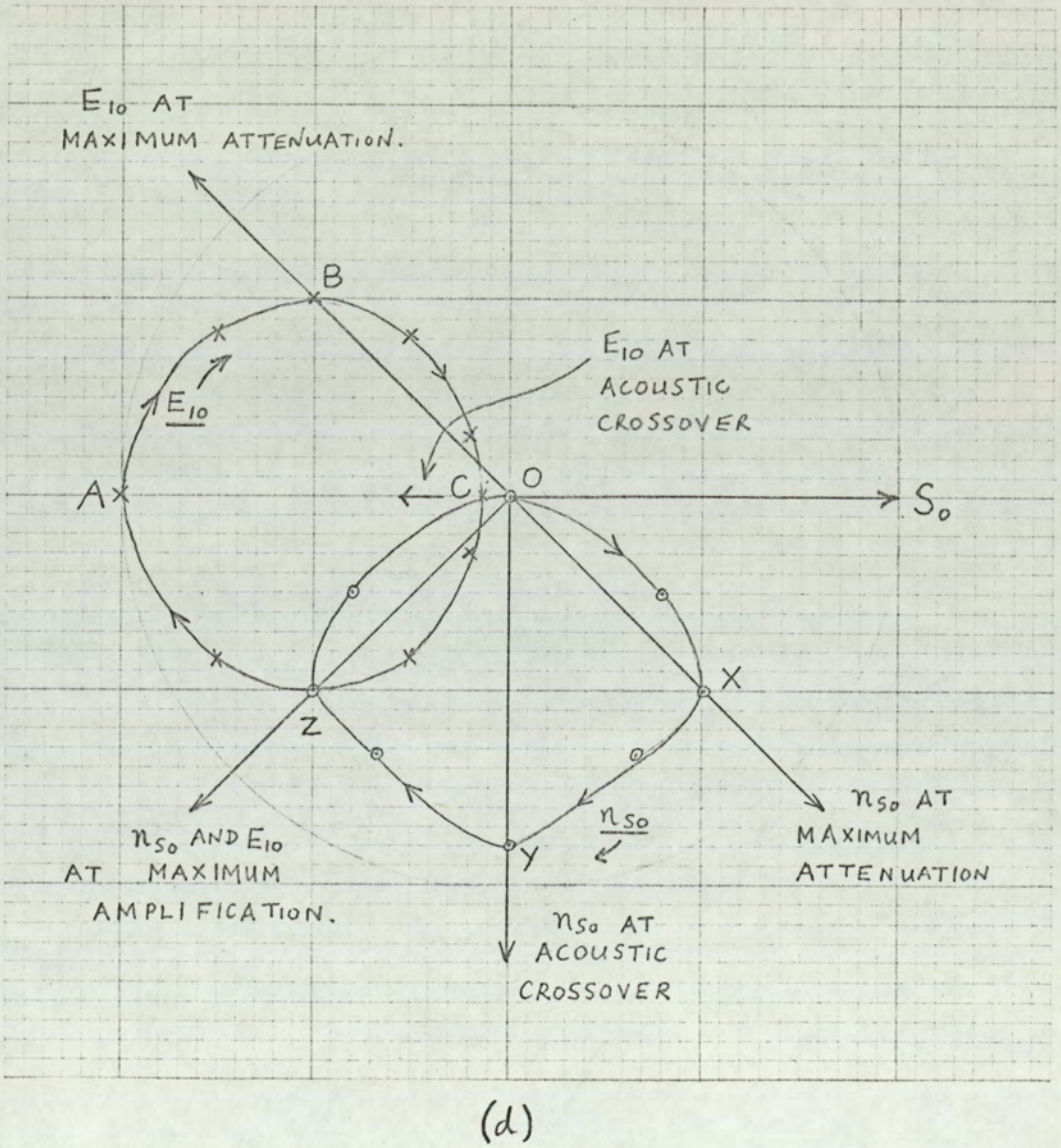

FIG. 7. RELATIVE ORIENTATION OF VECTORS AT (a) MAX. ATTENUATION . (b) CROSSOVER AND (c) MAX. AMPLIFICATION. DIAGRAM (d) INDICATES CHANGE IN n_{so} AND E_{1o} .

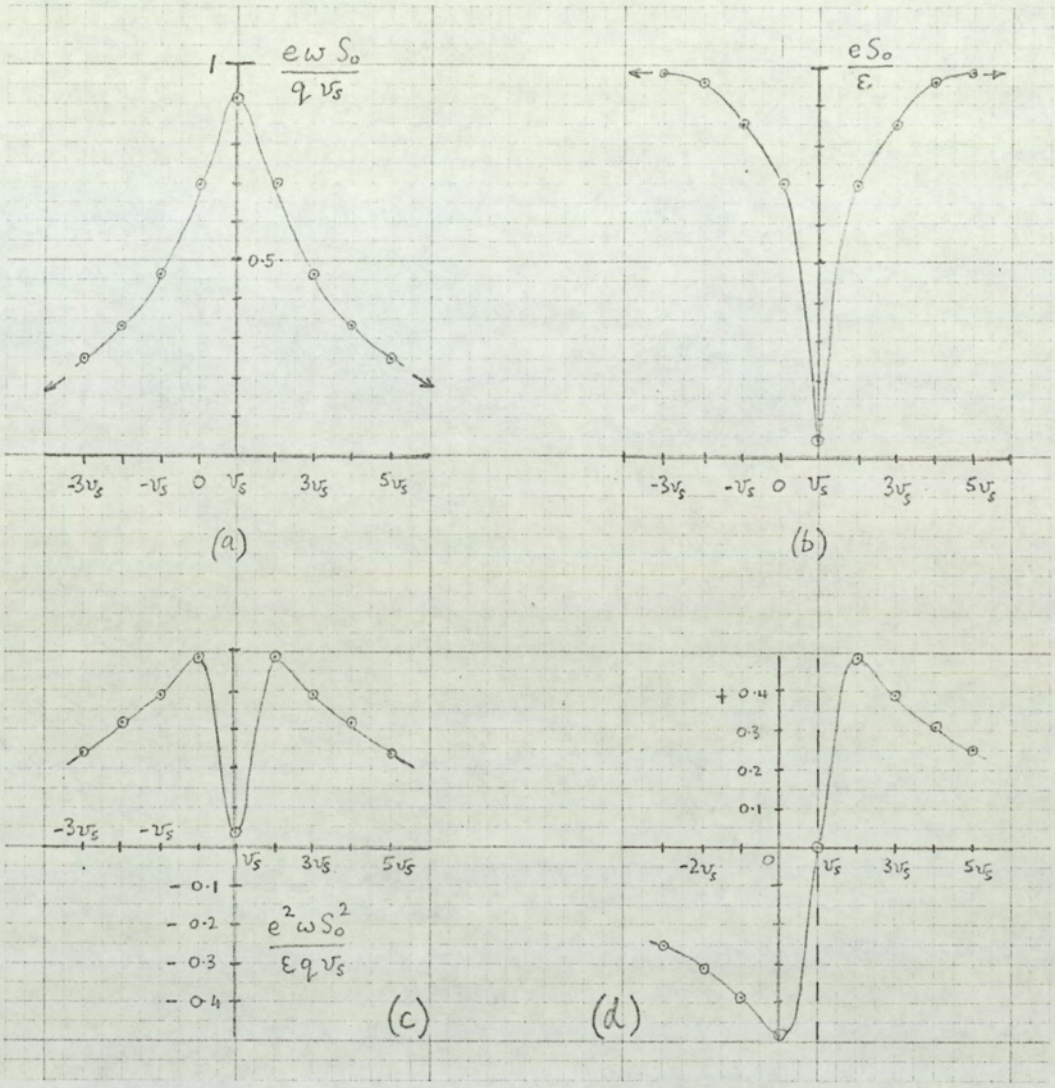

FIG. 8. VARIATION OF a) n_{s0}

b) E_{10}

c) $(n_{s0} E_{10})$

d) $(n_{s0} E_{10} \cos\theta)$

WITH ELECTRON DRIFT VELOCITY.

$$\frac{\omega_c}{\omega} = 1 \; ; \; \frac{\omega}{\omega_D} = 0.05 .$$

$\tilde{J}$ and $\tilde{E}_1$. Anticipating future discussion this results in reduced acoustic attenuation and amplification.

As γ is reduced to zero, v_d increases from zero to v_s, with v_d now in the same direction as v_s. Figure 8(a) shows n_{so} to increase to its maximum value which is a little less than that given by equation (2.22) because of electron diffusion. At the same time the piezoelectric field decreases almost to zero, (figure 8(b)).

The acoustic attenuation becomes zero when γ is zero (see equation 2.3) and this condition is known as acoustic crossover. This corresponds to the electrons drifting at the acoustic velocity. The acoustic attenuation is also zero for no drift field applied to the crystal if ω_c is zero. Consequently, measurement of α is made relative to the insulating, or no illumination, acoustic transmission through the sample. At acoustic crossover the phase angle between $\tilde{n}_s$ and $\tilde{E}_1$ (or $\tilde{J}$ and $\tilde{E}_1$) is 90° as shown in figure 6(d), figure 7(b), and also the points C and Y on figure 7(d) representing the amplitudes E_{10} and n_{so} respectively, at acoustic crossover.

As γ is made more negative v_d becomes greater than v_s, and figures 8(a) and 8(b) show n_{so} to decrease and E_{10} to increase respectively. Figure 7(d) shows the vectors representing $\tilde{n}_s$ and $\tilde{E}_1$ to continue swinging round in the direction of the arrows and eventually, for large negative γ, assume the same amplitudes as for large positive γ. However, figure 6(d) now indicates $\tilde{n}_s$ and $\tilde{E}_1$ to be in phase. In fact, figure 6(c) shows that it is only for values of v_d close to v_s that cosine θ is not nearly ± 1. The significance of this point will be discussed shortly. Maximum amplification occurs when v_d equals $2v_s$ - a consequence of choosing $\frac{\omega_c}{\omega}$ to equal unity - and figure 7(d) shows E_{10} and n_{so} at maximum amplification to intersect at Z. Here the effects of diffusion have been ignored for the sake of clarity. The true state of affairs is shown in figure 7(c) where $\tilde{E}_1$ and $\tilde{n}_s$ are not strictly parallel because of diffusion.

Two points need stressing. Firstly figure 7(d) gives no indication of the rates of change of ψ, the phase angle between $\tilde{E}_1$ and $\tilde{S}$, and of ϕ, the phase angle between $\tilde{n}_s$ and $\tilde{S}$, with electron drift velocity. This information must be derived from figures 4(d) and 5(d). Secondly, the figures are strictly valid for $\frac{\omega_c}{\omega}$ equal to unity, and this is rather a special case, although the basic features of the foregoing discussion will be unchanged for a different value of $\frac{\omega_c}{\omega}$. Returning to the point concerning the rate of change of ψ and ϕ it may be seen from figures 4(d) and 5(d) that whilst ϕ changes from 0° to -180° at a reasonably uniform rate over the entire range of v_d, the phase angle ψ undergoes a dramatic change near acoustic crossover. This must be borne in mind when studying figure 7(d).

Differentiation of equation (2.3) for α with respect to angular acoustic frequency ω shows that α_{MAX} results when $\omega = \sqrt{\omega_c \omega_D}$ Considering the definition of ω_c and ω_D given on page 34 and using the Einstein relation for the diffusion constant,

$$D_n = \frac{\mu k_o T}{q}$$

where k_o is Boltzmanns constant

T is the absolute temperature

μ is the electron mobility

it may be shown that

$$\frac{\omega^2}{\omega_c \omega_D} = k_s^2 \Lambda^2$$

where k_s is the acoustic wavevector and

$$\Lambda^2 = \frac{\varepsilon k_o T}{q^2 n_o}$$

Λ is known as the Debye screening length. If $k_s^2 \Lambda^2 << 1$ then the thermal motion of the electrons discourages electron bunching. If $k_s^2 \Lambda^2 >> 1$, that is, a high acoustic frequency, then the electron distribution cannot respond to the acoustic wave,

diffusion effects become important, and negligible bunching again occurs. This may be further illustrated by considering equation (2.18) expressing n_{so} in terms of the electron parameters, and the strain amplitude. Differentiating this expression with respect to acoustic frequency shows that the maximum possible value of n_{so} occurs when $\omega^2 = \omega_c \omega_D$. Thus for a given crystal conductivity, maximum possible electron bunching will occur when the acoustic wavelength is equal to the Debye length. It is apparent from equation (2.18) that for a given ω and ω_c, maximum bunching will occur when the electrons are drifting with the acoustic velocity, that is, when $\gamma = 0$. The bunched electron density may then be expressed

$$n_{so} = \frac{e S_o}{q v_s} \frac{\omega_c}{\left(\frac{\omega_c}{\omega} + \frac{\omega}{\omega_D}\right)} \quad - - - - - - (2.2.3)$$

For an acoustic frequency other than $\omega = (\omega_c \omega_D)^{\frac{1}{2}}$, n_{so} will be increased by increasing ω_c. However, the limiting value of n_{so} will be smaller than that obtained when $\omega = (\omega_c \omega_D)^{\frac{1}{2}}$. As concluded previously, in diffusion effects are very great, then $\frac{\omega}{\omega_D}$ may dominate the denominator of equation (2.23) and reduce n_{so}. This is more likely to occur at high acoustic frequencies.

The general relationship between $\tilde{E}_1$ and $\tilde{S}$ given by equation (2.5) shows the maximum piezoelectric field, described by equation (2.23) to be modified by the following term.

$$\frac{\gamma + j \frac{\omega}{\omega_D}}{\gamma + j\left(\frac{\omega_c}{\omega} + \frac{\omega}{\omega_D}\right)}$$

This term may thus be regarded as a screening factor. It gives an account of how the piezoelectric field is reduced under different conditions. The imaginary part of the screening factor has the same form as the attenuation of the acoustic wave.

The attenuation coefficient α may be described by

$$2\alpha = \frac{1}{2} \frac{\tilde{J} \cdot \tilde{E}_1}{Q} \quad - - - - (2.2.4)$$

where $\frac{1}{2}\tilde{J}.\tilde{E}$ is the scalar product of $\tilde{J}$ and $\tilde{E}_1$ and expresses the power loss of the acoustic wave per unit volume.

Q is the local acoustic intensity. $\frac{1}{2}\tilde{J}.\tilde{E}$ may also be expressed as $\frac{1}{2}$ Re $(\tilde{J}\tilde{E}_1^*)$, where Re $(\tilde{J}\tilde{E}_1^*)$ is the real part of the product of the alternating current density and the complex conjugate of the piezoelectric field. Thus

$$2\alpha = \frac{1}{2}\frac{J_o E_{10}}{Q}\cos(\theta - 180) \quad \text{---------} \quad (2.25)$$

Making use of equation (2.15) we obtain

$$2\alpha = -\frac{1}{2}\frac{q v_s}{Q} n_{so} E_{10} \cos\theta \quad \text{---------} \quad (2.26)$$

where θ is the phase angle between $\tilde{n}_s$ and $\tilde{E}_1$. Substituting for n_{so}, E_{10} and cos θ from equations (2.18), (2.16) and (2.20) respectively, and putting $Q = \frac{1}{2} c v_s S_o^2$ verifies equation (2.26). Rearrangement of equation (2.26) yields

$$\frac{n_s . E_1}{2} = -\frac{2\alpha Q}{q v_s} \quad \text{---------} \quad (2.27)$$

The non linear current term which was omitted in Whites treatment in order to obtain a linear solution of the complex wave equation may be shown to be given by $\mu q \tilde{n}_s \tilde{E}_1$. This product describes a d.c. current and a doubly periodic alternating current. The d.c. current is known as the acoustoelectric current J_{ae} and may be expressed

$$J_{ae} = \frac{1}{2} q\mu (n_s . \tilde{E}_1) \quad \text{---------} \quad (2.28)$$

Equations (2.27) and (2.28) then show

$$J_{ae} = -\left(\frac{\mu}{v_s}\right) 2\alpha Q$$

The open circuit acoustoelectric field E_{ae} is given by

$$E_{ae} = -\frac{J_{ae}}{\sigma} = -\frac{J_{ae}}{n_o q \mu}$$

Thus

$$E_{ae} = \frac{2\alpha Q}{n_o q v_s} \quad \text{---------} \quad (2.29)$$

This is the Weinreich relationship.

It may appear paradoxical to ignore a non linear term whilst deriving a linear theory, and then use the results of that theory to

investigate the non linear term. The approach is valid however, providing the condition $n_{so} \ll n_o$ is tenable.

From equations (2.26) and (2.28) the attenuation coefficient and the acoustoelectric current are both seen to be proportional to $n_{so} E_{10} \cos\theta$. Figure 8(c) illustrates the variation of the product $(n_{so} E_{10})$ with electron drift velocity. The product $(n_{so} E_{10} \cos\theta)$ is shown in figure 8 (d) as a function of v_d. This indicates the characteristic variation of α or J_{ae} with applied d.c. field. Since $\cos\theta$, shown in figure 6(c) significantly changes from ± 1 only when v_d approaches v_s it is apparent that the variation of α or J_{ae} for high crystal conductivities is due mainly to the change in the product $(n_{so} E_{10})$. However, maximum acoustic gain or loss occurs when $\gamma = \pm\left(\frac{\omega_c}{\omega} + \frac{\omega}{\omega_D}\right)$. Consequently for low crystal conductivities maximum $|\alpha|$ occurs at v_d closer to v_s. If the conductivity is sufficiently low then the electron drift velocity for $|\alpha_{MAX}|$ could be within the velocity region where $\cos\theta$ changes dramatically in magnitude. Then the maximum gain or loss becomes more dependent on the phase angle between $\tilde{n}_s$ and $\tilde{E}_1$.

Although this has not been an entirely comprehensive discussion of the phase relationships, it has served to illustrate some of the basic features of acoustic amplification and attenuation. The significance of some of the parameters involved in the interaction has also been described.

2.3. The Weinreich relationship

In section 2.2 it was noted that the d.c. part of the non linear current term omitted from White's [27] linear theory was given by

$$J_{ae} = \mu q \frac{\tilde{n}_s \cdot \tilde{E}_1}{2}$$

This d.c. current was termed the acoustoelectric current, and was first predicted by Parmenter[1]. A general discussion of the acoustoelectric effect has been given in chapter 1.

Weinreich was the first to suggest that the acoustoelectric field and the acoustic attenuation coefficient were closely related. The attenuation coefficient may be considered to describe the ratio of the average power lost by the electrons / unit volume to the local acoustic intensity. As shown in the last section this may be expressed

$$2\alpha = \frac{1}{2} \frac{\tilde{J} \cdot \tilde{E}_1}{Q}$$

If the acoustic wave and the electron distribution are considered to be otherwise isolated, the change in wave energy and momentum due to the acoustoelectric interaction must result in the same change in energy and momentum of the bunched electrons. This may be expressed as follows.

$$\frac{dE_x}{dx} = \frac{dp}{dt} \qquad \text{---------- (2.30)}$$

where E_x is the energy density of the acoustic wave and p is the momentum of the electrons. The attenuation coefficient may be written

$$2\alpha = -\frac{1}{Q_x} \frac{dQ_x}{dx} \qquad \text{---------- (2.31)}$$

where Q_x is the local acoustic intensity. Q_x is related to E_x as follows.

$$Q_x = v_s E_x \qquad \text{---------- (2.32)}$$

Thus equation (2.31) may be expressed as

$$2\alpha = -\frac{1}{Q_x} v_s \frac{dp}{dt} \qquad \text{---------- (2.33)}$$

The rate of change of electron momentum may be expressed as an average force acting on the electrons. This force can be written

$$F = -n_o q E_{ae} \qquad \text{---------- (2.34)}$$

Thus

$$2\alpha = \frac{1}{Q_x} v_s n_o q E_{ae} \qquad \text{---------- (2.35)}$$

Rearranging yields the Weinreich relationship. The above argument is independent of detailed mechanism, and is generally valid provided the initial postulate of equation (2.30) applies. The effects of carrier trapping on the Weinreich relationship will be considered later in this chapter, since this vitiates the assumption described by equation (2.30).

The purpose of this thesis is to study the validity of the Weinreich relationship. The acoustoelectric field, acoustic attenuation coefficient and input acoustic power density have been measured over a wide range of applied conditions and at different acoustic frequencies. These results are described in chapter 5. The measured values of the acoustoelectric field are dependent on the measurement technique used. In order to make a comparison between theory and experiment it is necessary therefore to consider the Weinreich relationship in a manner consistent with this measurement technique. Such an analysis is presented in the following section.

2.4. The Weinreich relationship modified for experimental test

The analysis to be presented in this section has been published [81].

A detailed description of the measurement techniques used to investigate the validity of the Weinreich relationship is given in chapter 4. The attenuation coefficient is determined by monitoring the change in amplitude of an input acoustic signal due to a single acoustic transit through the CdS crystal used. The resulting acoustoelectric effect is sumultaneously determined by measuring an acoustoelectric voltage which appears across a small resistor placed in series with the crystal. The duration of the input acoustic signal is chosen to be less than the acoustic transit time of the crystal sample. As the acoustic packet propagates through the crystal, the measured acoustoelectric voltage changes, in a manner descriptive of the change in acoustic amplitude. The

input acoustic packet is considered to be idealised such that the peak to peak amplitude is constant over the width. Experimentally, this assumption is not strictly true since the input r.f. signal is not truly rectangular. In practice therefore the half height width is measured.

Suppose the width of the acoustic packet when wholly within the crystal to be w cms., where $w < L$, the crystal length. Let the input acoustic intensity be Q_o watts $cm.^{-2}$ The acoustic signal is considered to propagate through the crystal in the positive x direction, where x is measured from the input face of the crystal. The acoustic intensity at a plane x in the crystal may then be expressed as

$$Q_x = Q_o \exp(-2\alpha x) \quad \text{-----(2.36)}$$

The acoustoelectric voltage produced by the acoustic signal within the crystal is given by $\int_{x_2}^{x_1} E_{ae}\, dx$. Here x_1 and x_2 are the distances from the input crystal face to the leading and trailing edge of the acoustic signal respectively. Combining equation (2.36) with the expression for the acoustoelectric field given by Weinreich and integrating yields

$$\overline{E}_{ae}(x_1 - x_2) = \frac{Q_o}{n_o q v_s}\left(e^{-2\alpha x_2} - e^{-2\alpha x_1}\right) \quad \text{--(2.37)}$$

where $\overline{E}_{ae}$ is the average acoustoelectric field produced by the acoustic signal.

If a small resistor R_m is placed in series with the crystal of resistance R_c, the acoustoelectric current through this resistor results in a measurable voltage V_{ae} across R_m. V_{ae} may be expressed, using Thevenin's theorem, as

$$V_{ae} = \frac{R_m}{(R_m + R_c)}\, \overline{E}_{ae}(x_1 - x_2) \quad \text{---(2.38)}$$

Combining equations (2.37) and (2.38), the measured acoustoelectric voltage produced by an acoustic signal entirely within the crystal

is given by

$$V_{ae} = \frac{R_m}{(R_m + R_c)} \frac{Q_o}{n_o q v_s} \left(e^{-2\alpha x_2} - e^{-2\alpha x_1} \right) \quad --(2.39)$$

Until the acoustic signal is wholly within the crystal x_1 may be considered to vary from zero to w and x_2 to be zero. Thus, the measured acoustoelectric voltage produced by the acoustic signal entering the crystal is given by

$$V_{ae} = \frac{R_m}{(R_m + R_c)} \frac{Q_o}{n_o q v_s} \left(1 - e^{-2\alpha x_1} \right) \quad --(2.40)$$

valid for $0 \leq x_1 \leq w$

When $x_1 = w$ in equation (2.40) the whole acoustic packet is just within the crystal. It then propagates through the crystal, and the measured acoustoelectric voltage is given by equation (2.39) with $(x_1 - x_2) = w$. Expressing V_{ae} in terms of x_1 this becomes

$$V_{ae} = \frac{R_m}{(R_m + R_c)} \frac{Q_o}{n_o q v_s} e^{-2\alpha x_1} \left(e^{2\alpha w} - 1 \right) \quad --(2.41)$$

When x_1, the distance from the input face of the crystal to the leading edge of the acoustic signal, equals L, acoustic reflection occurs. During reflection the measured voltage may be considered to be the linear sum of two components: that produced by the acoustic signal propagating out of the crystal, and that produced by an acoustic signal having an effective input intensity of $R Q_o e^{-2\alpha L}$, propagating in the opposite direction into the crystal. R is the reflection coefficient of the boundary. These two voltages are of opposite signs. Here it is convenient to define x_3 as the width of the acoustic signal travelling in the positive x direction during reflection. The corresponding net measured voltage is then given as

$$V_{ae} = \frac{R_m}{(R_m + R_c)} \frac{Q_o}{n_o q v_s} e^{-2\alpha L}\left[\left(e^{2\alpha x_3} - 1\right) - R\left(1 - e^{-2\alpha(w - x_3)}\right)\right] \quad (2.42)$$

where x_3 is considered to vary from w to zero during reflection.

The same argument may be applied to determine the measured voltage during the second and subsequent acoustic transits, if required.

If the crystal is attenuating, then α is positive and the maximum of the measured acoustoelectric voltage corresponds to the input acoustic packet just within the crystal. This is expressed by equation (2.40) with $x_1 = w$. If an external d.c. field is applied to the crystal sufficient to cause amplification then α is negative, and the maximum of the measured acoustoelectric voltage is given by equation (2.41) for $x_1 = L$, and α negative. This then becomes

$$V_{ae} = \frac{-R_m}{(R_m + R_c)} \frac{Q_o}{n_o q v_s} \left(1 - e^{-2\alpha w}\right) e^{2\alpha L} \quad -- (2.43)$$

The markedly larger acoustoelectric voltages measured under amplifying conditions, result from the positive exponential term in equation (2.43). The factor $\frac{R_m}{(R_m + R_c)} \frac{1}{n_o q v_s}$ appearing in the equations may be expressed differently.

Experimentally R_m is chosen to be much less than R_c for all illumination intensities. The crystal resistance R_c may be expressed in terms of the crystal conductivity σ as follows.

$$R_c = \frac{K}{\sigma} \quad - - - - - - (2.44)$$

where K is a constant depending on the crystal length and the d.c. contact area. The conductivity σ may be written

$$\sigma = n_o q \mu \quad - - - - - - - (2.45)$$

where μ is the electron mobility. Lastly, the drift field required for the onset of acoustic amplification may be introduced using the

relationship

$$E_{TH} = \frac{v_s}{\mu} \quad \text{------} \quad (2.46).$$

Making use of equations (2.44) to (2.46) leads to the following identity

$$\frac{R_m}{(R_m+R_c)} \frac{1}{n_o q v_s} \equiv \frac{R_m}{K E_{TH}} \quad \text{---} \quad (2.47)$$

The maximum of the measured acoustoelectric voltage, for α positive, is then given by

$$V_{ae} = \frac{R_m}{K E_{TH}} Q_o \left(1 - e^{-2\alpha w}\right) \quad \text{---} \quad (2.48)$$

and for α negative

$$V_{ae} = -\frac{R_m}{K E_{TH}} Q_o \left(1 - e^{-2\alpha w}\right) e^{2\alpha L} \quad \text{--} \quad (2.49)$$

Note that equation (2.49) predicts a negative acoustoelectric voltage, as expected. Many of the experimental results to be shown in chapter 5 are compared with those predicted, and it is these two equations which are used to calculate the predicted values.

The variation of V_{ae} as the acoustic signal propagates through the crystal may be calculated using equations (2.40) to (2.42), with the factor $\frac{R_m}{(R_m+R_c)} \frac{1}{n_o q v_s}$ modified as indicated by equation (2.47). Using the results of this analysis it has been possible to compare theory and experiment quantitatively in a manner previously not undertaken. The experimental results, their comparison with theory, and the conclusions drawn from this comparison are presented in chapters 5 and 6 of this thesis.

2.5. The effects of carrier trapping

2.5.1 Introduction

The Weinreich relationship has been shown to relate theoretically, the acoustoelectric field and the acoustic attenuation coefficient. In 1962 Wang [36] reported that contrary to theoretical

expectation, the acoustoelectric field changed sign at a lower applied drift field than the attenuation coefficient. Subsequent theoretical study [37,38] indicated that the Weinreich relationship was not invalidated by an applied electric field. Shortly afterwards Uchida et al [45,46] developed a suggestion, originally made by Greebe [40], that the trapped and mobile bunched space charge might not always be in phase. Uchida et al theoretically considered the implications of a complex trapping factor and showed that the expression for the attenuation coefficient derived by White [27], was considerably modified. Their theoretical conclusions were substantiated by experiment [46].

Southgate and Spector [47] extended the Uchida treatment to describe the effect of a complex trapping factor on the acoustoelectric field. They were thus able to show that the Weinreich relationship, accordingly modified, predicted a different d.c. crossover field for the acoustoelectric effect and the attenuation coefficient, in qualitative agreement with the experimental results reported by Wang [36].

A brief review of the trapping theory of Uchida et al, will now be presented, and the essential features of Southgate and Spector's work will be discussed. The relevance of this work, to the experimental results described in chapter 5 will be made apparent.

2.5.2. The trapping theory of Uchida et al

The essential feature of the theories describing the effects of carrier trapping on both the attenuation coefficient and acoustoelectric field is the inclusion of a complex trapping factor. Hutson and White, and White, considered that a fraction "f" of the bunched space charge was mobile, whilst the fraction (1-f) was bounded. The fraction "f" was assumed to be independent of acoustic frequency. This assumption is, however, justified only if the relaxation time τ of the electron trapping is much shorter than the periodic time of the acoustic wave $\frac{2\pi}{\omega}$. If $\omega\tau \simeq 1$ the phase difference between the mobile and trapped space charge becomes quite

appreciable.

Uchida et al considered a single trapping level and related f_o, the mobile fraction of the bunched space charge when $\omega\tau \ll 1$ - consistent with White's assumption - to the corresponding fraction f when $\omega\tau \gg 1$ or $\omega\tau \simeq 1$. This relationship was shown to be

$$f = \frac{f_o - j\omega\tau}{1 - j\omega\tau} \qquad (2.50)$$

When $\omega\tau \ll 1$, f tends to the value f_o, in agreement with White's assumption. The imaginary character of f becomes greatest when $\omega\tau = 1$; and when $\omega\tau \gg 1$ f approaches unity. This last condition implies no trapping to occur for high acoustic frequencies.

Uchida et al expressed equation (2.50) as

$$f = \frac{bf_o}{(1 + ja)} \qquad (2.51)$$

where

$$a = \frac{(1 - f_o)\omega\tau}{f_o + (\omega\tau)^2} \qquad (2.52)$$

and

$$bf_o = \frac{f_o^2 + (\omega\tau)^2}{f_o + (\omega\tau)^2} \qquad (2.53)$$

Even for a fixed acoustic frequency the quantities "a" and "b" will vary from one crystal to another, since the quantities f_o and τ will depend on trapping parameters.

It is considered unnecessary to detail the mathematical aspects of the Uchida analysis; however the following points are of importance.

The expression arc tangent "a" was shown to describe the phase difference between the mobile and trapped space charge. The quantity "a" was seen to be related to the gain and loss of the acoustic wave. Furthermore, the degree of unsymmetry of the acoustic gain versus applied drift field curve, described by the ratio of maximum acoustic gain to maximum acoustic loss was shown to be a function of "a". As "a" was increased from a = 0 the

the results of the analysis indicated that maximum gain would be significantly reduced. The applied d.c. field necessary for acoustic crossover was also seen to be increased, particularly at low crystal conductivities. It was concluded that a suitable crystal for good acoustic amplification should have a small value of "a"

2.5.3. The effect of carrier trapping on the Weinreich relationship

Southgate and Spector [47] extended the foregoing analysis to describe the effect of carrier trapping on the Weinreich relationship. They expressed the trapping factor f as the complex fraction

$$f = f_r + j f_j \qquad (2.54)$$

The comparison of equation (2.54) with equations (2.51) to (2.53) show that

$$f_r = \frac{\left(f_o + (\omega\tau)^2\right)}{1 + (\omega\tau)^2} \qquad (2.55)$$

and

$$f_j = -\frac{\omega\tau(1 - f_o)}{1 + (\omega\tau)^2} \qquad (2.56)$$

The White trapping factor "f" was replaced by the complex trapping factor and the following expressions were obtained for the attenuation coefficient and the acoustoelectric field.

$$\alpha = \frac{K^2}{2 v_s} \frac{\omega_c \left[1 - \left(\frac{v_d}{v_s}\right) f_r - \left(\frac{\omega}{\omega_D}\right) f_j\right]}{\left[1 - \left(\frac{v_d}{v_s}\right) f_r - \left(\frac{\omega}{\omega_D}\right) f_j\right]^2 + \left[\frac{\omega_c}{\omega} + \left(\frac{\omega}{\omega_D}\right) f_r - \left(\frac{v_d}{v_s}\right) f_j\right]^2} \qquad (2.57)$$

$$E_{ae} = \frac{Q_o K^2}{n_o q v_s^2} \frac{\omega_c \left[f_r - \left(\frac{v_d}{v_s}\right)\left(f_r^2 + f_j^2\right)\right]}{\left[1 - \left(\frac{v_d}{v_s}\right) f_r - \left(\frac{\omega}{\omega_D}\right) f_j\right]^2 + \left[\left(\frac{\omega_c}{\omega}\right) + \left(\frac{\omega}{\omega_D}\right) f_r - \left(\frac{v_d}{v_s}\right) f_j\right]^2} \qquad (2.58)$$

The symbols have been previously defined.

Combining these equations yielded the following expression for the Weinreich relationship.

$$E_{ae} = \frac{2Q_o\alpha}{n_o q v_s}\left[f_r + f_j\left[\frac{\frac{\omega}{\omega_D}f_r - \frac{v_d}{v_s}f_j}{1 - \frac{v_d}{v_s}f_r - \frac{\omega}{\omega_D}f_j}\right]\right] \quad - - - -(2.59)$$

For negligible trapping f_j tends to zero and f_r tends to unity. Equation (2.59) then reduces to the well established Weinreich relationship.

Since the trapped space charge may transfer momentum directly to the lattice, it is apparent that the expression

$$\frac{d\rho}{dt} = \frac{d E_x}{d x}$$

discussed in section 2.3 is no longer valid. The bracketed term in equation (2.59) describes the frequency and drift field dependence of the coefficient of proportionality between α and E_{ae} when the bunched space charge does not contribute equally to each.

From equations (2.57) and (2.58) it may be seen that

$$\left.\frac{v_d}{v_s}\right)_{\alpha=0} = \frac{1 - \left(\frac{\omega}{\omega_D}\right)f_j}{f_r} \quad - - - -(2.60)$$

whilst

$$\left.\frac{v_d}{v_s}\right)_{E_{ae}=0} = \frac{f_r}{\left(f_r^2 + f_j^2\right)} \quad - - - -(2.61)$$

Thus when $f \neq 0$; that is, when trapping is significant, the α and E_{ae} crossover points are unequally shifted along the applied voltage axis. Equating equations (2.60) and (2.61) suggests an equal shift if

$$f_j = \left(\frac{\omega}{\omega_D}\right)\left[f_r^2 + f_j^2\right] \quad - - - - -(2.62)$$

This possibility is excluded however since equation (2.56) implies f_j to be negative.

Expressions for the maximum and minimum values of α and E_{ae},

and the drift fields at which these occur were given by Southgate and Spector, in terms of the real and imaginary parts of the trapping factor. Of practical interest are the equations describing the ratios of the extrema of α and E_{ae} .

$$\left|\frac{\alpha_{MAX}}{\alpha_{MIN}}\right| = \left[\frac{\left(f_r^2 + f_j^2\right)^{\frac{1}{2}} - f_j}{\left(f_r^2 + f_j^2\right)^{\frac{1}{2}} + f_j}\right] \quad -----(2.63)$$

$$\left|\frac{E_{ae\ MAX}}{E_{ae\ MIN}}\right| = \left[\frac{f_r b - f_j\left(\frac{\omega_c}{\omega}\right)}{f_r b + f_j\left(\frac{\omega_c}{\omega}\right)}\right] \quad -----(2.64)$$

where

$$b = \left[\left[1 + \left(\frac{f_j^2}{f_r^2}\right)\right]\left\{\left[1 - \left(\frac{\omega}{\omega_D}\right)f_j\right]^2 + \left[\left(\frac{\omega_c}{\omega}\right) + \left(\frac{\omega}{\omega_D}\right)f_r\right]^2\right\} - 1 - 2\left(\frac{f_j}{f_r}\right)\left(\frac{\omega_c}{\omega}\right)\right]^{\frac{1}{2}} \quad ---(2.65)$$

It may be deduced from these equations that the greater the effects of trapping the more the ratios deviate from unity.

The experimental results described in chapter 5 demonstrate that it is easier to determine the ratio of maximum acoustic loss to maximum acoustic gain, than the corresponding ratio for the acoustoelectric field. This is mainly due to the method used for measuring the acoustoelectric signal, and the subsequent interpretation of this measurement, as described in section 2.4. It will also be made apparent that the acoustic crossover point is more accurately obtained than the acoustoelectric crossover point. Furthermore, whilst the expression describing $\left|\frac{\alpha_{MAX}}{\alpha_{MIN}}\right|$ given by equation (2.63) is reasonably simple, the expression for $\left|\frac{E_{ae\ MAX}}{E_{ae\ MIN}}\right|$ is extremely complicated.

Equations (2.55), (2.56), (2.60) and (2.63) have thus been used to obtain the following expressions for $\omega\tau$, f_j and f_r .

$$f_r = \left[P + \left(\frac{\omega}{\omega_D}\right)\frac{1}{X} \right]^{-1} \quad \text{- - - - - - (2.66)}$$

$$f_j = \left[X\left[P + \left(\frac{\omega}{\omega_D}\right)\frac{1}{X} \right] \right]^{-1} \quad \text{- - - - - - - (2.67)}$$

$$\omega\tau = \left[X(P-1) + \left(\frac{\omega}{\omega_D}\right) \right]^{-1} \quad \text{- - - - - - - (2.68)}$$

where

$$X = \left[\frac{4A}{(1-A)^2} \right]^{\frac{1}{2}} \quad \text{- - - - - - (2.69)}$$

$$A = \left| \frac{\alpha_{MAX}}{\alpha_{MIN}} \right| \quad \text{- - - - - - (2.70)}$$

$$P = \left(\frac{v_d}{v_s} \right)_{\alpha=0} \quad \text{- - - - - (2.71)}$$

Both A and P may be experimentally determined, and thus the important parameters of the trapping theory may be calculated. f_o may also be determined from equation (2.55) or (2.56)

Trap independent asymmetries of the acoustic gain versus applied drift field curve have been described by M.K. Parsons [82]. No published work has yet determined numerically whether the trapping theories consistently describe the change in crossover field and observed asymmmetry of both the attenuation coefficient and the acoustoelectric effect. Experimental results relating to the attenuation coefficient are used in chapter 5, to calculate the trapping parameters using equations (2.66) to (2.68). The calculated values are then substituted into equation (2.61) to determine the effect of possible trapping on the acoustoelectric field crossover. These results are then compared with those obtained experimentally to determine the extent of the trap dependence of the observed asymmetries.

2.6. Concluding remarks

The small signal theory of the acoustoelectric interaction has been reviewed. The dependence of acoustic amplitude on crystal conductivity, electron diffusion, acoustic frequency, and applied drift field have been discussed. The predicted variation of the amplitude and phase of the bunched space charge, piezoelectric field, and a.c. current density relative to acoustic strain have been described in a manner hitherto unreported.

The Weinreich relationship has been discussed, and an original analysis has been given, enabling quantitative comparison with experiment to be made. The effect of carrier trapping on the Weinreich relationship has also been reviewed, and a simple means of determining the trapping parameters experimentally from the observed behaviour of the acoustic signal has been indicated. Using these determined parameters the predicted effect of trapping on the acoustoelectric effect may then be calculated and compared with that observed. In this way, a means of deciding whether the trapping theories consistently describe the variation of acoustic and acoustoelectric crossover and asymmetry is possible.

A theoretical review of the many non linear theories appearing in the literature has not been included, since this would necessarily be extensive. The main features of some of the more prominent theories have been discussed in chapter 1. Particular conclusions of these theories relevant to the discussion of the experimental results presented in chapter 5, will be noted at the appropriate place in the text.

CHAPTER 3

The fabrication of an ultrasonic amplifier

3.1. Introduction

The ultrasonic amplifier used in this research was similar to that described by Uchida et al., and comprised a single crystal of CdS sandwiched between two Y-cut quartz transducers. Absent were the fused silica buffers included by Hutson, McFee and White [28] in their original amplifier (see figure 3). Two possible advantages accrue from the inclusion of buffers. The transducers, and, therefore, the equipment generating and detecting the ultrasonics, are isolated from the high voltage generating equipment. Secondly, a time delay exists between the acoustic generation and the entry of the acoustic signal into the CdS. The use of buffers introduces two extra bonds however, which was considered to more than offset their advantages. The prospect of being able to introduce higher acoustic powers into the crystal thus decided their exclusion. The consequent problem of isolating the d.c. leads from the r.f. terminals did not present any great difficulty, and the lack of any time delay between the generation of the acoustic signal and its propagation into the crystal was not found to be important.

This chapter describes the fabrication of the ultrasonic amplifier. Since the experimental results to be described later were all obtained using the same amplifier, the reasons for choosing the particular piece of CdS used are given. The orientation and preparation of the crystal is then described. The major problems associated with the fabrication of the device are considered, and their successful solution is detailed.

3.2. The choice of crystal

The acoustoelectric activity of one piece of CdS may be markedly different from that of another. A comparison of results obtained using different crystals would require a reasonable number of active crystals. Any difference in acoustoelectric behaviour could only then be properly interpreted if the crystals used were examined for any differences in their physical properties, inhomogeneity, and non-stoichiometry. Such an investigation would necessarily have meant undertaking a more limited number of acoustoelectric experiments. It was therefore considered more judicious to select a single crystal of assured activity and concentrate the experimental work on that one specimen.

The CdS crystals available for selection were all irregularly shaped single crystal boule fragments. It was decided that the final choice would depend upon three qualifications: the physical dimensions of the crystal, its photoconductivity, and finally, the more important assurance of acoustoelectric activity.

3.2.1. The physical dimensions of the crystal.

In order to propagate a piezoelectrically active shear acoustic wave through single crystal CdS, the wave propagation must be at right angles to the major crystallographic axis - the "c" axis - of the crystal, and the polarisation direction of the wave parallel to the "c" axis.

The minimum acceptable dimensions of the proposed amplifier were essentially dictated by the dimensions of the transducers to be used. These were 6.4 mm (0.25 ins.) in diameter, and demanded that the faces of the amplifier to which they were to be affixed were at least 7 mm.square. The length of the amplifier measured normally to these faces, and thus perpendicular to the "c" axis was also required to be about 7 mm.long.

Each available crystal was therefore examined to determine

the approximate direction of the "c" axis, and thus whether an amplifier of sufficient size could be obtained. In many cases the roughly shaped crystals tended to be elongated in this direction, and often striations parallel to the "c" axis were visible on cleavage surfaces. This preliminary visual examination was supplemented by an examination of each crystal in polarised light. Since CdS is optically anistropic, rotation of the crystal about a normal to the plane of crossed polaroids produces a variation of optical transmission which correlates with the directions of optical anistropy. No variation in transmission is noted however, for light travelling parallel to the "c" axis. Some of the crystals were so irregularly shaped, that it was first necessary to grind and polish small flats on the crystal before the polarisation technique could be used. A quick identification of the "c" axis direction was thus possible. Of six crystals examined in this way, only four were considered to be suitable for possible use as an amplifier.

3.2.2. The photoconductivity of the crystal

Having determined which crystals were capable physically of yielding an amplifier, it was next necessary to determine their photoconductive performance.

The small signal theory of White [27] discussed in chapter 2 predicts that the crystal conductivity σ necessary to give maximum gain of an acoustic wave of angular frequency ω is

$$\sigma = \varepsilon \frac{\omega^2}{\omega_D^2} \qquad - - - - - - - (3.1)$$

where ε is the dielectric permittivity at constant strain and ω_D is the diffusion frequency. A typical value of $\omega_D = 4{\cdot}8.10^9$ sec.$^{-1}$ may be calculated using the Einstein relationship for the diffusion constant, and the defining equation for ω_D as given in section 2.2. The trapping factor appearing in the definition of ω_D was assumed to be unity, and the electron drift mobility typically 200 cm^2.(volt sec)$^{-1}$. Substitution of this value of ω_D into equation (3.1), and allowing ω

to take those values of experimental interest, enables the determination of the required conductivity variation necessary for optimum amplifier performance at these frequencies. For $\frac{\omega}{2\pi}$ from 15 MHz to 135 MHz this was calculated to be 10^{-6} to 10^{-4} $(\text{ohm cm})^{-1}$.

Small parallel flats were ground on opposite faces of each crystal to enable a d.c. contact to be made to each. The d.c. contacts were prepared by evaporating indium onto each of the flats (Haydl [83] has suggested that quick d.c. contact may be achieved by rubbing the crystal face with gallium. This method was tried but was found to be unreliable). The crystal was then heated radiantly to just over the melting point of indium in an inert nitrogen atmosphere. This increased the diffusion rate of indium into the crystal. The ambient atmosphere during the heating was required to be inert in order to prevent oxidation of the indium during the diffusion process. A special perspex manipulator box was constructed to enable wires to be attached to the indium coated surfaces of the crystals, without difficulty, in an inert atmosphere.

The variation of crystal resistance with illumination was then noted. Of the four crystals investigated one showed very little photoconductivity; two were found to have the desired range of conductivity variation; and the fourth appeared to be of very high conductivity.

The selection process was concluded by assessing the acoustoelectric activity of the two crystals, satisfying both dimensional and photoconductive requirements.

3.2.3. Acoustoelectric activity

The simplest means of assessing the acoustoelectric activity of a given crystal is to investigate its current-voltage (I-V) characteristic. A discussion of the current saturation produced by the amplification of thermally generated broadband acoustic flux has been given in chapter 1. The degree of activity may be qualitatively assessed from the non linearity of the I-V plot. Since only those

flux components which are piezoelectrically active will be amplified it was considered advisable now to orient each of the two crystals carefully. Anticipating that shear acoustic wave propagation would eventually be investigated the crystals were oriented for shear wave coupling, using an x-ray technique. A description of this technique, and of the cutting and polishing of the crystal faces is described in the following sections.

D.c. contacts were then made to each crystal so that an applied field could be applied perpendicular to the "c" axis. An I-V characteristic was plotted for each of the two crystals and these are shown in figure 9. The measurement technique used to obtain the I-V curves is described in chapter 5. The I-V characteristic of figure 9 (a) indicates very little acoustoelectric current saturation. The rather involved selection process was thus seen to be well justified, since the inconvenience of making an inactive amplifier using this crystal was avoided. Figure 9 (b) indicates a very active crystal, and this was selected for the amplifier. This proved to be a successful choice, as the results described in chapter 5 testify. The chosen crystal was obtained from Eagle Picher [84] and was described as a grade B crystal.

3.3. Crystal orientation

A more detailed description will now be given of the preparation of a carefully orientated crystal, suitably shaped for amplifier use, from an irregularly shaped boule fragment.

The problem is essentially twofold. Appropriate crystallographic planes have to be identified very accurately using an x-ray technique. Provision must then be made for the cutting, grinding, and polishing of the crystal faces parallel to these planes. In practice, this was achieved without any lack of confidence in the orientation of the crystal faces, by using a jig similar to that described by Bond [85]. This allowed precise movement of the crystal during the x-raying, and

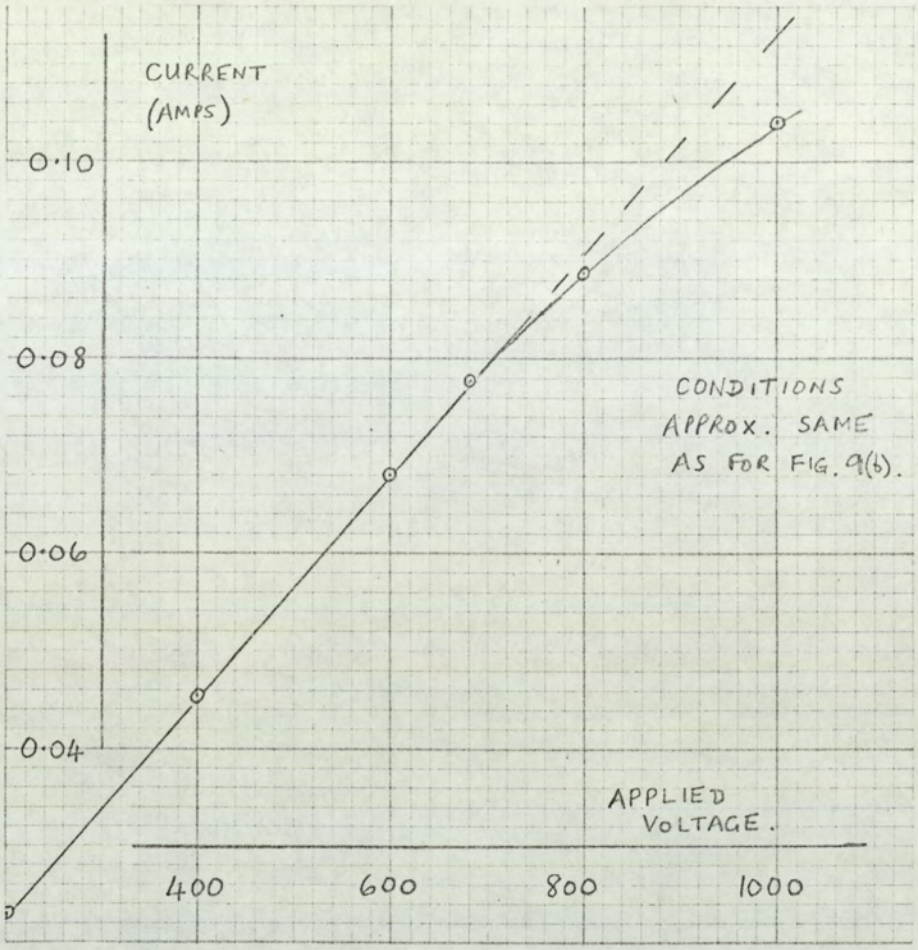

(b)

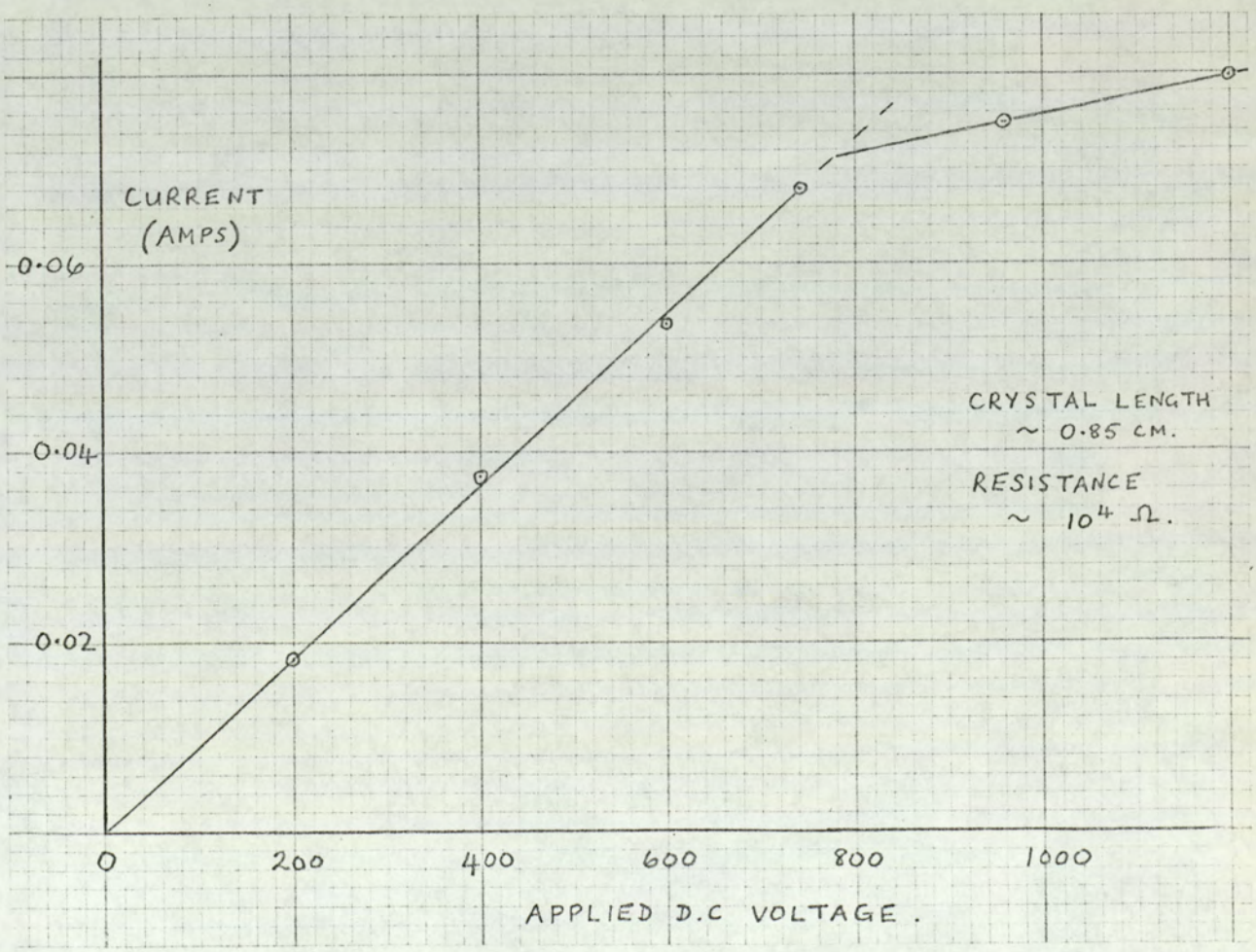

FIG. 9. I-V CHARACTERISTICS SHOWING (b) TO BE MORE ACOUSTOELECTRICALLY ACTIVE.

then the grinding and polishing of the crystal faces without further disturbing the orientation.

A Laue back reflection x-ray method was used to determine the crystallographic planes to be exposed by cutting. The most convenient means of achieving piezoelectrically active shear wave propagation is to attach the Y-cut quartz transducers used for acoustic generation and detection to either the $(11\bar{2}0)$ or $(1\bar{1}00)$ planes; the z axis of the transducer being parallel to the "c" axis of the CdS. The planes $(11\bar{2}0)$, $(1\bar{1}00)$ and (0001) are mutually orthogonal and each results in an easily recognisable diffraction pattern for perpendicularly incident x-rays. The crystal faces were chosen to be parallel to these planes. Figure 10 shows the relative orientation of these planes in the crystal and a sketch of the diffraction pattern obtained when each family of planes is perpendicular to the incident x-ray beam. "White" x-radiation was used in order to reduce the time for each exposure from forty minutes for filtered radiation to some ten minutes.

The general procedure starting from the irregularly shaped crystal was to identify visually the approximate direction of the "c" axis. The crystal was then affixed, with thermo-setting wax, to a small brass table, which was later fitted to a Philips' goniometer head. This was adjusted on the arm of an x-ray generator so that the "c" axis of the crystal was approximately parallel to the incident x-ray beam. A Laue back-reflection photograph was taken and the crystal position specifically adjusted to achieve two objectives. The hexagonally symmetric diffraction pattern was centralised, and a line drawn through two opposite images of the diffraction pattern was made horizontal. Using a small set square , lines were then drawn on the crystal to mark the three principal directions. Three exposures were considered necessary to obtain the required directions to within $\pm 2^{\circ}$.

The crystal was then cut to expose the $(11\bar{2}0)$, $(1\bar{1}00)$ and

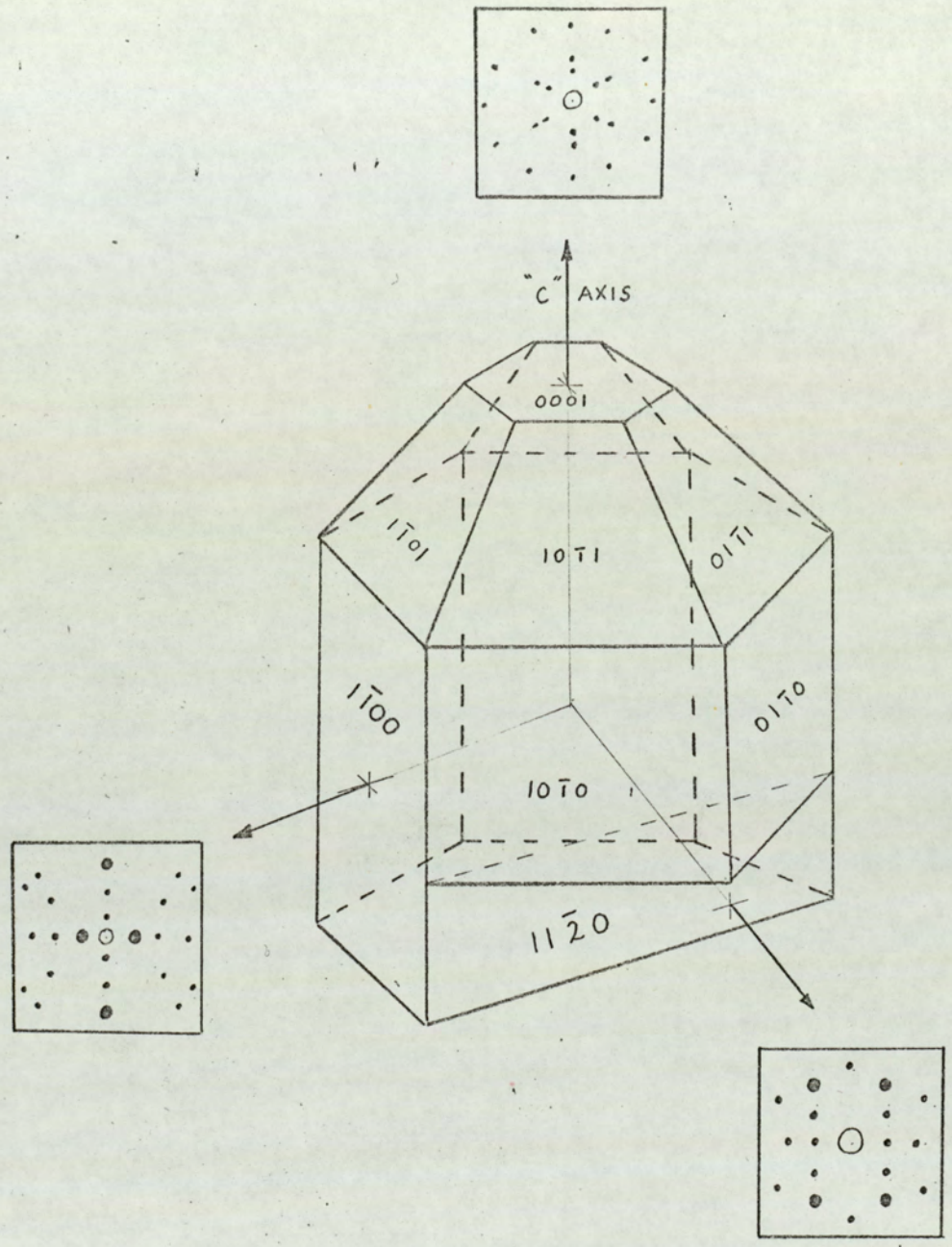

FIG. 10. RELATIVE ORIENTATION OF CRYSTAL PLANES IN CdS, AND LAUE X-RAY DIFFRACTION PATTERNS CORRESPONDING TO THE PRINCIPAL PLANES

(0001) planes to within this accuracy, using an available diamond saw of the type described by Fynn and Powell [86].

It was at this stage in the preparative programme that I-V plots were made to determine the acoustoelectric activity of the two crystals which were being considered for possible amplifier use. The crystal showing marked activity was then orientated extremely carefully using the orientation-polishing jig [85]. In order to obtain an orientation accuracy of thirty minutes of arc, a large sample-film distance was chosen to increase the sensitivity of the method. After a satisfactory Laue photograph had been obtained for a given crystal orientation, the crystal face perpendicular to the incident x-ray beam was ground and polished to the desired standards without detaching the crystal from the jig. Each crystal face was prepared in turn. Once one face had been polished, the x-raying required to orientate the opposite parallel crystal face was minimal.

3.4. Grinding and polishing of crystals

The grinding of each crystal face was achieved by hand, using 600 grade silicon carbide paper with water as the lubricant. The widely accepted technique of a figure of eight grinding path was adopted, and slow rotation of the major axis of the figure eight allowed uniform grinding of the entire surface to be achieved. The last few grinding strokes were executed in the same direction to ensure an even, unidirectional scratch finish. After careful washing of the crystal face, the surface finish was improved by using successively finer and finer grades of levigated alumina. This fine polishing was carried out on a "Sylvet" cloth which was thoroughly washed at each alumina change. The surface finish and parallelism of the crystal faces was then inspected optically.

Parallelism of the faces was checked by obtaining fringes with plane polarised monochromatic light of 5800 $\mathring{A}$ wavelength, between crossed polaroids. A set of very nearly parallel fringes

obtained for those faces to which the transducers were to be attached, indicated that these faces were individually plane but not quite parallel. The measurement of the fringe spacing enabled the wedge angle to be calculated. This was determined to be (30 $\pm$ 5) minutes of arc. The surface finish was inspected visually for any marked scratches. A Taylor-Hobson Talysurf metrology machine was available for monitoring surface contour. This was not used, however, since the diamond stylus would inevitably have scratched the crystal surfaces. The surface topography was thus observed using the Newton's rings technique. The lack of local fringes suggested a satisfactory surface finish.

The final stage in the crystal preparation was to degrease and etch the crystal prior to evaporating indium contacts. The etchant considered most suitable was dilute chromic acid. A sufficient quantity was prepared by dissolving 70 gms of chromium trioxide in 200 mL. of distilled water and adding 10 mL. of concentrated sulphuric acid. This solution was then diluted three times using distilled water. The crystal was immersed for three minutes with the solution at 70°c. The etchant was then continuously diluted with distilled water until the beaker effectively contained only distilled water. This obviated removing the crystal through a contaminating skin which invariably formed on the chromic acid surface. The etched crystal was then washed in isopropyl alcohol and dried in air.

3.5. Choice of contact material

The intended amplifier design required that shear quartz transducers were directly affixed to the CdS crystal. Since acoustic buffers were not to be included, the transducer - crystal bonds had also to serve as the d.c. contacts to the crystal. The choice of suitable bonding material was somewhat limited. Commonly used materials such as silver, gold, copper, carbon, platinum etc., do not make good electric contact to CdS. The current-voltage characteristic for low applied voltages is found to be non linear, indicating rectifying

contacts. Smith [87] has shown that the diffusion of indium or gallium into the CdS produces ohmic contacts. A gallium - indium alloy has also been used, but experiments revealed that this alloy was liquid at room temperature over a wide range of composition. The melting point of gallium is only 29.8 °c and this renders it unsuitable. The example of Hutson et al [28], Uchida et al [45], Southgate and Spector [47] and others, in using indium as the d.c. contact material recommended it as the most suitable bonding material.

The other important consideration concerns acoustic transmission through the bond. Kinsler and Frey [88] have given an expression for the transmission coefficient of an acoustic wave through one medium into a second medium, separated from the first by a third medium. This was shown to be a function of the specific acoustic impedence of each media, the bond thickness and the acoustic wavenumber. Substitution of the appropriate values into the derived expression resulted in an assurance that an indium bond would theoretically allow a high acoustic transmission.

3.6. The choice and preparation of the transducers

Originally it was intended to purchase correctly orientated gold chrome plated quartz transducers of the desired thickness for 15 MHz fundamental acoustic generation, and then attach leads using a thermosetting silver paste. This proved to be an unnecessary technical problem however, since coaxially plated Y-cut quartz transducers, having two leads already attached were commercially available from the Valpey Corporation [89]. The dimensions and orientation of these transducers are described in figure 11. The presence of the two wires solved one problem and created another. In order to fabricate the amplifier it was necessary to evaporate indium onto both the crystal and the front-face of the transducers. It was then required to bond the transducers to the crystal, whilst ensuring that their orientation with respect to the crystals axes was as demanded from acoustoelectric considerations.

The problem of bonding two articles using indium has been

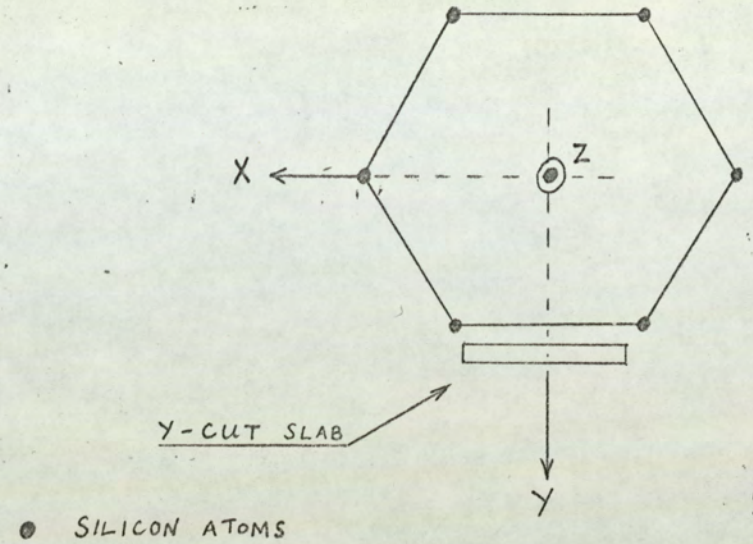

α - QUARTZ

PLAN OF UNIT CELL.

PLANE PERPENDICULAR

TO Z - AXIS

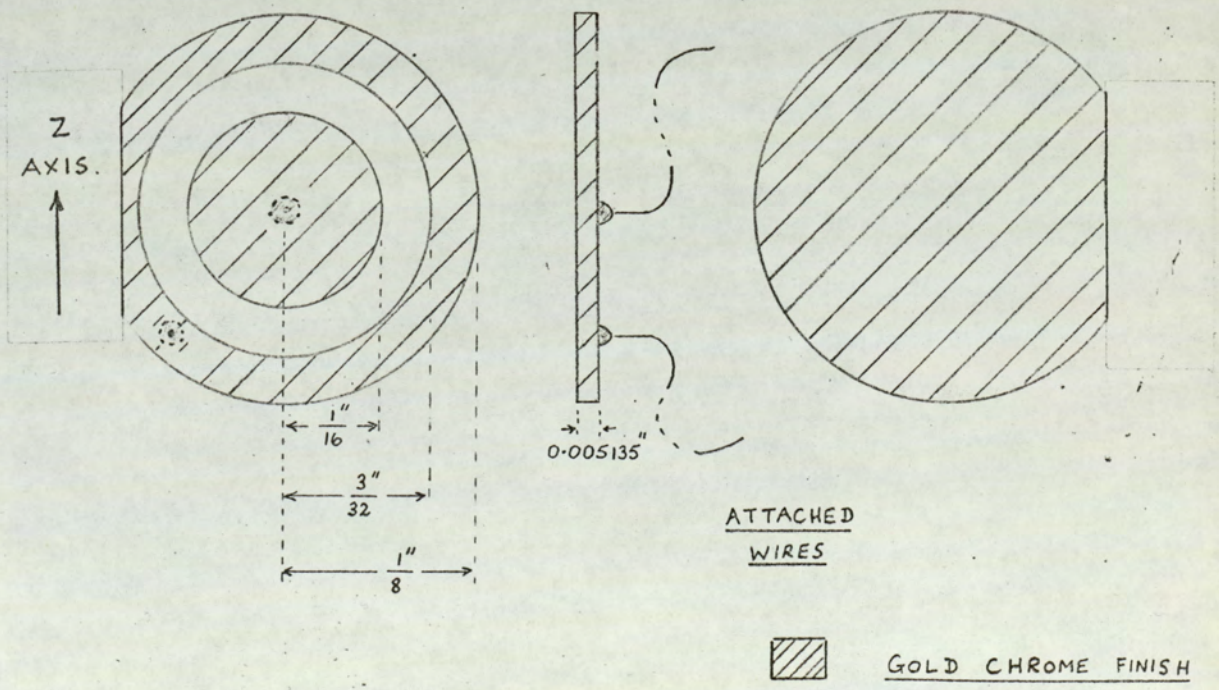

FIG. 11. DIMENSIONS AND ORIENTATION OF Y-CUT COAXIALLY PLATED QUARTZ TRANSDUCERS

investigated by Brew [90], and Arenburg [91]. However, their suggested method involved effecting a cold weld using pressures in excess of 1200 psi. Early experiments indicated that this was prohibited by the fragile nature of the transducers to be used. Furthermore, the presence of the attached wires were found to be a source of embarrassment since any attempt to press the transducer to the crystal faces had to incorporate some means of avoiding these wires. Since the transducer diameter was only 0.25 ins. this proved to be quite difficult.

In order to protect the wires and also enable the transducers to be more easily pressed against the crystal faces for bonding, it was decided to provide solid backing to each transducer. The choice of backing material was dependent on the following criteria.

(1) Material easily machinable.

(2) Preferably available in rod form.

(3) Non conducting.

(4) An ability to withstand an ambient temperature of 160°c without softening.

(5) High acoustic absorption coefficient.

The material considered to be the most suitable was Nylon 66. Assurance of the first three criteria being satisfied was obtained before purchase. The specified melting point was 260°c. Whether the nylon would soften appreciably, during heating to the melting point of indium, was not known. Subsequent experimental investigation showed that it did not.

Some 5/16" O.D. nylon 66 rod was purchased, and six one inch offcuts were taken. These 1" long nylon rods were pushed into a hole of 5/16" clearance in the centre of a small brass block, having carefully measured orthogonal edges. This enabled end faces perpendicular to the major axis of the rod to be ground and polished. Two small diameter holes, one centrally sited and one towards the edge of the rod cross-section, were then drilled through the entire

rod length. These were to take the transducer wires. The holes were slightly countersunk to allow space for the solder used to attach the wires to the transducer. With the exception of the quarter inch of rod nearest to the face to which the transducer was to be attached, the nylon rods were then tapped with a 5/16" B.S.F. thread. Each of the six one inch pieces were prepared in this way.

It was decided to attach the transducers to the machined nylon rods using Araldite 820. Both the epoxy resin and hardener are liquids, and their mixture may be thinned using toluene. The following experimental tests were made to determine the feasibility of the proposed method of transducer presentation.

The Araldite was tested by affixing small squares of thin quartz to the nylon. Experience gained here indicated that room temperature setting of the araldite was best, although it also took the longest. Heating the Araldite too quickly reduced the strength of the bond. The Araldite solution was best applied with a fine brush and with suitable care, the process could be accomplished without getting any Araldite on the upper surface of the quartz square.

The effect of the nylon backing on the acoustic performance of the transducers was investigated by attaching a transducer to the nylon using Salol (phenyl salycylate). The nylon backed transducer was then attached to a fused silica buffer, using in one case, Salol, and another gallium. The transducer was used to generate an acoustic signal having a frequency of 45 MHz., and also to detect the resulting acoustic echoes. A typical echo train, as displayed using an oscilloscope,is shown in figure 12(a).The quartz buffer used in the experiment was 9.0 mm. long, and the time between successive echoes is due to acoustic round trip travel in the quartz. There is no indication of any received echoes due to acoustic propagation in the nylon. This indicates a high acoustic absorption coefficient for the nylon. Figure 12(b), obtained using a 5 mm long buffer, affirms this.

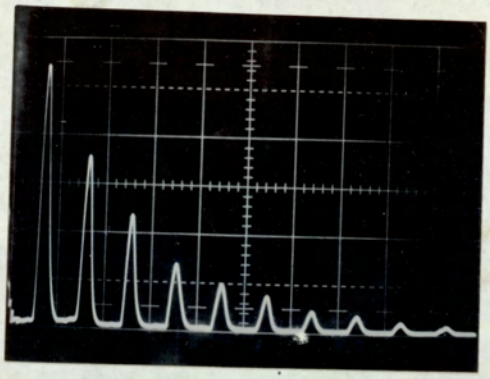

(a)

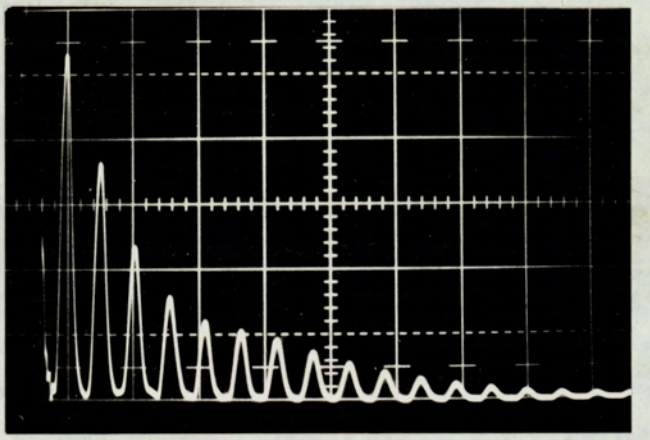

(b)

GENERAL :

HORIZONTAL 5 μsecs / SQUARE

BUFFER LENGTH a) 9 mm.
b) 5 mm.

SHEAR ACOUSTIC VELOCITY $3.75\ 10^5$ CMS/SEC.

FIG 12 ACOUSTIC ECHO TRAIN OBSERVED IN QUARTZ BUFFER SYSTEMS - SINGLE TRANSDUCER OPERATION, NYLON BACKED.

Two of the machined nylon rods were then degreased using trichloroethylene, and boiled in distilled water; washed in alcohol and air dried. Each was supported vertically, and a thinned Araldite solution was brushed over each of the faces due to receive a transducer. The transducers were also stringently cleaned and a little Araldite applied to each transducer surface to which the wires were attached. All the Araldite painted surfaces were closely inspected to ensure that no air bubbles were entrapped in them. The transducer wires were then carefully threaded into the small holes drilled through the nylon and each transducer seated onto the nylon surface, with each solder blob adequately accommodated by the countersunk regions. In deciding beforehand, which of the prepared nylon rods and transducers were to be used, care was taken to ensure that the transducers would seat down perfectly on the appropriate nylon surface.

Earlier work carried out with the fused silica squares indicated the correct amount of Araldite required to give a good bond without any overflow onto the top face of the silica. A small cylindrical brass weight of diameter less than the transducer was centrally placed on each transducer to counteract any tendency for the transducers to rise off the nylon during the setting of the Araldite bond. The transducer surfaces were protected by a piece of tissue paper of diameter equal to that of the brass weight. The excess Araldite squeezed out from between the nylon and the transducer tended to obscure easy identification of the transducer flat. The excess in the region of the flat was removed using a very soft brush dipped in toluene. After the Araldite bonds had set, the transducers were ready to receive an indium coating.

3.7 The indium evaporation technique

A simple means of evaporating indium onto each transducer face, and the $(11\bar{2}0)$ faces of the crystal was devised. This is

shown in figure 13 with the crystal and transducers in situ. The crystal and transducers are shown fixed to a brass platform P, which is supported by clips on two pillars of a brass stand. The height of the platform P could be varied by altering the position of the clips on the pillars. The construction and use of the evaporating jig will now be described.

Two ⅜" diameter holes were drilled through the platform to allow the tapped nylon rods carrying the transducers, to be fixed to the platform P using 5/16" B.S.F. nuts. A 1.1 cm. hole was centrally drilled through P between the two ⅜" diameter holes. The diameter of this central hole was obtained semi-empirically, and was just large enough to allow the crystal free passage through it. A circular region concentric with the drilled central hole was then recessed into the platform P to a depth of 2 mm. The diameter of the recess was 2.0 cm. A hollow brass cylinder of inside diameter 1.1 cm.and outside diameter 2.0 cm. was then carefully machined so that the cylinder height plus the thickness of the platform P within the recessed region was equal to the crystal dimension perpendicular to the $(11\bar{2}0)$ crystal faces. Four small holes were then drilled vertically through the cylinder wall and the recessed region of the platform. These holes allowed the cylinder and two copper masks to be bolted to the platform. The copper masks were circular, of outside diameter 2.0 cms.and with a central hole of 0.25 ins. diameter. They too, had four small holes appropriately drilled.

The final assembly of the crystal arrangement was as follows. One of the copper masks was placed over the central hole of the brass platform, on the side which had not been recessed. Four 8 B.A. bolts were then pushed through the holes drilled in the mask and platform. The brass cylinder was sited in the recessed region with the four bolts locating the appropriate holes drilled through the cylinder, and the crystal was carefully lowered into the brass cylinder. The

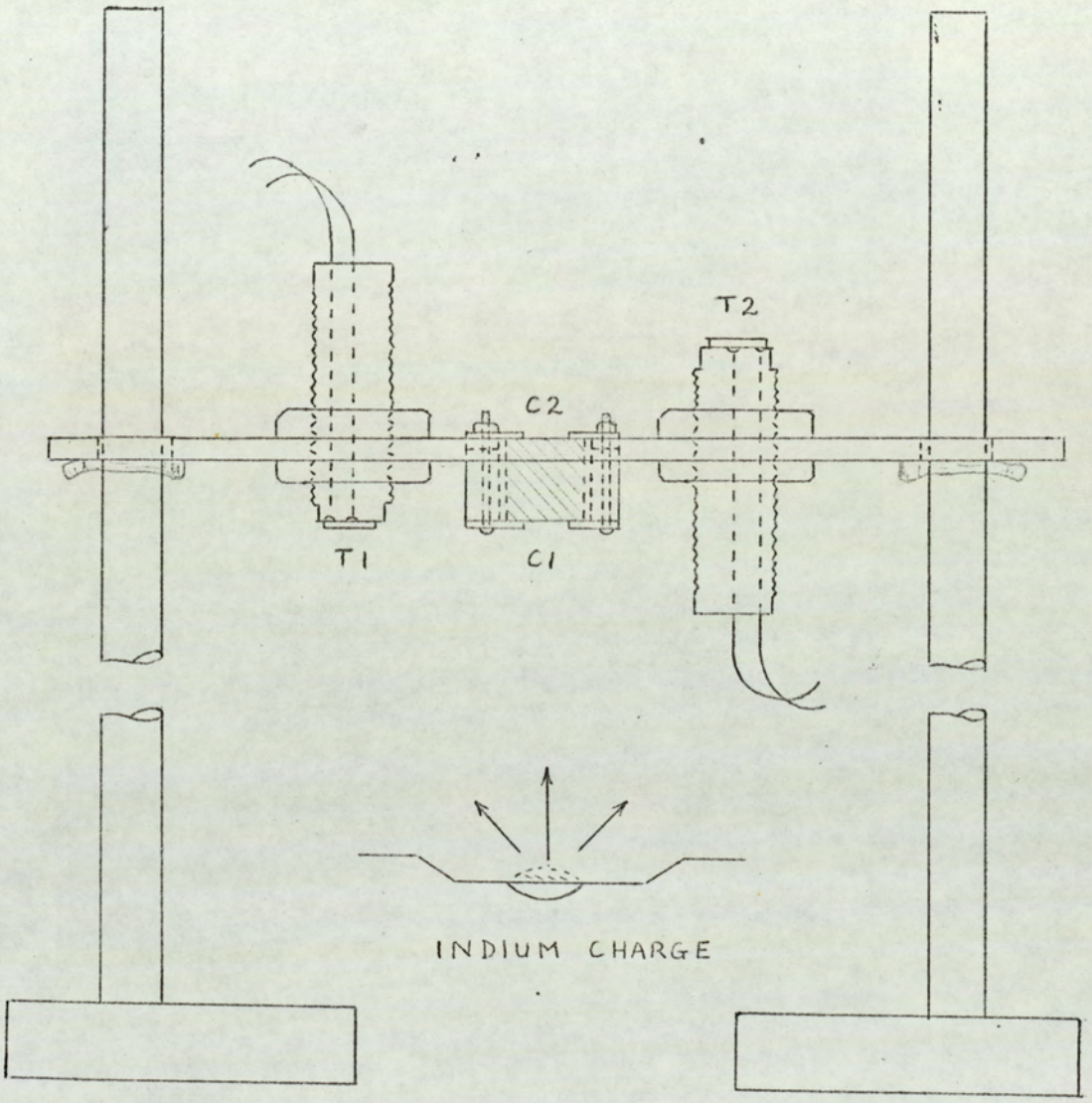

CADMIUM SULPHIDE

T1, T2 TRANSDUCERS

FIG. 13

DIAGRAM OF EVAPORATION TECHNIQUE

careful machining of the cylinder ensured that the upper surface of the crystal was flush with the top face of the cylinder. A second copper mask was placed on this crystal face with the bolts coming through the small holes drilled in the top mask. The entire arrangement was then firmly fixed with 8 B.A. nuts. During this procedure, care was taken to ensure that the crystal was centrally sited within the cylinder. Thus, both faces of the crystal which were to receive the evaporated indium were exposed simultaneously, yet the crystal was firmly supported.

The nylon rods to which the transducers were attached, were bolted to the brass platform so that the transducer T 1 (see figure 13) faced in an opposite direction to transducer T 2. Indium was then evaporated onto crystal face C1 and transducer T1. The brass platform was removed from the supporting pillars, upturned, and replaced on the pillars. An evaporation onto C2 and T2 was then carried out. During evaporation small copper caps were placed on the ends of the nylon rods from which the transducer wires extended, in order to prevent possible subsequent electrical shorting of the wires due to the indium.

The geometry of the evaporation technique allowed the assumption that an equal thickness of indium was deposited on both transducer and crystal face during a given evaporation. In case the amount of indium evaporated during the first evaporation differed slightly from that during the second evaporation, the amplifier was built with T1 in intimate contact with C2; and C1 in contact with T2. This ensured that each indium bond would be equally thick.

Prior to evaporating, all the jig and evaporator components were scrupulously cleaned, to avoid possible contamination of the bonds. The evaporation of the indium was carried out in a high vacuum system, comprising an Edwards E S 50 rotary pump, E O 4 diffusion pump, and a liquid nitrogen trap. The pressure before evaporation was 10^{-6} torr. Possible contamination was further reduced by using

Viton gaskets, with no vacuum grease, a low backstreaming rate diffusion pump fluid, and minimum exposure of the evaporation chamber to the rotary pump.

For each evaporation 2.5 cms. of ultrahigh purity indium wire was balled and placed on a molybdenum strip heater. The brass platform of the evaporation jig was sited six inches above the molybdenum boat. The thickness of the evaporated indium layer was estimated to be about a micron. Care was taken to ensure that the evaporation rate was sufficiently low to avoid spitting of indium blobs onto the receiving surfaces. A slag was observed to form on the surface of the evaporating indium within the molybdenum boat. The evaporation was halted in time to avoid the evaporation of this slag. After both evaporations had been completed, the nylon rods and crystal were carefully removed from the jig, ready for amplifier fabrication.

3.8 Amplifier fabrication

Preliminary experimental work concerned with transducer bonding showed that large bonding pressures following preheating of the evaporated indium surface to encourage diffusion, resulted in much transducer breakage. It was therefore considered more sensible to use small bonding pressures with the crystal and transducers in contact at an ambient temperature above the melting point of indium. Figure 14 describes the jig used to successfully achieve amplifier fabrication.

The base plate and the top plate served to strengthen the jig, and ensure that the pillars did not move during jig use. Transducer plate A was secured to the brass pillars as shown, with a nylon rod and transducer affixed at its centre. The second transducer nylon rod assembly was secured to transducer plate B and by sliding this plate onto the four pillars, the two transducers were brought into near contact. To safeguard the indium evaporated surfaces on each transducer, physical contact was prohibited. The orientation of the top transducer relative to the lower fixed

transducer was adjusted until both transducer flats were parallel. To enable this to be achieved accurately, two fiducial marks indicating the position of the transducer flat had been made on the side of each nylon rod. A telescope having a crosshatched graticule was used to line up these marks. The top transducer rod was then firmly secured to transducer plate B to prevent further independent movement of the transducer rod. Transducer plate B was removed from the jig whilst the crystal was correctly orientated with respect to the lower fixed transducer.

The transducer flat marked the Z-direction of the quartz. Acoustoelectric consideration requires the c-axis of the CdS to be parallel to this flat. The crystal was carefully placed on the transducer with the indium evaporated regions exactly overlapping. The necessary relative orientation was achieved using the telescope vertically. Transducer plate B was then reintroduced onto the pillars, and the four load plates were lowered onto the transducer plate. The large central hole of the load plates allowed easy clearance of the nuts securing the nylon rod to the transducer plate. Thus loaded, the transducer plate was slowly lowered until the second transducer was in contact with the upper crystal face. The indium covered areas were again noted to be exactly overlapping. The top plate was then secured, and the final arrangement was as shown in figure 14.

The jig was then heated in an ambient temperature of 165°c for eight hours. This was sufficient to melt the indium. The bonding pressure was calculated to be about 2.5 p.s.i. After cooling, the amplifier was removed from the jig. This was straightforward but required great care. It was then mounted in a metal box as shown in figure 15.

Two drilled perspex blocks supported the amplifier, and the wires from the transducers were soldered to B.N.C. sockets. A 1" diameter hole cut in each side of the box, allowed opposite crystal

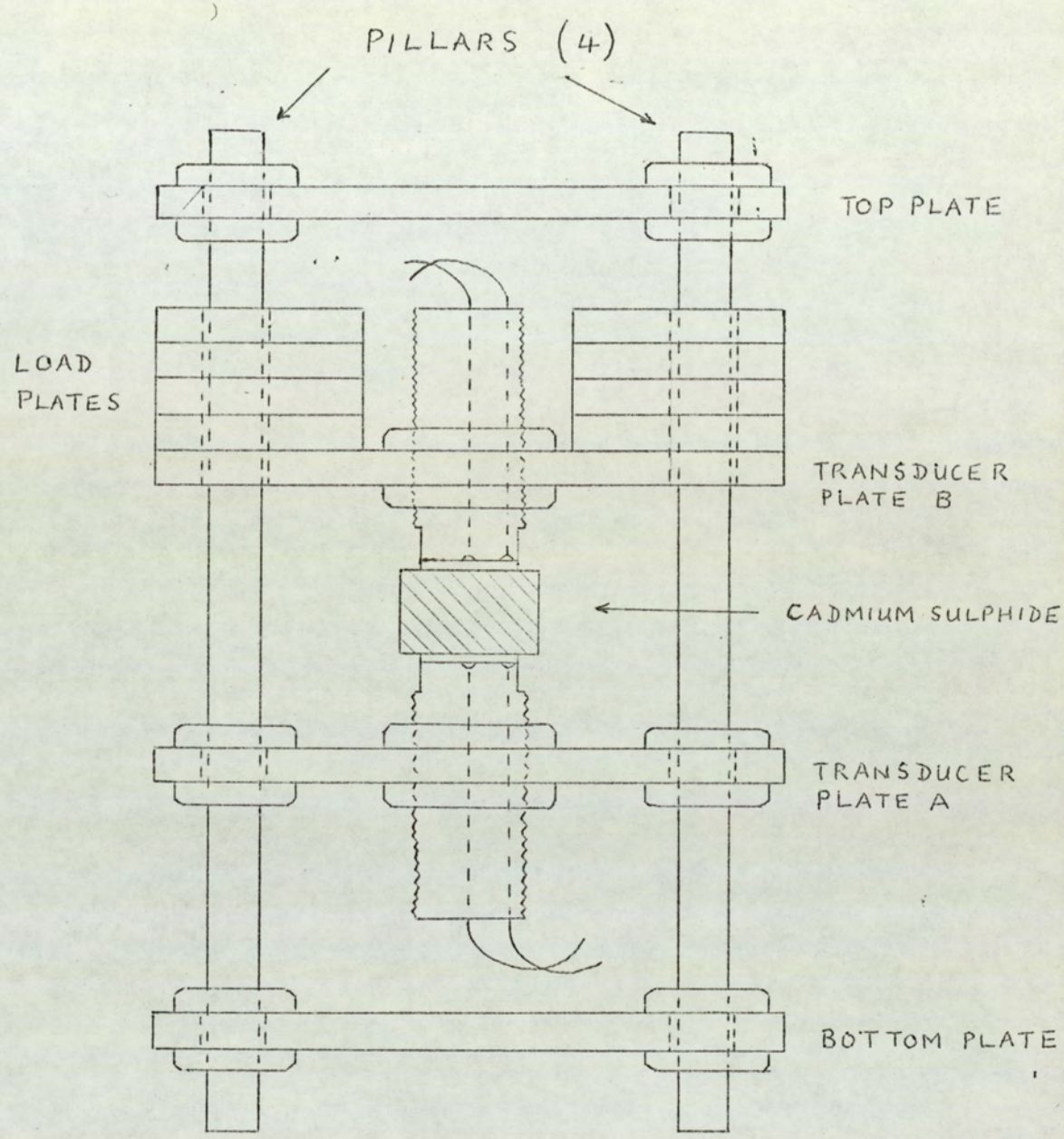

FIG. 14. AMPLIFIER ASSEMBLY JIG.

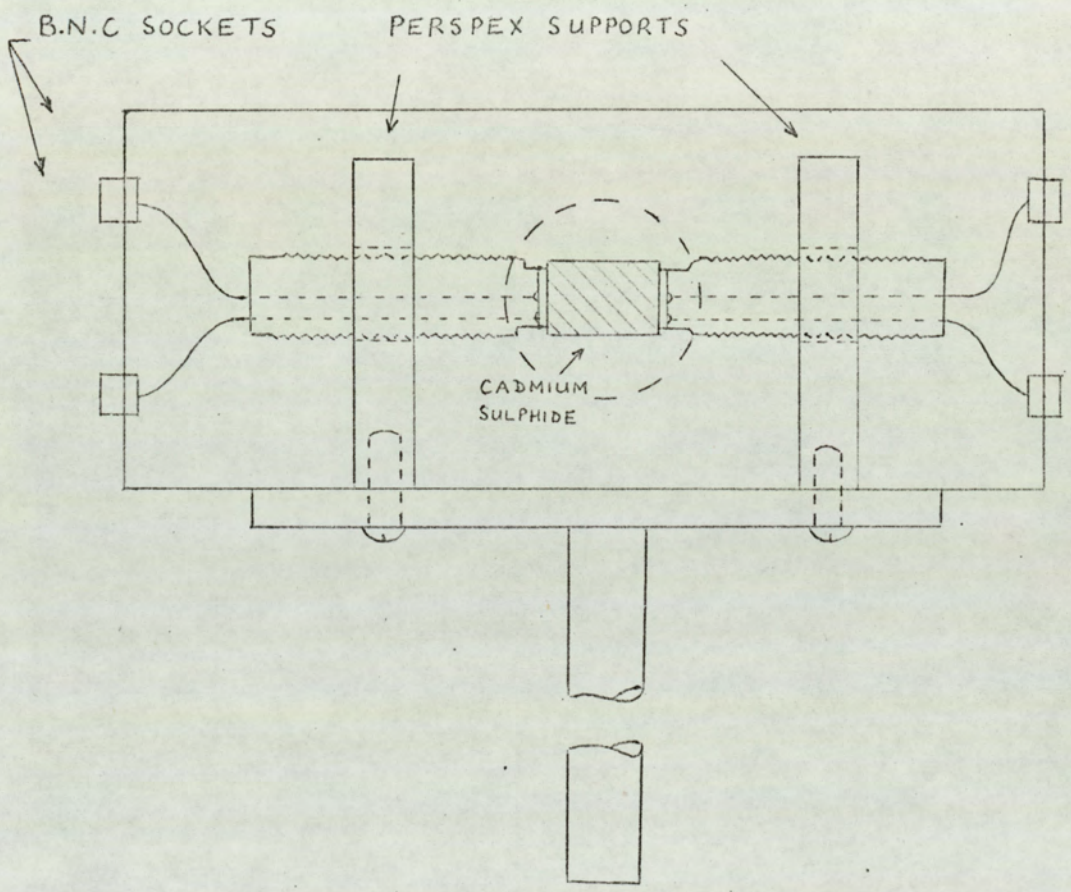

FIG. 15 THE AMPLIFIER MOUNTED FOR USE.

faces to be illuminated simultaneously.

The experimental arrangement and measurement techniques used to obtain the experimental results are described in the following chapter.

CHAPTER 4

Experimental equipment and measurement techniques

4.1. Introduction

This chapter presents a description of the equipment and techniques used to measure simultaneously the acoustic attenuation coefficient and acoustoelectric voltage, under a wide range of experimental conditions. A means of determining the acoustic intensity input to the crystal at different acoustic frequencies is also given. This makes use of the acoustoelectric effect to enable a more accurate determination of acoustic intensity to be made.

The care taken in determining these parameters, necessary for an accurate quantitative investigation of the Weinreich relationship, is emphasised by the calibration graphs appearing in this chapter.

4.2. General experimental arrangement

The overall experimental arrangement is shown in block form in figure 16. A photograph of the equipment as used for much of the experimental work, is shown in figure 17 and a key to this photograph is given by figure 18.

R.f. electrical signals, optionally variable in amplitude, duration, and frequency, were propagated through the CdS as acoustic signals, detected, and displayed on an oscilloscope. At the same time a high voltage d.c. pulse of up to 1 Kv could be applied to the crystal. Electrical isolation of the d.c. and r.f. circuits was achieved by transformer coupling of the r.f. to the crystal transducers. A triggering arrangement which enabled the d.c. field to be applied to the crystal up to 50 μ secs before or after the generation of the acoustic signal was incorporated, and simultaneous oscilloscope display of the acoustic echo train, acoustoelectric field, and applied d.c.

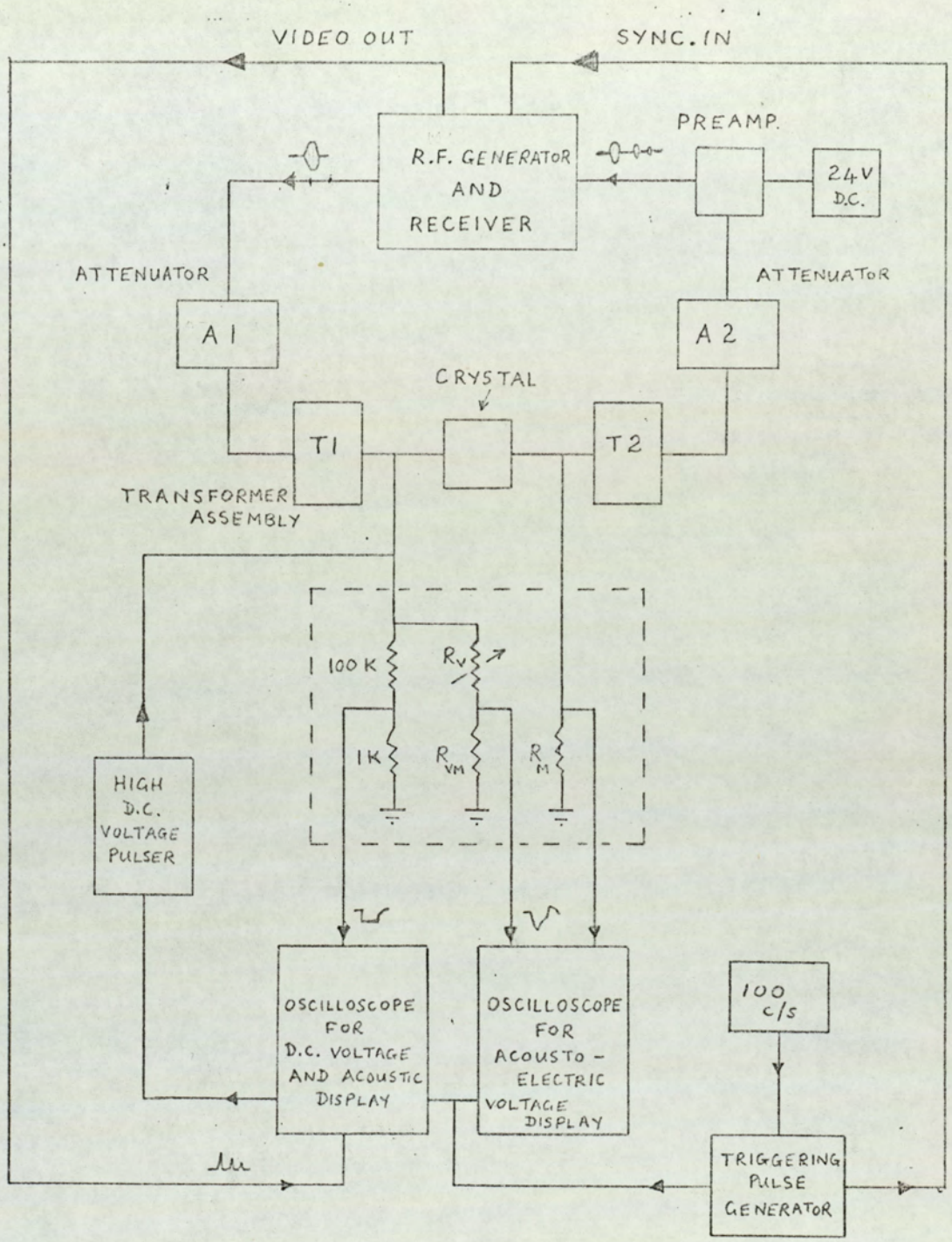

FIG 16. BLOCK DIAGRAM OF EXPERIMENTAL ARRANGEMENT

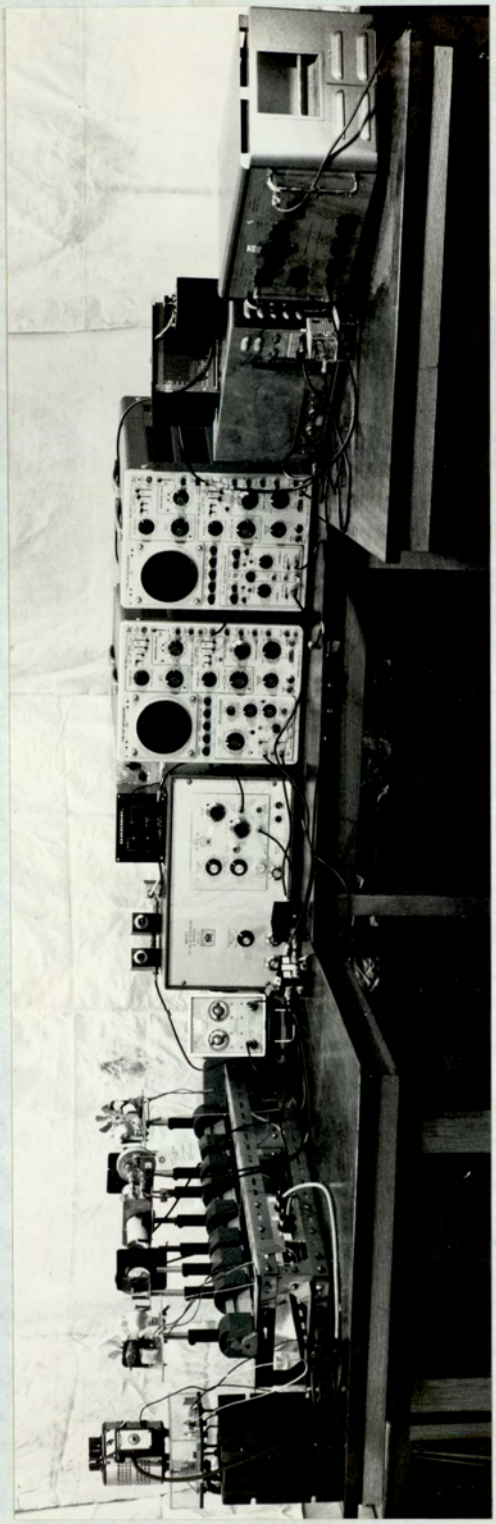

FIG. 17 EXPERIMENTAL ARRANGEMENT

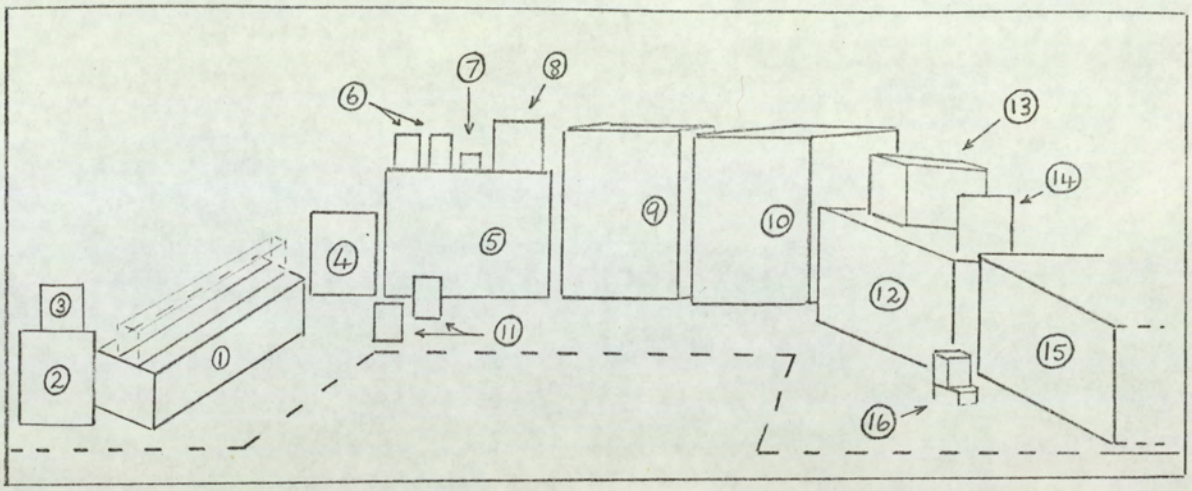

KEY

1. Optical System
2. Transformer for lamp supply
3. Variac to control crystal illumination
4. R.f. input attenuator (A1)
5. R.f. generator and receiver
6. R.f. output attenuators (A2)
7. Preamplifier
8. Preamplifier power supply
9. and 10. Oscilloscopes
11. Resistance chains
12. High d.c. voltage pulse generator
13. Mains frequency doubler
14. Variable capacitor for trigger phasing
15. Trigger pulse generator
16. D.c. voltage risetime control

FIG. 18. KEY TO FIGURE 17.

field was possible. The crystal conductivity could be varied by altering the illumination intensity.

The following sections describe each aspect of the overall experimental arrangement in more detail.

4.2.1. The optical system

A photograph of the optical system is shown in figure 19. The CdS crystal was illuminated from each side, by filtered light from a 100 W 12 V tungsten lamp. During use, each of the lamps was air cooled using a fan. A simple lens arrangement and careful alignment of the optical system ensured that the light incident onto the crystal was sensibly parallel and uniformly intense. This was checked using an EPY 80 photocell and a microammeter. A Variac in the lamp supply line enabled the illumination intensity, and hence, the crystal conductivity to be varied. In order to improve the stability of the illumination intensity a voltage stabiliser was used in the lamp supply line. Furthermore, switches on each lamp supply enabled their separate or joint use.

To ensure a uniform distribution of photoelectrons throughout the crystal, the white light from the tungsten lamps was suitably filtered so as to be weakly absorbed by the CdS. Illumination from opposite sides was also considered to improve the uniformity of bulk illumination. A Unicam SP 800 spectrophotometer was used to obtain the optical absorbance of single crystal CdS as a function of wavelength. A typical result is shown in figure 20. Incident light of wavelength less than 5200 $\mathring{A}$ is seen to be strongly absorbed, and corresponds to a photon energy just sufficient to transfer an electron from the valence band to the conduction band. The band gap of CdS may be determined from this to be 2.45 ev.

Light incident onto a crystal face will be absorbed as it travels through the crystal. Figure 20 shows that the absorption coefficient will depend strongly on the wavelength of the light.

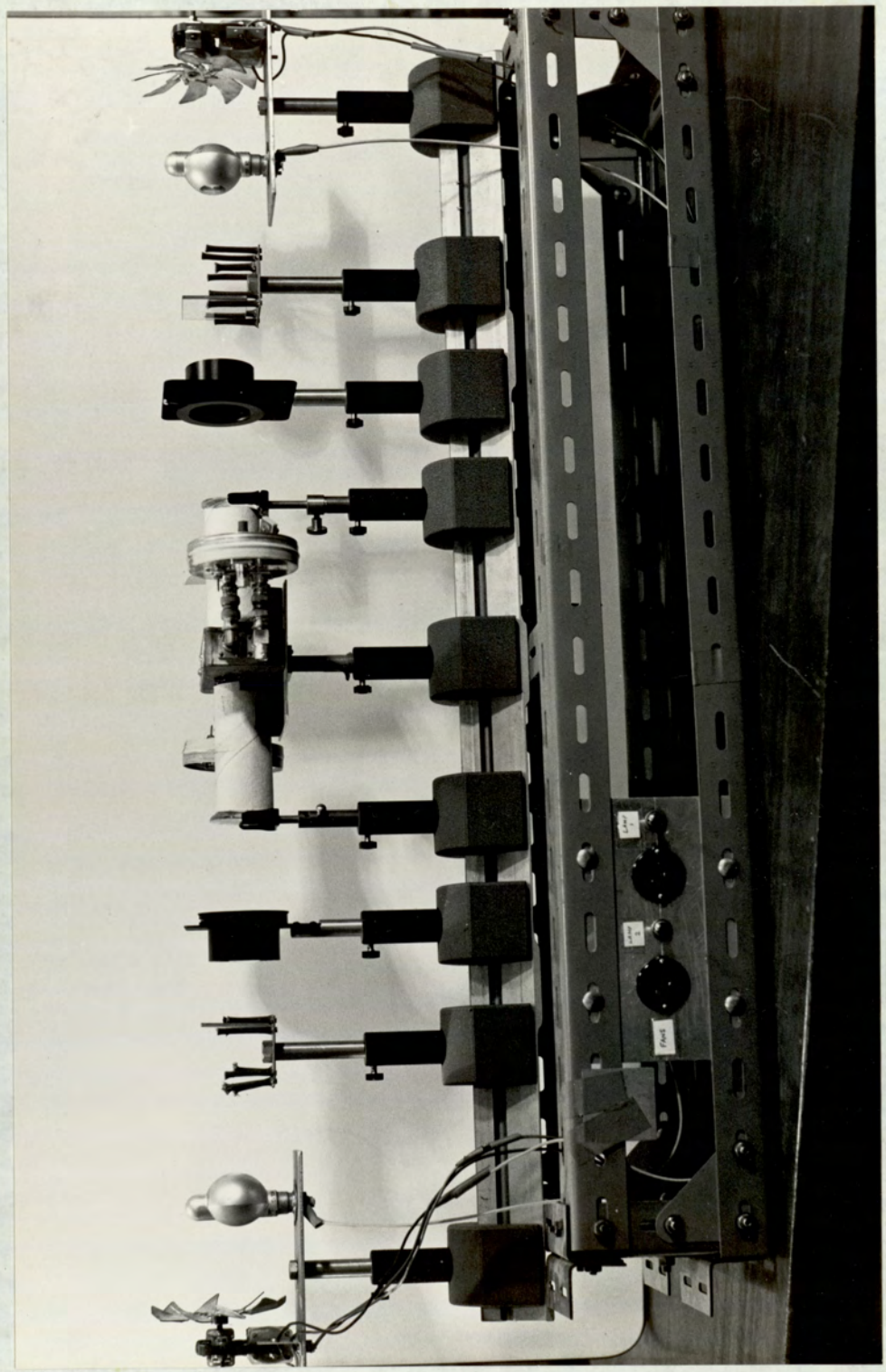

FIG. 19 THE OPTICAL SYSTEM

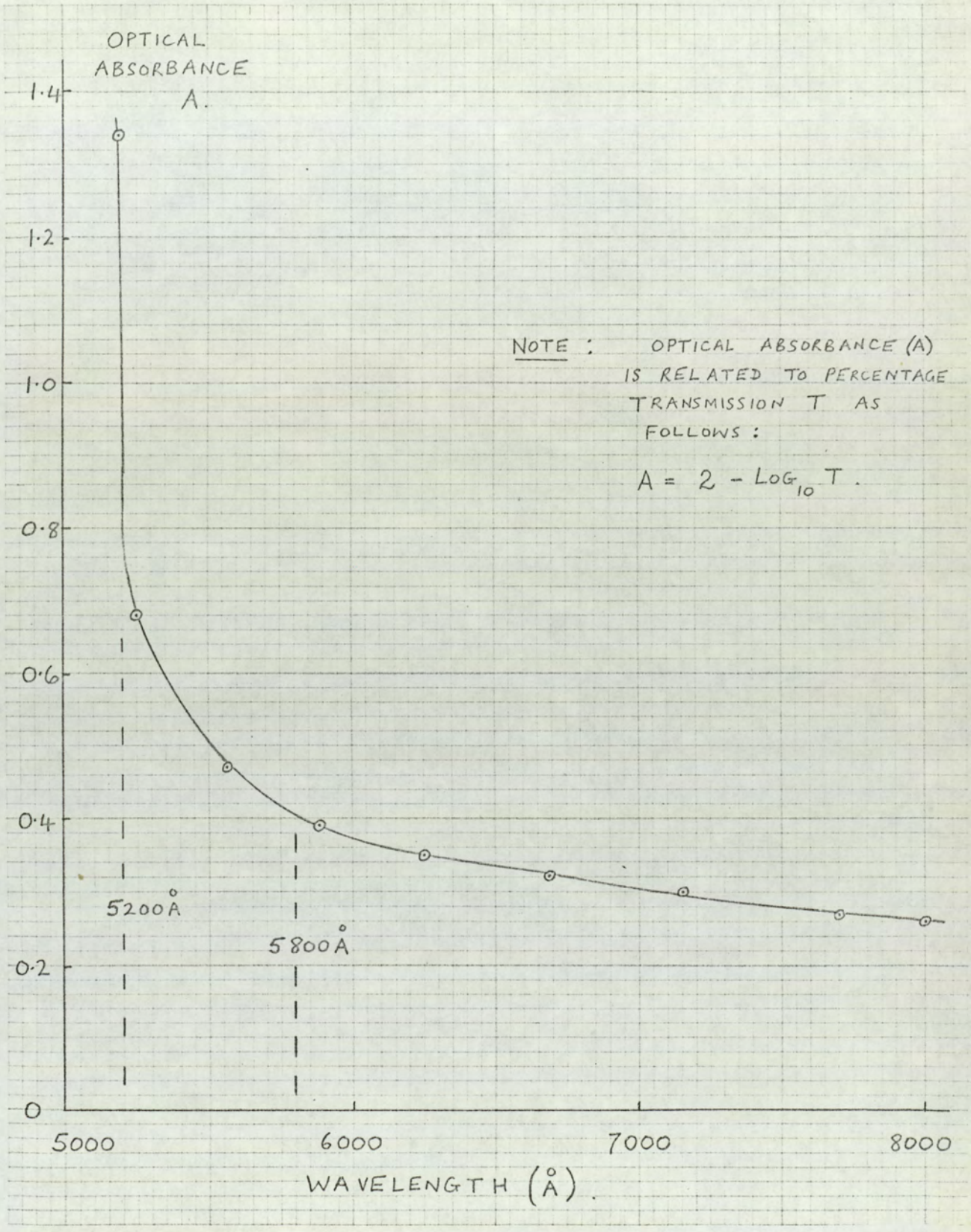

FIG. 20. OPTICAL ABSORBANCE VERSUS WAVELENGTH FOR CADMIUM SULPHIDE

Since the active area of the transducers used in the construction of the amplifier was only 3 m.m. in diameter (see figure 11), acoustic propagation took place down the central volume of the crystal. Light incident normally to the acoustic propagation direction will be absorbed as it travels through this central acoustically disturbed region, and it is therefore important to consider the possible effects of transverse non-uniform illumination. Davis and Drews [92] have investigated theoretically the effects of transverse and longitudinal variation in crystal resistivity on ultrasonic propagation. They considered the acoustic beam to cover the entire cross-sectional area of the crystal, and predicted that for strongly absorbed light, transverse non-uniform illumination could change considerably the photosensitive attenuation of a propagating acoustic wave.

Experiments were carried out to determine whether the acoustoelectric effects to be investigated were noticeably dependent on the spectral composition of the incident light. Various interference filters, each having a bandwidth of about 80 $\mathring{A}$, were used to obtain incident light having peak wavelengths between 4540 $\mathring{A}$ and 5800 $\mathring{A}$. It was concluded from noting the acoustic absorption coefficient and acoustoelectric field, both with and without an applied drift field that providing the illumination intensity was adjusted to result in the same crystal conductivity, the effects of transverse non-uniform illumination were negligible. Henrich and Weinreich [42] argue that a longitudinal variation in conductivity, that is, a variation parallel to acoustic propagation, would result in acoustoelectric voltage waveforms dependent on the direction of acoustic propagation in the crystal. Experiments carried out at different crystal conductivities with the amplifier used in this research, showed that the acoustoelectric voltage waveform was essentially the same for acoustic propagation in each direction through the crystal. Accordingly, the effects of longitudinal conductivity variation were here considered negligible.

The experimental results to be described in the next chapter were obtained with the crystal illuminated by light having a peak wavelength of 5800 Å. A Chance HAI filter, to remove all infra-red radiation, was placed near each tungsten lamp, and a combination of an interference filter having a bandwidth of 80 Å and peak transmission at 5800 Å, and a Wratten 23 A filter to reduce the short wavelength tail of the interference filter, were placed near the crystal. The spectral transmission curves, obtained using the spectrophotometer, of the interference filter and Wratten filter are shown in figure 21.

Cylindrical cardboard shields placed as shown in figure 19, were included to minimise the effect of roomlight on the determination of the reference dark condition. It was noted that the presence of the shields reduced considerably the acoustoelectric field observed even with the tungsten lamps switched off. The electronic attenuation coefficient of the CdS in roomlight, without the shields was estimated to be 0.5 db/cm. ; shield inclusion reduced this to 0.05 db/cm.

4.2.2. R.f. generation, detection and display

4.2.2.1. General description

That part of the overall experimental arrangement which describes the r.f. circuit is shown in figure 22. A Matec 6000 r.f. generator and receiver having a model 960 plug-in unit, was used to generate and detect the r.f. signals. The instrument provided r.f. generation and receiver tuning capabilities over the frequency range from 10 MHz to 310 MHz. The transducers bonded to the CdS had a fundamental of 15 MHz., and experiments were carried out at this frequency, and at the overtone frequencies up to 105 MHz. The generated r.f. packet was variable in duration from 0.6 μ sec. to 5.0 μ sec. although for most of the experimental work a 1 μ sec. duration r.f. packet was used. The rise and fall times of the generated r.f. packet were reasonably symmetrical, and the rise time to maximum amplitude for a 1 μ sec. half height width packet was approximately 0.2 μ sec.

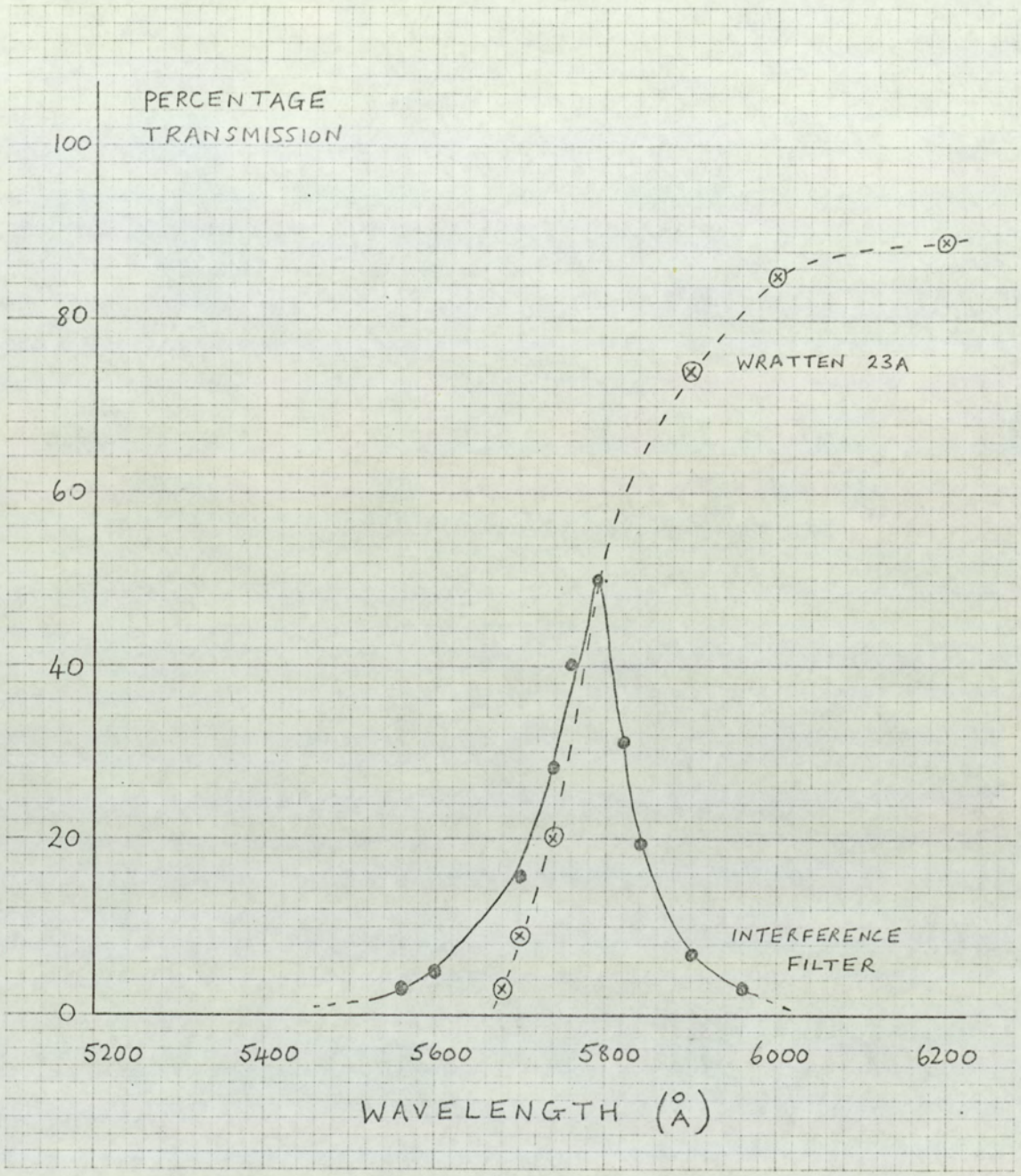

FIG. 21. SPECTRAL TRANSMISSION CURVES OF FILTERS.

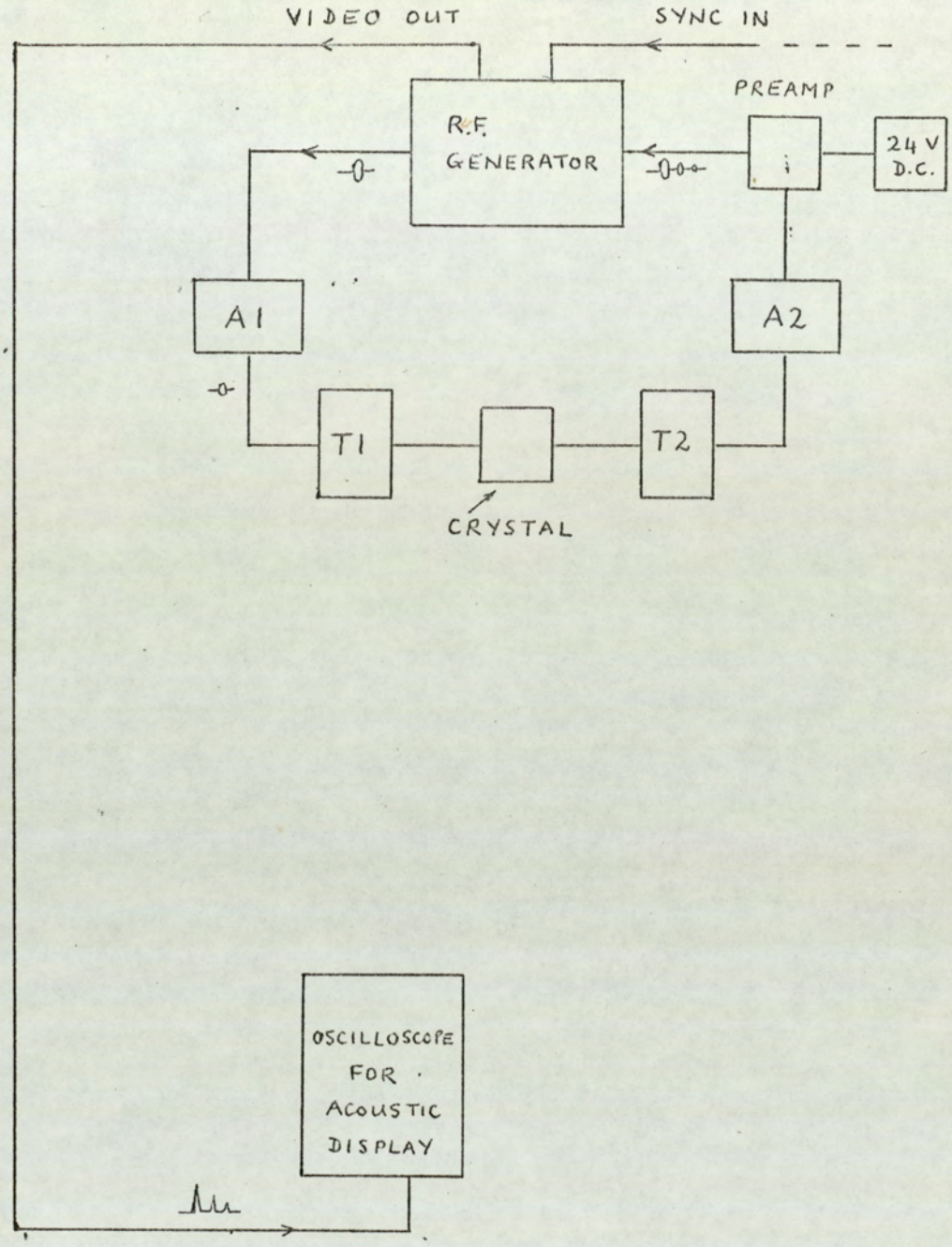

A1 AND A2 — CALIBRATED STEP ATTENUATORS.

T1 AND T2 — TRANSFORMER MATCHING ASSEMBLIES.

FIG. 22. R.F. CIRCUITRY.

A calibrated step attenuator A1 was used on the r.f. input side of the crystal to enable the input acoustic intensity to the crystal to be varied by known amounts. A similar attenuator A2 was used on the output side of the crystal to control the receiver input r.f. amplitude. A preamplifier on the output side of the crystal enabled small amplitude r.f. signals to be detected. Transformers T1 and T2 were constructed to couple the r.f. to and from the crystal. These allowed a high d.c. voltage pulse to be applied directly to the crystal without risk to the r.f. equipment. They also provided impedance matching of the transducers to the attenuators.

The detected acoustic echo train was displayed using a 547 Tektronix oscilloscope having a 1A1 dual channel plug-in. The video output and receiver of the Matec was shown to be linear over the signal amplitude range of the experiments. The r.f. generator was externally triggered at a repetition rate of 100 p.p.s. The triggering arrangement will be described in section 4.2.5.

4.2.2.2. The step attenuators

A Marconi U.H.F. switched attenuator (type T.F. 2163) was used on the crystal input side, and is designated A1. The instrument had a range of 142 dbs in 1 db steps and a frequency range from d.c. to 1 GHz. The switching networks allowed steps of 20 dbs. and 1 db, and the input and output impedance was 50 ohms. The insertion loss was 0.3 db per 100 MHz.

Two Hewlett - Packard V.H.F. attenuators were used in series on the output side of the crystal. These are designated A2. Model 355D covered a range of 120 dbs in 10 db steps, and model 355 C had a range of 12 dbs in 1 db steps. The specification of each was the same as the Marconi attenuator (A1).

No difference was noted in the behaviour of A1 and A2 throughout the experimental work, and each behaved as expected.

4.2.2.3. The Preamplifier

A Decca preamplifier (Model I.F. 45 - 25P) having a nominal

gain of 50 dbs and a centre frequency of 45 MHz., was included between the attenuator A2 and the Matec receiver during experimental work at 15 MHz. and 45 MHz. The frequency response of the preamplifier was experimentally determined (see figure 23), and although the gain was reduced by nearly 20 dbs at 15 MHz. operation, inclusion of the instrument at this frequency was found to be merited.

A similar preamplifier (model I.F. 100 - 20P) but centred on 100 MHz., was used during experimental work at frequencies of 75 MHz and higher. Both preamplifiers required a 24 V d.c. high stability line voltage. Both behaved linearly.

4.2.2.4. R.f. coupling and impedance matching

The problem of isolating the d.c. equipment from the r.f. equipment during amplifier operation, was successfully overcome by transformer coupling of the r.f. to the transducers. Figure 24 shows the transformer circuitry adopted. As well as achieving r.f. coupling, the transformer arrangement had also to provide impedance matching of the transducers to the 50 ohm impedance of the attenuators A1 and A2.

The equivalent circuit of a transducer has been shown to consist of a resistor, a capacitor and an inductor in series, together with a capacitor shunting this series arrangement [93]. The values of the equivalent circuit components depend largely on the loading and mounting of the transducer, and no attempt at their determination was made for the transducers used.

The admittance of a transducer at a given ultrasonic frequency (ω) may be represented by a resistance $R(\omega)$ in parallel with an impedance $X(\omega)$ as shown in figure 25. In order to ensure maximum transfer of r.f. energy to and from the transducers, the transformer should alter the effective resistance across PP to 50 ohms. At a given frequency, this requires a certain effective turns ratio. The impedance $X(\omega)$ will also be transformed and some other reactance from the transformer itself will be introduced. Both these may be

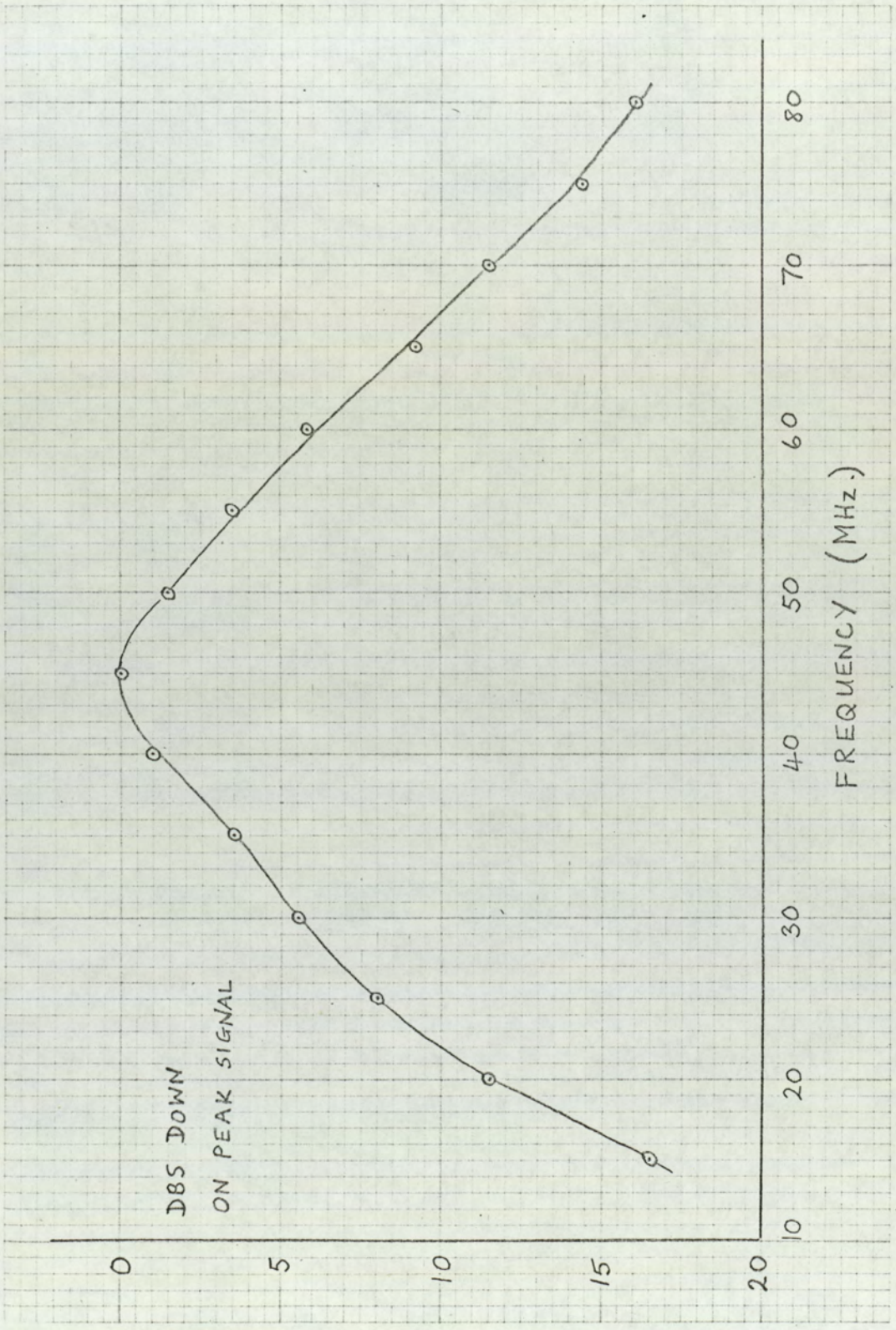

FIG. 23. FREQUENCY RESPONSE OF 45 MHz. PREAMPLIFIER

tuned out with a variable capacitor C1 in parallel with the transformer secondary. In practice, the choice of transformer turns ratio, and the value of the tuning capacitance were obtained empirically. The capacitor C2 shown in figure 24. earthed the r.f. The determination of the frequency response of the matching assemblies indicated reasonable peaking at the desired frequencies, with typically a 4 MHz bandwidth (3db down point). A typical measured frequency response is shown in figure 26.

The experimental work was carried out at different acoustic frequencies and at a given frequency, the matching of each transducer to the respective attenuator was achieved using identical matching assemblies. As the ultrasonic frequency was increased, a smaller transformer turns ratio was required for optimum matching. Consequently a different set of two transformer matching assemblies was built for use at each frequency. In use, the matching assemblies were joined directly to the amplifier housing via BNC couplers (see figure 19). This arrangement allowed a speedy change of matching networks when the ultrasonic frequency was changed.

The effective turns ratio of a given transformer was varied using a ferrite core, and at a particular ultrasonic frequency the transformer turns ratio and the capacitor C1 of each of the two matching assemblies in use at that frequency, were varied so as to give maximum transmission of ultrasonic power through the crystal. With the crystal illuminated using a low intensity light, the matching arrangement on the r.f. input side was tuned to give a maximum observed acoustoelectric voltage. (It will be shown in chapter 5 that for a given crystal conductivity, the measured acoustoelectric voltage is directly proportional to the input acoustic intensity. This knowledge is exploited several times to obtain a quick and reliable estimation of relative acoustic intensity input). The matching arrangement on the crystal output side was then tuned to give a maximum displayed

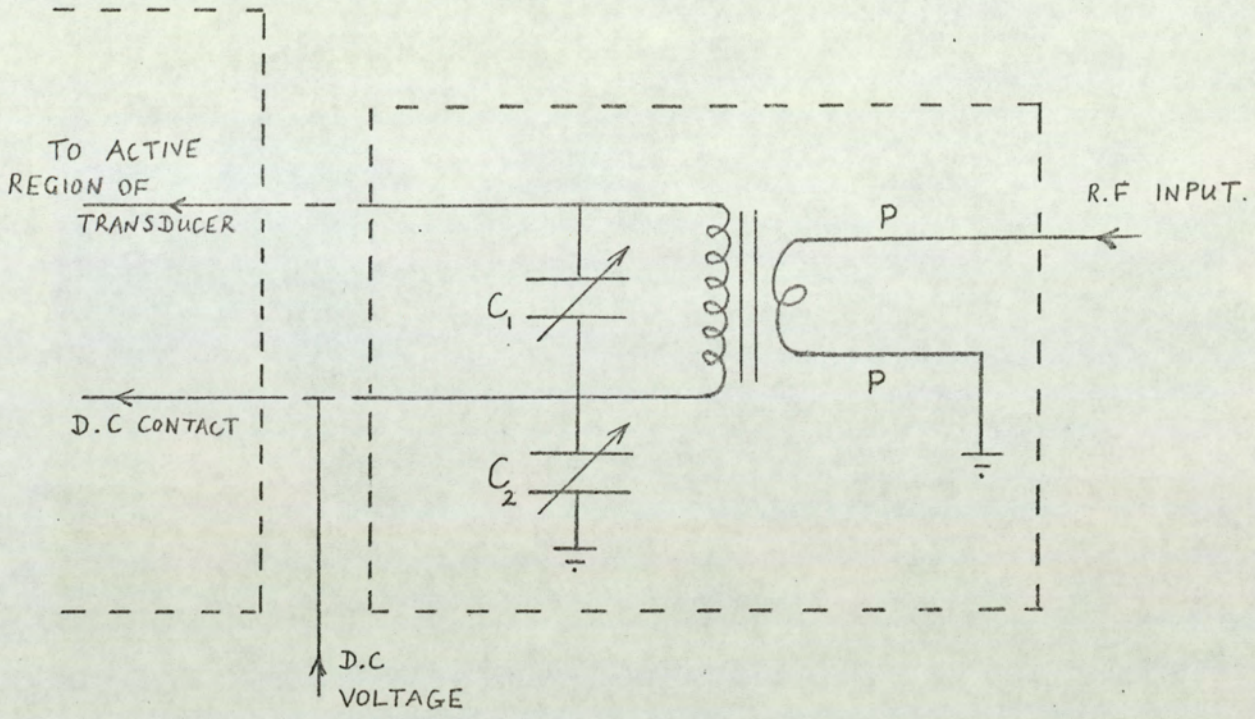

FIG. 24. TRANSFORMER ASSEMBLY

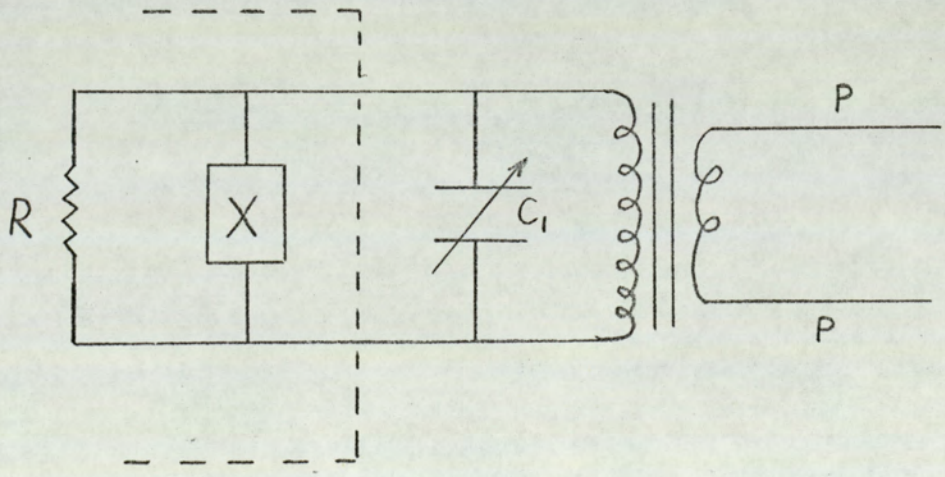

FIG. 25. EQUIVALENT CIRCUIT

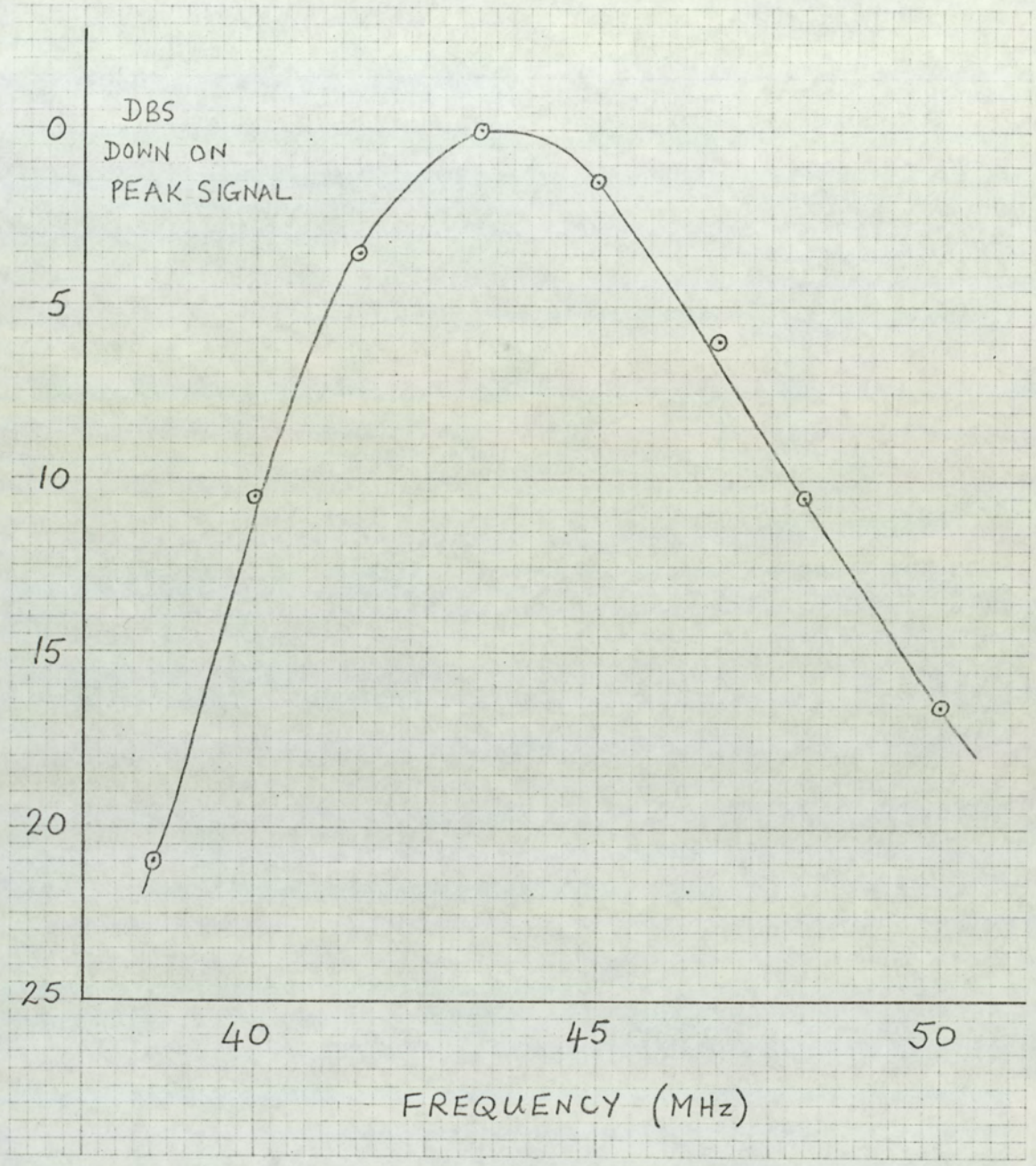

FIG. 26. FREQUENCY RESPONSE OF TRANSFORMER MATCHING ASSEMBLY.

acoustic transmission. The direction of acoustic propagation was reversed, and under the same applied conditions, the resulting acoustoelectric voltage and acoustic transmission were noted for comparison. Invariably, these were found to be almost the same. However, on occasions, a significant difference was noted, and this was found to be indicative of mismatching. The method of noting the acoustoelectric voltage, as well as acoustic transmission allowed conclusions to be drawn regarding the source of the mismatch.

The efficacy of the transformer matching assemblies was further tested by noting that varying the coaxial cable length from each attenuator to each respective matching arrangement did not affect either the observed acoustoelectric voltage, or acoustic transmission, indicating that the transformer was presenting a 50 ohm load to the cable.

4.2.3. Applied d.c. circuitry

Flat topped high d.c. voltage pulses were applied to the crystal from a d.c. pulse generator. The measurement of the applied d.c. pulse amplitude was achieved by putting a fixed resistance chain comprising a 100 K ohm and a 1 K ohm resistor, both high stability, in parallel with the crystal, as shown in figure 27. Within experimental error the assumption of a 1% "tap off" from the 1 K Ω resistor was justified, and the d.c. voltage appearing across this resistor was measured on an oscilloscope. The resistor R_m in series with the crystal, and the resistance chain comprising the variable resistor R_v and the resistor R_{vm} , in parallel with the crystal shown dashed in figure 27 were included for acoustoelectric voltage measurement and will be discussed in a later section. The r.f. circuitry at each side of the crystal is also shown dashed to correlate with figure 22.

The d.c. pulse generator was activated by a 20 v flat topped pulse from gate A of the oscilloscope. This switching pulse, and hence the applied d.c. pulse, could be varied in width from 1 to 50 μsecs. In order to reduce ohmic heating of the crystal, a low duty cycle of

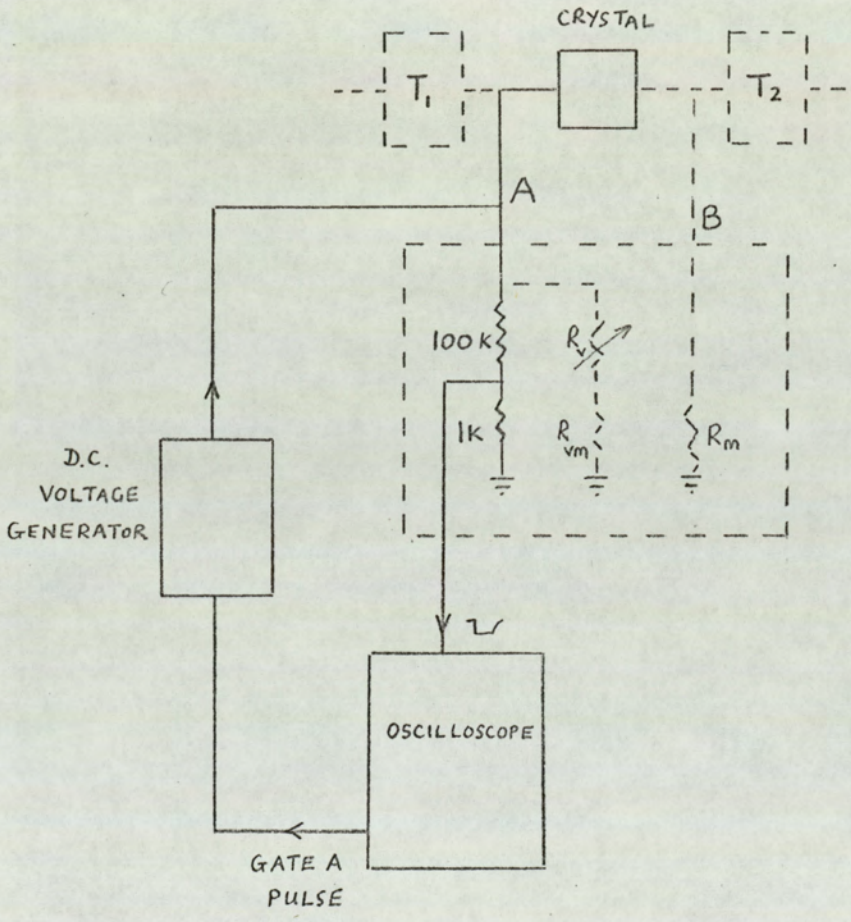

FIG. 27. D.C. CIRCUITRY

100 pps was chosen. The rise time of the applied d.c. pulse was also variable from 0.2 to 10μsecs. In order to minimise the possibility of crystal breakdown, particularly at high crystal conductivities, d.c. voltages up to 1 Kv only were applied to the crystal, although the capability of the pulse generator extended to 4 Kv. The applied voltage amplitude was varied using a Variac incorporated in the d.c. pulse generator design.

The two resistance chains and the resistor R_m were housed in a metal box well removed from the crystal. This allowed the measuring resistors, and associated capacitors (which have not yet been indicated) to be changed without any disturbance of the crystal mounting whatsoever. A second, more important, advantage of the d.c. measuring arrangement was that it allowed the d.c. leads to the crystal to be interchanged easily at points A and B in figure 27. This enabled the high voltage pulses to be applied to the crystal in either direction, and thus, the effects of carrier drift in an opposite direction to r.f. propagation could also be studied without difficulty.

4.2.4. The choice of oscilloscopes

During this research three Tektronix oscilloscopes were used. The acoustic echoes and the applied d.c. voltage were displayed simultaneously using the two channel 1A1 plug - in of a type 547 oscilloscope. The bandwidth of this oscilloscope was d.c. to 50 MHz. and the acoustic intensity input to the crystal for r.f. frequencies of 15 MHz. and 45 MHz. were determined using this oscilloscope in the manner to be described in section 4.5. To ensure an accurate determination of acoustic intensity at 45 MHz. the frequency response of the oscilloscope was measured using a Marconi standard signal generator. The resulting graph is shown in figure 28 (a).

Acoustic intensity determination at higher frequencies was accomplished using a type 581 A oscilloscope, having a type 86 plug-in unit. This oscilloscope has a bandwidth extending to 80 MHz. The

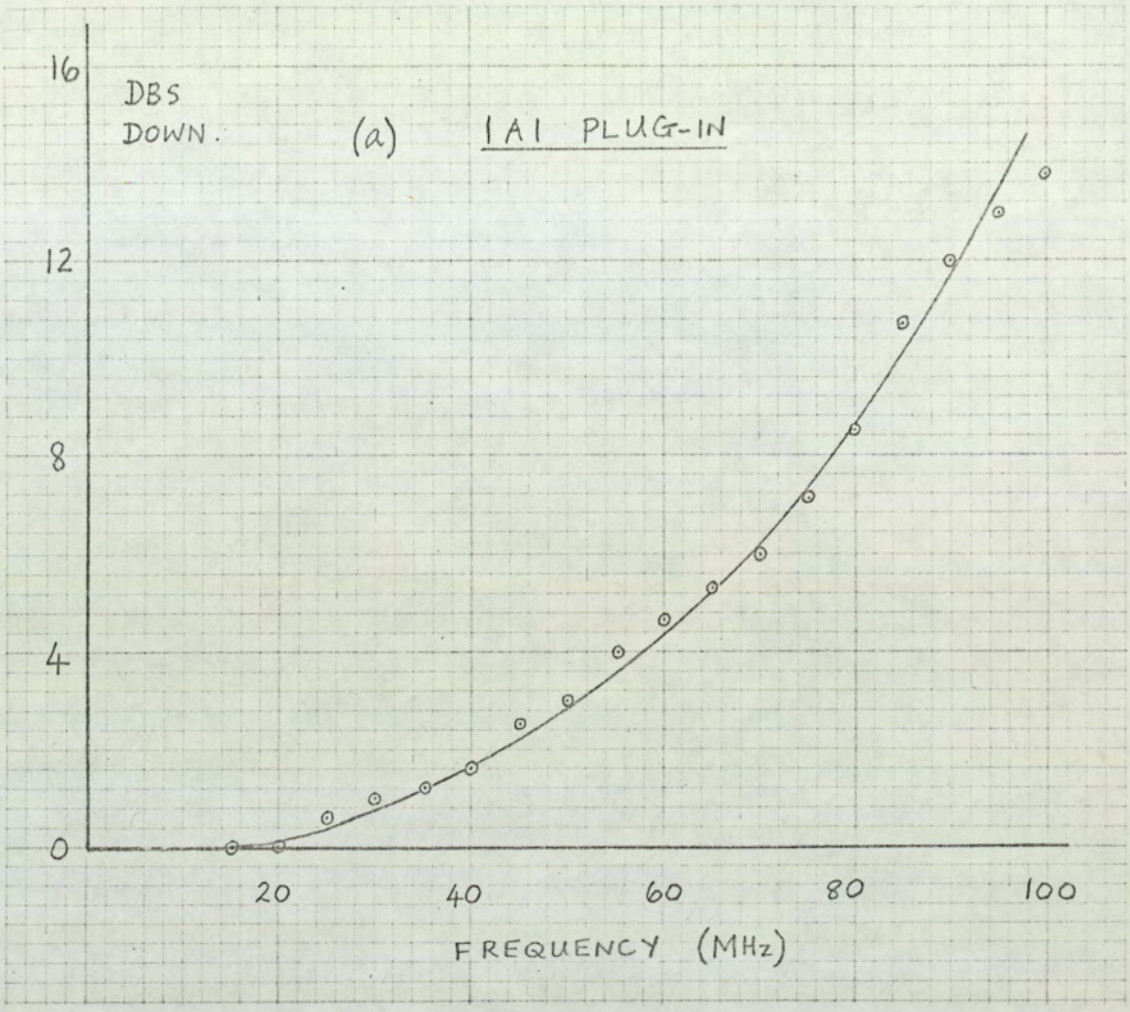

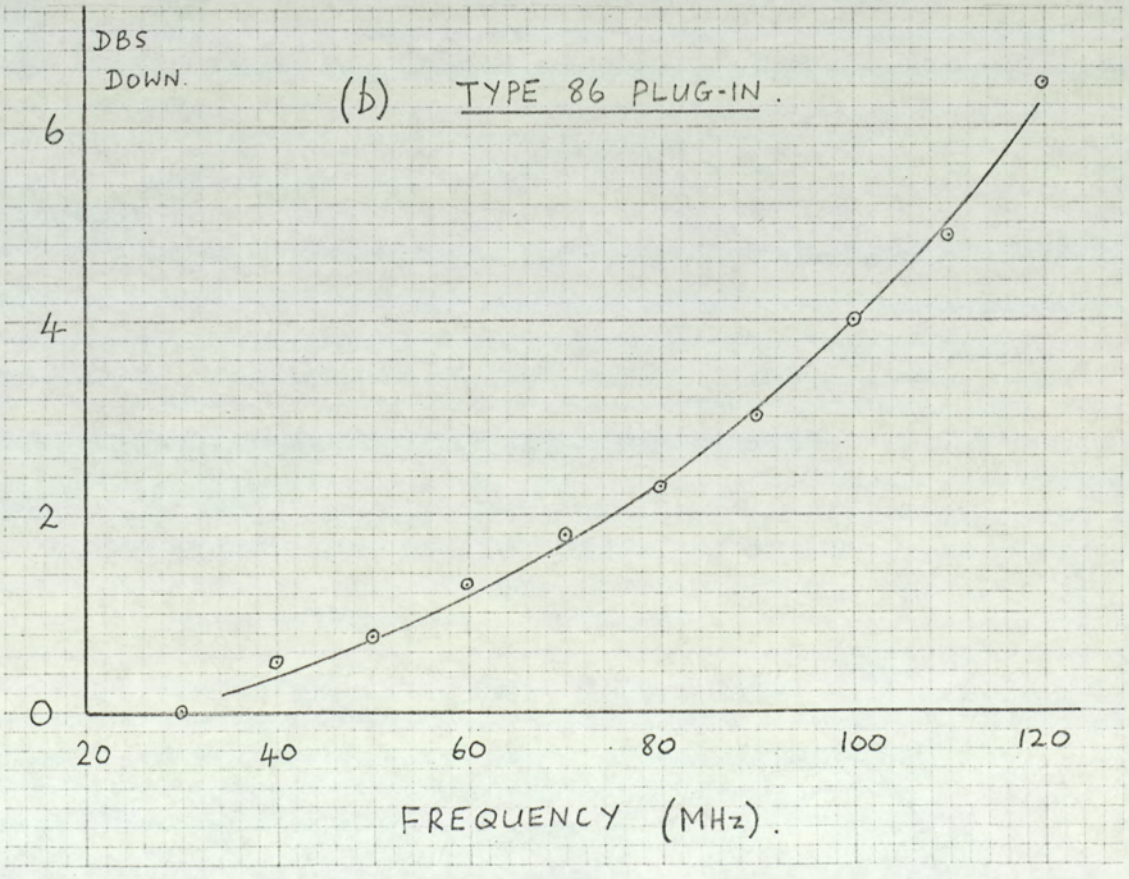

FIG. 28. FREQUENCY RESPONSE OF OSCILLOSCOPES.

frequency response of this instrument was also measured and this is shown in figure 28(b). The direct display of higher frequency harmonics to be described in chapter 5, was also accomplished using this oscilloscope.

Acoustoelectric voltage display, to be described in section 4.4., was achieved using a type 1A1 oscilloscope having a 1A7 high gain differential amplifier plug-in.

4.2.5. The overall triggering arrangement

A Solatron pulse generator, externally triggered at twice the mains frequency was used to provide a 5 volt positive going voltage pulse to the Matec r.f. generator synchronisation input (sync in). A negative going pulse from the Solatron pulse generator was used to trigger both oscilloscopes, as shown in figure 16. As noted in the previous section, a variable width voltage pulse from gate A of one of the oscilloscopes triggered the high d.c. voltage generator. The Matec triggering pulse from the Solatron pulse generator could be delayed up to 50μ secs with respect to the oscilloscope triggering pulse. Furthermore, the oscilloscope gate A output to the high voltage generator could be delayed up to 50μsecs with respect to the r.f. generator controlling pulse. This allowed the relative time of application, and the duration, of the applied d.c. voltage to the crystal, to be varied with respect to the acoustic signal into the crystal.

4.3. Acoustic attenuation measurement

The single transit attenuation of an acoustic signal after propagation through the crystal was measured under a wide range of applied conditions. Each measurement was made relative to the corresponding acoustic transmission with the crystal in the dark, and no drift field applied. The crystal is considered to be insulating when in the dark - measurement of the dark crystal conductivity indicating a value less than 10^{-9} $(\text{ohm cm})^{-1}$ - and no acoustoelectric interaction occurs. The non electronic attenuation of 50 MHz acoustic waves in CdS has been reported to be only of the order of

0.3 db/cm.[94].

The measured attenuations reported in chapter 5 are however solely due to the acoustoelectric interaction since measurement is made relative to the dark value. The experimental procedure enabling a measure of electronic attenuation to be achieved within an accuracy of $\pm$ 0.5 db. will now be described.

With the crystal in the dark, and for a given input acoustic intensity the single transit acoustic signal and subsequent echoes were displayed using the oscilloscope. Optimum matching of the crystal to the r.f. attenuators A1 and A2 was achieved in the manner described in section 4.2.2.4. The linear behaviour of the attenuators, preamplifier, and r.f. receiver was indicated by altering the db setting of the input attenuator A1 in 1 db. steps and noting that the height of the displayed acoustic echoes remained constant after corresponding changes in the db setting of the output attenuator A2. For a given, noted, db. setting of each attenuator the Matec receiver gain was adjusted to make the first echo of the acoustic display - that due to a single crystal transit - a convenient reference height. Throughout the experimental work this was chosen to be 6 volts on the 2 volts/cm. setting of the volts/cm range of the oscilloscope. Thus the chosen reference displayed height of the first echo was 3 cms.

For a given input acoustic intensity, dictated by the db. setting of the calibrated input attenuator A1, the attenuation of the acoustic signal for any crystal illumination and applied d.c. voltage, could then be measured by noting the required db. setting on the output attenuator A2 necessary for a displayed first echo height of 3 cms. The difference between that attenuator setting, and the dark crystal setting corresponding to the particular input attenuator setting, gave a measure of the electronic attenuation. In most cases the displayed height was not quite 3 cms. and an accuracy of $\pm$ 0.5 db. in the attenuation measurement was achieved

by then noting the echo height to within 0.1 cm., and using appropriate db. tables, relating the displayed height to the reference 3 cm. height.

4.4. Acoustoelectric voltage measurement

Figure 29 shows the experimental arrangement used to measure the acoustoelectric effect under a wide range of applied conditions. Initially, some difficulties were encountered in displaying the measured acoustoelectric voltage. These will be discussed after an account has been given of the basic measurement technique adopted.

A resistor R_m which was chosen to be much less than the lowest value of the crystal resistance R_c encountered experimentally, was put in series with the crystal. The acoustoelectric field generated in the crystal by an acoustic signal propagating through it, resulted in an acoustoelectric current through R_m and thus, a measurable voltage across R_m . A theoretical description of this voltage has been given in chapter 2. For much of the experimental work, a high d.c. voltage was applied to the crystal as discussed in section 4.2.3. The acoustoelectric voltage appearing across R_m was then superimposed on the much larger d.c. field also appearing across R_m . To allow the acoustoelectric voltage only to be displayed, a variable resistance chain was put in parallel with the crystal. This comprised a variable resistance R_V which covered the entire crystal resistance range, and a fixed resistor R_{Vm} chosen to be equal to R_m . The voltages appearing across R_m and R_{Vm} were then applied to the two inputs of the differential amplifier plug-in of the type 547 oscilloscope. For a given crystal illumination, the variable resistor R_V was adjusted so that its value was equal to the crystal resistance. The d.c. voltage across both R_m and R_{Vm} were then equal, and resulted in a null display on the oscilloscope. The acoustoelectric voltage appearing across R_m did not however appear across R_{Vm} , and consequently the displayed acoustoelectric

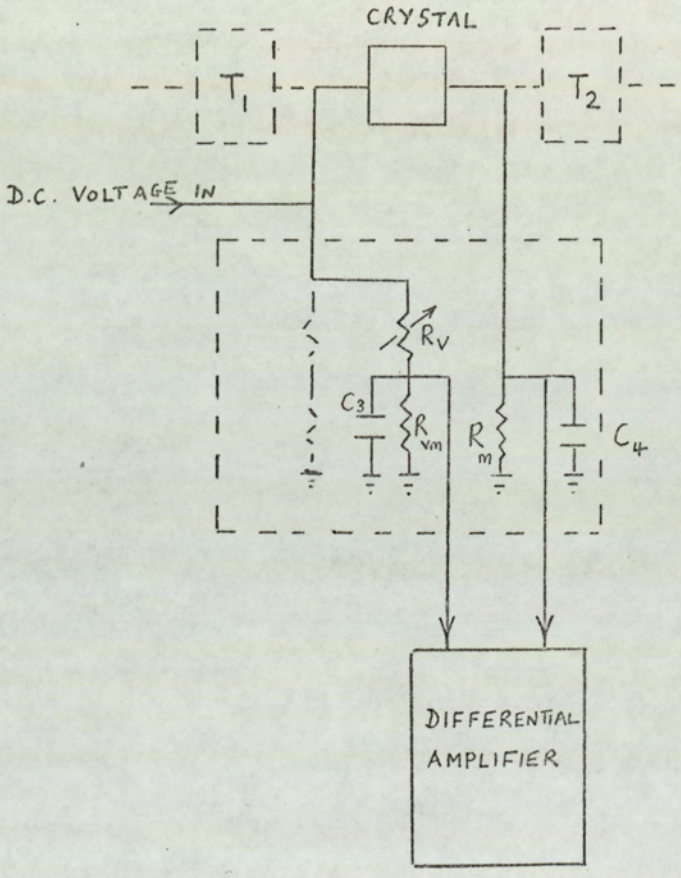

FIG. 29. ACOUSTOELECTRIC VOLTAGE MEASUREMENT CIRCUITRY.

voltage was entirely that across R_m . Further discussion of this observation will be given shortly. Using this technique acoustoelectric voltages of only ten millivolts or so, could be measured to within 10% accuracy in the presence of an applied d.c. field of 1 Kv.

The chosen value of R_m was 520 ohms. compared to the lowest attainable crystal resistance of 10^4 ohms. At first, direct measurement of the acoustoelectric voltage across the crystal for no applied drift field was attempted. The resulting oscilloscope display is shown diagrammatically in figure 30 (a). This indicates a capacitative effect which was considered to be associated with the crystal, and which is shown dotted in figure 29. Wang [36] has given an equivalent circuit for the amplifier which includes a parallel capacitor. No attempt was made in this research to investigate this.

Acoustoelectric voltage measurement across various series resistors was then tried. Series resistors of less than 4 KΩ gave a reasonable waveform display but it was noted that for resistors above 700Ω a rounding of the acoustoelectric voltage maxima occurred. Thus, for a given crystal illumination, the acoustoelectric voltage measured across 1 KΩ was not quite twice that measured across 500 Ω. No capacitative rounding was noted for values of R_m less than 700Ω .

A second difficulty concerned the unwanted display of r.f. pickup, particularly at the start of the acoustoelectric voltage trace. An example of this is shown diagrammatically in figure 30 (b). The presence of an r.f. current through the measuring resistor chains was thought due to the inevitable stay capacitances associated with the experimental arrangement. It was noted that capacitors C_3 and C_4 placed as shown in figure 29 entirely removed the pick-up. It was considered that these provided an effective by-pass for the r.f. current. A more definite reason for the inclusion of these capacitors was not sought, since their presence convincingly removed the r.f. pick-up and did not, in any way, affect the displayed

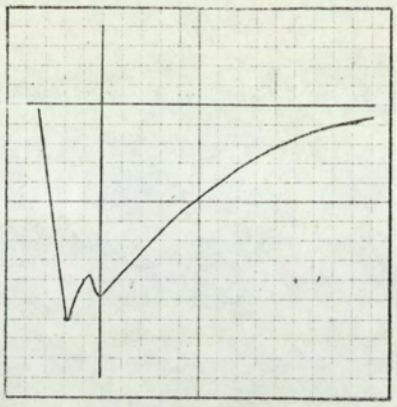

(a) LONG "ONE SIDED" DISPLAY

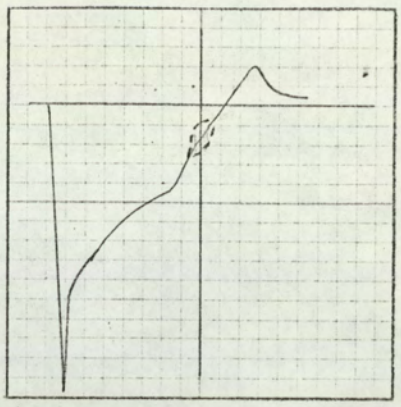

(b) R.F. PICKUP

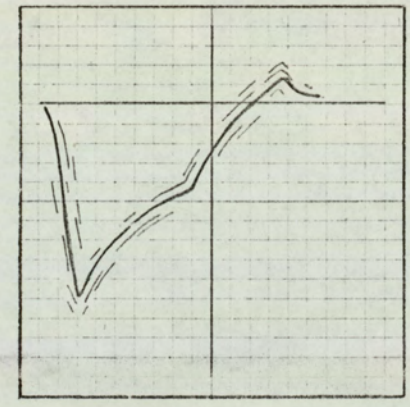

(c) "JITTER"

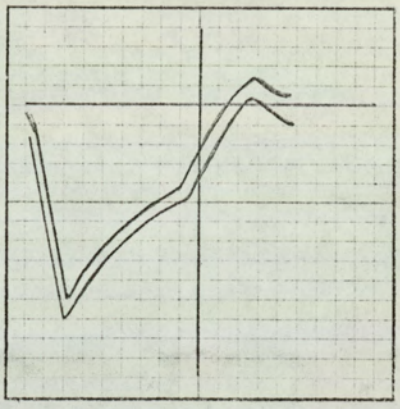

(d) STATIC DOUBLE TRACE

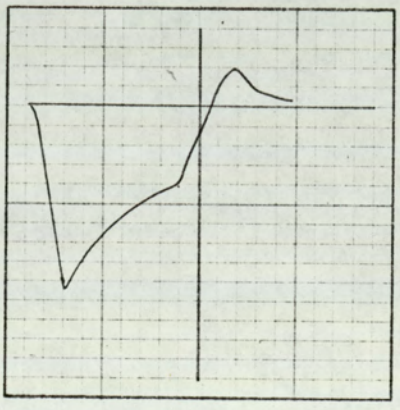

(e) DESIRED TRACE

FIG. 30. ACOUSTOELECTRIC VOLTAGE DISPLAY PROBLEMS.

acoustic signal, or true acoustoelectric voltage display.

It has been noted that the acoustoelectric voltage appearing across R_m did not appear across R_{Vm}. This was most convenient, since the appearance of an acoustoelectric voltage across R_{Vm} would have contributed to the acoustoelectric voltage display. Essentially, the effective resistance across which the acoustoelectric voltage is measured, and the value of which must be known for predicted acoustoelectric voltages to be calculated using the theory of section 2.3, would not then be that of R_m only. A possible explanation for this convenient absence of acoustoelectric voltage across R_{Vm}, is that a low impedance path by-passing R_{Vm} is available to the acoustoelectric current. When R_V was made less than 4 K ohm. an acoustoelectric voltage was detected across R_{Vm}. This was seen to increase as R_V was further reduced. Whilst this occurred, no reduction in the measured acoustoelectric voltage across R_m was noted. Thus reducing R_V below 4 KΩ was considered to provide an alternate more agreeable path for the acoustoelectric current, through R_{Vm} and R_V. The low impedance path in parallel with R_{Vm} and R_V, for high values of R_V, was thought to be due to a capacitor across the variable resistance chain. During the entire experimental work R_V was always greater than 10^4 ohms, and the displayed acoustoelectric voltage was always entirely due to the acoustoelectric current through R_m. No contribution to the displayed acoustoelectric voltage was ever observed from R_{Vm}.

Two other refinements to the experimental equipment were adopted. Initially the triggering of the r.f. generator and the d.c. pulse generator was made at 50 p.p.s. with the Solatron pulse generator triggered from the mains. The displayed acoustoelectric voltage and acoustic echoes were then observed to jitter as shown in figure 30 (c). The Solatron was then triggered at twice the mains frequency from a frequency doubler. This prevented the jitter and

resulted in a static doubling of the trace as shown for the acoustoelectric display in figure 30 (d). A large variable capacitor was included in the frequency doubler circuit to enable the phase of the approximately 100 cycle a.c. trigger to the Solatron pulse generator to be varied. This resulted in the desired single trace, a typical example of which is shown in figure 30 (e).

The steps taken to produce a displayed acoustoelectric voltage devoid of spurious pick-up, and other unwanted effects, are acknowledged to be semi-empirical. However, great care was taken to ensure that the acoustoelectric voltage measurement and the acoustic transmission were not affected in any way whatsoever, by these steps. Since this was the desired objective a thorough investigation into the causes of the spurious effects which, at first, prevented a useful display, was not undertaken.

4.5. Input acoustic intensity measurement

The input acoustic intensity to the crystal at a particular acoustic frequency was determined by first measuring the total insertion loss of the matching transformer assemblies T1 and T2, the transducers, and the insulating crystal, after optimum matching had been achieved.

The output from the r.f. generator was applied to the calibrated attenuator A1 and the attenuator output was terminated in 50 ohms. at the input of the particular oscilloscope used (see section 4.2.4.) This arrangement is shown in figure 31 (a). The half-height width of the r.f. signal was adjusted to be 1 μs and the peak to peak amplitude of the displayed r.f. packet was measured for different values of attenuation in the signal line. The r.f. signal for a given input attenuation was then applied to the crystal via the input matching assembly T1. The output line from T2 was terminated in 50 ohms at the oscilloscope input as shown in figure 31 (b), and the corresponding output signal displayed and measured. The input peak to peak

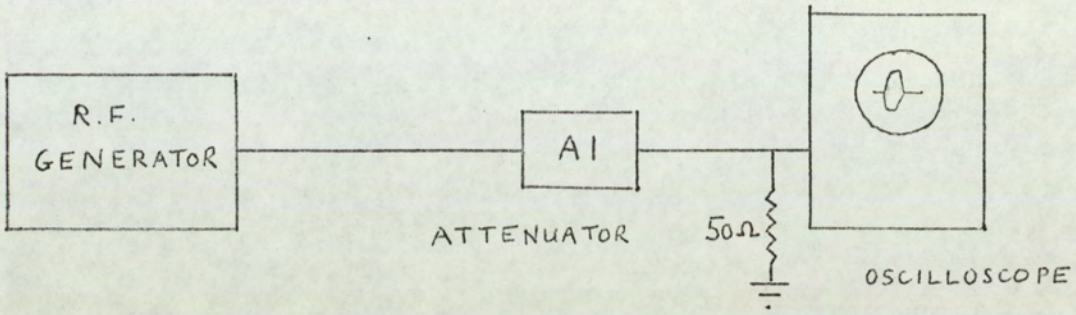

(a) MEASUREMENT OF V_{pp} IN.

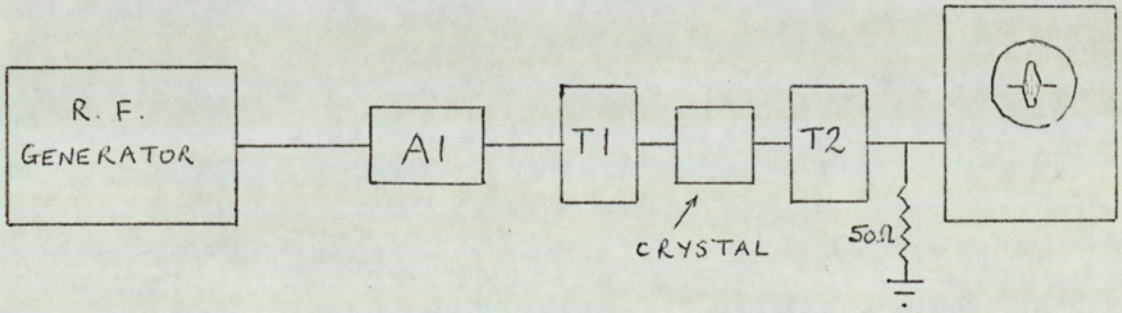

T1 AND T2 MATCHING TRANSFORMER ASSEMBLIES.

(b) MEASUREMENT OF V_{pp} OUT.

FIG. 31. INSERTION LOSS DETERMINATION

EXPERIMENTAL ARRANGEMENT.

amplitude was then plotted against the output peak to peak amplitude over a wide range of input acoustic intensities. A typical graph so obtained at 45 MHz. is shown in figure 32. The slope of the straight line plot gave the input-output signal amplitude ratio. The total insertion loss of the crystal, the transducers, and the matching circuitry could then be calculated.

In order to determine whether this loss was shared equally between each matching assembly and associated transducer, the crystal was weakly illuminated and the acoustoelectric voltage produced by the acoustic signal propagating through the crystal in each direction was noted. It has already been pointed out that the measured acoustoelectric voltage is linearly related to the input acoustic intensity. Consequently, equal acoustoelectric voltages observed for acoustic transmission in each direction through the crystal indicated an equal acoustic intensity input to each side of the crystal. Thus, for a given r.f. signal applied to each matching assembly, prior to transduction and subsequent propagation through the crystal, the observation of equal acoustoelectric voltages allows the assumption of an equal share of the total insertion loss.

If, however, the measured acoustoelectric voltages are not quite equal, and the difference is not due to mismatching as suggested in the previous section, then the measured insertion loss is not equally shared between each matching assembly and transducer. A correction must then be made to ensure an accurate determination of acoustic intensity input to the crystal. The correction term, as a function of the relative acoustoelectric voltages is derived in appendix 3.

The r.f. power applied to the input matching assembly T1 was calculated from the measured peak to peak amplitude of the input r.f. signal, assuming an input load of 50 ohms. The frequency response of the oscilloscope used to display the r.f. signal must be taken into account in the determination of true input r.f. amplitude. No correction to the determined input-output r.f. signal ratio is

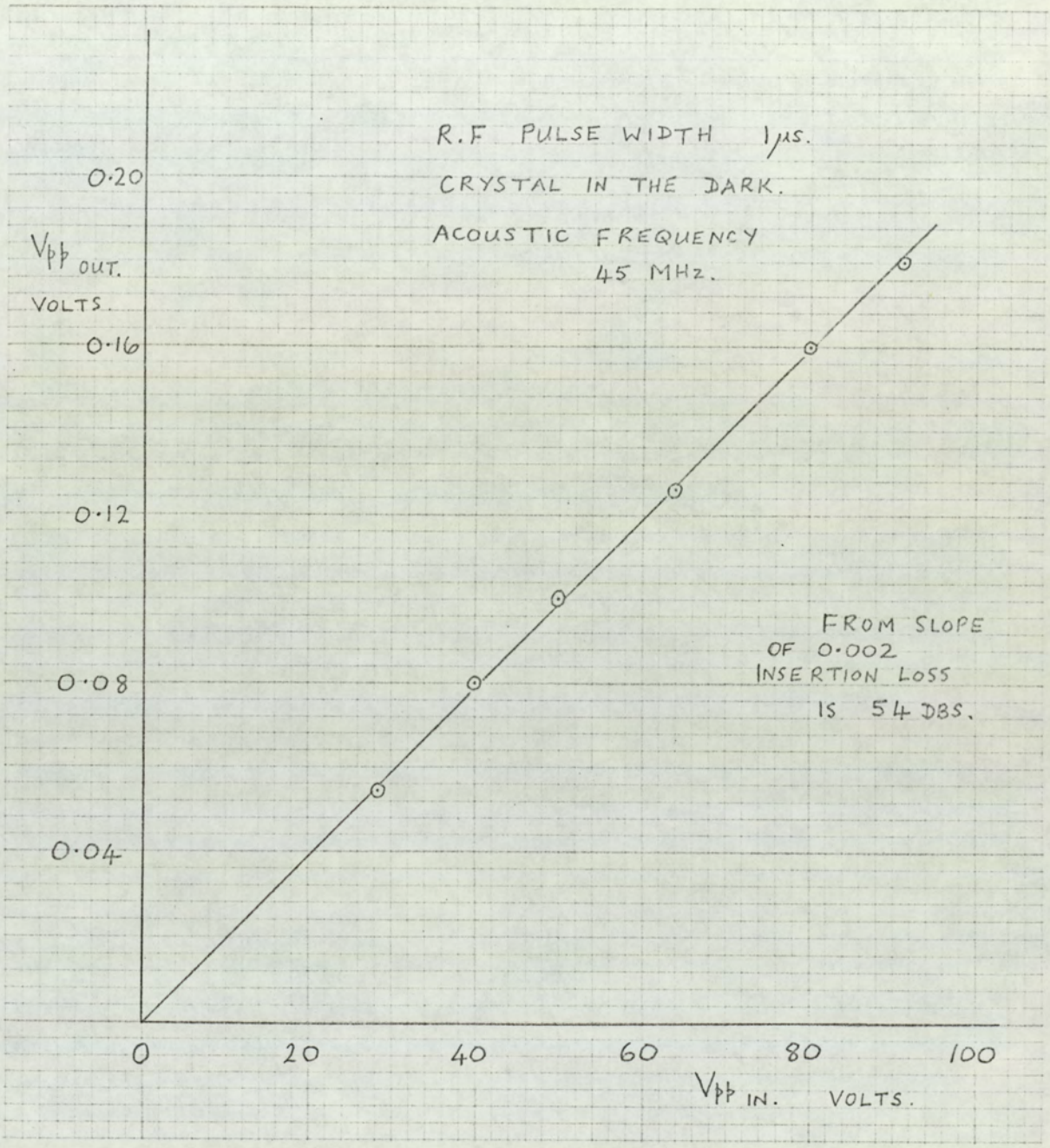

FIG. 32. DETERMINATION OF THE INPUT - OUTPUT SIGNAL AMPLITUDE RATIO, AND HENCE, THE INSERTION LOSS AT 45 MHz.

necessary however. Having taken into account any asymmetry in the total insertion loss and also the frequency response of the oscilloscope, the acoustic intensity into the crystal for a given setting of the input attenuator may be calculated. As indicated in appendix 4, the active area of the transducers is also taken into consideration, in order to obtain a value of input acoustic intensity in watts/sq.cm. A calibration graph was plotted at each acoustic frequency, giving the peak to peak r.f. amplitude input to T1 and the corresponding attenuator A1 setting versus acoustic intensity input to the crystal. These graphs for acoustic frequencies of 15 to 105 MHz are given as figures 33 to 36. They play an important role in the calculation of predicted acoustoelectric voltage using the theory of section 2.3.

The following calibration procedure was adopted prior to any experimental work, to ensure that results taken on different days could be compared.

The matching assemblies were tuned for optimum matching as previously described in section 4.2.2.4. With the crystal in the dark, the r.f. generator amplitude control and r.f. width control were adjusted to give a 1 μsec. half height width r.f. pulse of peak to peak amplitude, - as measured in the manner indicated by figure 31(a), and as specified by the previously determined calibration graph relevant to that particular acoustic frequency, - for a given db setting of the input attenuator. The peak to peak amplitude of the displayed r.f. pulse was then checked against the calibration graph for agreement at several other attenuator settings. With a given attenuator setting the r.f. was applied to the matching assembly T1 and the output signal from T2 was displayed as indicated in figure 31(b). The peak to peak amplitude of the output signal was checked, for several input amplitudes, using the input-output amplitude calibration graph used to determine the total insertion loss. The output r.f. signal from T2 was then applied to attenuator A2, which was connected to the

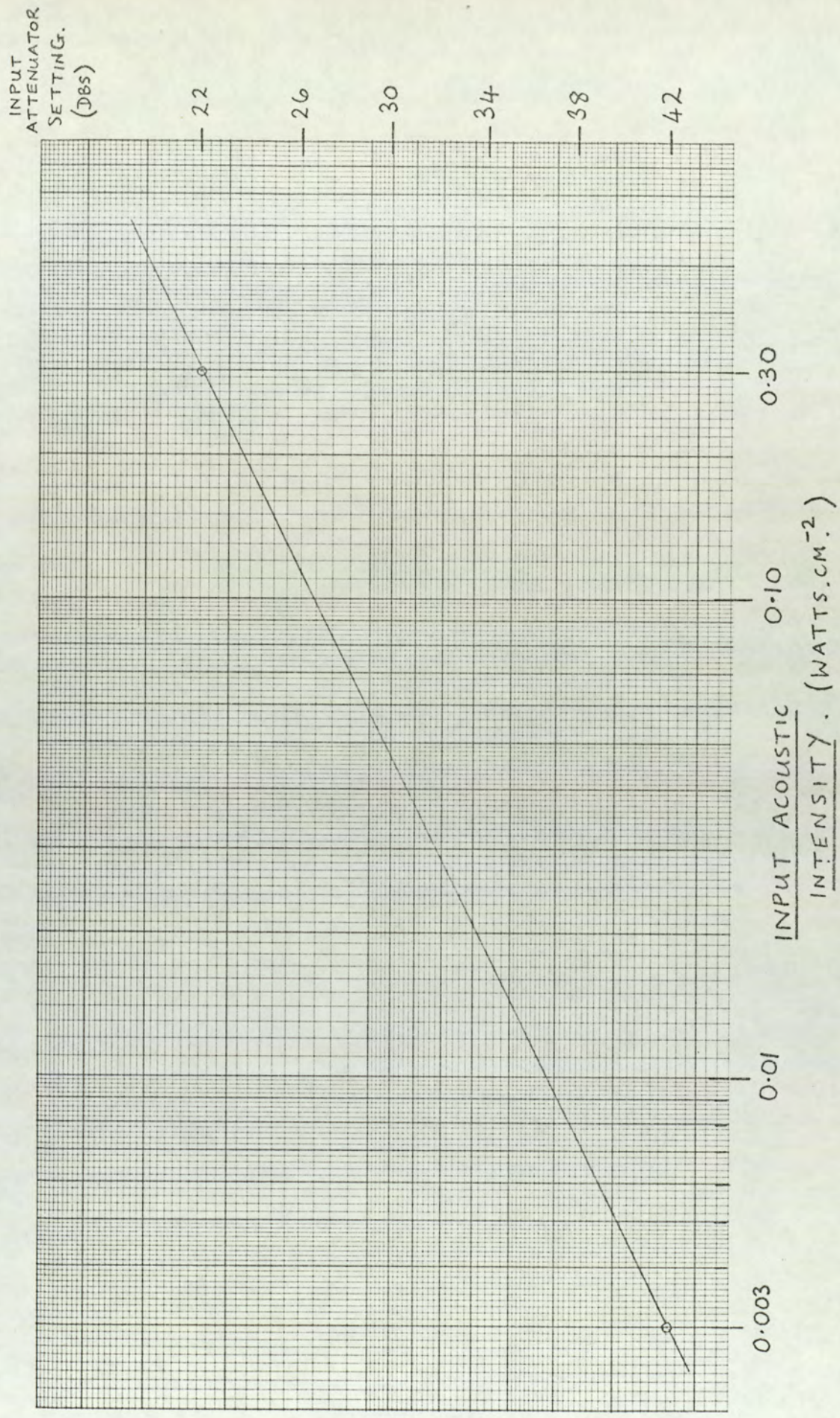

FIG. 33. INPUT ACOUSTIC INTENSITY VERSUS INPUT ATTENUATOR SETTING. 15 MHz.

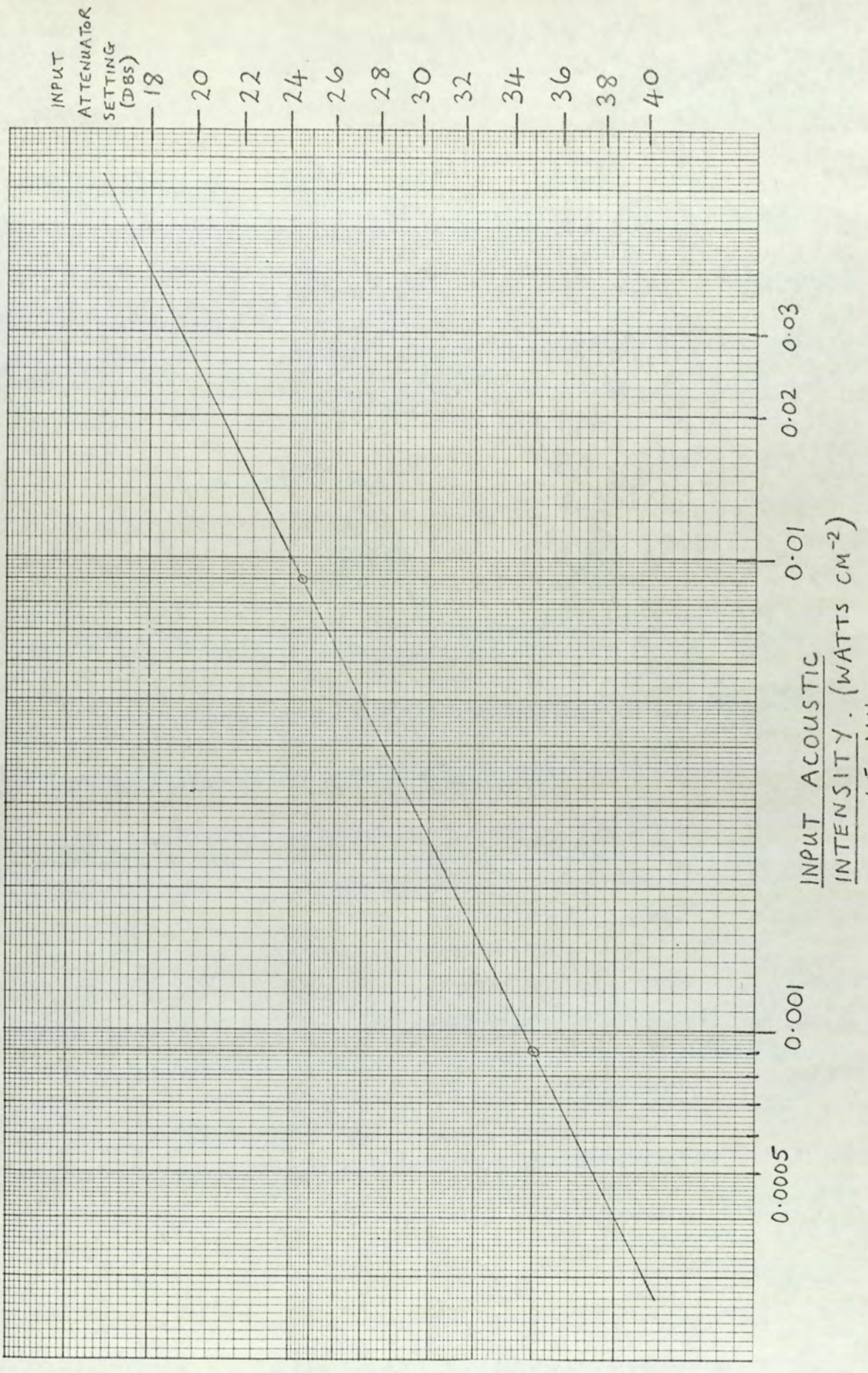

FIG 34. INPUT ACOUSTIC INTENSITY VERSUS INPUT ATTENUATOR SETTING. 45 MHz.

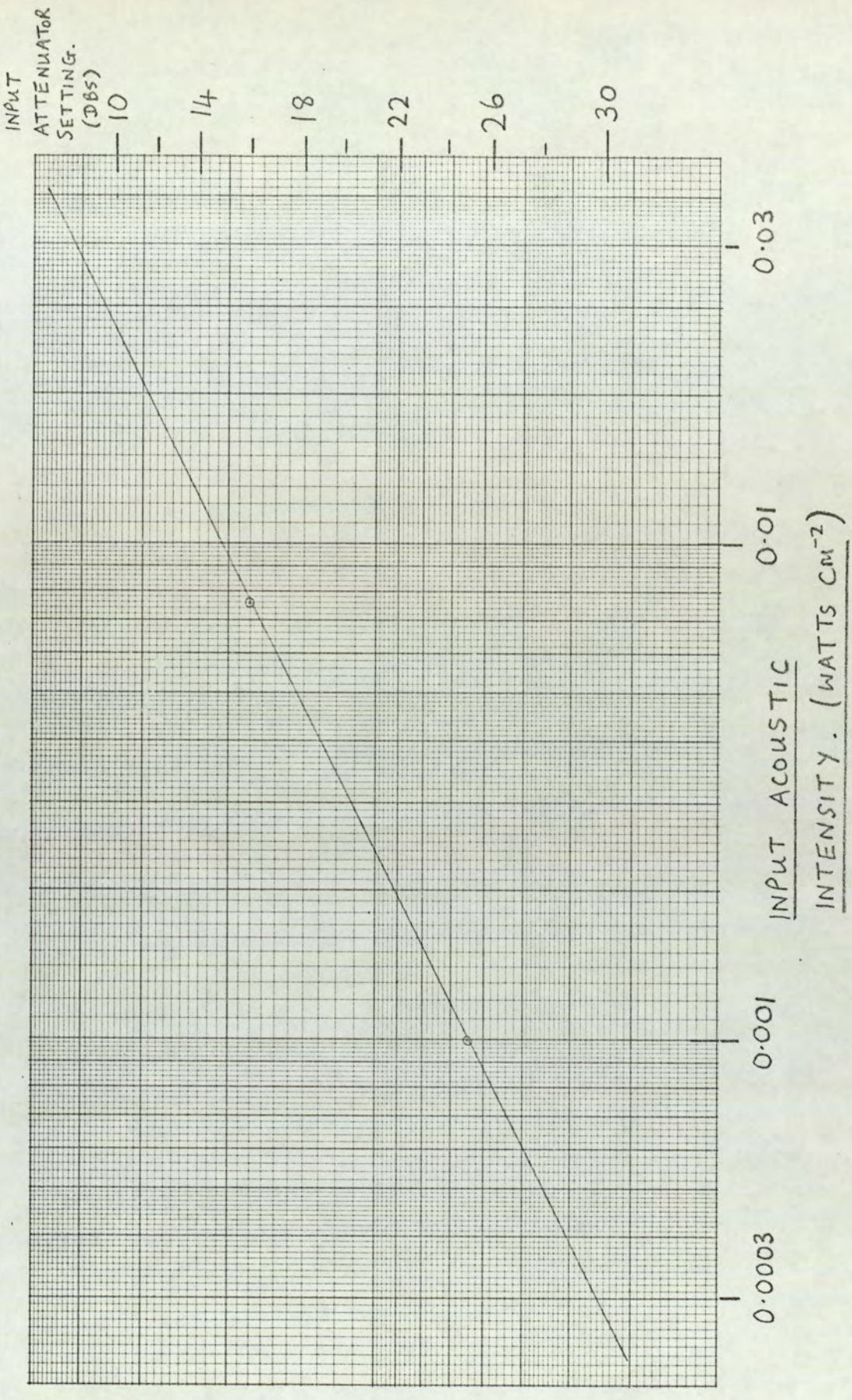

FIG. 35. INPUT ACOUSTIC INTENSITY VERSUS INPUT ATTENUATOR SETTING. 75 MHz.

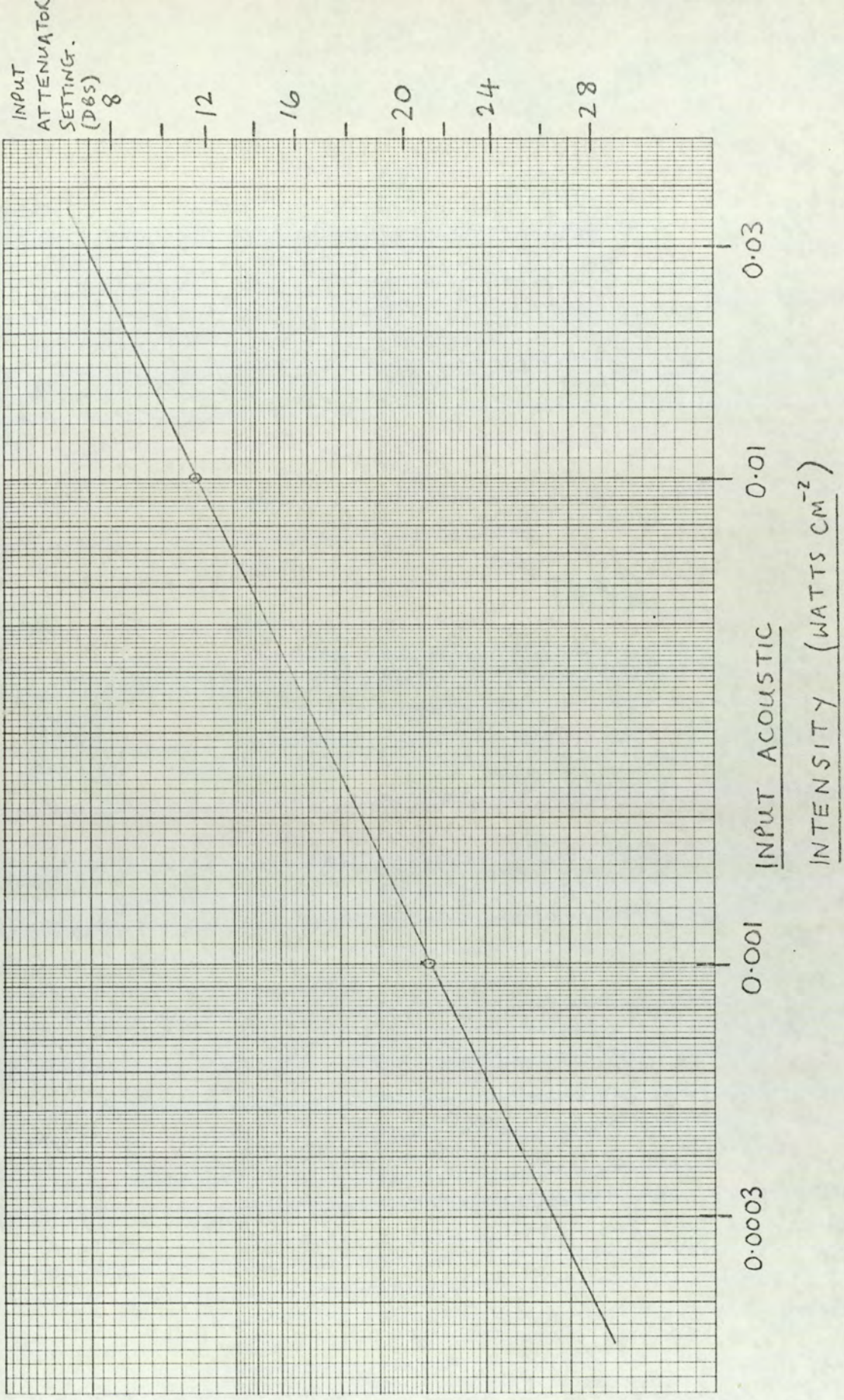

FIG. 36. INPUT ACOUSTIC INTENSITY VERSUS INPUT ATTENUATOR SETTING 105 MHz.

preamplifier and r.f. receiver. The db. settings of A1 and A2 were adjusted to make the displayed single transit echo height almost 3 cms. on the 2 volt/cm. setting of the oscilloscope volts/cm. range. Final adjustment of the displayed echo height to 3 cms. was achieved using the receiver gain control. The attenuator settings were adjusted to the same values each time, and providing the calibration procedure had been carried out correctly, the displayed height of the first echo was always very nearly 3 cms. before receiver gain adjustment.

This procedure was carried out several times during each experimental period to ensure that the acoustic intensity calibration graph was always valid. This allowed the acoustic intensity input to the crystal to be known immediately, for a given attenuator A1 setting.

4.6. Concluding remarks

A comprehensive description has been given of the equipment used in this research, and the manner in which it was used. The measurement techniques allowing an accurate simultaneous measure of the acoustoelectric voltage and acoustic attenuation coefficient have also been described. The method used, of determining the input acoustic intensity to the crystal - a method which makes use of the acoustoelectric effect to obtain a more accurate determination of input intensity - has been given.

CHAPTER 5

Experimental results

5.1. Introduction

This chapter describes the experimental work which has been carried out in order to assess the validity of the Weinreich relationship over a wide range of applied conditions. The analysis presented in chapter 2 has enabled this assessment to be quantitative. It has not been the purpose of this work to investigate comprehensively the acoustic behaviour of the crystal, with a view to comparing critically the observed behaviour with that predicted by White's theory. Rather, it has been the aim to determine to what extent the observed acoustic behaviour, and the simultaneously observed acoustoelectric effect are related. Such an investigation could be carried out using any crystal exhibiting acoustoelectric behaviour, and the fact that the particular crystal used might not be considered a "good" amplifier is irrelevant. The opportunity to assess the Weinreich relationship over a wide range of applied conditions does demand an active crystal however, and the care taken in choosing such a crystal has been described in chapter 3.

The results to be reported indicate strong non linear behaviour which has enabled the study of the Weinreich relationship to be made under both linear, and non linear conditions, and also to be extended to include harmonic generation. It has been necessary to restrict substantially the reported experimental work, since a description of all the experimental work carried out would be impractical. Typical results are reported, and in many cases

these have been repeated on separate occasions with satisfactory agreement.

With the exception of the general observations describing the amplification of broadband acoustic flux, and the consequent current saturation and oscillation, presented in the final section of this chapter, the experimental results relate the behaviour of an input acoustic signal to the acoustoelectric voltage thereby produced. The range of input acoustic intensity employed, extended over four orders of magnitude to a maximum of several watts cm^{-2}. Some results are reported at an acoustic frequency of 105 MHz., although the majority of the experimental work has been carried out at 15, 45 and 75 MHz. The crystal conductivity was varied from the dark conductivity, - about 10^{-9} $(ohm.cm)^{-1}$ - to nearly 10^{-4} $(ohm.cm)^{-1}$, and d.c. voltages of up to 1000 volts were applied to the crystal.

Section 5.2. describes the results obtained with no drift voltage applied to the crystal. Section 5.3. then presents the results obtained with an applied d.c. voltage, and since this section is extensive it comprises four main subsections. A general assessment of the Weinreich relationship over the entire, indicated, range of applied conditions is given in section 5.3.1. The following two sections present the work carried out on harmonic generation, and the suggestion of Tien [71], and independently, Butcher and Ogg [77], that the Weinreich relationship is valid for each harmonic is tested quantitatively. Section 5.3.4 is concerned with the effects of carrier trapping on the Weinreich relationship and an attempt is made to test experimentally the prominent trapping theories as described in chapter 2. Finally section 5.3.5. concludes the experimental results with some general observations on current saturation and oscillation. No more than a preliminary discussion of these results has been given in this chapter. The results are discussed in detail in chapter 6.

5.2. Experimental results, with no drift voltage applied to the crystal.

5.2.1. The variation of attenuation coefficient with crystal conductivity

The small-signal linear theory of White, outlined in chapter 2, predicts the acoustic attenuation of an acoustic wave propagating through a piezoelectric semiconducting medium in the absence of an applied d.c. voltage to be

$$\alpha = \frac{K^2}{2v_s}\left[\frac{\omega_c}{1+\left(\frac{\omega_c}{\omega}+\frac{\omega}{\omega_D}\right)^2}\right] \qquad -------(5.1.)$$

where the symbols have already been defined.

It may be seen that for small crystal conductivities, that is, small ω_c and for $\omega \ll \omega_D$ the bracketted term in the denominator of equation 5.1 is small compared to unity, and under such conditions the attenuation coefficient is given by

$$\alpha = \frac{K^2}{2v_s}\,\omega_c \qquad -------(5.2)$$

Thus an indication of the electromechanical coupling factor, K, at a given acoustic frequency, may be obtained experimentally from a determination of the slope of α versus ω_c in the region of small ω_c.

Figures 37 to 39 show the measured variation of attenuation coefficient with crystal conductivity, at acoustic frequencies of 15 to 105 MHz. For convenience the conductivity has been plotted as the ratio $\left(\frac{\omega_c}{\omega}\right)$. The achieved range of conductivity was such that only at 15 MHz was the ratio $\left(\frac{\omega_c}{\omega}\right)$ significant compared to unity, and it is only at this acoustic frequency that special attention has been paid to the determination of the slope of the

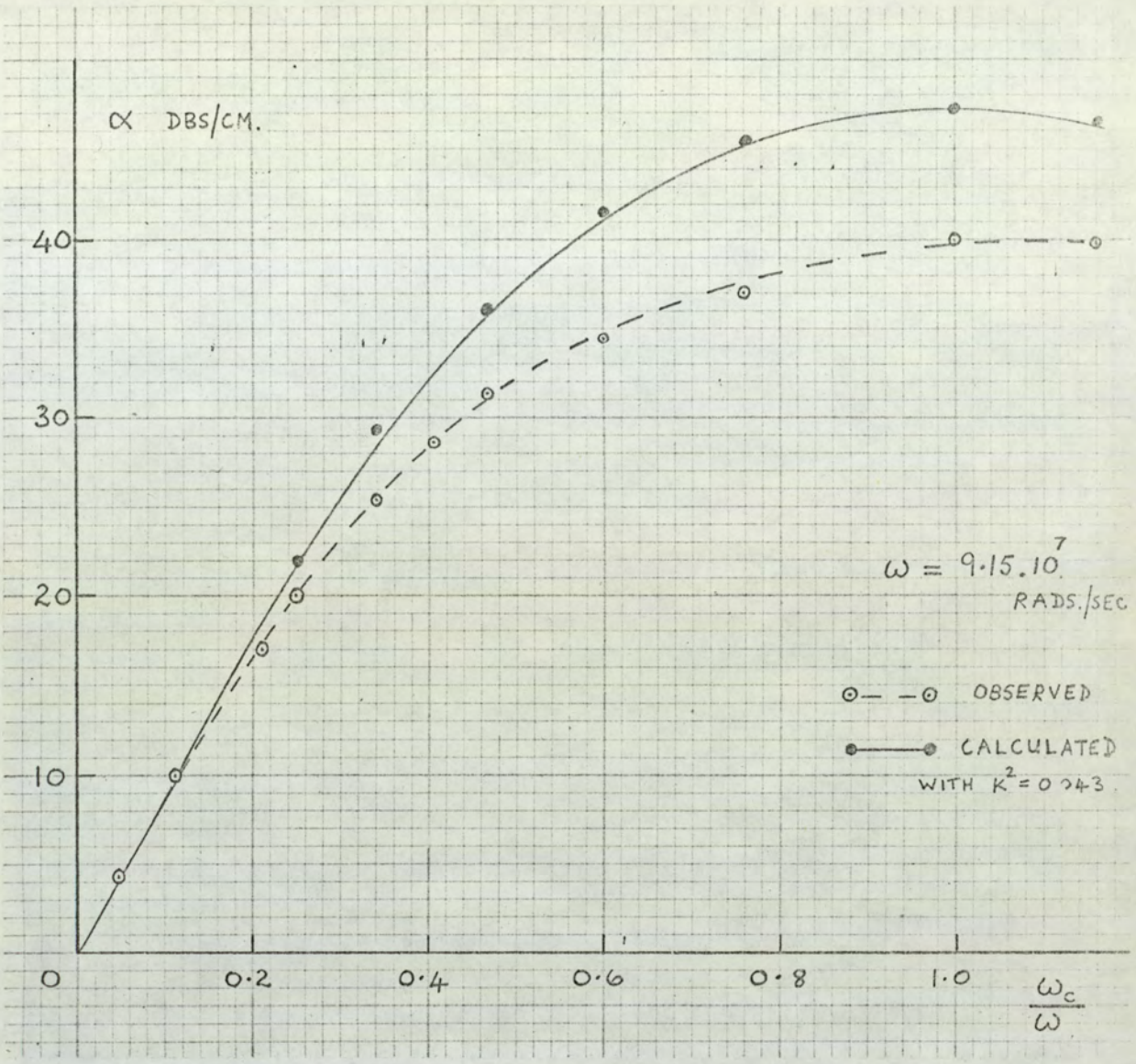

(a)

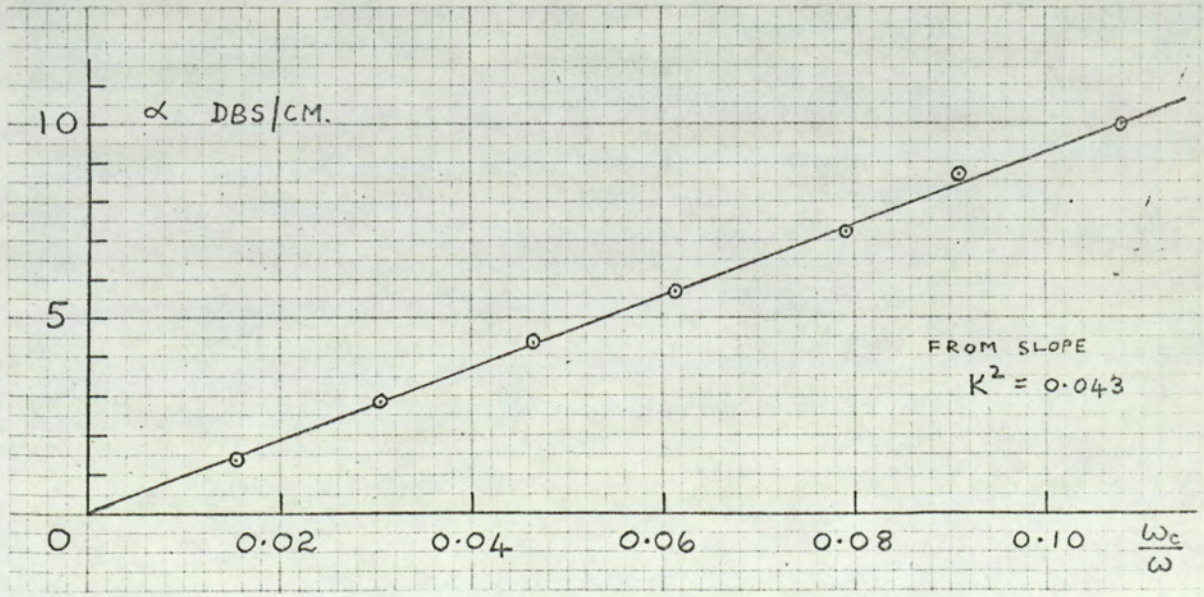

(b)

FIG. 37 THE VARIATION OF ATTENUATION WITH CRYSTAL CONDUCTIVITY AT 15 MHz. NO APPLIED D.C. VOLTAGE.

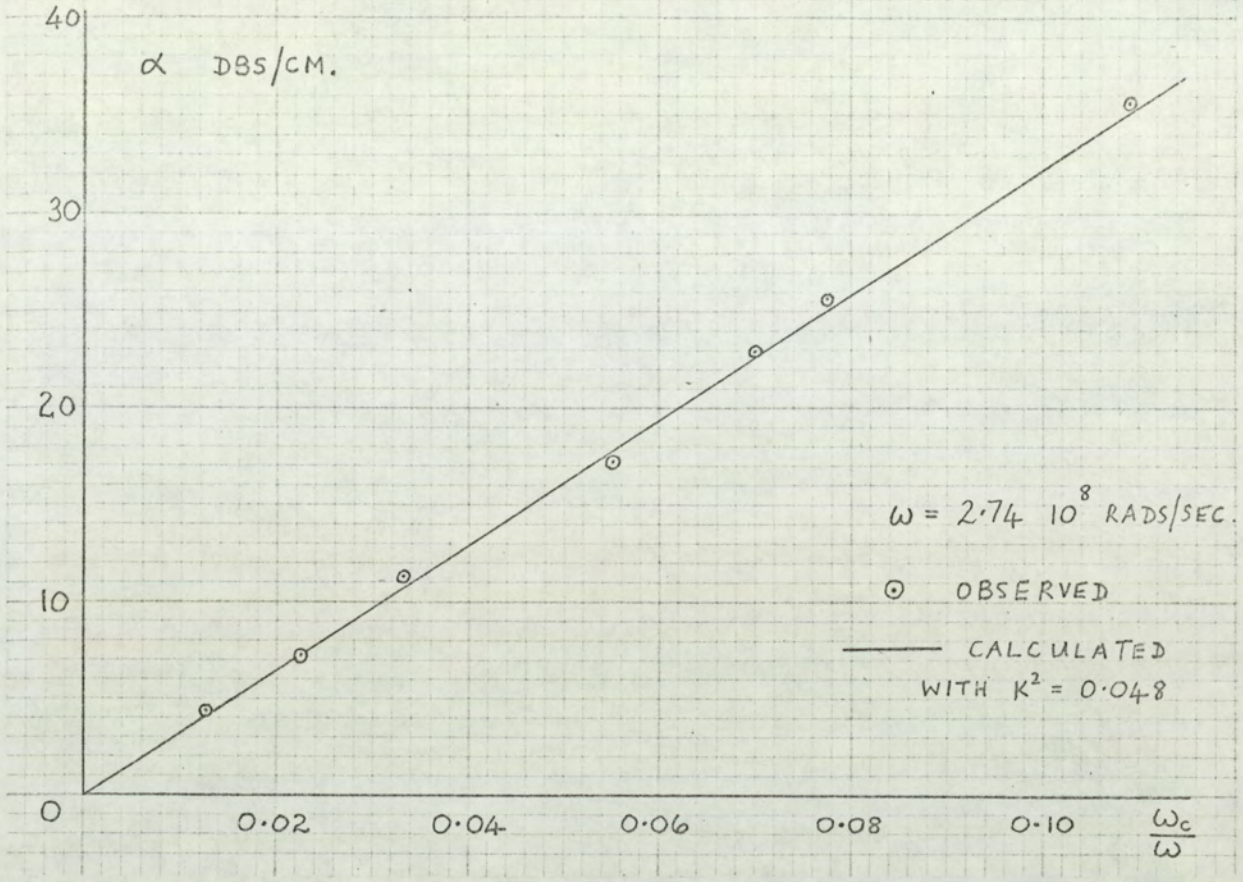

(a)

(b)

FIG. 38. THE VARIATION OF ATTENUATION WITH CRYSTAL CONDUCTIVITY AT 45 MHz.
NO APPLIED D.C. VOLTAGE

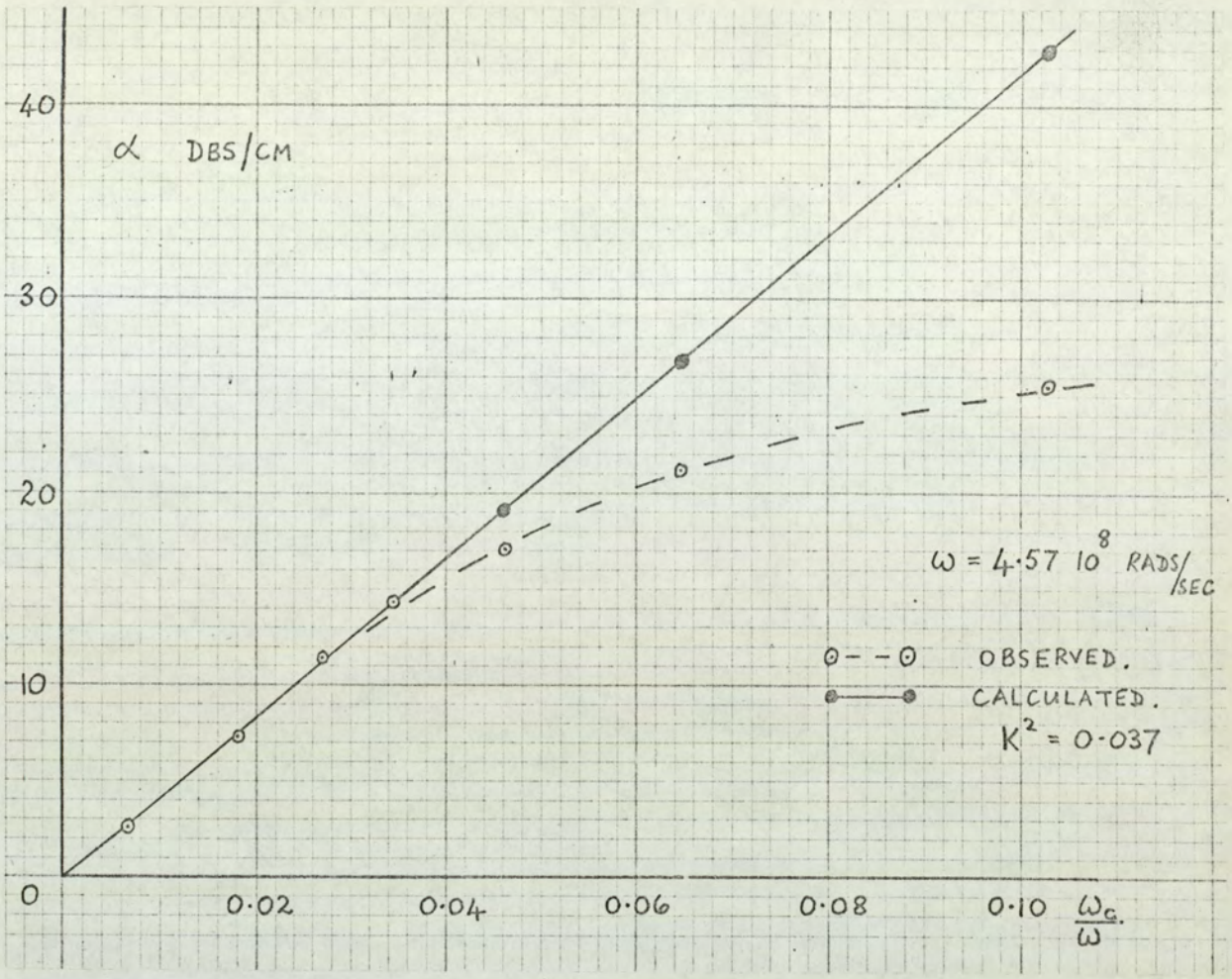

(a)

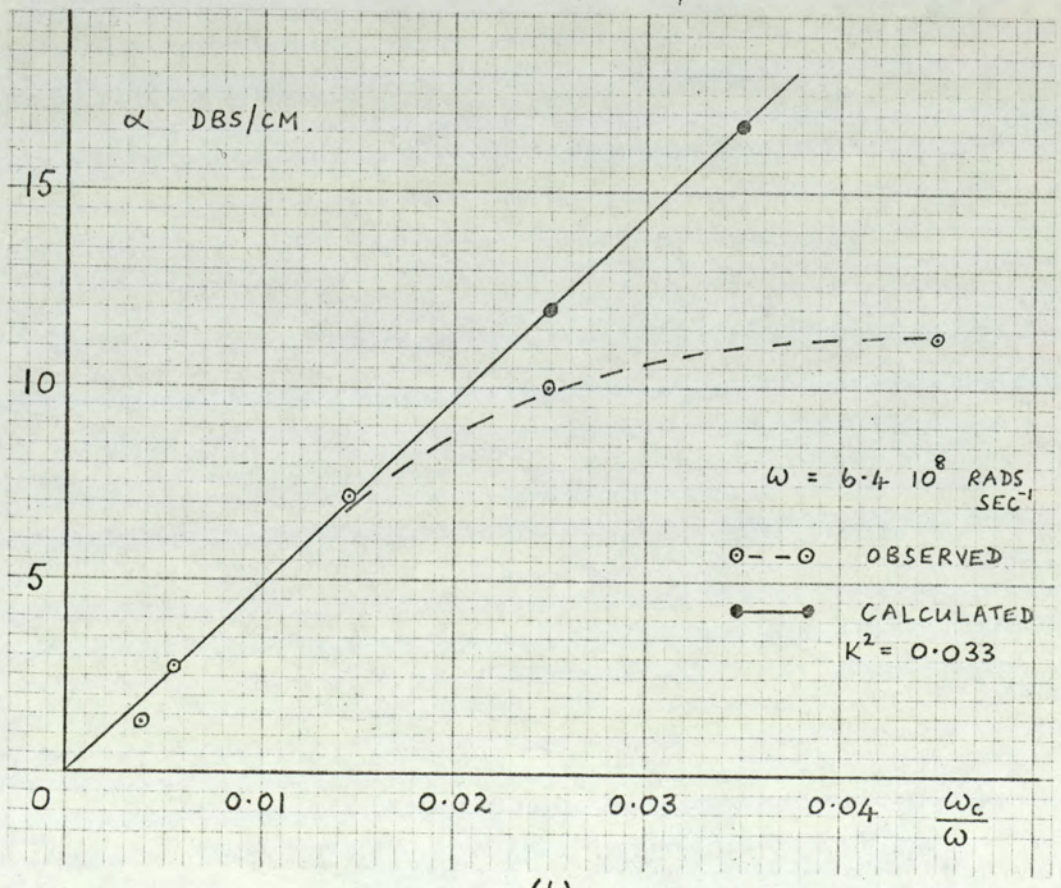

(b)

FIG. 39 THE VARIATION OF ATTENUATION WITH CRYSTAL CONDUCTIVITY AT (a) 75 MHz. (b) 105 MHz. NO APPLIED D.C. VOLTAGE.

curve near the origin (figure 37 (b)). The values of K^2 thus determined at each acoustic frequency are tabulated below.

TABLE 1.

Acoustic Frequency (MHz)	K^2
14.4	0.043
43.2	0.048
72.0	0.037
100.8	0.033

The acoustic frequencies will be referred to as being nominally 15, 45, 75 and 105 MHz. although as table 1 indicates, careful measurement of each acoustic frequency when maximum acoustic transmission through the crystal had been established as described in section 4.3. , indicated frequencies differing slightly from these nominal values. Figure 40 allows the crystal conductivity to be determined at each acoustic frequency, for a given value of $\left(\frac{\omega_c}{\omega}\right)$.

Throughout the experimental work the crystal conductivity was determined by applying 600 volts d.c. to the crystal resistance chain (see section 4.4) and measuring the voltage drop across the 520 ohm resistor R_m in series with the crystal. This enabled the crystal resistance to be calculated. The conversion to crystal conductivity involves the d.c. contact area (circular, of radius 0.25 ins.) and the crystal length (0.70 cms). The conversion factor was determined to be 2.2 cm^{-1}. The dielectric relaxation frequency ω_c was obtained from the conductivity and dielectric permittivity at constant strain $\left(\varepsilon = 8 \times 10^{-13} \text{ F. cm}^{-1}\right)$ [39].

Using the determined values of K^2 , the variation of α

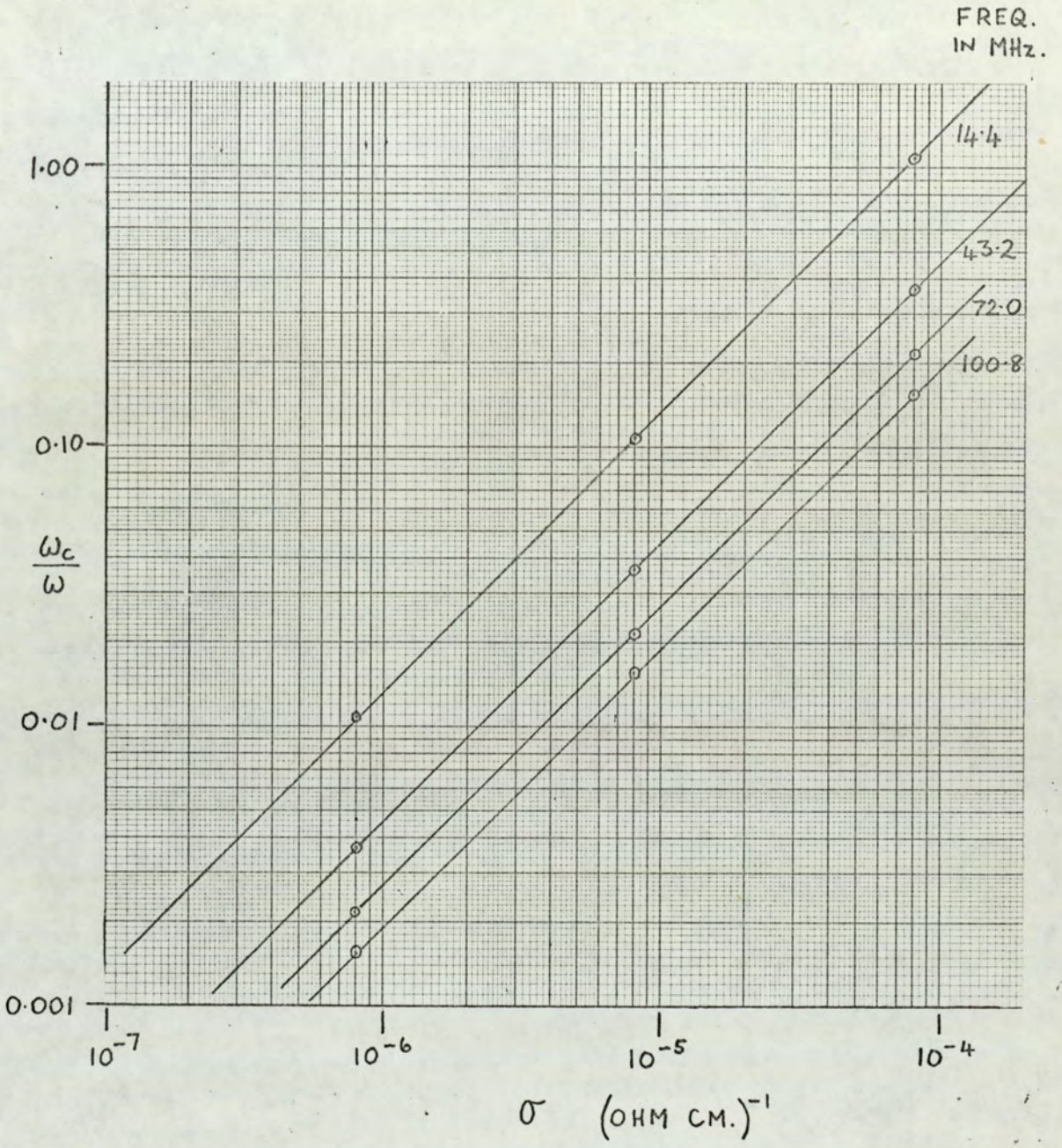

FIG. 40 $\frac{\omega_c}{\omega}$ VERSUS CRYSTAL CONDUCTIVITY

with $\frac{\omega_c}{\omega}$ was calculated using equation (5.1), to enable a comparison of theoretical and experimental attenuation coefficient over the experimental range of $\frac{\omega_c}{\omega}$ at each frequency. The theoretical variation of α is also plotted in figures 37 to 39. The value of ω_D used in the calculation of α from equation (5.1) was determined as indicated on page 60 using a value of 200 cm^2/volt sec. for drift mobility. This value of mobility was determined using the threshold field for acoustic amplification observed in the absence of any trapping or power effects.

5.2.2. The acoustoelectric voltage during acoustic transit.

In section 2.3 a theoretical description, derived using the Weinreich relationship, was given of the acoustoelectric voltage measured in the manner described in section 4.4.

An acoustic signal of a given input intensity Q_o watts cm^{-2} and finite width W, propagating through the crystal and being attenuated, was shown to result in an acoustoelectric voltage described by the following equations.

As the acoustic signal enters the crystal,

$$V_{ae.} = \frac{R_m}{K E_{th}} Q_o \left(1 - exp.(-2\alpha x_1)\right) \quad ----(5.3)$$

where X_1 is the distance from the input face of the crystal to the leading edge of the acoustic signal. If the crystal is attenuating the maximum of the acoustoelectric voltage is given by equation (5.3) with $X_1 = W$. This corresponds to the acoustic signal just within the crystal. As the acoustic signal propagates through the crystal it was shown that

$$V_{ae.} = \frac{R_m}{K E_{th}} Q_o \left(exp.(2\alpha W) - 1\right) exp.(-2\alpha x_1) \quad -----(5.4)$$

Acoustic reflection, occurring when $X_1 = L$, the crystal length, resulted in a predicted acoustoelectric voltage given by

$$V_{ae.} = \frac{R_m}{K E_{th}} Q_o e^{-2\alpha L} \left[\left(e^{2\alpha x_3} - 1 \right) - R \left(1 - e^{-2\alpha (w - x_3)} \right) \right] \quad --(5.5)$$

where X_3 is the width of the acoustic signal travelling in the positive X - direction during reflection, this being the acoustic propagation direction before reflection.

Equations (5.3) to (5.5) thus enable calculation of the acoustoelectric voltage during the propagation of an acoustic signal through the crystal. Figure 41 compares the predicted variation of acoustoelectric voltage with that observed for two values of attenuation coefficient at 45 MHz. The input acoustic intensity and the attenuation coefficient were determined experimentally as described in chapter 4. The threshold drift field, for the onset of acoustic amplification, was observed to be 870 volts cm^{-1}, and the acoustoelectric voltage was measured across 520 ohms.

For convenience, the equations used to calculate the acoustoelectric voltage have been derived in terms of the distance L, X and W, whilst the calculated values are plotted as a function of time. The conversion from one to the other involves the acoustic velocity only. Also, the value of reflection coefficient R, used to calculate the acoustoelectric voltage during the reflection period was assumed to be unity. This assumption is discussed in chapter 6. Figure 42 shows a qualitative comparison between theory and experiment for a high value of attenuation coefficient; that is, a high crystal conductivity.

The experimentally determined values of acoustoelectric voltage to be described with the crystal both attenuating and amplifying,

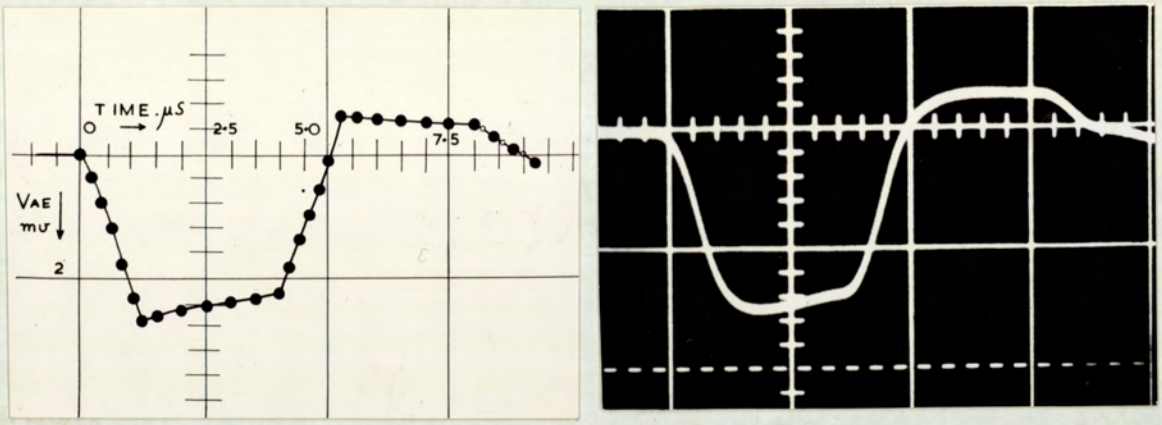

α = 1·0 DBS/L

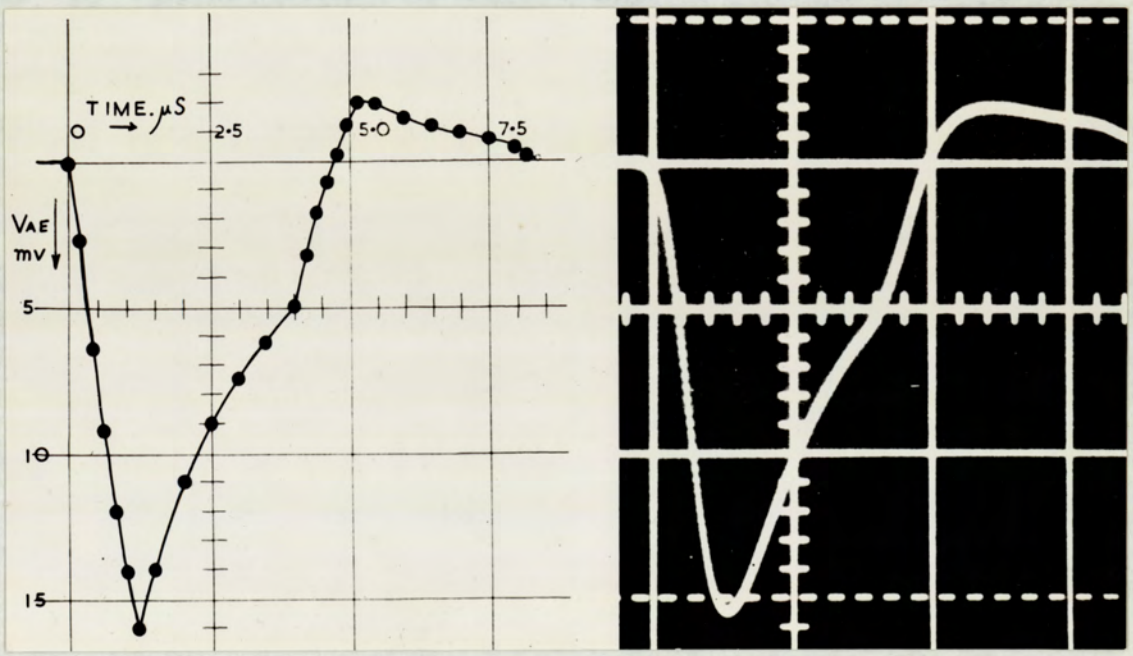

α = 7·5 DBS/L

GENERAL : Q_o = 0·16 WATT/SQ.CM

R_m = 520 OHMS.

$V_{D.C.}$ = 0. VOLTS.

ACOUSTIC FREQUENCY = 45 MHz.

FIG. 41. PREDICTED AND OBSERVED ACOUSTOELECTRIC VOLTAGE AS ACOUSTIC SIGNAL PROPAGATES THROUGH CRYSTAL.

(a)

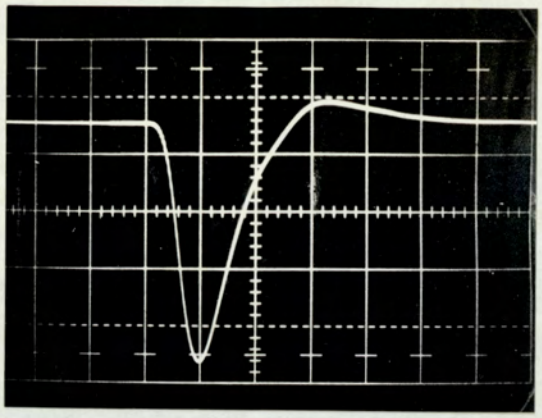

HORIZONTAL : 2·5 μs / SQ.

(b)

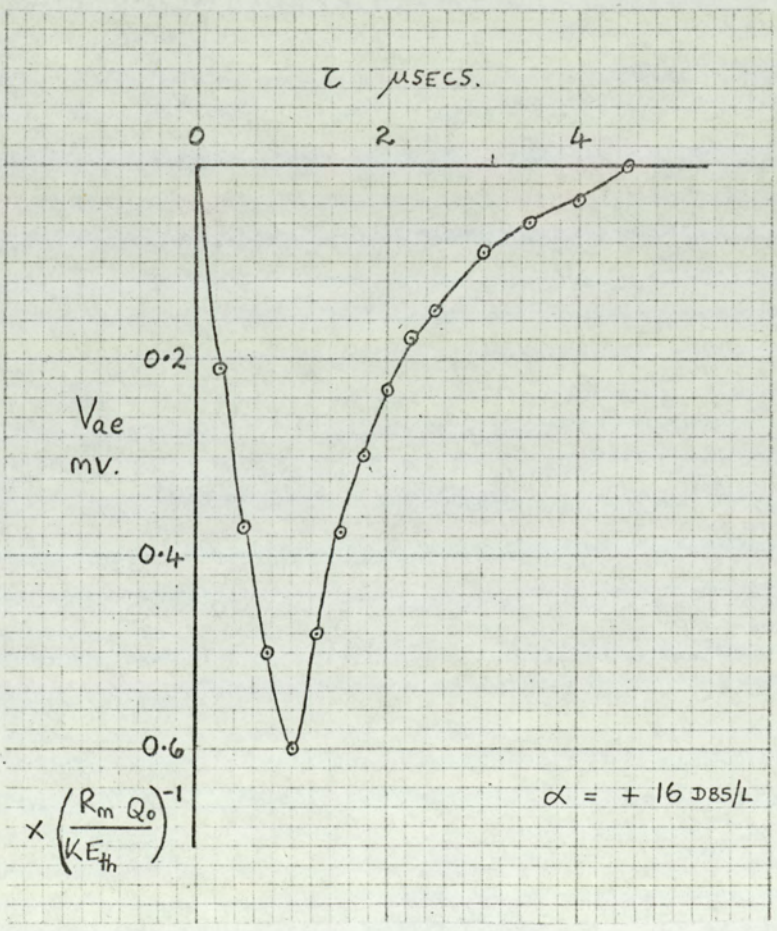

FIG 42 QUALITATIVE COMPARISON OF THEORY (b) AND EXPERIMENT (a) FOR A LARGE ATTENUATION COEFFICIENT

where not specified as a function of time as in figures 40 and 41, were all measured at the maximum value. Under attenuating conditions this corresponds to the acoustic signal just within the crystal, and comparison of these results with theory is made using equation (5.3) with $X_1 = W$. Under amplifying conditions, the equation used to calculate the acoustoelectric voltage was equation (5.4), with $X_1 = L$ and α negative, and this corresponds to the leading edge of the acoustic signal having just completed a single acoustic transit.

To emphasise the advantage of using an input acoustic signal of half height width less than the acoustic transit time of the medium figure 43 shows an acoustoelectric voltage trace obtained for an input acoustic signal of 40 μsecs duration. Although the initial maximum may be used to determine the acoustoelectric voltage due to an acoustic signal travelling in the forward direction, the displayed acoustoelectric voltage thereafter, describes the effect of acoustic propagation in both directions, and may not be interpreted as simply as for a small width signal. Furthermore, if a small width acoustic input is used, a comparison between theory and experiment of that part of the acoustoelectric voltage trace due to the propagation of the acoustic signal through the crystal after its introduction into the crystal, gives some indication of the uniformity of the attenuation throughout most of the crystal. This information cannot be so obtained from using an input acoustic signal of duration greater than the crystal transit time.

The following sub-sections compare the experimental and theoretical variation of acoustoelectric voltage with input acoustic intensity and acoustic pulse width. A graph giving the value of the exponential factor $\left[1 - \exp.(-2\alpha w)\right]$ appearing in equation (5.3) for $X_1 = W$, was used extensively during the calculation of the expected acoustoelectric voltage and is given as figure 44(a).

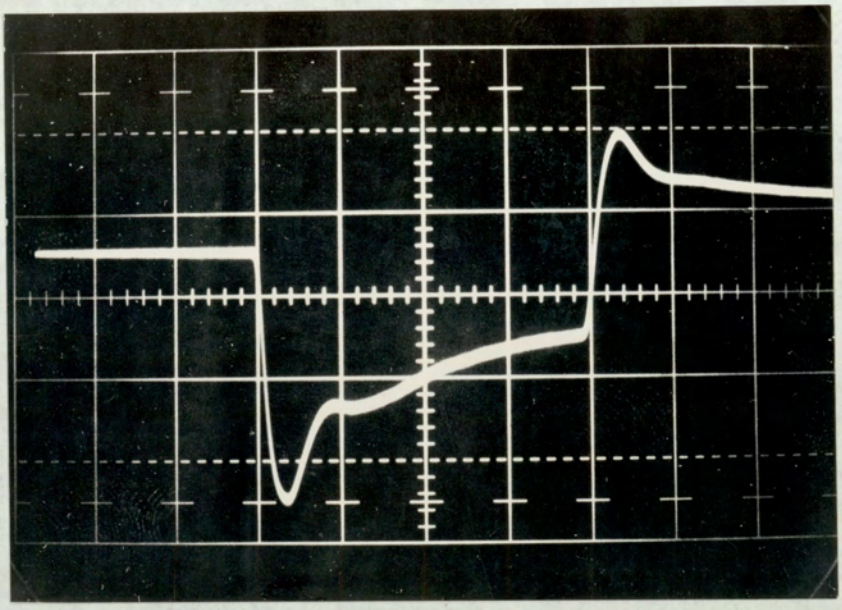

HORIZONTAL : 10 μSECS / SQUARE.

DURATION OF INPUT ACOUSTIC SIGNAL = 40 μsecs.

CRYSTAL TRANSIT TIME = 4 μsecs.

FIG. 43. ACOUSTOELECTRIC VOLTAGE GENERATED BY AN ACOUSTIC SIGNAL OF DURATION MUCH GREATER THAN THE ACOUSTIC TRANSIT TIME OF THE CRYSTAL

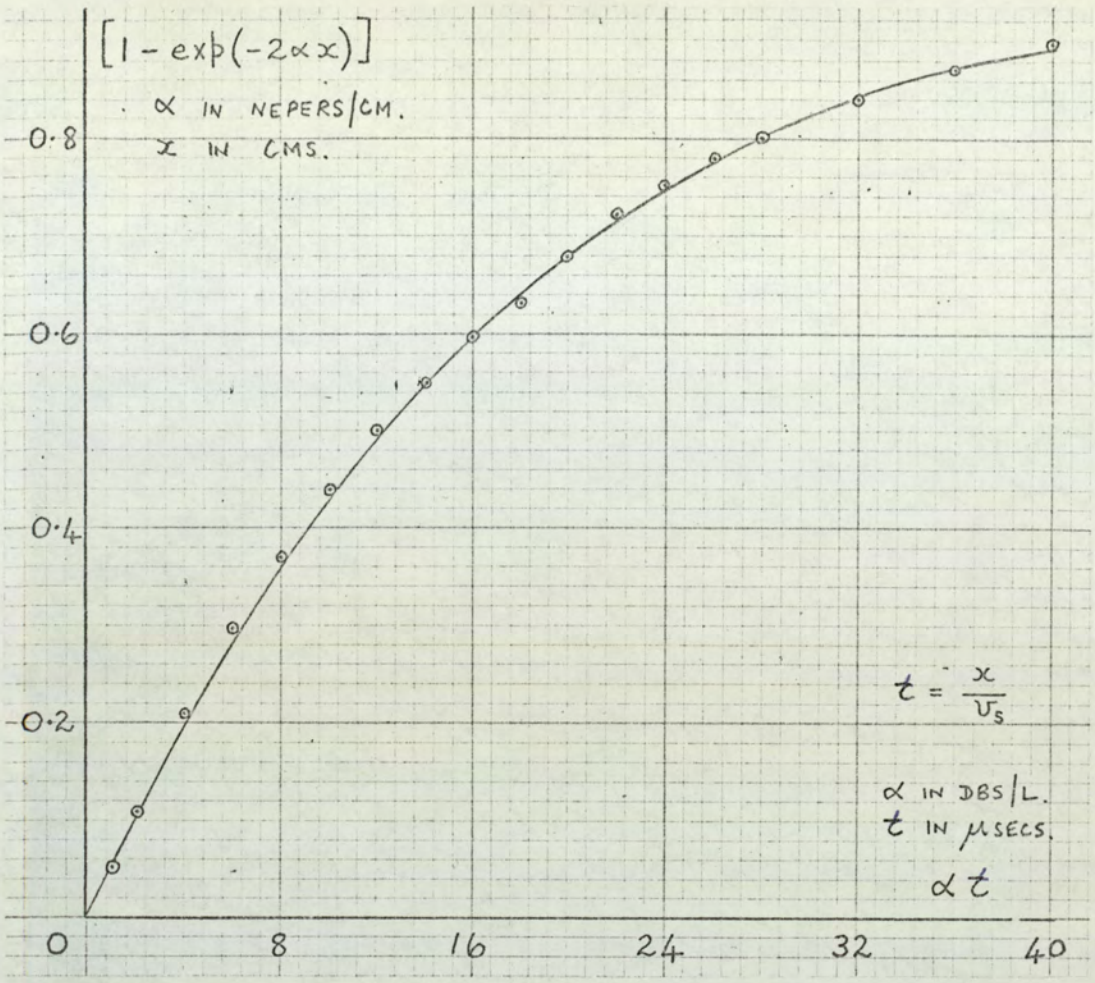

(a)

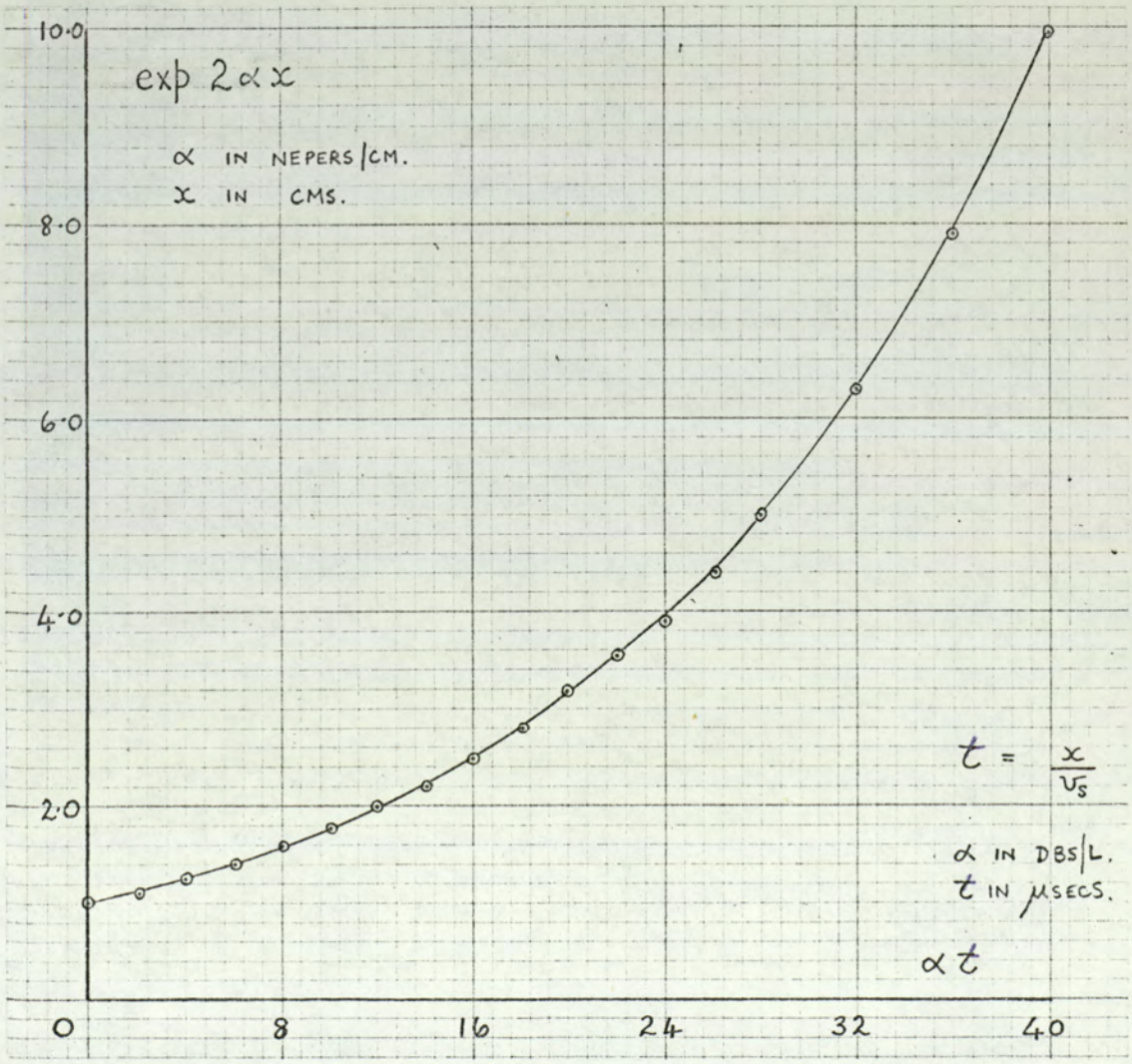

(b)

FIG 44 GRAPHS FOR V_{AE} CALCULATION

This calibration graph gives the value of the exponential factor, for α expressed in nepers/cm. and W in cms. as a function of the product of α as measured, in dbs/crystal length and t, the width of the acoustic signal within the crystal expressed in microseconds. Figure 44(b) enables the exponential factor (exp $2\alpha L$) to be determined similarly. This positive exponential factor is included in the equations describing the acoustoelectric voltage under amplifying conditions, and will be referred to later.

5.2.3. The variation of acoustoelectric voltage with input acoustic intensity

The variation of acoustoelectric voltage and attenuation coefficient with input acoustic intensity was measured for several crystal conductivities, at each of the four acoustic frequencies indicated in table 1, and the results are compared with theory in figures 45 to 48. For small input acoustic intensities, the attenuation coefficient was found to be independent of input intensity and remained a constant. At large acoustic inputs however, the attenuation coefficient was observed to decrease. At each acoustic frequency, the slope of the experimental curves over the input acoustic intensity range where the attenuation coefficient remains a constant, is seen to be unity as predicted by equation (5.3). The reduction in slope at high input intensities is due to the decrease in attenuation coefficient, and good agreement between theory and experiment is maintained by taking this decrease into account. This is particularly noticeable with the results obtained at 45 MHz. Although it would seem that quantitative agreement is poor at acoustic frequencies other than 45 MHz, the qualitative variation of the acoustoelectric voltage as a function of input acoustic intensity, at each frequency, is as predicted. The direct proportionality between the measured acoustoelectric voltage and the input acoustic intensity has been usefully exploited to assess relative acoustic intensity input to the crystal, as described in

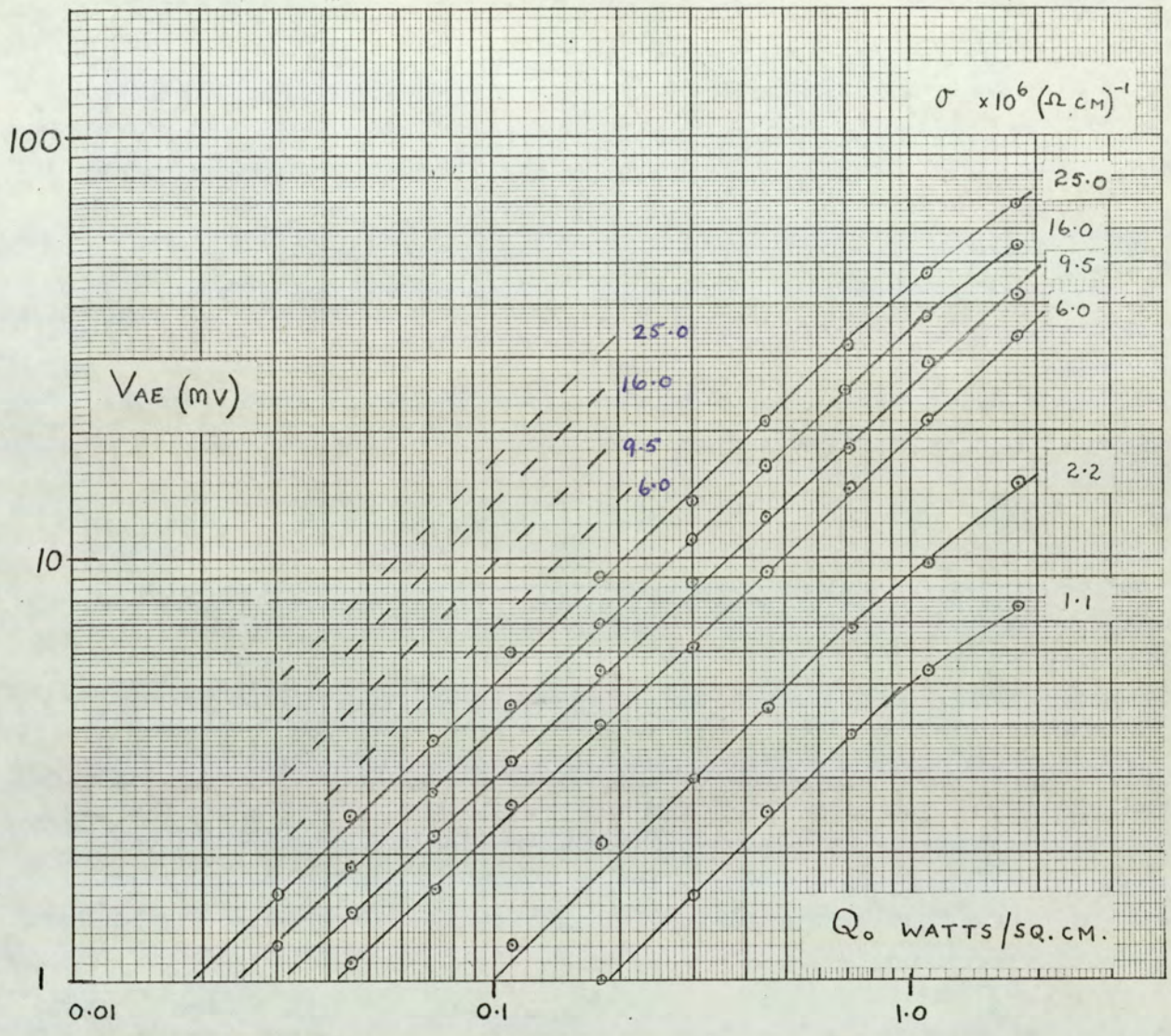

σ (Ω CM)⁻¹ x10⁶	α DBS/L
1·1	1·0
2·2	2·0
6·0	5·0
9·5	8·0
16·0	12·0
25·0	18·0

⊙——⊙ OBSERVED

– – – PREDICTED

FIG 45 ACOUSTOELECTRIC VOLTAGE VERSUS INPUT ACOUSTIC INTENSITY NO D.C. VOLTAGE APPLIED - 15 MHz.

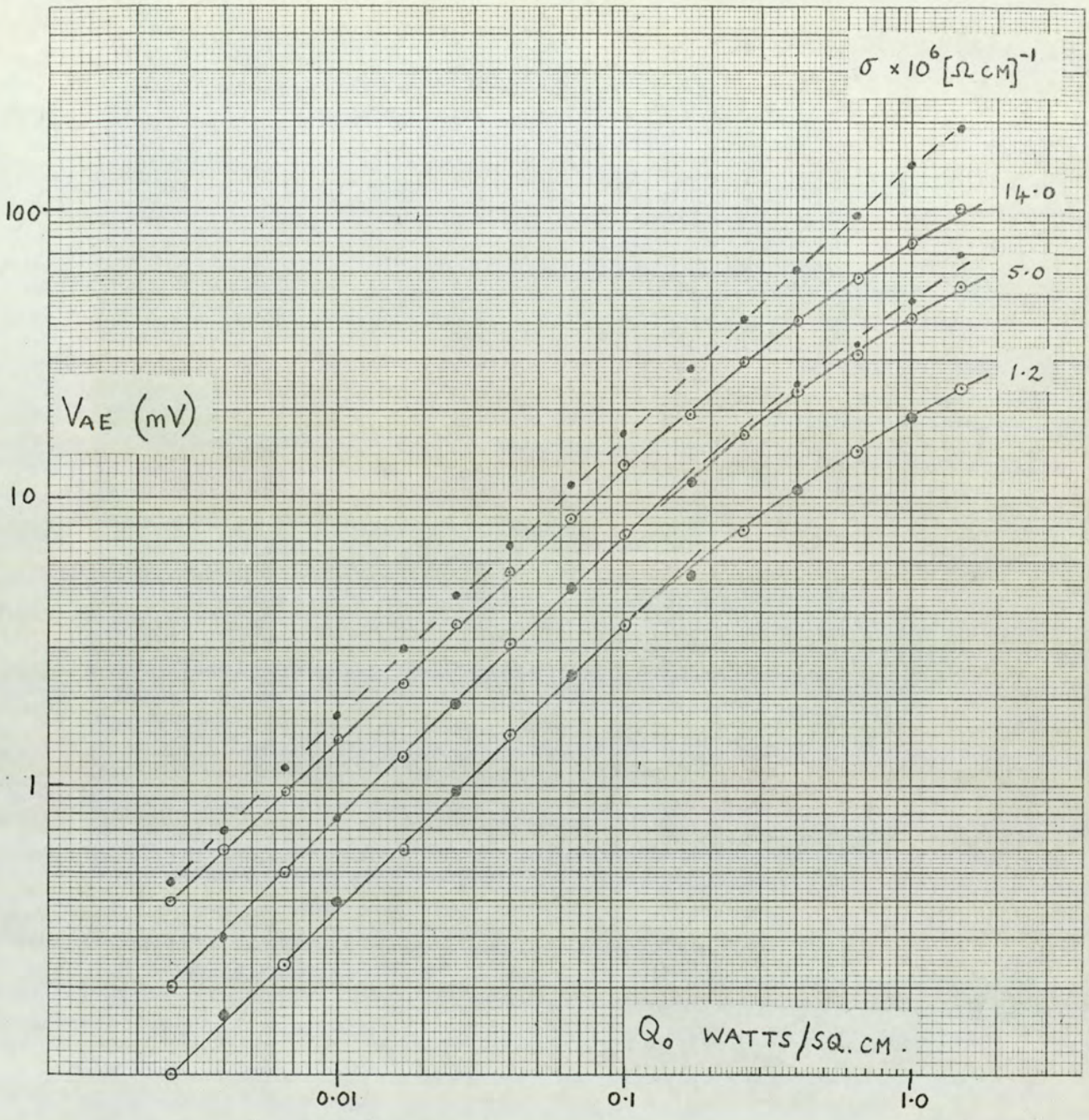

σ $(\Omega\,\mathrm{CM})^{-1}$ $\times 10^6$	α DBS/L
1·2	2·0
5·0	5·0
14·0	15·0

OBSERVED

PREDICTED

FIG. 46 ACOUSTOELECTRIC VOLTAGE VERSUS INPUT ACOUSTIC INTENSITY NO D.C. VOLTAGE APPLIED. — 45 MHz.

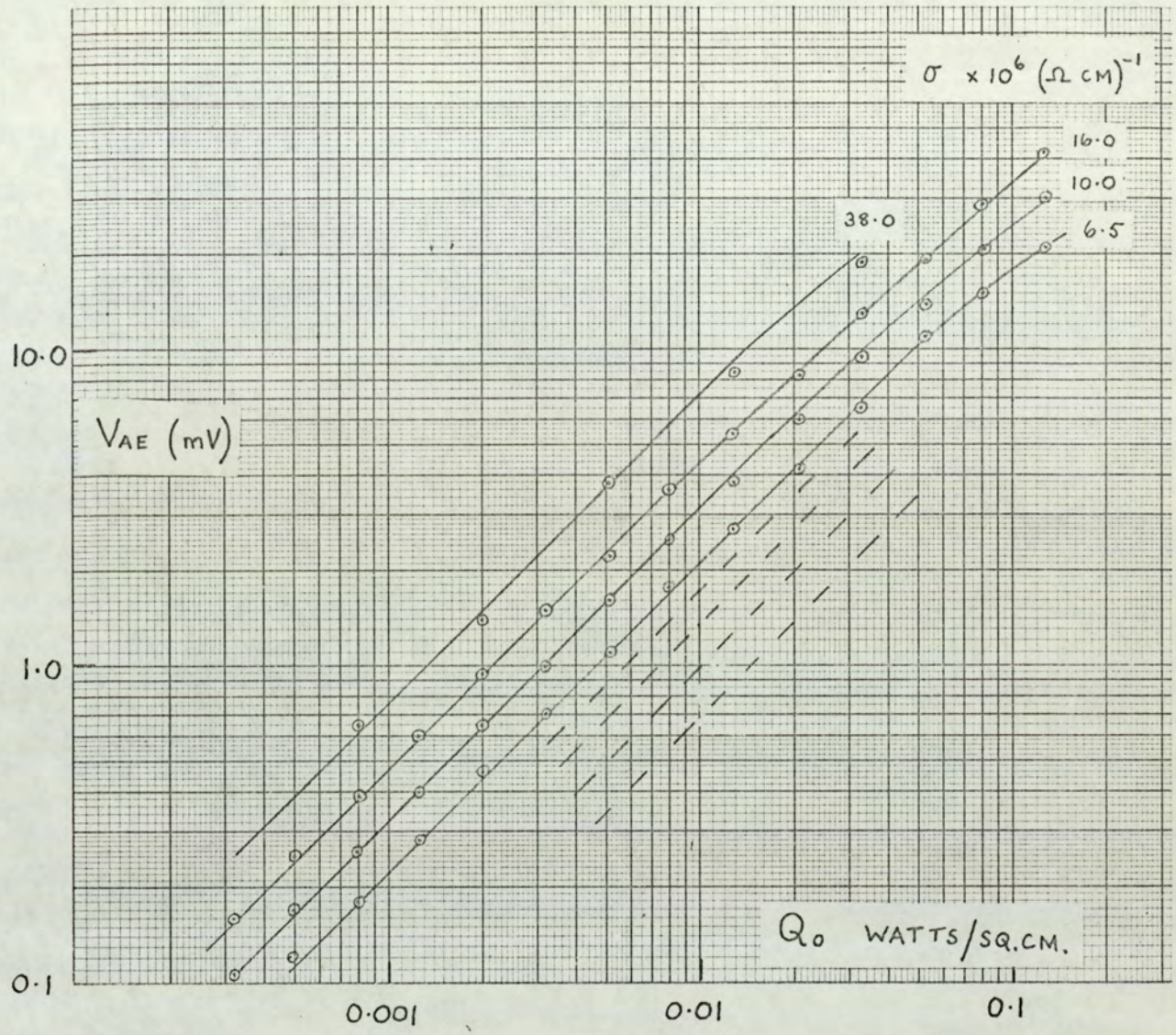

σ $(\Omega\,cm)^{-1}$ x 10^6	α DBS/L
6·5	5·0
10·0	8·0
16·0	12·0
38·0	18·0

⊙——⊙ OBSERVED

– – – PREDICTED

FIG 47. ACOUSTOELECTRIC VOLTAGE VERSUS INPUT ACOUSTIC INTENSITY. NO D.C. VOLTAGE APPLIED. – 75 MHz.

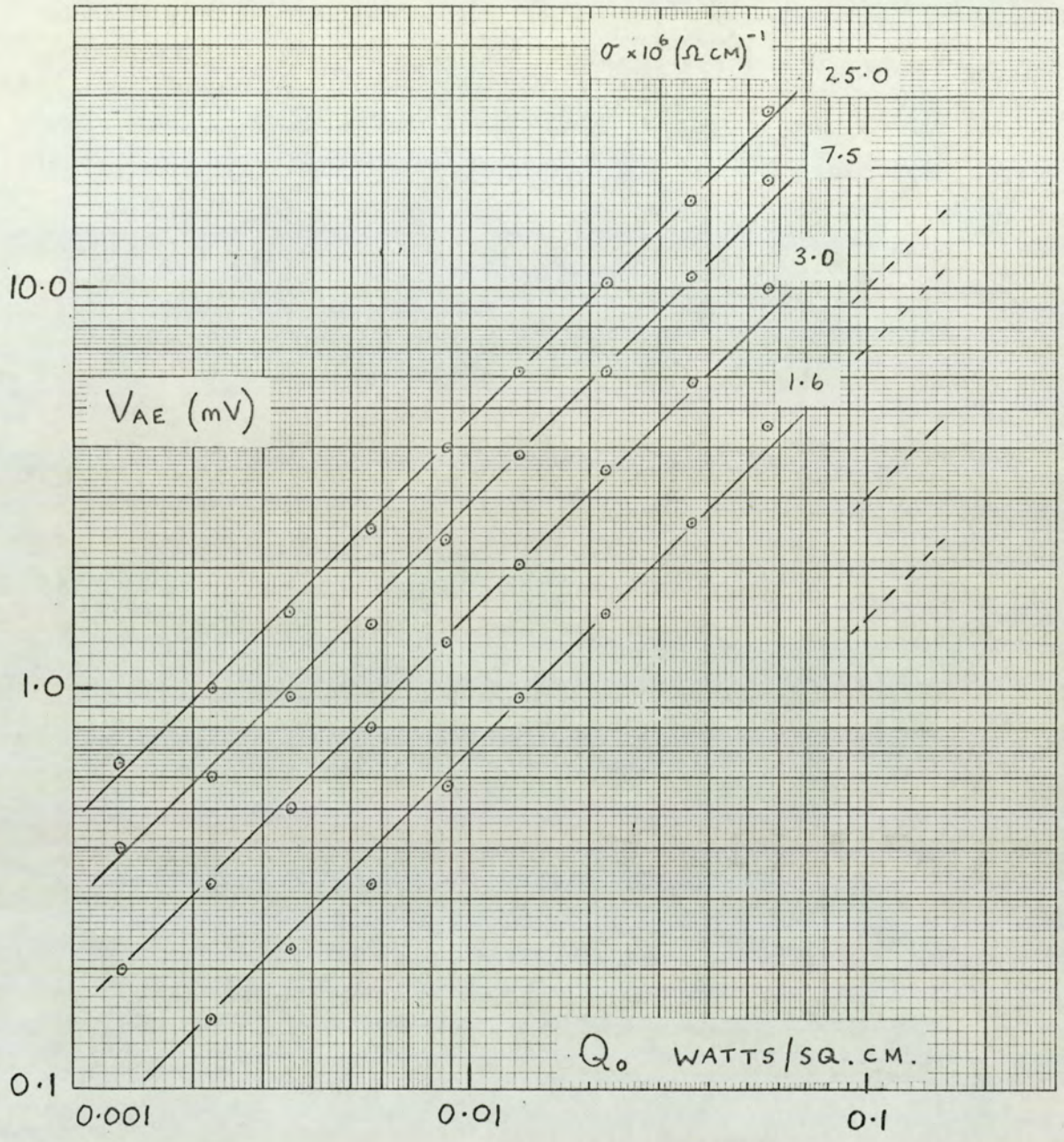

$\sigma\ (\Omega\,cm)^{-1} \times 10^6$	α DBS/L
1·6	1·0
3·0	2·0
7·5	5·0
25·0	8·0

FIG. 48. ACOUSTOELECTRIC VOLTAGE VERSUS INPUT ACOUSTIC INTENSITY NO D.C. VOLTAGE APPLIED - 105 MHz.

chapter 4.

5.2.4. The variation of acoustoelectric voltage with input acoustic pulse width.

Equation (5.2) indicates a dependence of $V_{ae.}$ on pulse width W. To investigate this the acoustoelectric voltage was measured as a function of acoustic signal width for several crystal conductivities at 45 MHz. The experimental and corresponding theoretical results are given in figure 49. The pulse width was determined as the half height width since the generated r.f. pulses were not truly rectangular. A typical example of an input acoustic packet is shown in figure 78(a). For each pulse width, the peak to peak amplitude of the input r.f. was adjusted to be the same, thus ensuring that the input acoustic intensity remained a constant. It was noted however, that with the crystal in the dark, altering the r.f. pulse width from its minimum value of 0.5 μsec, though keeping the peak to peak amplitude a constant, resulted in a small change in displayed height of the single transit signal. This was considered to be due to the transducer response to the different width signals. The acoustic intensity graphs of figures 33 to 36 were obtained using an input acoustic signal of 1 μsec half height width. Accordingly, a note was made of the change in displayed first echo height for differing pulse widths and a correction made to the value of input power used in the calculations for acoustic pulse widths other than 1 μsec. It was assumed that the change in height of the first echo expressed in dbs was due equally to each transducer, and the input acoustic intensity correction was thus half the observed change in dbs.

The total response of the transducers to various width acoustic signals is shown in figure 50, where the output signal measured for a given input signal width is related to the output signal using a 1 μsec input signal width.

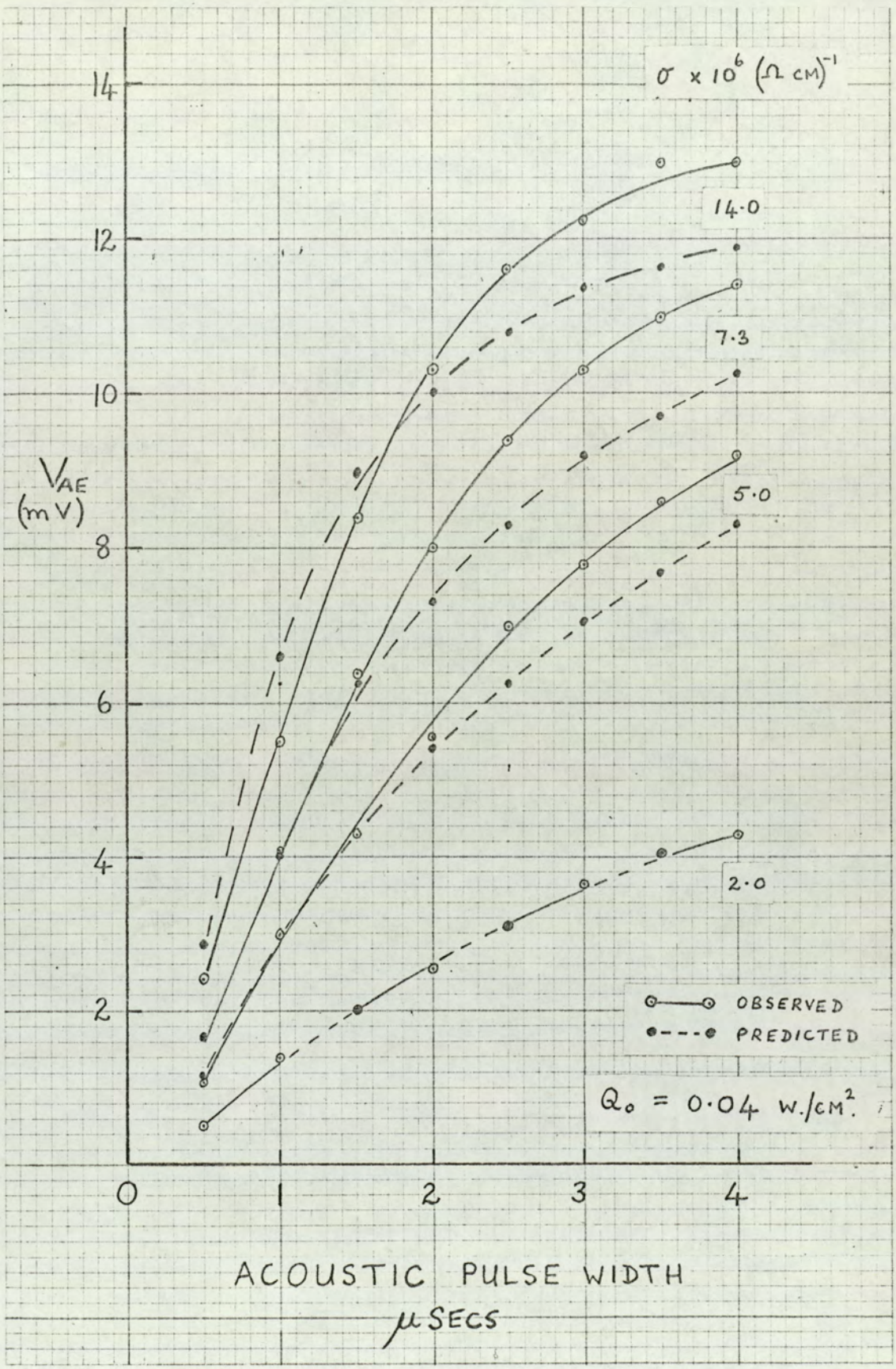

FIG 49. ACOUSTOELECTRIC VOLTAGE VERSUS INPUT ACOUSTIC SIGNAL WIDTH. NO APPLIED D.C. VOLTS - 45 MHz.

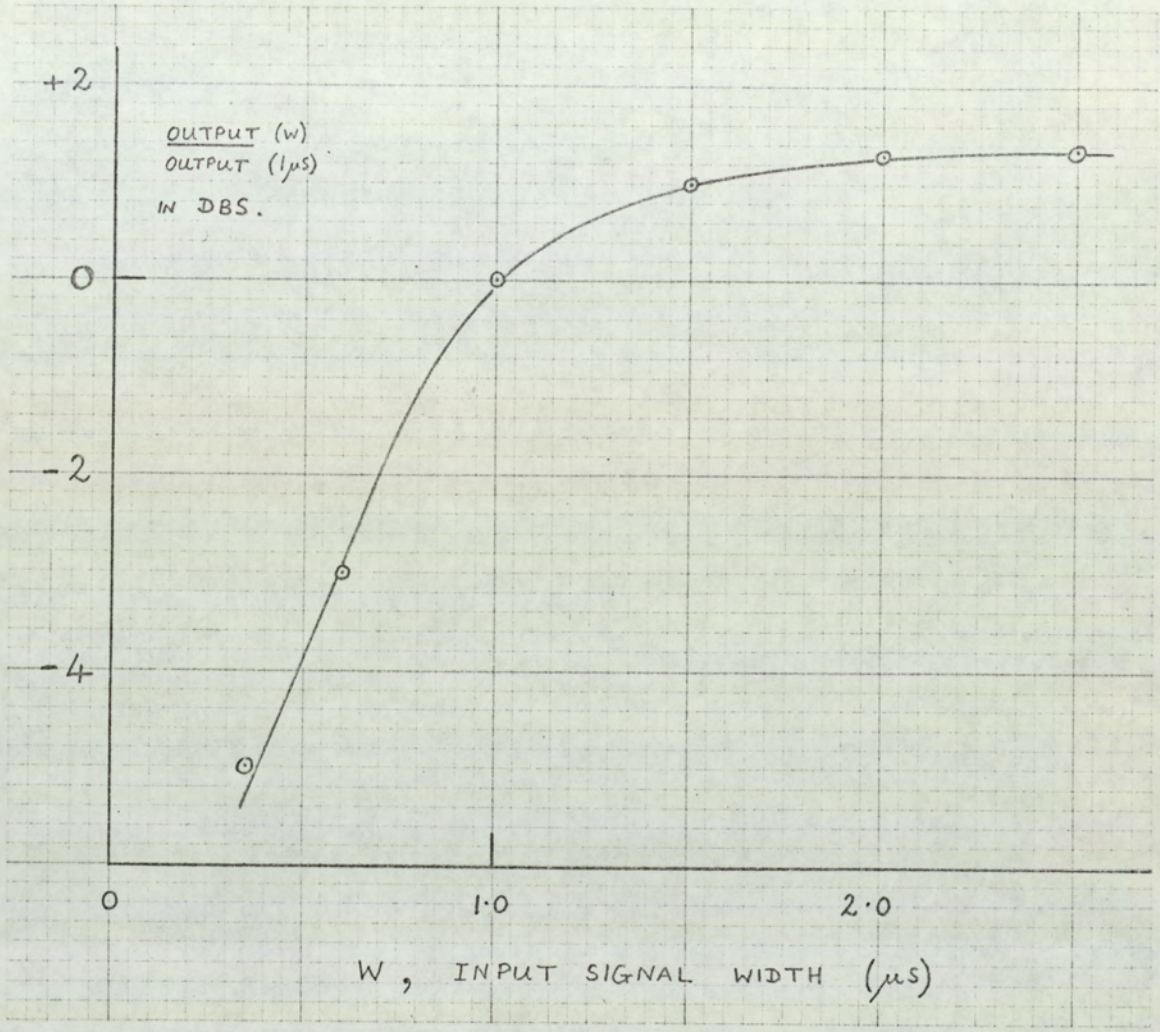

FIG. 50. TRANSDUCER RESPONSE TO ACOUSTIC SIGNALS OF VARIOUS WIDTHS - RELATED TO A 1μsec. WIDTH.

The variation of acoustoelectric voltage with input signal width shown in figure 49 is typical, and qualitatively similar results were obtained at other frequencies.

5.2.5. A note on the experimental results obtained at 75 MHz and 105 MHz.

Although a full discussion of all the results will be given in chapter 6, the quantitative discrepancy already indicated by the results at 75 MHz. and 105 MHz. demand preliminary discussion here.

The results indicate the measured acoustoelectric voltage to be several times larger than that predicted. An examination of equation (5.2) which was used to calculate the acoustoelectric voltage indicates the following sources of possible error.

a) Determination of the factor $\frac{R_m}{K E_{th}}$.

b) Determination of the attenuation coefficient.

c) Input acoustic intensity determination.

These were carefully checked several times and the following conclusions were drawn from this assessment of the possible sources of error.

5.2.5.1. The determination of the factor $\frac{R_m}{KE_{th}}$

The value of K, which relates the crystal conductivity to the crystal resistance was considered to be a fixed constant for all experimental work. This constant was determined from the crystal length and d.c. contact area, neither of which is a function of acoustic frequency.

The value of R_m was chosen to be 520 ohms and this resistor, placed in series with the crystal allows the measurement of the acoustoelectric voltage. At both 75 MHz. and 105 MHz. the effective value of the resistance across which the acoustoelectric voltage was measured, was checked by shunting R_m with 50 ohms, and comparing the measured acoustoelectric voltage with that previously obtained. At

each frequency the ratio of the two measurements, for a given set of applied conditions was about 10 as expected. Thus the value of 520 ohms for R_m was considered appropriate.

The threshold field E_{th}, was checked for small acoustic inputs at various crystal conductivities. This was observed to be 870 volts/cm. at both 75 MHz. and 105 MHz., in agreement with the previously used value.

In conclusion the anomalous results were not considered to arise from the calculation of the factor $\frac{R_m}{KE_{th}}$. The experimental error involved in the evaluation of this factor was also considered to be very small.

5.2.5.2. Acoustic attenuation determination.

The dependence of the calculated acoustoelectric voltage on the attenuation coefficient is given by the factor $\left(1 - e^{-2\alpha w}\right)$ appearing in equation (5.3) The maximum possible value this factor may take is unity when, theoretically, the attenuation coefficient would be infinite. Reference to figure 44(a) indicates that if the attenuation coefficient were determined to be say, 5 dbs/L for a 1 μsec half height width input acoustic signal, then $\left(1 - e^{-2\alpha w}\right) = 0.25$. In order that this factor is some four times bigger the effective attenuation coefficient would then have to be extremely large. Indeed, for measured attenuation coefficients above 5 dbs/L, the discrepancies are too large for a possible error in attenuation measurement to be the sole cause.

A more sophisticated check on the determination of attenuation coefficient is afforded by noting the shape of the acoustoelectric voltage display. Qualitatively, the rate at which the acoustoelectric voltage is reduced, as the input acoustic signal propagates through the crystal is indicative of the acoustic attenuation coefficient. As figure 41 (a) indicates, a low attenuation coefficient results in rather a flat acoustoelectric voltage trace corresponding to

acoustic propagation through the crystal. As the attenuation coefficient increases, the rate of change of acoustoelectric voltage increases, figure 41 (b), and for a high acoustic attenuation the displayed acoustoelectric voltage trace becomes very pointed as illustrated by figure 42. For a given crystal conductivity, and thus, attenuation coefficient, the acoustoelectric voltage display shape was not changed much by altering the input acoustic intensity; only the magnitude changed.

The crystal conductivity was adjusted so that the measured attenuation was the same at each acoustic frequency, and the displayed acoustoelectric voltage shape was observed. The only significant discrepancy to be noted was that whilst the shape was quite similar at 15 MHz, 45 MHz and 75MHz, a much larger attenuation coefficient than that measured was indicated at 105 MHz. The acoustoelectric voltage shape was seen to be much more spiky at this frequency, than that observed at the other frequencies. The crystal conductivity was then reduced until the acoustoelectric voltage shape at 105 MHz. was similar to those previously noted at the other frequencies. The attenuation coefficient was again measured and found to be only 4 dbs/L whereas the measured attenuation resulting in the same acoustoelectric voltage shape at the other acoustic frequencies was 8 dbs/L.

This investigation was cursary and the theory developed in chapter 2 really allows a more quantitative approach. However, the discrepancies noted at 75 MHz. and 105 MHz. were too large to be entirely attributed to an error in the determination of attenuation coefficient. Therefore, the investigation was not pursued in detail. The results did serve to indicate that at 105 MHz some of the disagreement between the calculated acoustoelectric voltage and that observed may be due to an anomaly in attenuation measurement. It should be emphasised that the method of measuring the attenuation

coefficient, as described in section 4.3, and as used throughout the experimental work is not suspect. The variation of acoustoelectric voltage with input acoustic intensity at 75 MHz. and 105 MHz. given in figures 47 and 48 show the disagreement to be unaffected by crystal conductivity.

The overall conclusion must be that the discrepancy arises from an error in the input acoustic intensity determination.

5.2.5.3. The determination of input acoustic intensity at 75 MHz. and 105 MHz.

The conclusion reached at the end of the previous section is most unwelcome since it casts doubt on the method of intensity determination described in section 4.5., although the results obtained at 45 MHz. would seem to testify as to the accuracy of this method. A comprehensive check was therefore carried out into every stage of the acoustic intensity measurement at 75 MHz. and 105 MHz.

The frequency response of the oscilloscope used to display the peak to peak voltage of the input and output r.f. signal, as described by figure 31. was checked and found to be as previously determined and given by figure 28 (b). The insertion loss of the attenuator A1 on the signal input side of the crystal was measured and determined to be 0.2 db at 75 MHz and 0.5 db at 105 MHz in reasonable agreement with the manufacturer's specification (see section 4.2.2.2.). The acoustoelectric voltage display was measured using the type 1A1 plug-in of a type 547 Tektronix oscilloscope and was found to agree with that obtained using the 1A7 differential amplifier plug-in.

Various lead lengths on the input and output side of the transformer assemblies were tried without any change in either the input peak to peak r.f. signal or the output r.f. signal. A stub tuner was inserted in the input and output line and tuned for maximum transmission without producing any change in the maximum

input and output r.f. signals, and therefore without providing any justification for a different insertion loss determination. This itself was checked several times at each acoustic frequency by completely off tuning the matching transformers and then retuning for maximum transmission as indicated in section 4.2.2.4.

A review of the input acoustic intensity determination indicated that if an error of the required magnitude were present then the measurement of peak to peak voltage of both the input and output r.f. signal would have to be about one half the true value. On the other hand, if the overall error were entirely attributed to an error in measuring the output signal amplitude, then this error would be of the order of 12 dbs. Such an error would certainly have been identified by the careful and systematic checks carried out.

Thus the conclusions are somewhat contradictory. All experimental evidence points to an error in input intensity determination whilst the checks carried out to determine this error have proved negative. The major experimental work has been carried out at 15 MHz. and 45 MHz. and lack of time has resulted in this disagreement observed at the higher frequencies remaining unexplained.

One possibility which has not been pursued is that the output r.f. signal measured with the crystal in the dark, and used to determine the insertion loss of the matching transformers and associated transducers has been correctly measured, but does not give a true indication of the insertion loss. In determining the input acoustic intensity it was assumed that the acoustic attenuation of the dark crystal was negligible, and thus, the total measured insertion loss was attributed to the transformers and transducers only. However, if the dark attenuation of a 75 MHz. and 105 MHz. acoustic signal is not negligible, then the measured insertion loss should be shared between the transformers, transducers and crystal. If the

crystal is not credited with its share of the total insertion loss, then the determined insertion loss of each transformer and associated transducer would be too large. This would then result in a calculated value of the input acoustic intensity which was smaller than the true value. The acoustoelectric voltages calculated using these acoustic intensities would then be smaller than expected.

This has been a tentative suggestion which would seem to offer a possible explanation of the observed disagreement.

5.2.6. Concluding remarks

The results obtained with no applied d.c. voltage largely indicate a good qualitative agreement with theory. Quantitatively, the results obtained at 15 MHz. indicate the Weinreich relationship to predict a larger acoustoelectric voltage than that actually measured. However, a discussion of this, without first presenting the results obtained with the crystal amplifying at this frequency will be seen to be premature.

The results at 45 MHz. indicate excellent quantitative agreement between theory and experiment. The variation of acoustoelectric voltage with input acoustic intensity, pulse width and time all agree well with theory.

The results at 75 MHz. and 105 MHz. have already received some discussion, and it was concluded that the disagreement between theory and experiment - a disagreement considered to be due to an error in the input acoustic intensity determination - had not been satisfactorily identified. The results of the investigation into the disagreement did suggest, however, that the measurement of input and output peak to peak r.f. amplitude leading to acoustic intensity determination, was, in itself correct. Rather, the discrepancy arose from an appreciably reduced output peak to peak r.f. signal, probably due to anomalous attenuation during acoustic propagation through the dark crystal.

The results obtained with a d.c. field applied to the crystal will now be presented.

5.3. Experimental results with a drift voltage applied to the crystal.

5.3.1. General acoustoelectric behaviour

The acoustic attenuation coefficient and the acoustoelectric voltage were measured simultaneously over a wide and comprehensive range of input acoustic intensity and crystal conductivity with various applied d.c. voltages at 15 MHz and 45 MHz. Similar results, though of a less comprehensive nature, were obtained at 75 MHz.

Figure 51 presents the variation of output acoustic intensity as a function of input acoustic intensity with d.c. voltages applied to the crystal within the range zero to 1000 volts, and for a given crystal conductivity at an acoustic frequency of 15 MHz. These results, and similar results to follow are described as the input-output characteristics. The output signal has been measured relative to the dark level signal output as described in section 4.3. and both the input and output are plotted in dbs. The input acoustic intensity corresponding to a particular db. setting of the attenuator A1 on the input side of the crystal may be obtained from figure 33. The procedure to obtain the results of figure 51 was as follows.

The system was first tuned for maximum acoustic transmission and the acoustic intensity calibration graph shown in figure 33 was checked to be valid. With the crystal unilluminated and with no d.c. voltage applied, the db. setting of the input attenuator A1 was then altered in steps of five dbs. and the output attenuator setting was adjusted to maintain the same display height of the single transit acoustic echo. This technique has been explained in detail in section 4.3. The output attenuator setting was plotted against the input attenuator setting over a wide range of input acoustic

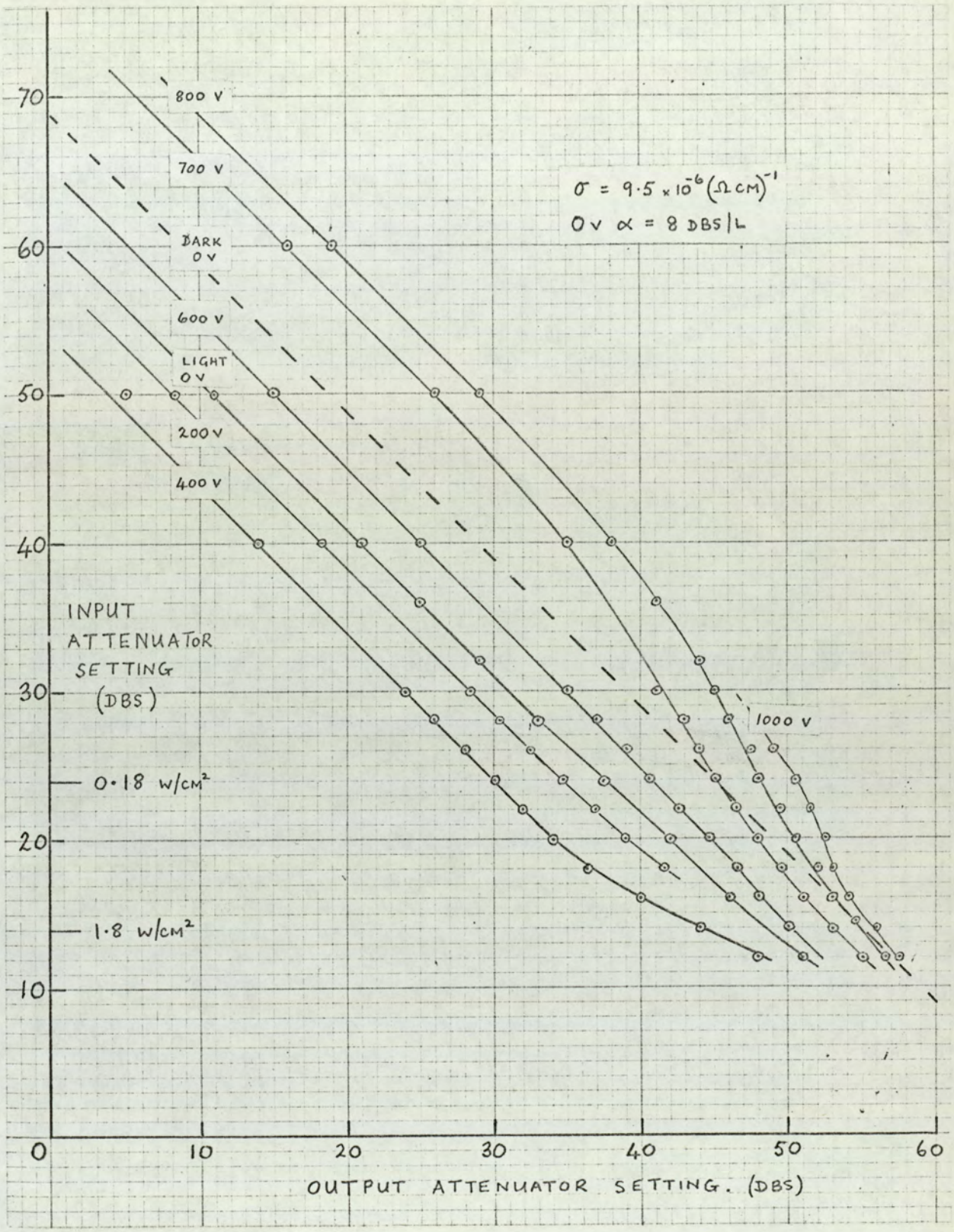

FIG. 51. INPUT - OUTPUT CHARACTERISTICS

15 MHz . $\sigma = 9{\cdot}5 \times 10^{-6}\ (\Omega\ \mathrm{cm})^{-1}$

intensity and this plot constituted the dark level plot shown by the dashed line in figure 51 et seq. The crystal was then illuminated to result in a given attenuation of a small acoustic input, and the crystal conductivity measured in the manner described in section 5.2.1. and checked against the attenuation - conductivity graph of figure 37(a). Various d.c. voltages were applied to the crystal and, for each applied voltage, the setting of the output attenuator necessary to maintain the reference display height of the first received acoustic echo over a large range of input attenuator settings was noted, and plotted against the input attenuator settings. In figure 51, for example, 400 volts applied to the crystal and an input signal corresponding to the 40 dbs. Setting of the input attenuator, resulted in an output signal which was displayed as a 3 cm high echo on the 2 vol:/cm range of the oscilloscope, when the db. setting of the output attenuator was 14 dbs. Comparison with the dark level db. setting of the output attenuator corresponding to the same input intensity enables the accustic attenuation to be determined for that particular input power, under the specified applied conditions of illumination and d.c. voltage. For the example considered the attenuation is seen to be 15 dbs/L (L is the acoustic transit length of the crystal). Note that in figure 51 the measured attenuation is independent of input acoustic intensity for small acoustic inputs since the input-output curves at the various applied voltages are parallel to the dark level plot. In the case of large acoustic inputs however, which correspond to a small number of dbs. in the input attenuator, the output signal becomes power dependent and both attenuation and amplification are seen to be reduced. The acoustic crossover, indicated in figure 51 by the intersection of any of the curves with the dark level line, is also seen to be strongly affected by input acoustic intensity and the applied d.c. voltage necessary for crossover is seen to increase as the input acoustic intensity is increased.

Figure 52 presents the acoustoelectric voltage measured simultaneously, under the same applied conditions as for figure 51. Thus figures 51 and 52 present the measured attenuation coefficient and acoustoelectric voltage as a function of input acoustic intensity and applied d.c. voltage for one crystal conductivity at 15 MHz. Figures 53 and 54, 55 and 56 present similar results obtained at two different crystal conductivities.

Three general observations may be concluded from these results. A comparison of figures 51, 53 and 55 indicates larger power effects at higher crystal conductivities. The amplification is also seen to be greater. The acoustoelectric voltage is greater under amplifying conditions than for attenuating conditions. Equation 5.4. predicts this for $X_1 = L$ and α negative, by the presence of the positive exponential factor, $exp.(2\alpha L)$. This factor is absent in equation (5.3) which predicts the acoustoelectric voltage under attenuating conditions. This is clearly illustrated in figure 57 where for a given input acoustic intensity, Q_o, the predicted acoustoelectric voltage is plotted as a function of positive and negative attenuation coefficient. Note that the acoustoelectric voltage scale for a negative attenuation coefficient is different by a factor of one thousand, to the corresponding scale for positive attenuation. Also note that the predicted acoustoelectric voltage increases more rapidly as α increases for amplification than for attenuation. For this reason it will be apparent that when the crystal is attenuating a measurable acoustoelectric voltage is generated for large input intensities only. This, unfortunately, has meant that in many cases the acoustoelectric voltage could not be measured for small input acoustic signals when the crystal was in an attenuating condition. Consequently, most of the reported acoustoelectric voltage measurements have been obtained for those input intensities

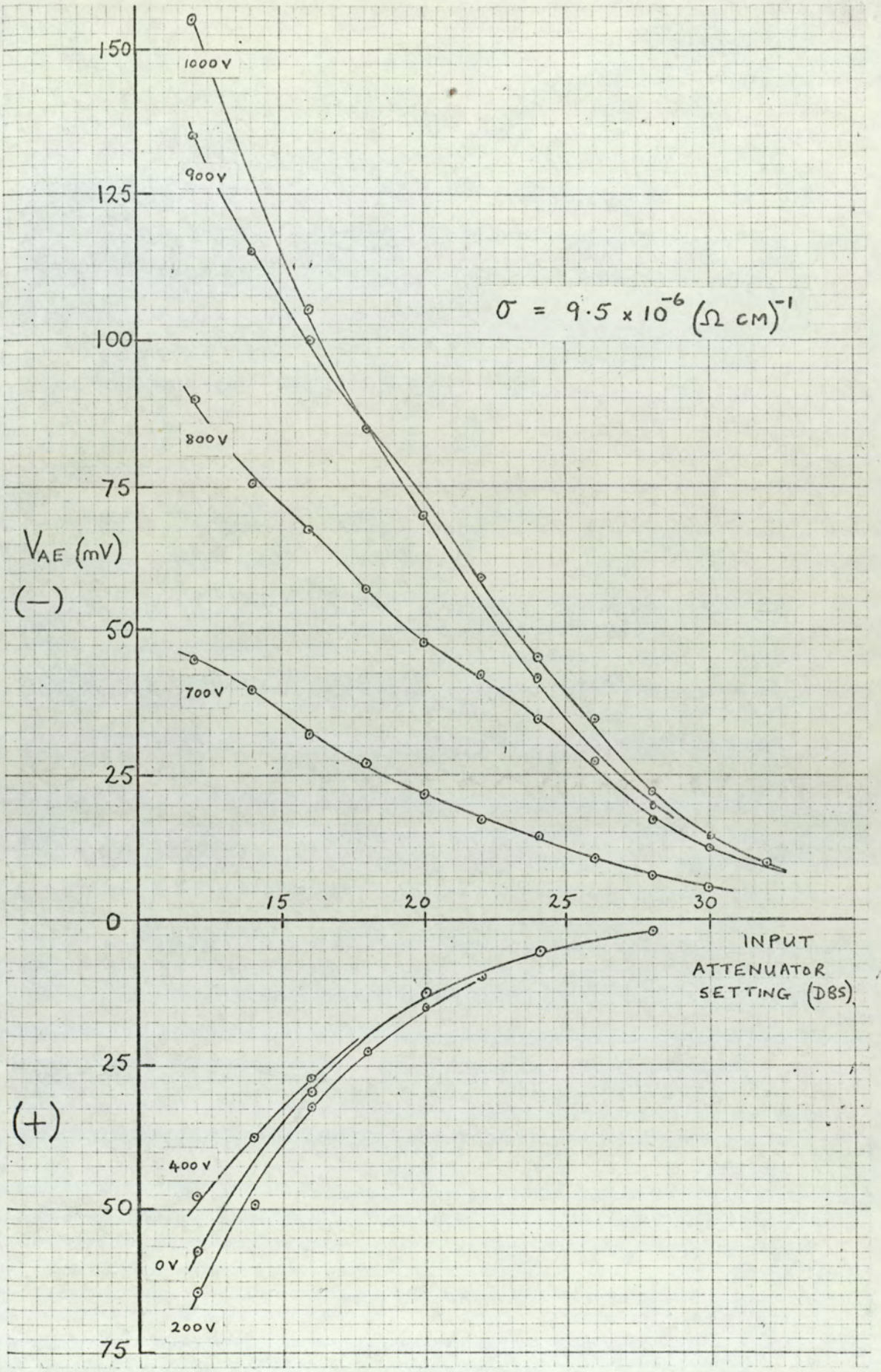

FIG 52. ACOUSTOELECTRIC VOLTAGE VARIATION . 15 MHz. - $\sigma = 9.5\ 10^{-6} (\Omega cm)^{-1}$

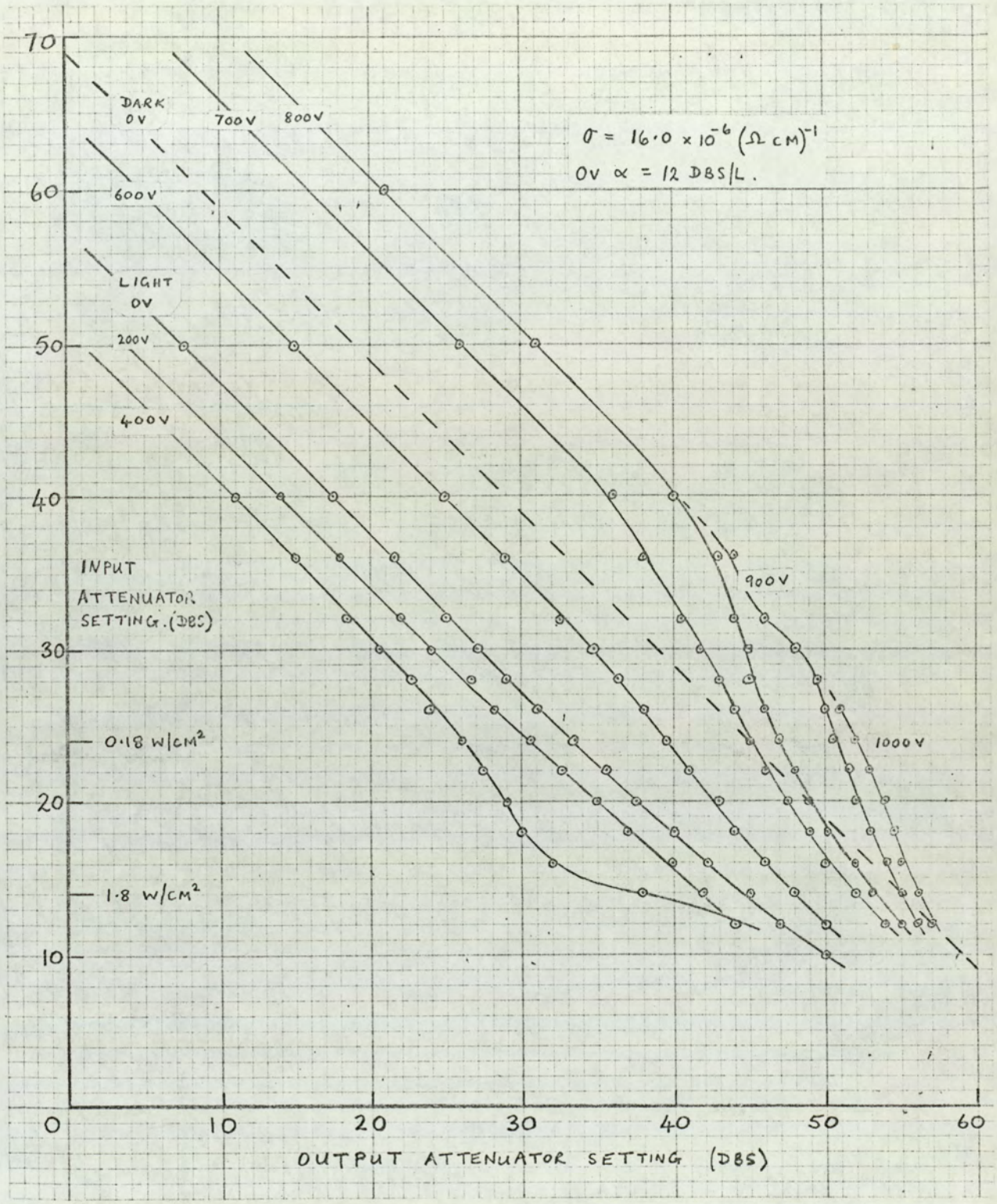

FIG. 53. INPUT - OUTPUT CHARACTERISTICS

15 MHz. $\sigma = 16{\cdot}0 \times 10^{-6}\ (\Omega\ \mathrm{CM})^{-1}$

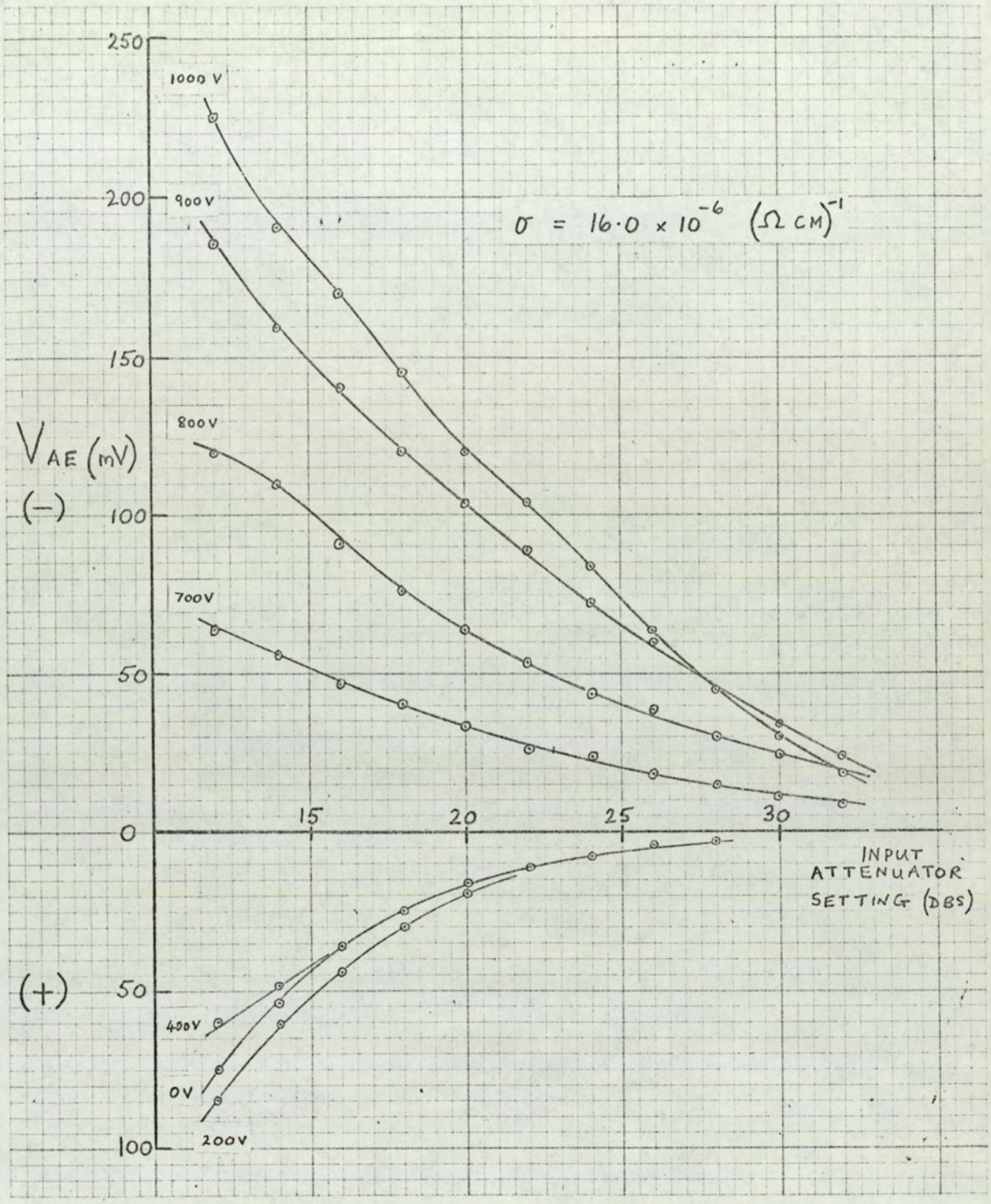

FIG. 54. ACOUSTOELECTRIC VOLTAGE VARIATION. 15 MHz. $\sigma = 16{\cdot}0\ 10^{-6}(\Omega CM)^{-1}$

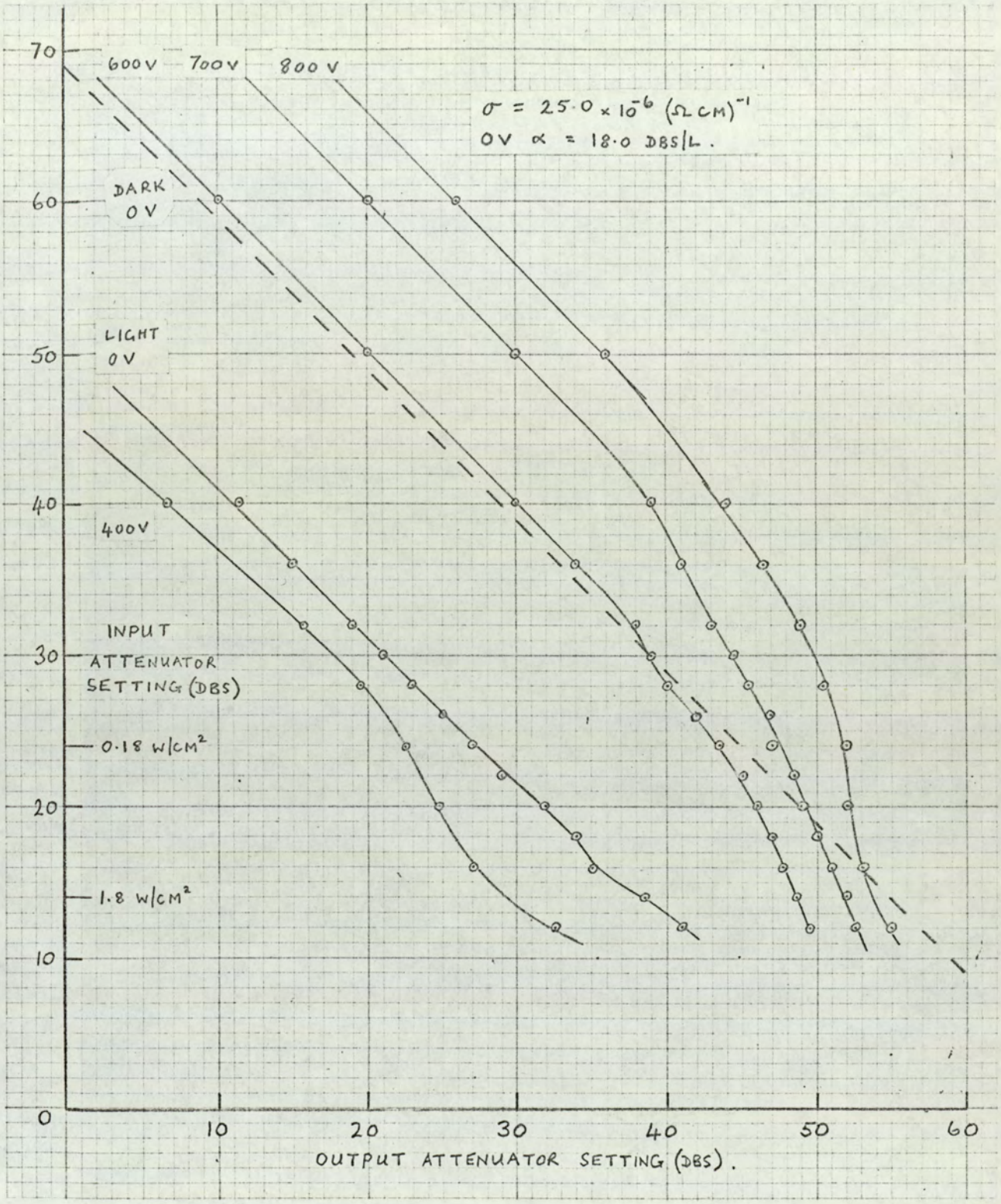

FIG. 55. INPUT - OUTPUT CHARACTERISTICS

15 MHz. $\sigma = 25{\cdot}0 \times 10^{-6}\ (\Omega\,\mathrm{cm})^{-1}$

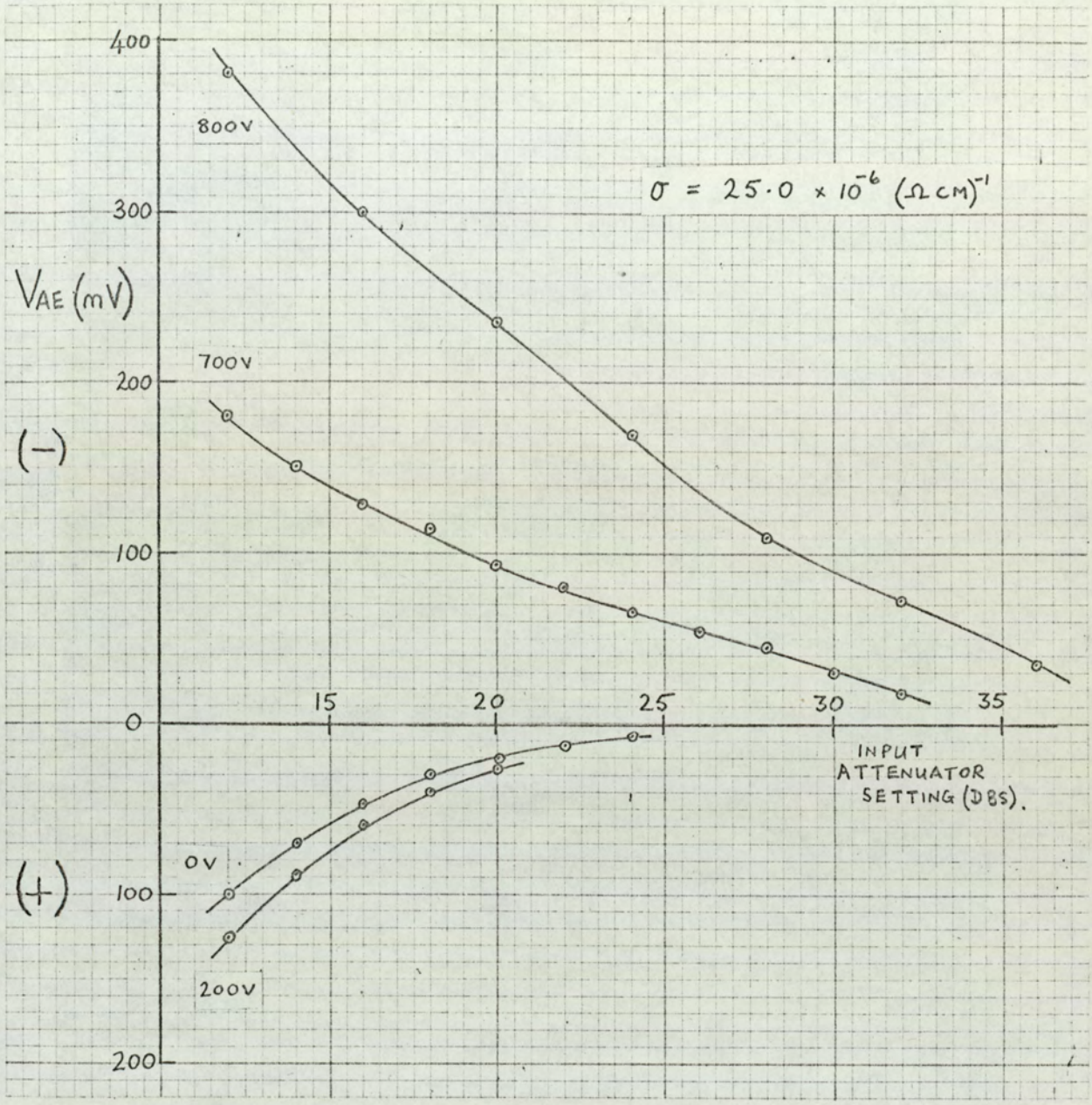

FIG. 56. ACOUSTOELECTRIC VOLTAGE VARIATION. 15 MHz. $\sigma = 25.0\ 10^{-6}\ (\Omega CM)^{-1}$

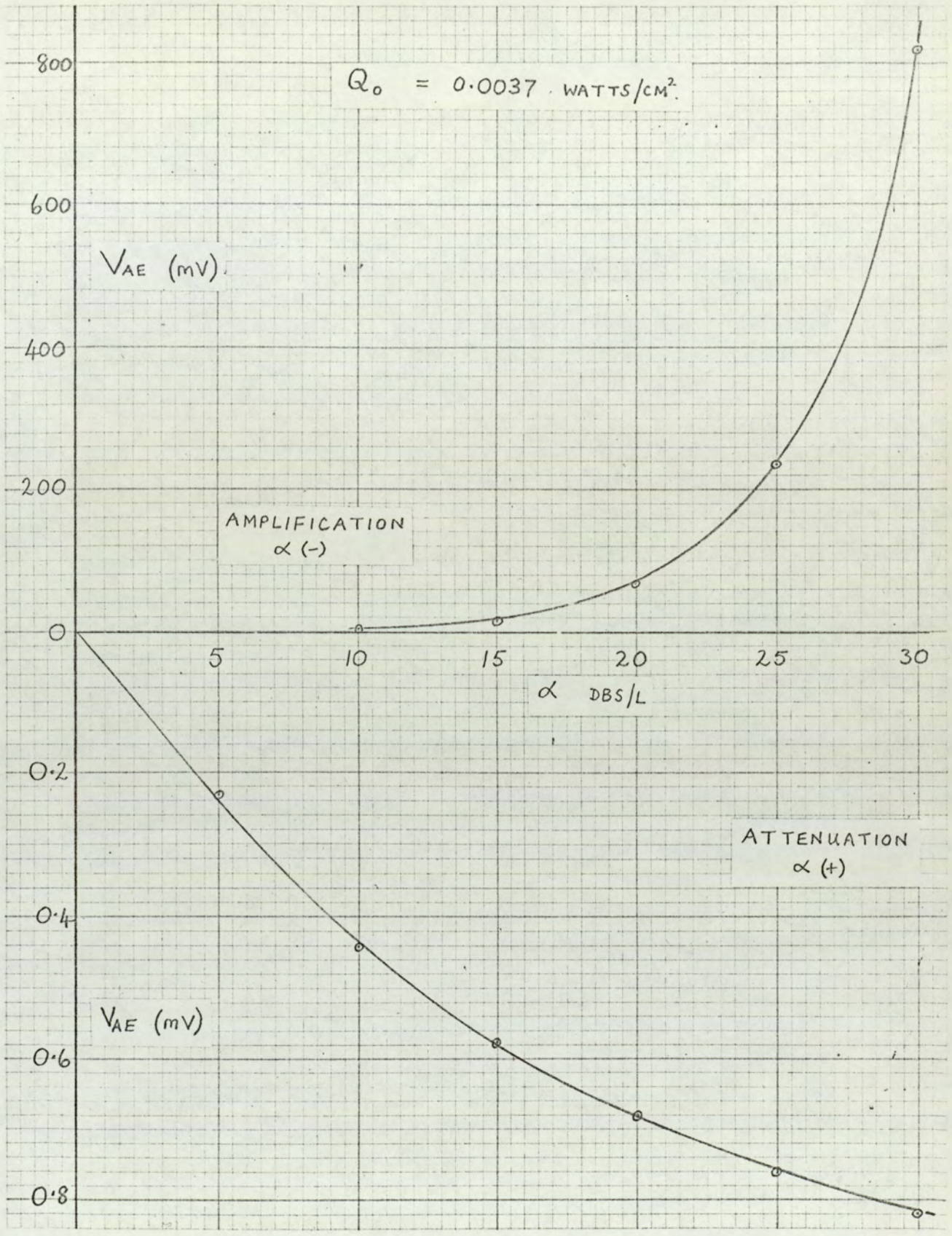

FIG. 57. PREDICTED ACOUSTOELECTRIC VOLTAGE AS A FUNCTION OF BOTH POSITIVE AND NEGATIVE ATTENUATION COEFFICIENTS.

where non-linear acoustoelectric behaviour has been noted. Sufficient evidence will be presented however establishing the validity of the Weinreich relationship for small input signals.

Returning to the general results given in figures 51 to 56, it is possible to compare the measured acoustoelectric voltage under a given set of applied conditions to that calculated using either equation (5.3) or (5.4), depending on whether the crystal is attenuating or amplifying. It is also possible to calculate what attenuation coefficient would be required for a given set of applied conditions to result in the measured acoustoelectric voltage. Typical results are presented in figures 58 to 61. The measured values of attenuation coefficient and acoustoelectric voltage have been taken from figures 53 and 54. In figure 58 the solid line in the top graph gives the measured attenuation coefficient as a function of input acoustic intensity. The input acoustic intensity increases as the input attenuator setting becomes smaller. The solid line in the lower graph records the simultaneously measured acoustoelectric voltage. Reference to the operating information given in figure 58 indicates the applied d.c. voltage to be 200 volts, and the same information given by the solid curves of figure 58 may be found in figures 53 and 54 for an applied voltage of 200 volts over the relevant input acoustic intensity range indicated in figure 58. The dashed line of the upper graph in figure 58 records the calculated attenuation coefficient which theoretically should result in the measured acoustoelectric voltage given in the lower graph. The dashed line of the lower graph records the calculated acoustoelectric voltage which theoretically is consistent with the measured attenuation coefficient given in the top graph. Figure 59 describes a similar comparison between theory and experiment with 400 volts applied to the crystal. Figures 58 and 59 indicate that the measured acoustoelectric voltage is smaller than that predicted by theory for the measured attenuation coefficients, and that a much

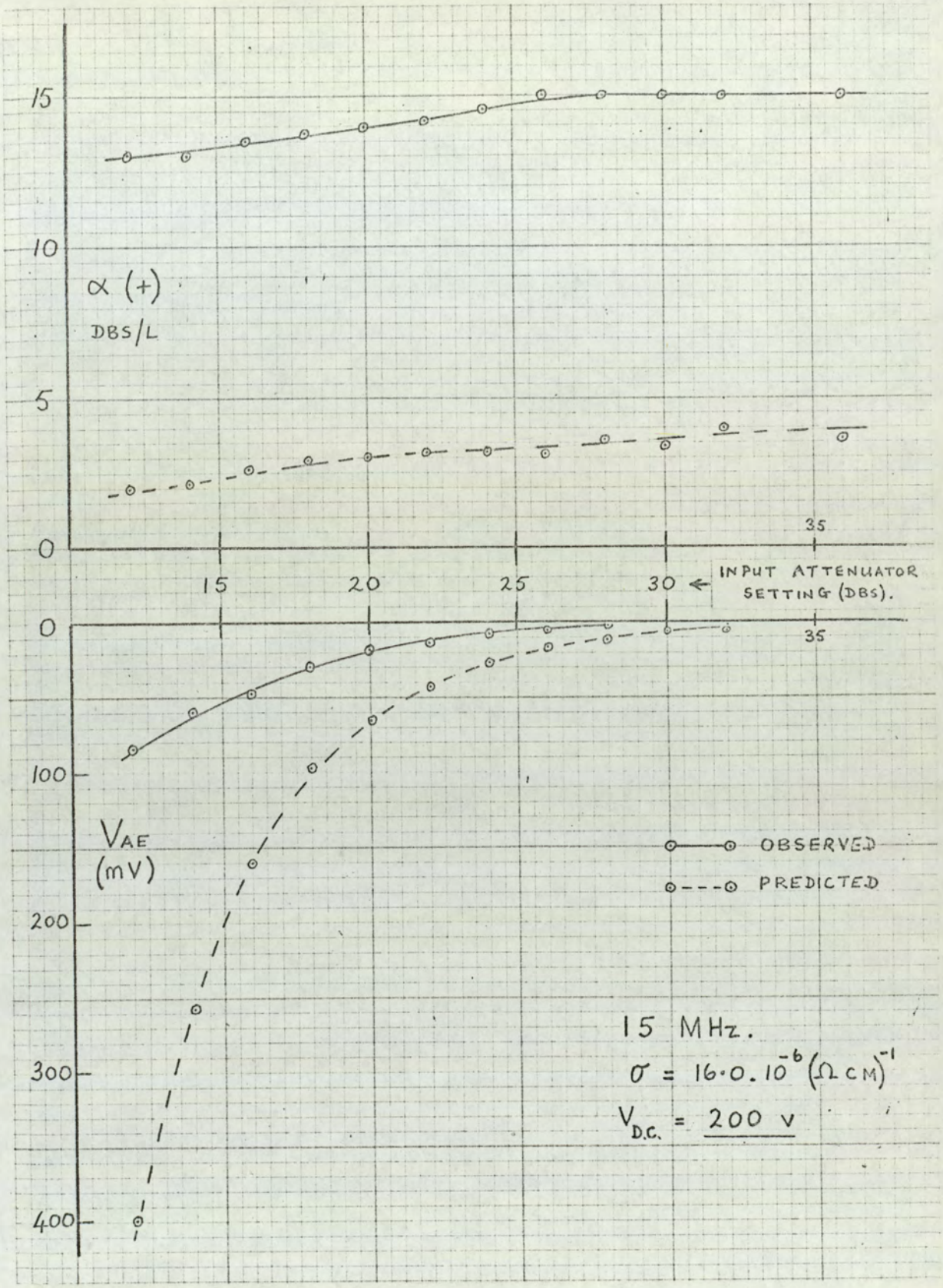

FIG. 58. EXPERIMENTAL AND CORRESPONDING THEORETICAL VALUES OF ATTENUATION COEFFICIENT AND ACOUSTOELECTRIC VOLTAGE 15 MHz. $\sigma = 16.0\ 10^{-6}(\Omega\,\mathrm{cm})^{-1}$. $V_{DC} = 200$ V

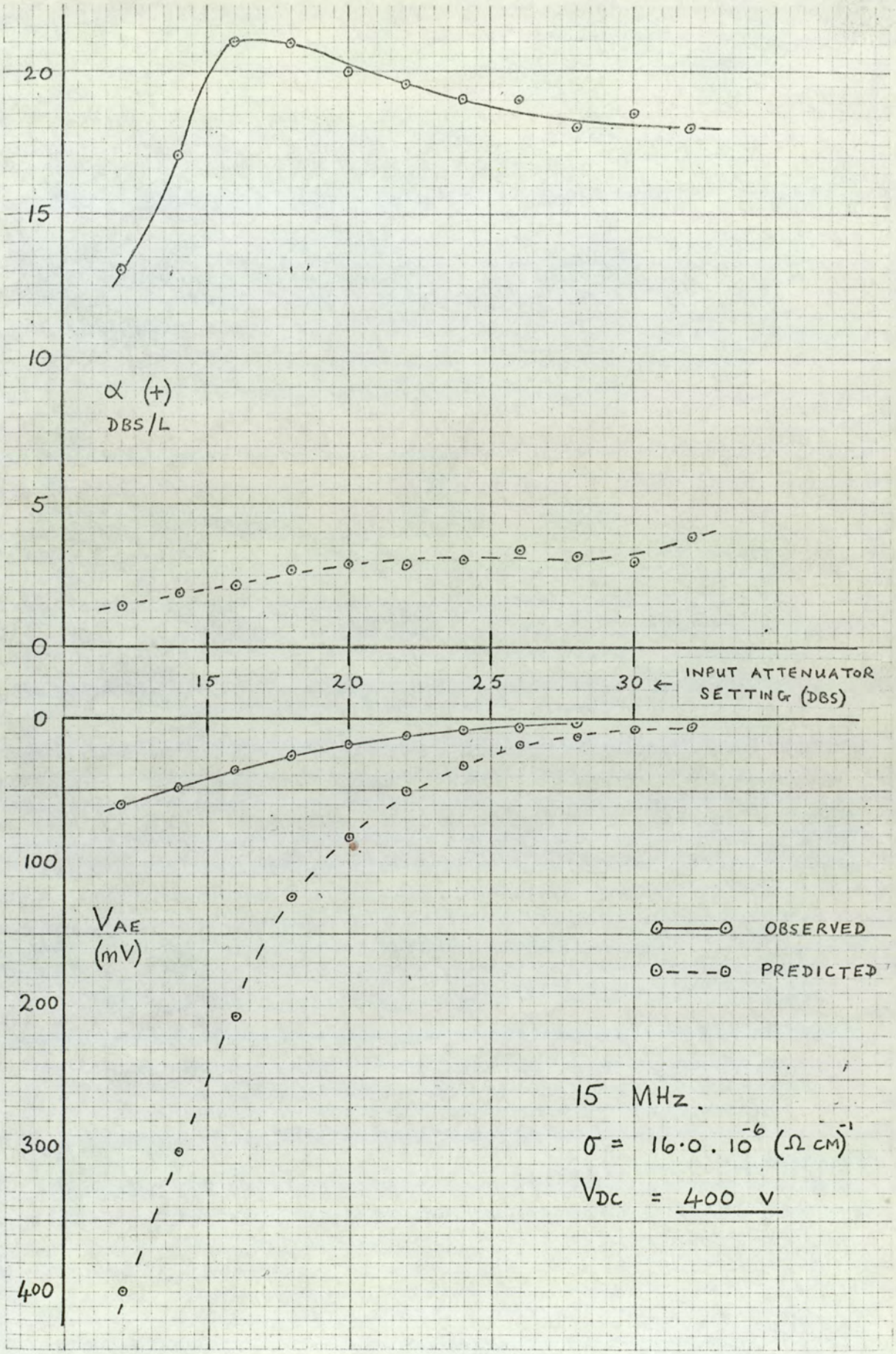

FIG. 59. GENERAL TITLE AS FIG. 58.

15 MHz. $\sigma = 16{\cdot}0\ 10^{-6}\ (\Omega\,\mathrm{cm})^{-1}$. $V_{DC} = 400\mathrm{V}$

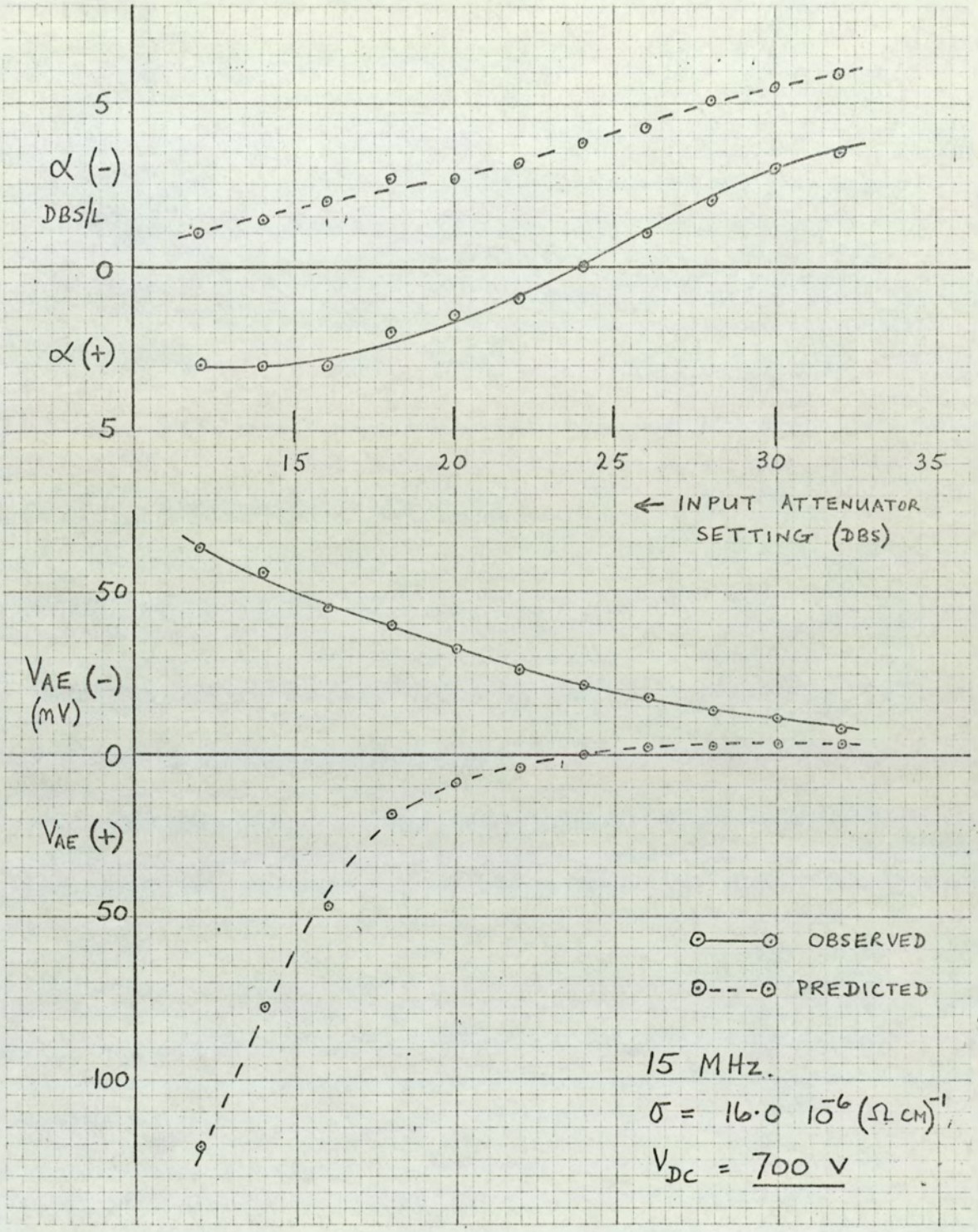

FIG. 60. GENERAL TITLE AS FIG. 58.

15 MHz. $\sigma = 16{\cdot}0\ 10^{-6}\ (\Omega\,\mathrm{CM})^{-1}$ $V_{DC} = 700$ V.

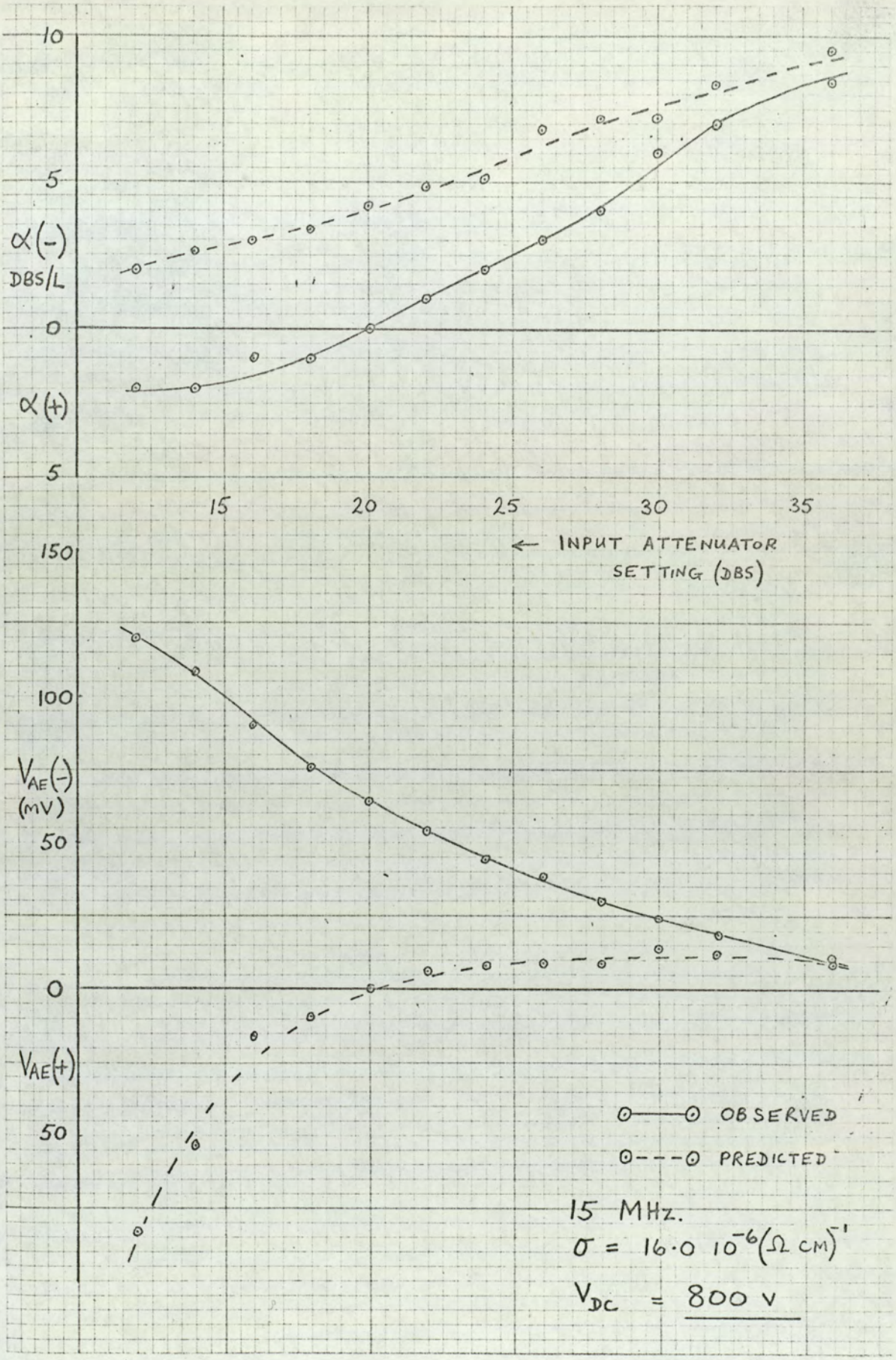

FIG. 61 GENERAL TITLE AS FIG. 58.

15 MHz. $\sigma = 16{\cdot}0.10^{-6}\,(\Omega\,\mathrm{CM})^{-1}$. $V_{DC} = 800\,V$

reduced attenuation coefficient would be necessary if the calculated acoustoelectric voltage were to be in agreement with that observed. This conclusion is in agreement with the 0 volts results obtained at 15 MHz given in figure 45. It might possibly be concluded therefore, that the input acoustic intensity determination at 15 MHz is in error. However, the same comparison for amplifying voltages (figures 60 and 61) indicates that for small acoustic inputs theory and experiment are in better agreement. As the acoustic intensity is increased with the crystal amplifying it will be noted from either figure 60 or 61 that the measured amplification coefficient is reduced until acoustic crossover occurs. The measured acoustoelectric voltage is seen to increase steadily however, and no crossover is observed. A more comprehensive discussion of these, and other results to be reported for amplifier operation at 45 MHz and 75 MHz., will be given in chapter 6.

The variation of both attenuation coefficient and acoustoelectric voltage, with applied d.c. voltage and input acoustic intensity at 45 MHz for two crystal conductivities, is given in figures 62 to 65. Figures 66 to 68 present the comparison between theory and experiment of the acoustoelectric voltage and attenuation coefficient for three applied d.c. voltages. The experimental results plotted in figures 66 to 68 are taken from figures 64 and 65.

Figure 69 shows the input-output characteristics for one crystal conductivity at 75 MHz and figure 70 the corresponding measured acoustoelectric voltage. The results are qualitatively similar to the 15 MHz and 45 MHz results.

It was shown in section 5.2. . that a useful quantitative assessment of the Weinreich relationship at 75 MHz was not a viable proposition because the determination of input acoustic intensity seemed to be suspect, due to a tentatively suggested anomaly in the attenuation determination. The calculated acoustoelectric voltage for a given input acoustic intensity and attenuation coefficient was

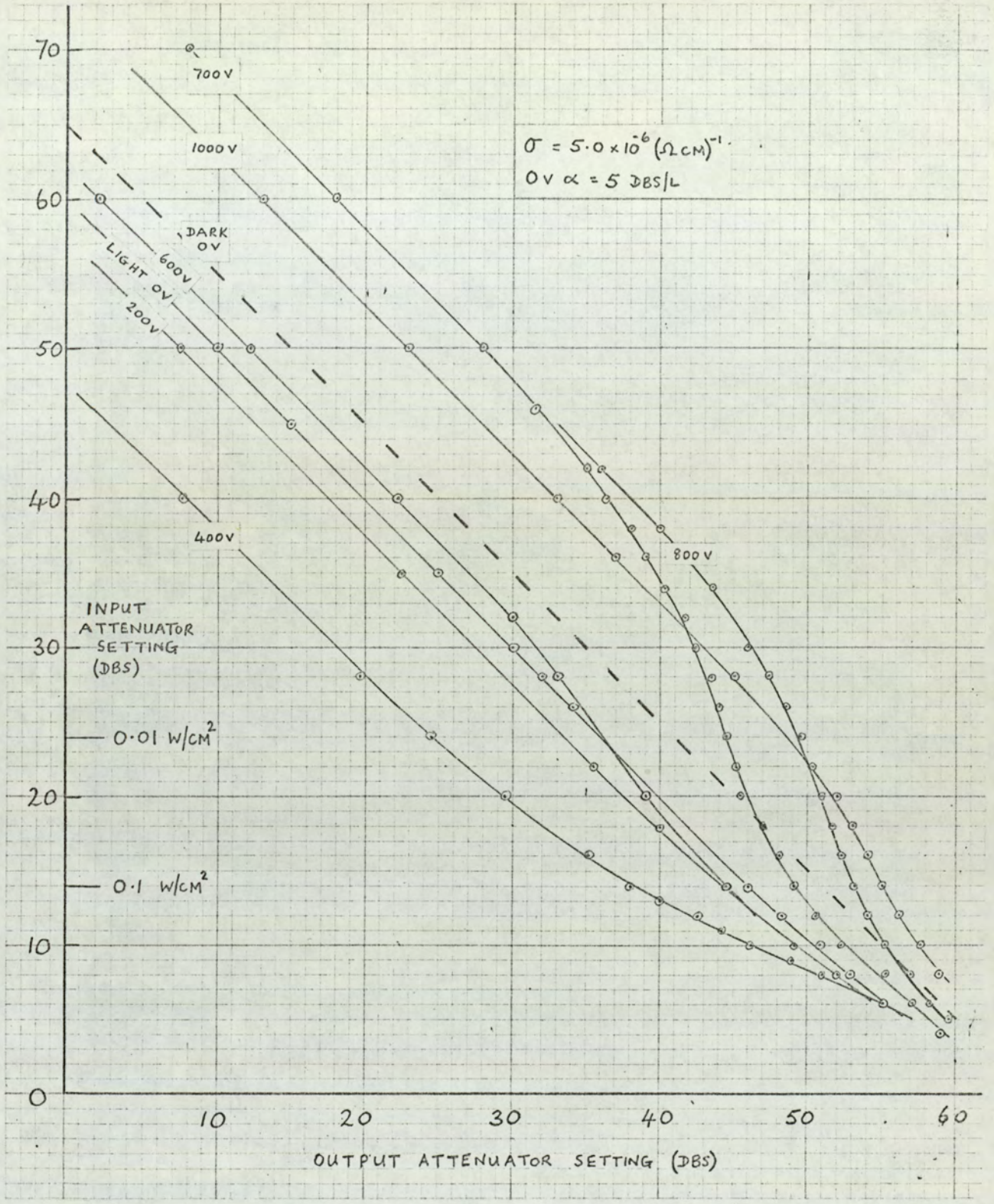

FIG. 62. INPUT - OUTPUT CHARACTERISTICS

45 MHz. $\sigma = 5{\cdot}0\ 10^{-6}\ (\Omega\ \mathrm{cm})^{-1}$

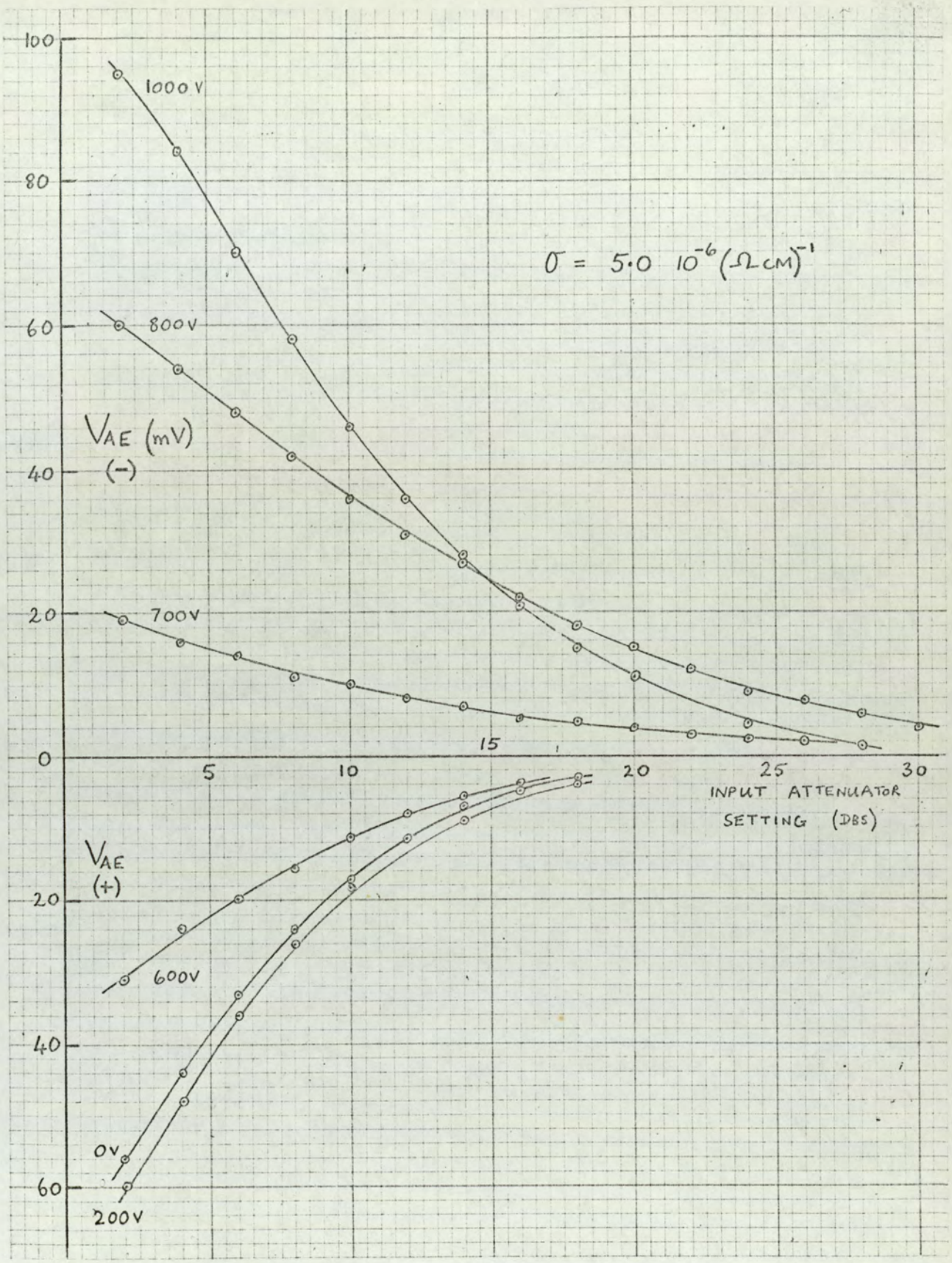

FIG. 63. ACOUSTOELECTRIC VOLTAGE VARIATION. 45 MHz. $\sigma = 5.0\ 10^{-6} (\Omega CM)^{-1}$

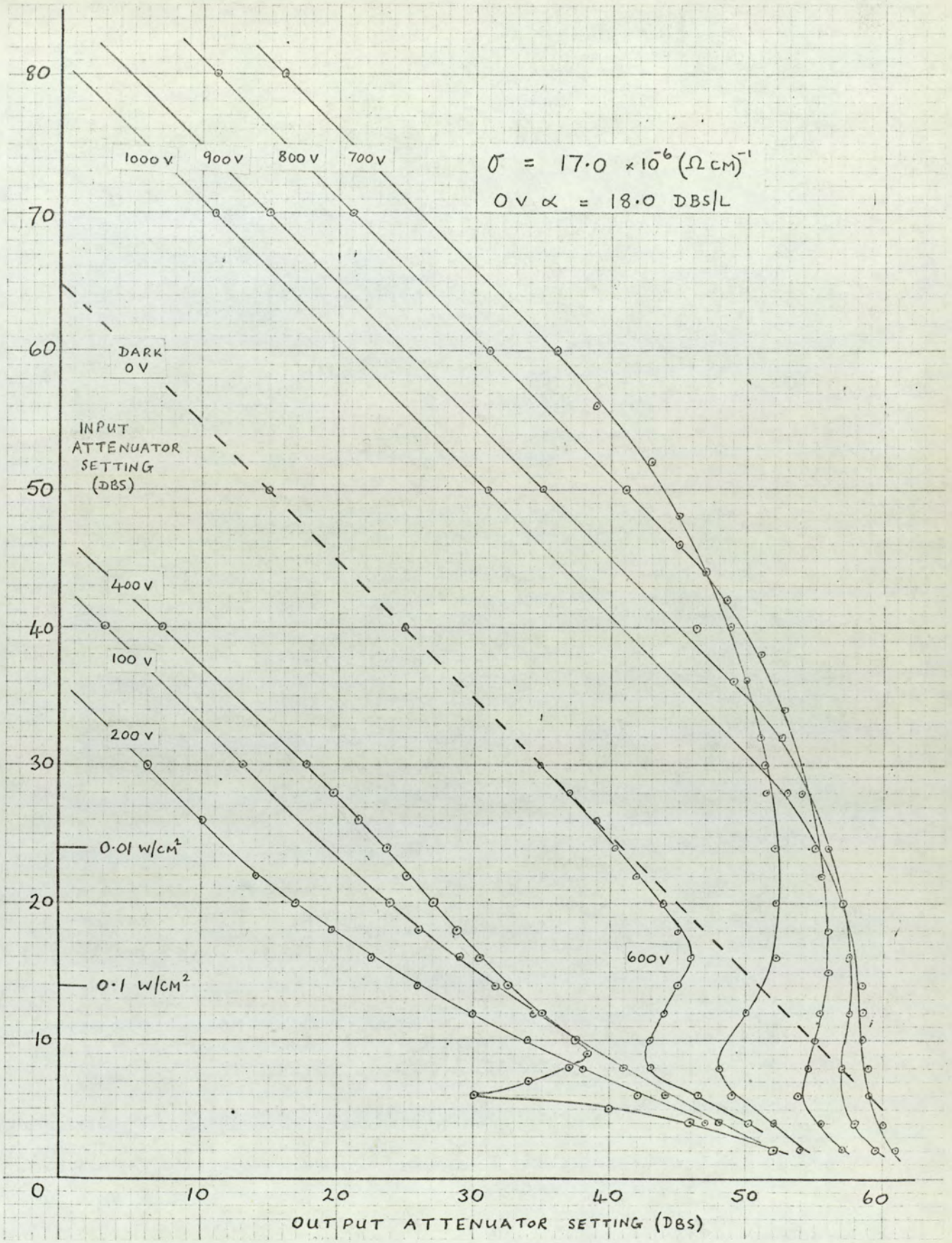

FIG. 64. INPUT - OUTPUT CHARACTERISTICS

45 MHz. $\sigma = 17{\cdot}0\ 10^{-6}\ (\Omega\ \mathrm{CM})^{-1}$

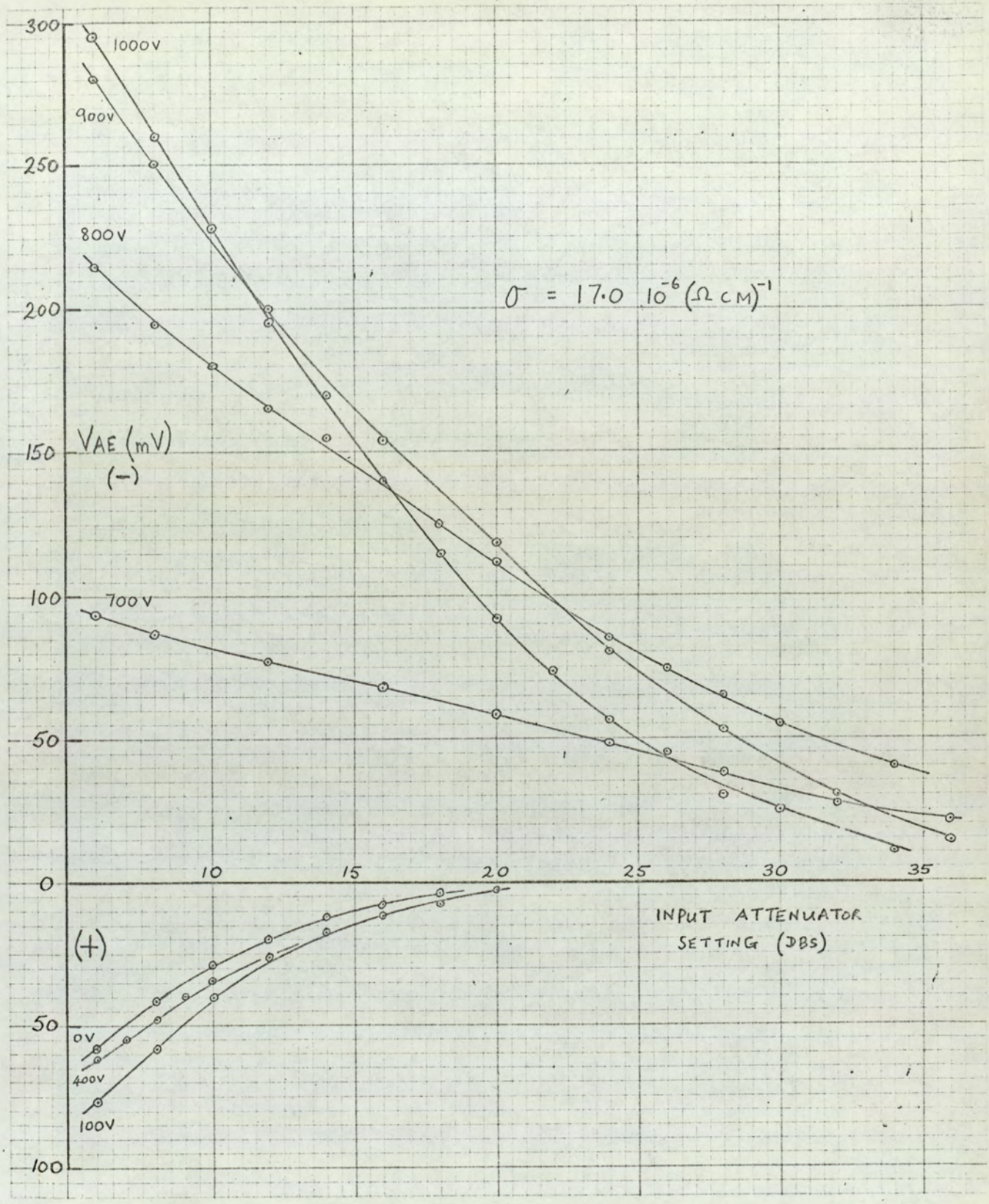

FIG. 65. ACOUSTOELECTRIC VOLTAGE VARIATION. 45 MHz. $\sigma = 17.0\ 10^{-6}(\Omega\,\mathrm{CM})^{-1}$

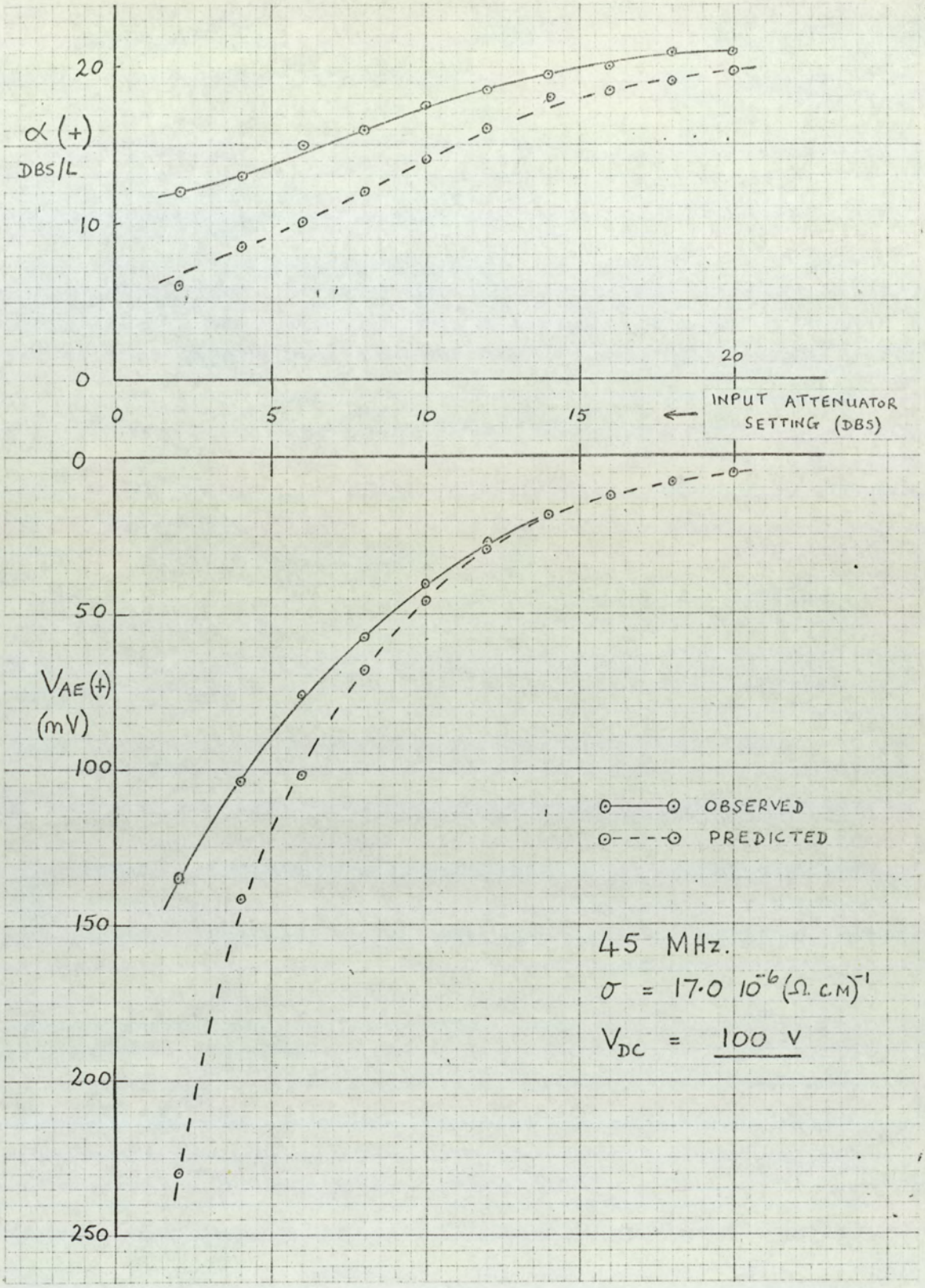

FIG. 66. GENERAL TITLE AS FIG. 58.

45 MHz $\sigma = 17{\cdot}0\ 10^{-6}\ (\Omega\ \mathrm{CM})^{-1}$. $V_{DC} = 100$ V

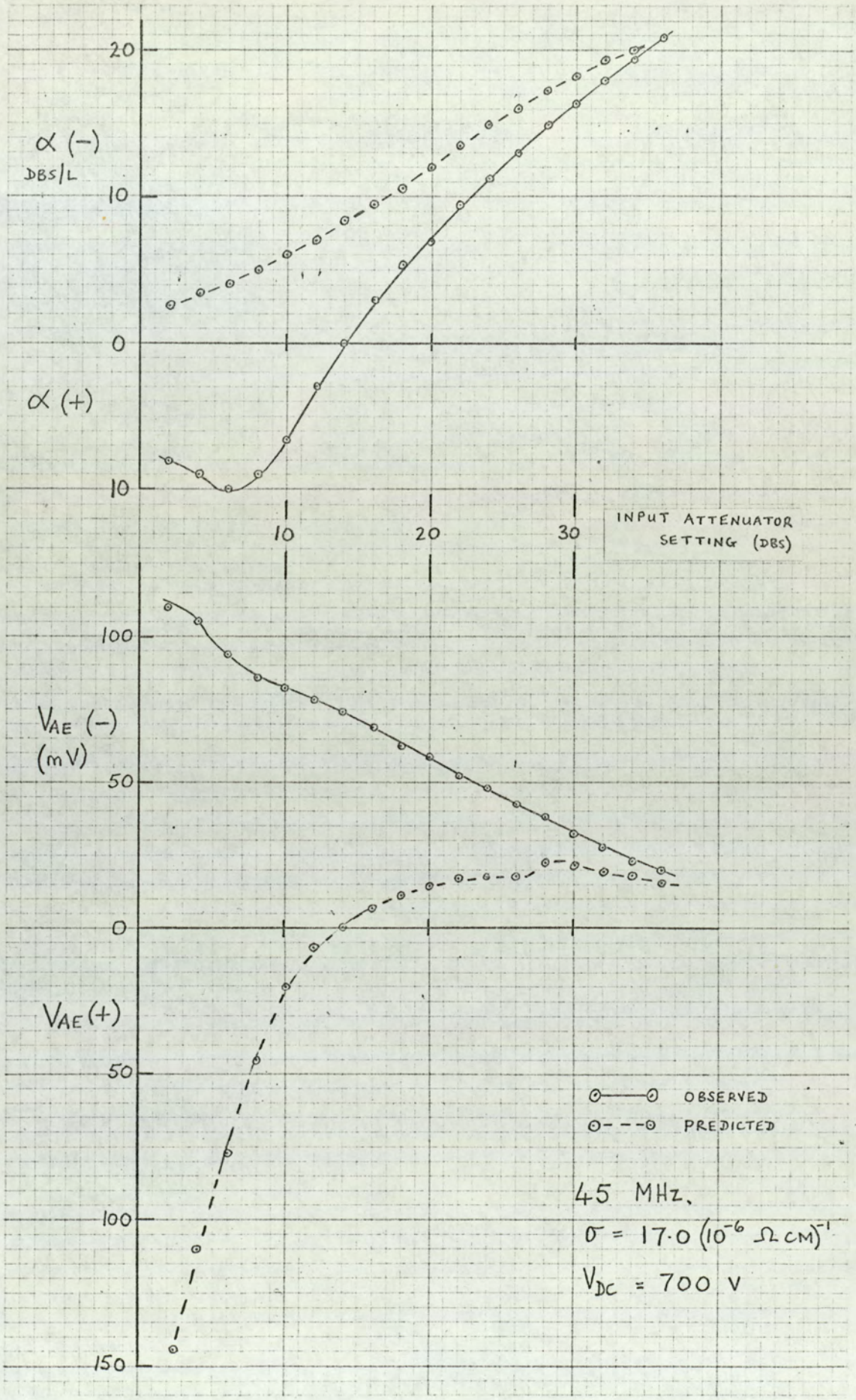

FIG. 67. GENERAL TITLE AS FIG. 58.

45 MHz. $\sigma = 17{\cdot}0\ 10^{-6}\ (\Omega\,\mathrm{CM})^{-1}$ $V_{DC} = 700\,\mathrm{V}$.

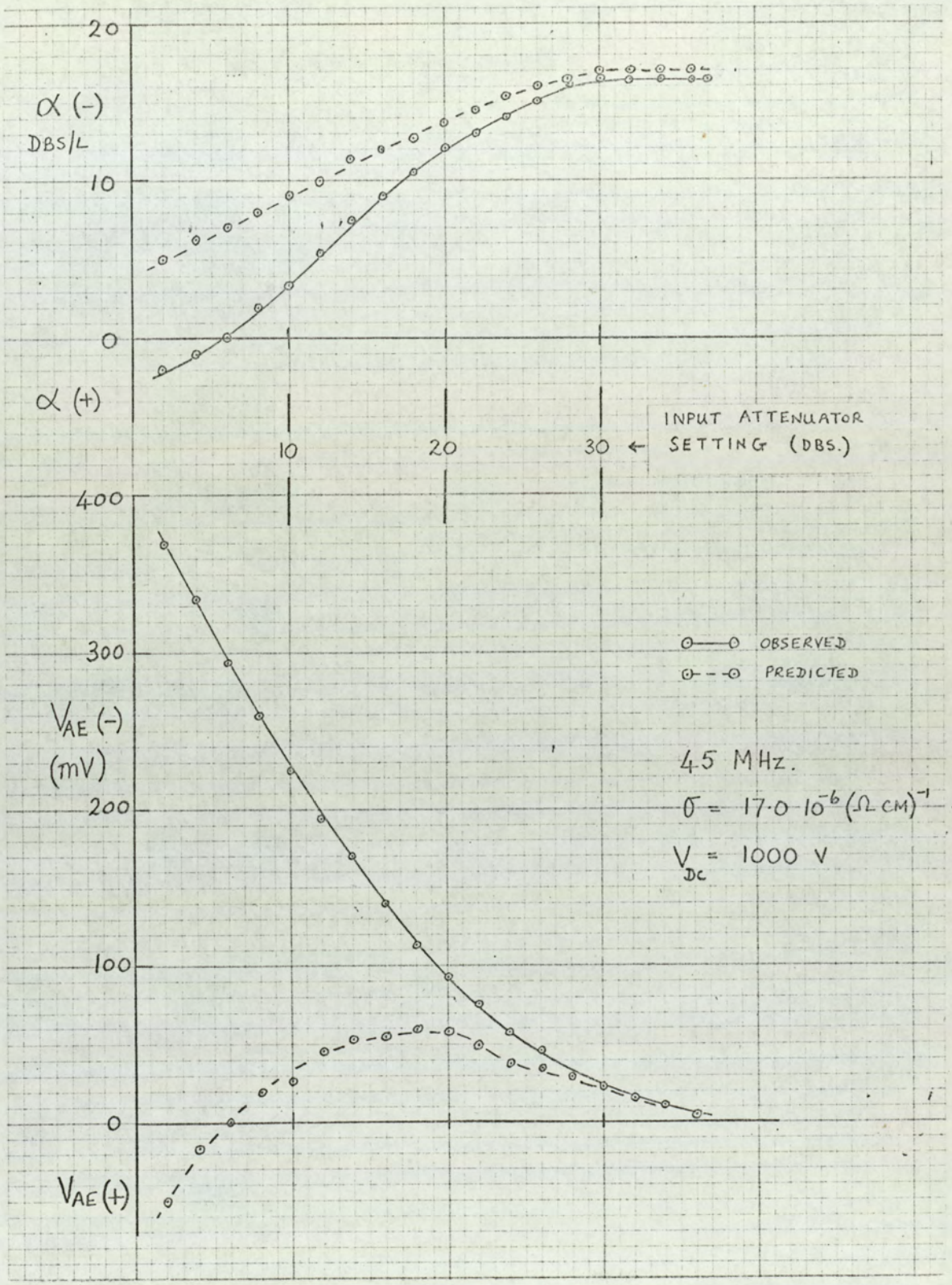

FIG. 68. GENERAL TITLE AS FIG. 58.

4.5 MHz. $\sigma = 17.0\ 10^{-6}\ (\Omega\,\mathrm{CM})^{-1}$. $V_{DC} = 1000\,V$

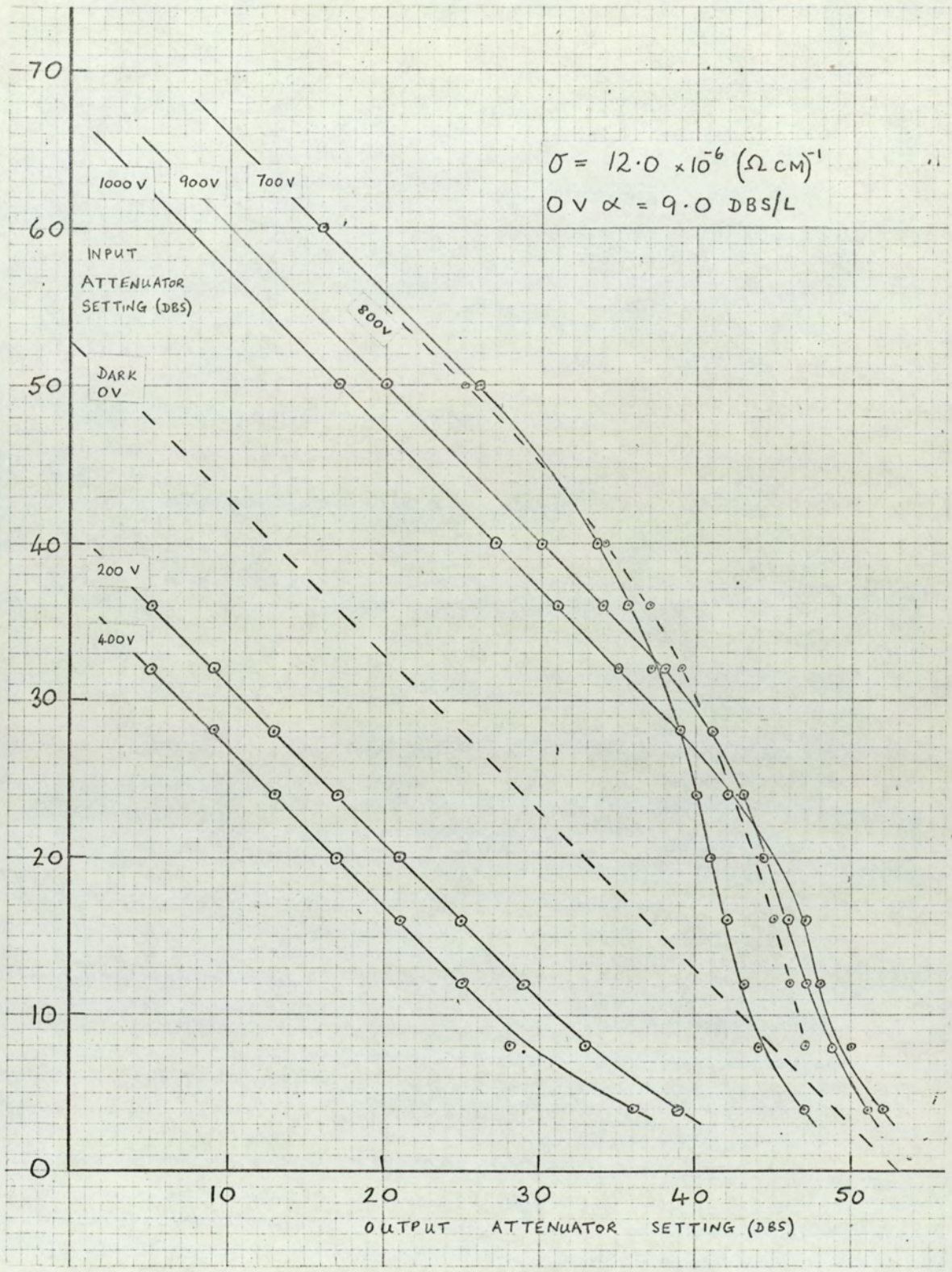

FIG. 69. INPUT - OUTPUT CHARACTERISTICS

75 MHz. $\sigma = 12{\cdot}0\ 10^{-6}\ (\Omega\ \mathrm{CM})^{-1}$

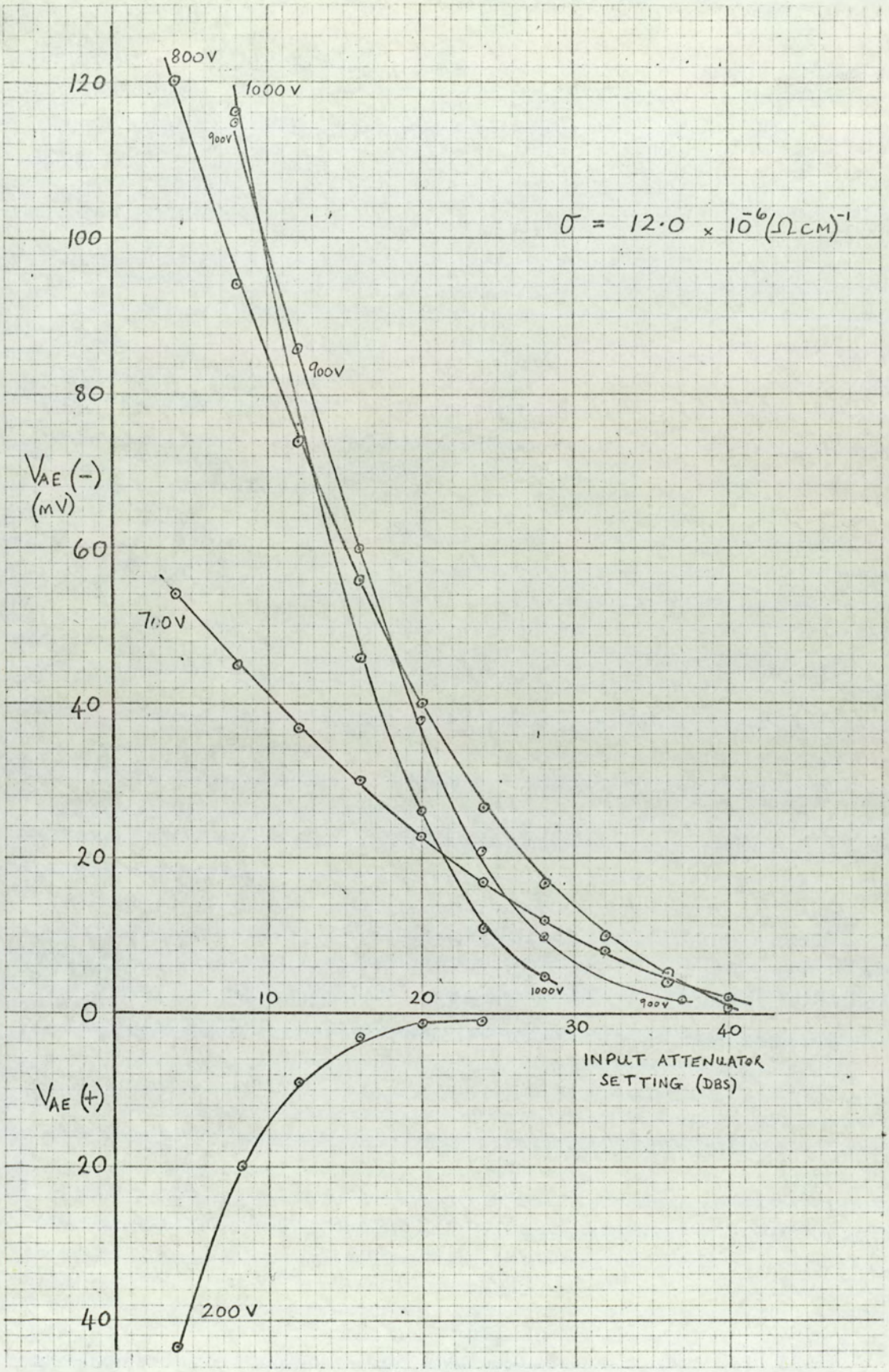

FIG. 70. ACOUSTOELECTRIC VOLTAGE VARIATION. 75 MHz. $\sigma = 12.0\ 10^{-6} (\Omega CM)^{-1}$

seen to be some four times smaller than that observed. However the results obtained at 15 MHz (figure 45) indicated that though agreement between theory and experiment was poor under attenuating conditions, agreement was better when the crystal was amplifying a small input acoustic intensity (figure 61). Consequently it was considered useful to compare theory and experiment under amplifying conditions at 75 MHz to determine whether a more favourable comparison would result. Figure 71 accordingly presents such a comparison. The experimental results plotted in figure 71 are taken from figures 69 and 70. Figure 72 showing the variation of attenuation coefficient with input acoustic intensity at 75 MHz under amplifying conditions for a high crystal conductivity is included for reference when harmonic generation is considered later.

A full discussion of the results presented so far will be given in the next chapter though a few general remarks are appropriate here.

The measured variation of attenuation coefficient and acoustoelectric voltage with input acoustic intensity and applied d.c. voltage for various crystal conductivities at several acoustic frequencies show that the amplification and attenuation at a given acoustic frequency increases with crystal conductivity. The effect of increasing the input acoustic intensity is seen generally to reduce amplification and also to reduce attenuation. Many of the input-output characteristics indicate that the plotted curves - each corresponding to a particular applied d.c. voltage - cross one another in the power dependent region. The measured acoustoelectric voltage curves, presented with each of the input - output characteristics also intersect in a manner similar to the amplification curves. The input - output characteristics presented all show a marked saturation of gain to occur as the input acoustic intensity is increased. Furthermore this saturation starts for quite modest input intensities.

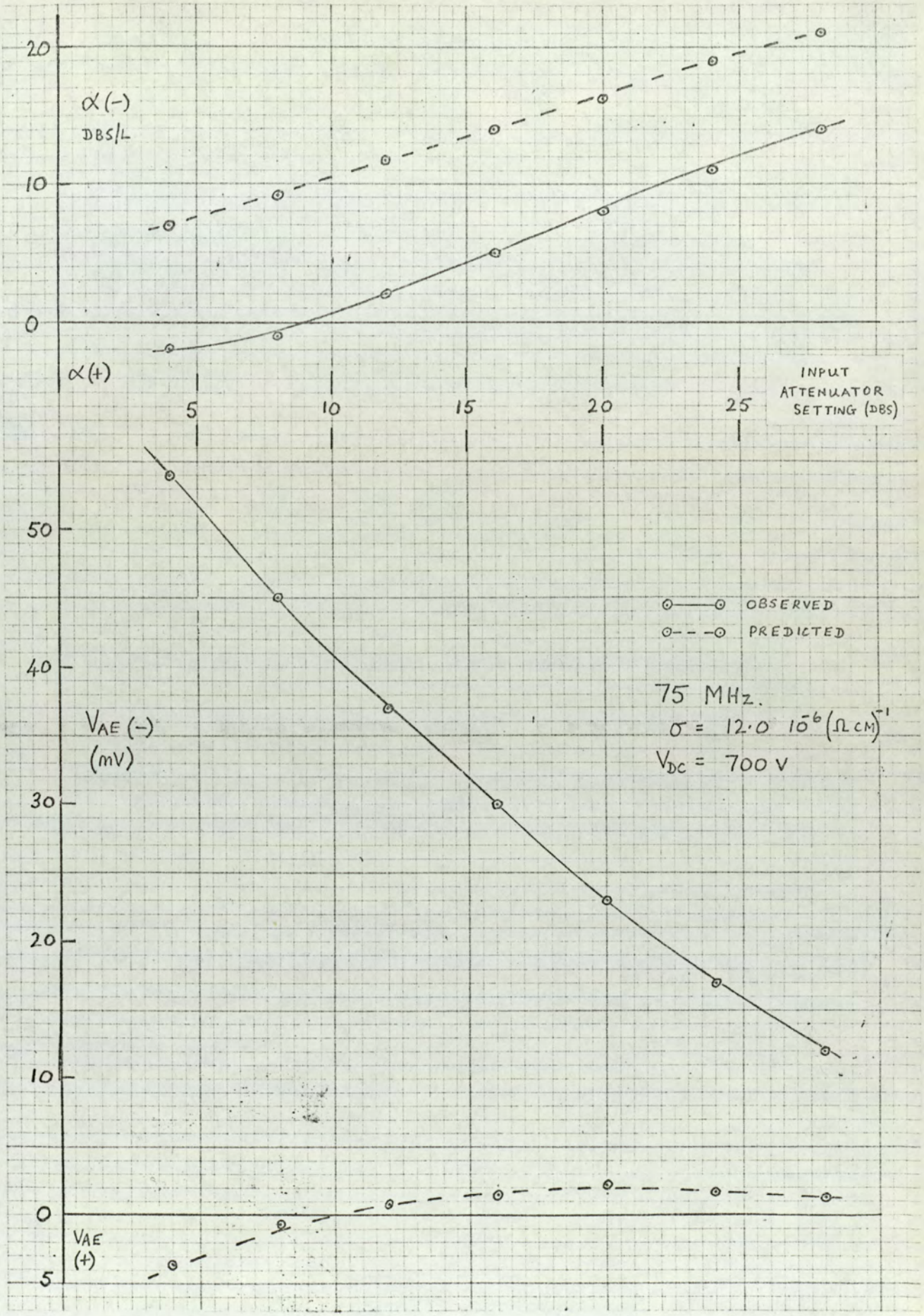

FIG. 71. GENERAL TITLE AS FIG. 58.

75 MHz. $\sigma = 12{\cdot}0\ 10^{-6}(\Omega\,\mathrm{CM})^{-1}$. $V_{DC} = 700$ V.

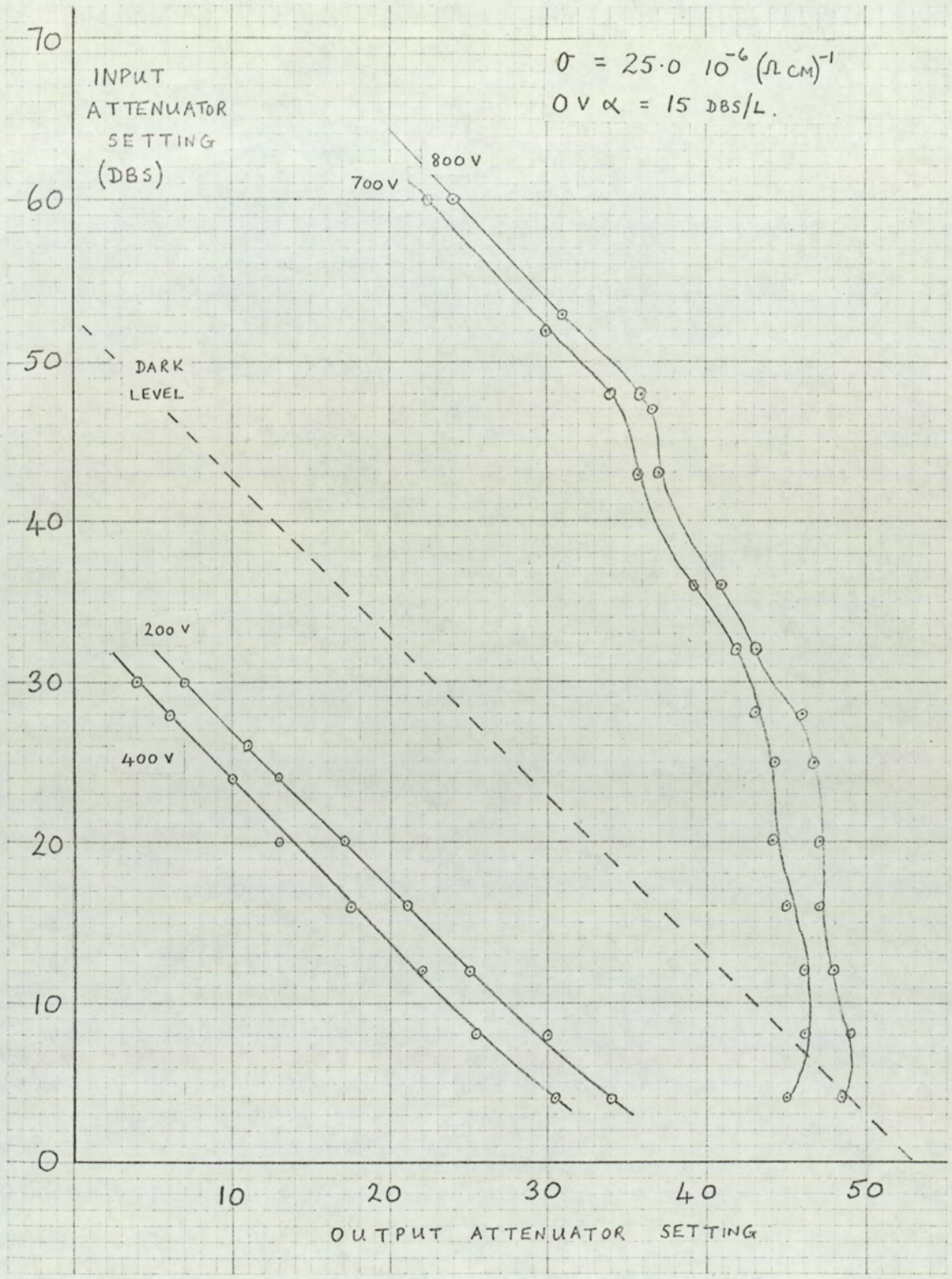

FIG. 72. INPUT - OUTPUT CHARACTERISTICS

75 MHz. $\sigma = 25{\cdot}0\ 10^{-6}\ (\Omega\,\mathrm{cm})^{-1}$

An investigation of the Weinreich relationship under amplifying conditions in the absence of such gain saturation thus requires acoustoelectric voltage measurement for very small acoustic inputs. Since the measured acoustoelectric voltage is a function of input acoustic intensity this also requires the measurement of small acoustoelectric voltages in the presence of large applied d.c.voltages. Figure 57 shows the acoustoelectric voltage to increase as an exponential function of attenuation coefficient when the crystal is amplifying. This increase is very marked as the amplification coefficient becomes large.

An examination of the input - output characteristics at 15 MHz and 45 MHz indicates that the onset of gain saturation occurs at larger input acoustic intensities at 15 MHz than at 45 MHz. The use of the calibration graphs given in figures 33 and 34 is necessary for this conclusion to be drawn. On the other hand, the observed amplification is smaller at 15 MHz than at 45 MHz. To cite a specific example - the maximum amplification coefficient observed at 15 MHz for σ = 17.0 10^{-6} (ohm cm)$^{-1}$ is seen to be about 11 dbs./L (figure 53). For the same crystal conductivity gain reduction is seen to start with an input attenuator setting of about 40 dbs. which according to figure 33 corresponds to an input acoustic intensity of 0.005 watts/sq.cm. Theory accordingly predicts an acoustoelectric voltage of 7.3 mv. At 45 MHz for the same crystal conductivity, figure 64 indicates a maximum amplification coefficient of about 26 dbs/L. Gain reduction is again seen to initiate at an input attenuator setting of 40 dbs, although according to figure 34 this corresponds to the lower input acoustic intensity of about 0.0003 watts/sq cm. However, in this case theory predicts a measured acoustoelectric voltage of 24.5 mv. Moreover, the observation of high amplification over a much wider range of crystal conductivity at 45 MHz recommends this frequency as the more suitable for power

independent acoustoelectric voltage measurement.

Figure 73 presents the observed variation of small signal amplification and simultaneously measured acoustoelectric voltage for three crystal conductivities at 45 MHz. The input acoustic intensity was maintained constant and was chosen to be the smallest input intensity which enabled reasonable measurement of acoustoelectric voltage. The dashed lines in the lower graph indicate the predicted acoustoelectric voltage for the measured amplification variation shown in the upper graph. The Weinreich relationship indicates that if the input acoustic intensity and amplification coefficient are constant then the acoustoelectric voltage should also be constant. This is verified experimentally in figure 73 for an amplification coefficient of 20 dbs/L and 25 db/L. The measured acoustoelectric voltage corresponding to an amplification coefficient of 25 db/L is shown to be reasonably constant, and independent of applied d.c. voltage or crystal conductivity. A similar comparison for an amplification coefficient of 20 dbs/L also indicates satisfactory agreement with theory.

5.3.2. The variation of acoustoelectric voltage with input acoustic intensity

The variation of the attenuation coefficient under a wide range of applied conditions has been given in the preceding section. The results indicate a marked reduction in amplification for a given applied d.c. voltage and crystal conductivity as the input intensity is increased. An investigation was carried out to determine the variation of acoustoelectric voltage with input acoustic intensity under both amplifying and attenuating conditions. Since the investigation demanded that input intensity was the only variable, the applied d.c. voltage was adjusted each time the input intensity was increased in order to maintain the same measured attenuation coefficient. For the sake of clarity a negative attenuation coefficient

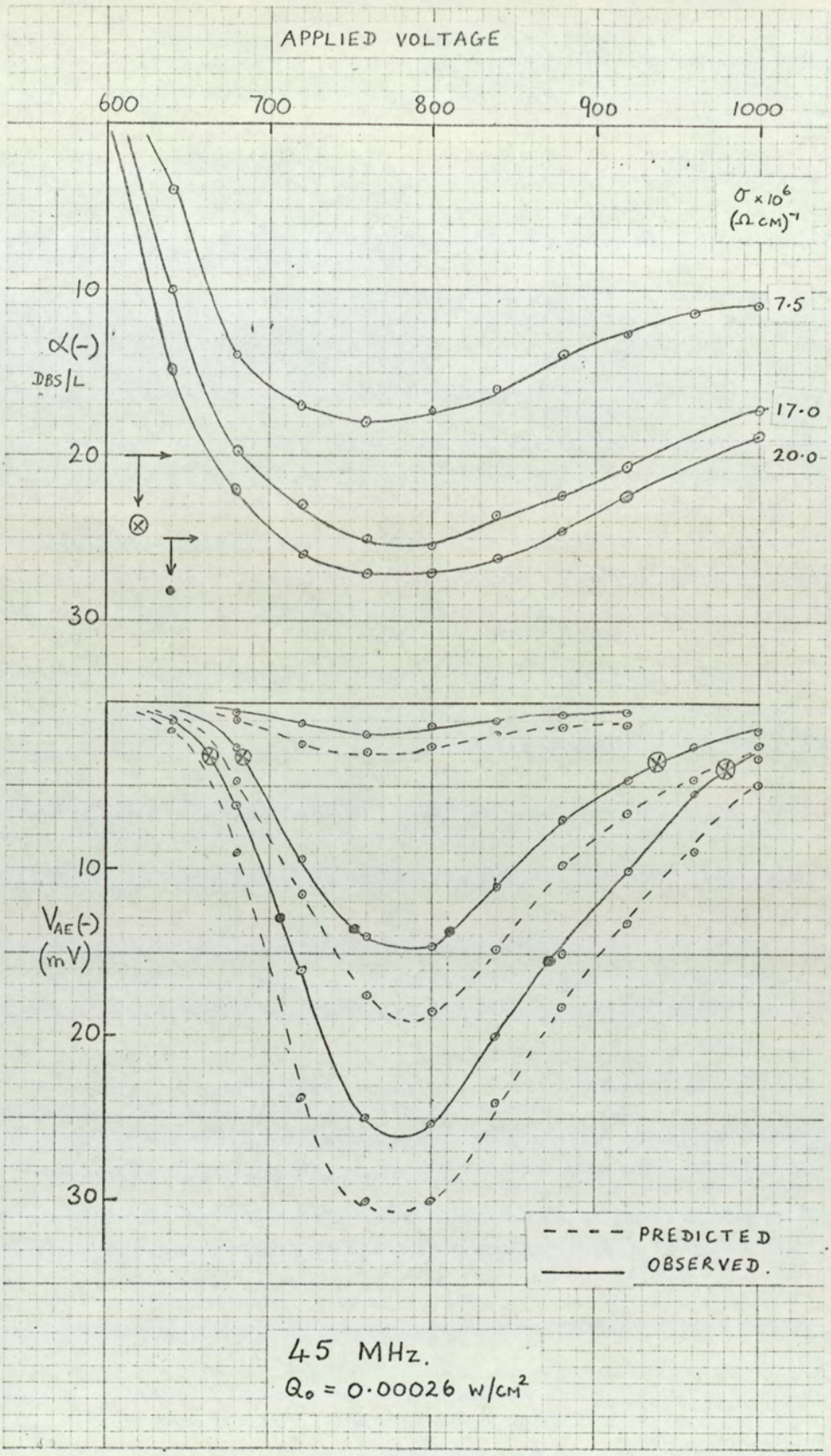

FIG. 73. SMALL SIGNAL GAIN AND ACOUSTOELECTRIC VOLTAGE.

D.C. VOLTAGE VARIED - 45 MHz.

will henceforth be referred to as the amplification coefficient. Figures 74 and 75 show the measured acoustoelectric voltage as a function of input acoustic intensity for an attenuation coefficient of 14 dbs/L and an amplification coefficient of 6 dbs/L respectively of a 15 MHz input acoustic signal. The range of applied d.c. voltage necessary to maintain the chosen attenuation coefficient as the input acoustic intensity was increased is indicated. The results were obtained for various crystal conductivities, although the acoustoelectric voltage was always measured when the input acoustic signal was being attenuated by the specified amount. The measurement of acoustoelectric voltage for each crystal conductivity was terminated when a d.c. voltage greater than 1000 volts was necessary to obtain the chosen value of attenuation coefficient. The solid line in figure 74 indicates the predicted values of acoustoelectric voltage. The measured acoustoelectric voltage is seen, in figure 74, to be proportional to the input acoustic intensity and independent of crystal conductivity. Quantitatively, the measured acoustoelectric voltage is seen to be several times smaller than that predicted. This disagreement is similar to that previously recorded for no volts applied to the crystal at this acoustic frequency. Figure 75 presents the measured acoustoelectric voltage as a function of input acoustic intensity, for a maintained amplification coefficient of 6 dbs/L. A low amplification coefficient was chosen since this value could be achieved over a wide range of crystal conductivity at high input acoustic intensities by increasing the applied d.c. voltage as necessary within the range 600 to 1000 volts. The predicted acoustoelectric voltage is again indicated by the solid line in figure 75. It may be noted that as the crystal conductivity is increased, the measured acoustoelectric voltage becomes greater than that predicted. Good agreement between theory and experiment is recorded for a low crystal conductivity of $9.5\ 10^{-6}$ $(\text{ohm cm})^{-1}$ over much of the input acoustic intensity range considered.

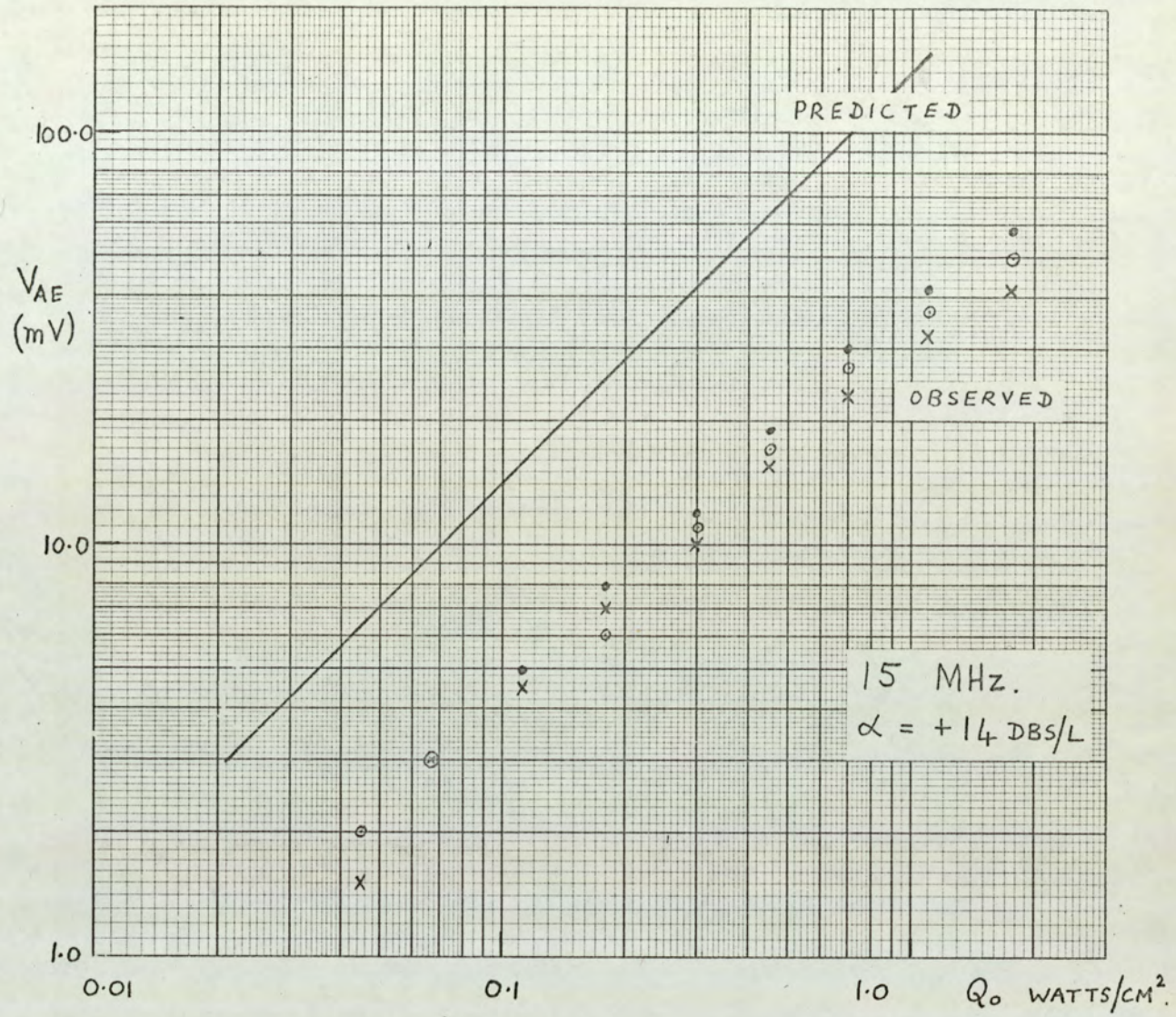

SYMBOL	$\sigma \times 10^6$ $(\Omega\,CM)^{-1}$	$V_{D.C.}$ RANGE Q_o INCREASING
●	16·0	150 → 210
X	20·0	500 → 470
⊙	25·0	500 → 470

FIG. 74. ACOUSTOELECTRIC VOLTAGE VERSUS INPUT ACOUSTIC INTENSITY.

D.C. VOLTAGE APPLIED . 15 MHz. α = +14 DBS/L.

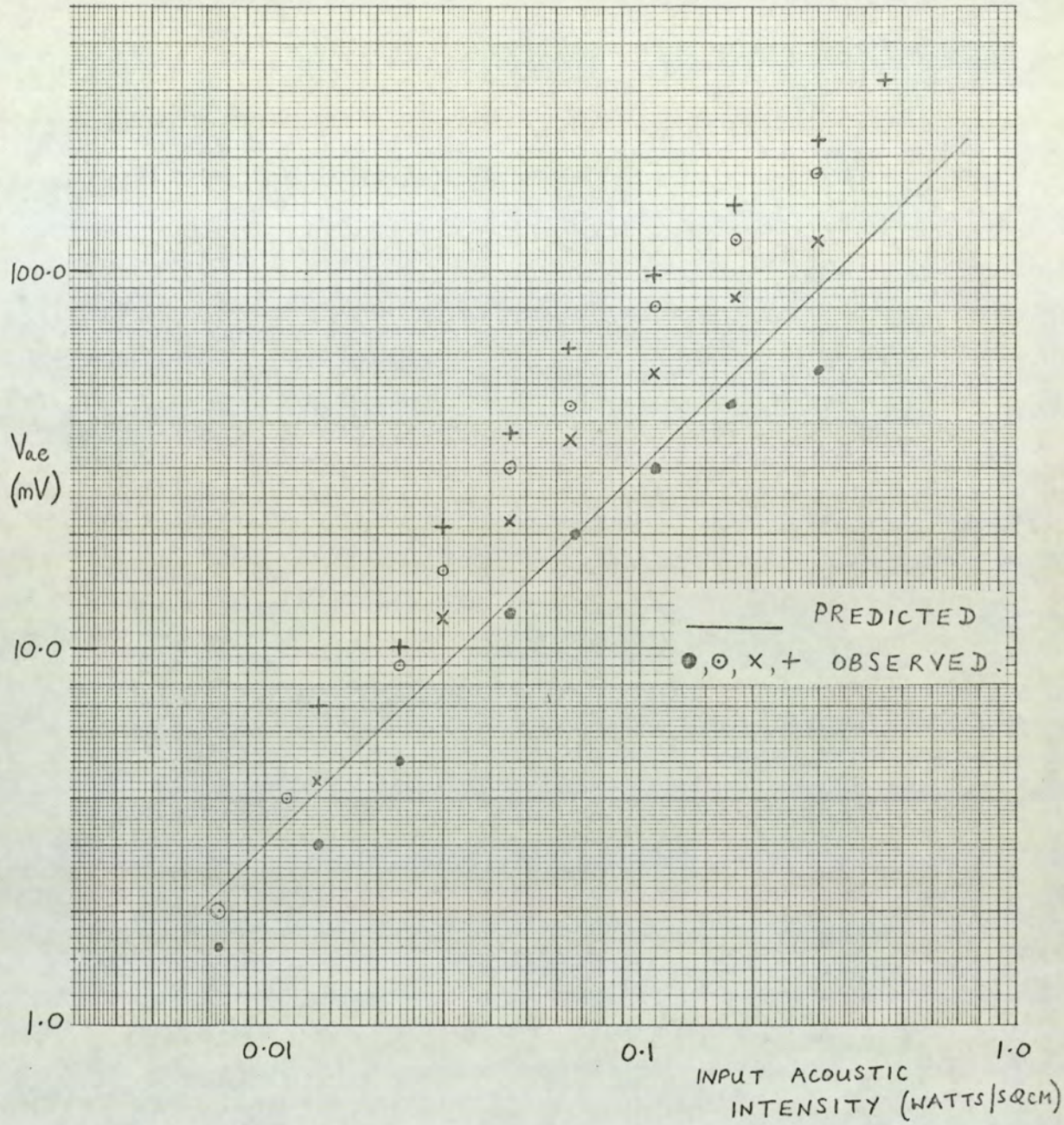

SYMBOL	$\sigma \times 10^6$ $(\Omega\,CM)^{-1}$	V_{DC}. RANGE Q_0 INCREASING
●	9·5	710 → 1040
×	16·0	680 → 920
⊙	20·0	650 → 900
+	25·0	650 → 900

FIG. 75. ACOUSTOELECTRIC VOLTAGE VERSUS INPUT ACOUSTIC INTENSITY D.C. VOLTAGE APPLIED. 15 MHz. $\alpha = -6$ DBS/L.

Prior to drawing any conclusions from these results it was thought advisable to carry out the same experiment for a 45 MHz. input acoustic signal. The results of this work are shown in figures 76 and 77. Figure 76 (a) compares the observed variation of acoustoelectric voltage with input acoustic intensity for an attenuation coefficient of 8 dbs/L, and figure 76(b) for an attenuation coefficient of 18 dbs/L. The results of figure 76 were obtained for more than one crystal conductivity and although there is some experimental spread, the agreement between theory and experiment is quite impressive. Figure 77 shows results obtained under amplifying conditions, for two values of amplification coefficient. The experiment was carried out over a wide range of crystal conductivity as the table in figure 77 indicates. The results obtained for an amplification coefficient of 16 dbs/L are seen to have been obtained at lower input powers than those obtained for an amplification coefficient of 6 dbs/L. The reduction in amplification due to an input signal greater than 0.01 watt/sq.cm. was such that an amplification coefficient of 16 dbs/L could not be achieved, even by increasing the applied d.c. voltage to 1000 volts.

The results obtained for an amplification coefficient of 6 dbs/L shows an increase in measured acoustoelectric voltage with crystal conductivity and input intensity similar to that obtained at 15 MHz. and given in figure 75. Again the measured acoustoelectric voltage is seen to be greater than that predicted although at small input powers agreement is better. Unfortunately, the extent of this agreement could not be pursued for an input acoustic intensity less than 0.003 watt/sq.cm. because the acoustoelectric voltage generated was too small to permit accurate measurement. It was concluded from the results obtained at both 15 MHz. and 45 MHz. and given as figures 75 and 77 that the disagreement between theory and experiment noted under amplifying conditions was general. This disagreement

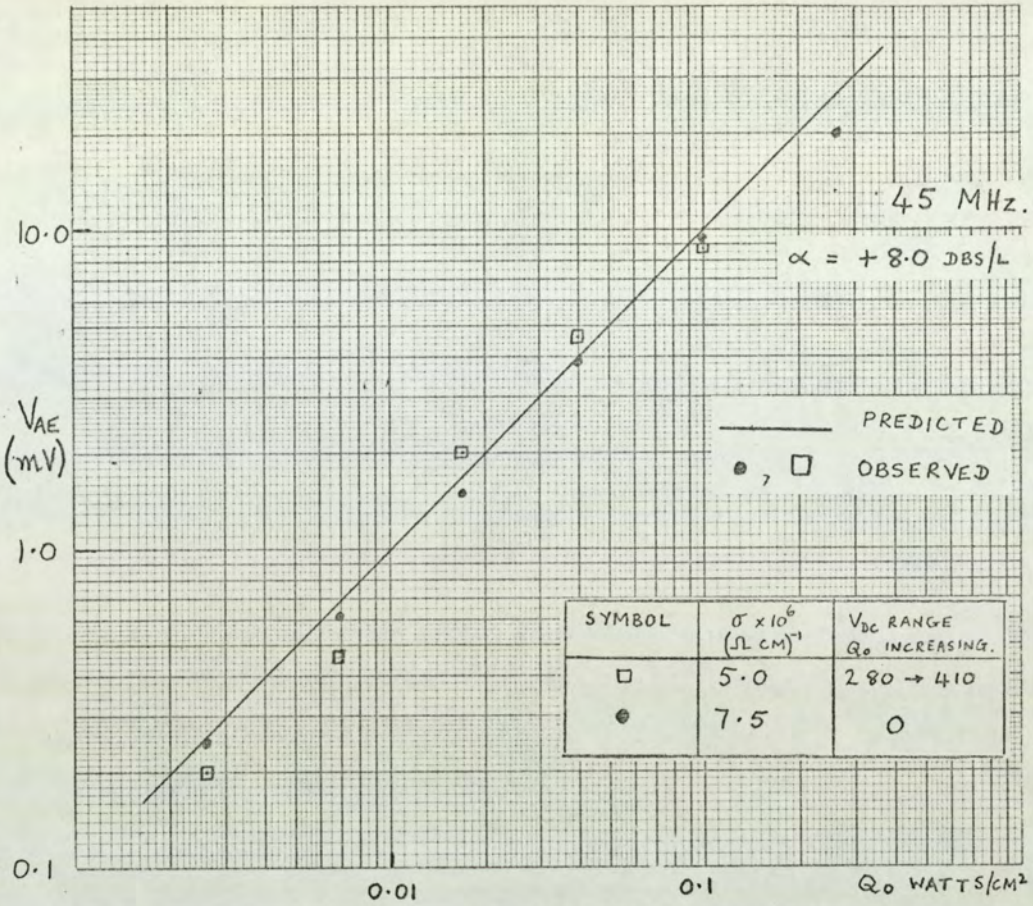

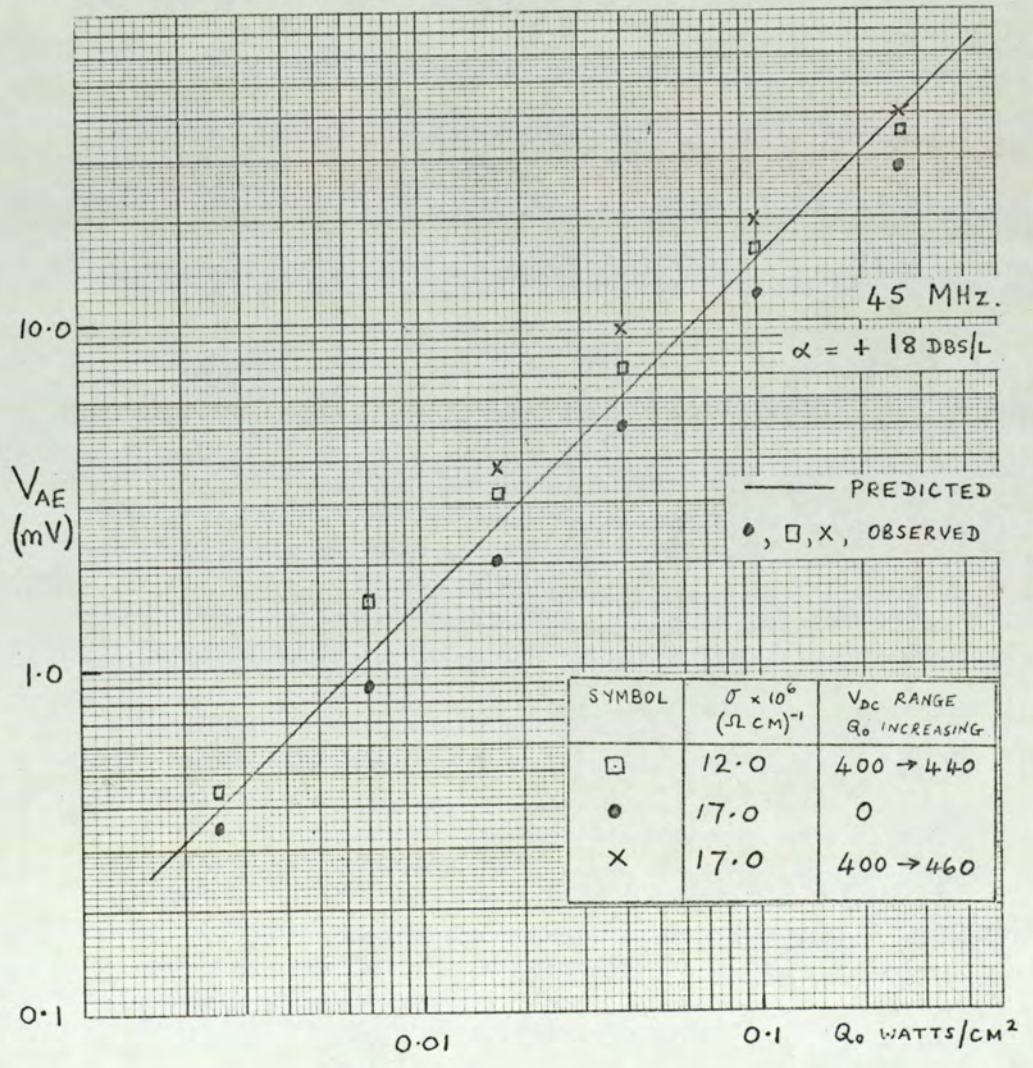

FIG. 76. ACOUSTOELECTRIC VOLTAGE VERSUS INPUT ACOUSTIC INTENSITY. D.C VOLTS APPLIED.

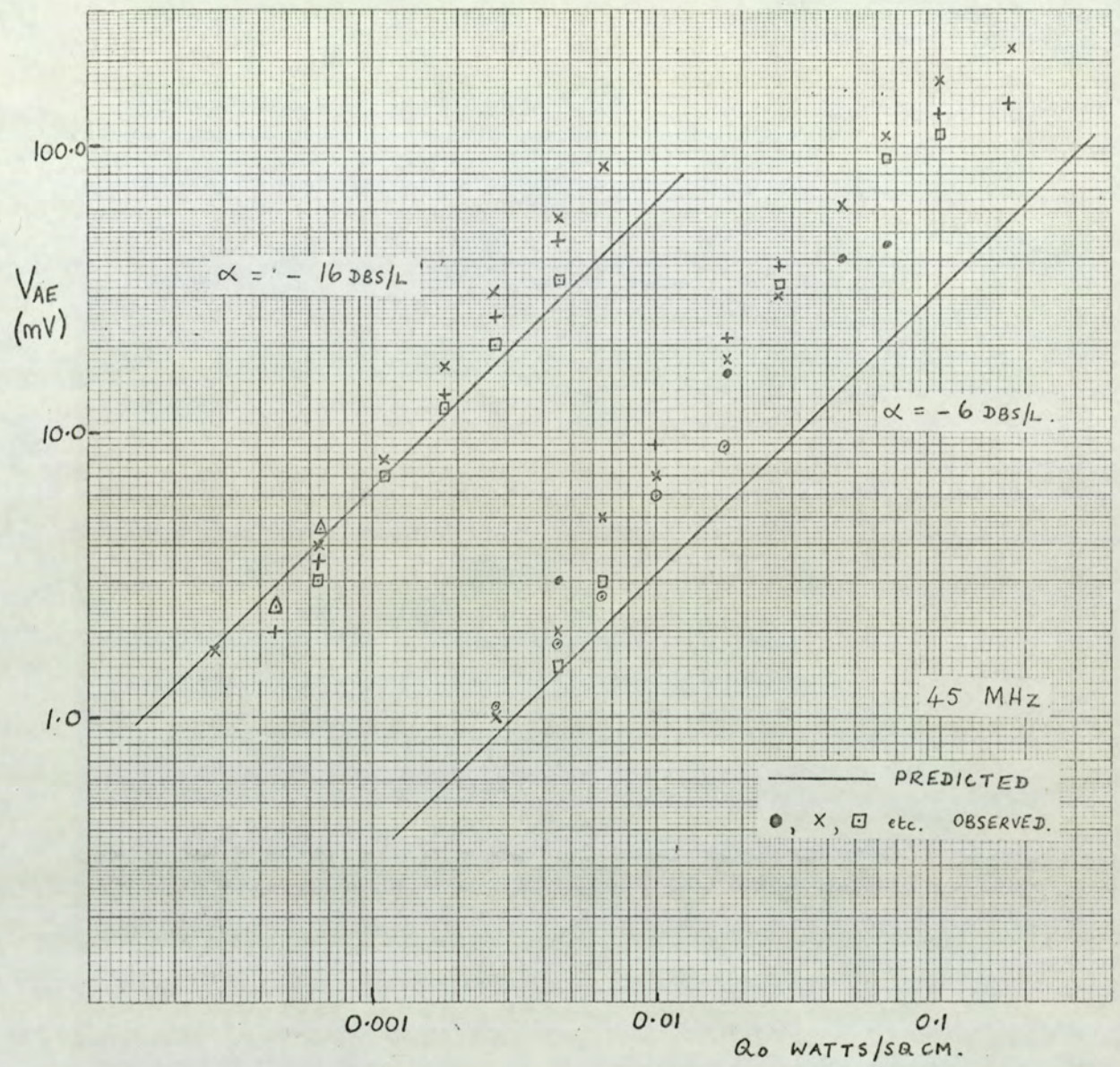

SYMBOL	$\sigma \times 10^6$ $(\Omega CM)^{-1}$	V_{DC} RANGE Q_0 INCREASING
⊙	5·0	700 → 840
△	7·5	700 → 780
●	9·5	640 → 980
⊡	12·0	630 → 940
+	14·0	620 → 1050
X	17·0	620 → 950

FIG. 77. ACOUSTOELECTRIC VOLTAGE VERSUS INPUT ACOUSTIC INTENSITY. 45 MHz. CRYSTAL AMPLIFYING

was attributed to the generation of harmonics. It was argued that the generated harmonics were amplified during transit though the crystal, and since the acoustic intensity of the harmonics was likely to be small, their amplification coefficient would be large. Figure 57 indicates that the acoustoelectric voltage increases rapidly for large amplification coefficients, and thus the acoustoelectric voltage generated by the harmonics might be appreciable. The measurement of acoustoelectric voltage cannot distinguish between that due to the input acoustic signal, and that due to harmonics, and consequently, the measured acoustoelectric voltage would be that due to both. An experimental programme was therefore initiated to determine whether the observed disagreement between theory and experiment illustrated by figures 75 and 77 could be attributed to harmonic generation as postulated.

5.3.3. Harmonic generation

The results described so far indicate that for a given crystal conductivity and applied d.c. voltage the amplification, and to a lesser extent, the attenuation, of an input acoustic signal is substantially reduced as the input acoustic intensity is increased. For a given crystal conductivity therefore, it is necessary to adjust the applied d.c. voltage as the input acoustic intensity is increased, if the amplification coefficient is to be maintained a constant over the range of acoustic intensity in question. A comparison between experiment and theory of the variation of acoustoelectric voltage with input acoustic intensity, for such a constant amplification coefficient, at various crystal conductivities indicates a measured acoustoelectric voltage which is larger than that predicted. In order to determine whether this disagreement may be attributed to the generation of harmonics which contribute to the measured acoustoelectric voltage it was necessary to measure the harmonic output and then to assess the possible contribution of the

generated harmonics.

It was considered sufficient to concentrate on the possible harmonic generation due to a 15 MHz. input acoustic signal, which then allows harmonic output signals of frequency 45 MHz. 75 MHz., and if necessary, 105 MHz. to be measured. The investigation of harmonic generation due to a 45 MHz. input signal would require the detection of output frequencies of 135 MHz. and 225 MHz. and these were considered to be outside the frequency range suitable for measurement. The investigation into harmonic generation was therefore carried out for an input signal of 15 MHz. and a reasonably high crystal conductivity. Figure 75 indicates that the disagreement between theory and experiment increases with crystal conductivity. Accordingly the investigation was carried out at a crystal conductivity of 25.0×10^{-6} (ohm cm.)$^{-1}$.

Harmonic generation was detected and measured by tuning the r.f. receiver to the particular harmonic frequency to be monitored, and by changing the 15 MHz. transformer matching assembly on the output side of the crystal for the assembly corresponding to the harmonic frequency in question.

The validity of the input acoustic intensity versus input attenuator (A1) setting calibration graph at 15 MHz.(figure 33) was first checked in the manner described in section 4.5, before changing the output transformer matching assembly from 15 MHz. to that relevant to the required harmonic frequency, and before retuning the r.f. receiver to the new frequency.

The harmonic output was displayed directly on the oscilloscope in the manner indicated by figure 31(b). Figure 78 shows typical displays obtained, for each harmonic frequency. Figure 78(a) shows the input r.f. signal at 15 MHz. Figures 78 (b,c,d) show the harmonic output at 45 MHz., 75 MHz., and 105 MHz. respectively. For most of the investigation the acoustic output from the crystal was

TYPICAL INPUT SIGNAL. 15 MHz.

HORIZONTAL SCALE
0·2 μSECS/SQUARE

(a)

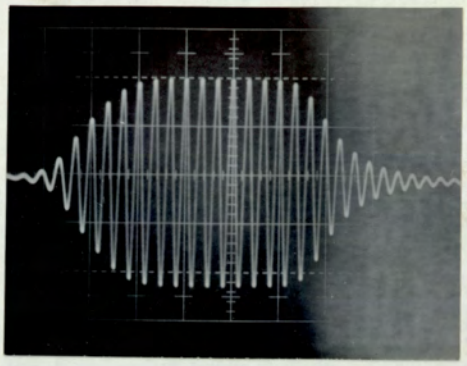

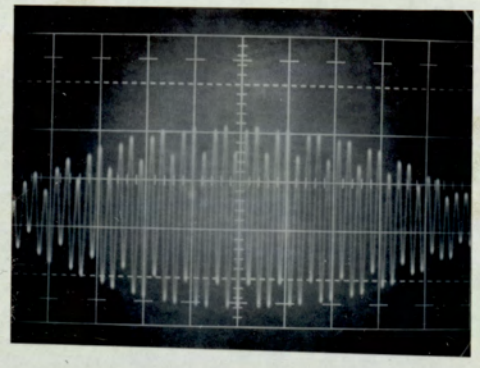

(b)

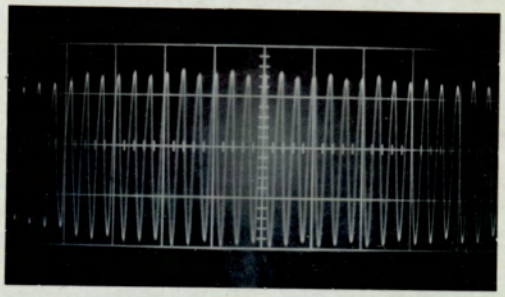

(c)

DETECTED HARMONICS

b) 45 MHz ~0·1 μs/sq.

c) 75 MHz ~0·04 μs/sq.

d) 105 MHz ~0·1 μs/sq.

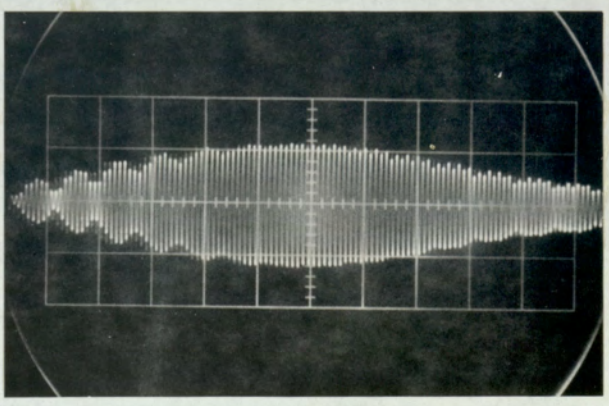

(d)

FIG. 78. HARMONIC GENERATION

fed into the r.f. receiver via the output attenuator A2, and the appropriate preamplifier, and displayed on the oscilloscope as an echo train. The effect of crystal conductivity, input acoustic intensity and applied d.c. voltage were then noted in terms of the output attenuator setting necessary for a displayed signal transit echo height of 3 cms on the 2 volt/cm scale of the oscilloscope.

At each harmonic frequency the peak to peak amplitude of the harmonic output corresponding to various, noted, output attenuator settings was measured by direct oscilloscope display. In order to determine from this the harmonic acoustic intensity within the crystal, immediately prior to transduction and subsequent detection, it was necessary to take into account the insertion loss of the particular transformer assembly being used on the output side of the crystal. It was assumed that this insertion loss was as previously determined from normal operation at that frequency. Normal operation is taken to mean acoustic generation and detection at the same frequency. If, for example, the 45 MHz. harmonic was to be monitored, the transformer matching assembly on the output side of the crystal was the same assembly used on the output side during normal operation at 45 MHz. The returning of this transformer assembly to obtain maximum transmission of the harmonic was minimal and thus the previously determined insertion loss was considered to be applicable. The acoustic intensity of the harmonic at the output face of the crystal was calculated in a similar way to that shown in appendix 4. A calibration graph of output attenuator setting versus harmonic intensity, Q_L, at the output crystal face was thus obtained for each harmonic frequency investigated. This graph appears as figure 79. Previous experimental work has indicated that the determined insertion loss of the 75 MHz transformer assemblies is in error and that calculated values of acoustic intensity at this frequency should be some four times greater than those obtained using this insertion loss. The 75 MHz. calibration plot given in figure 79

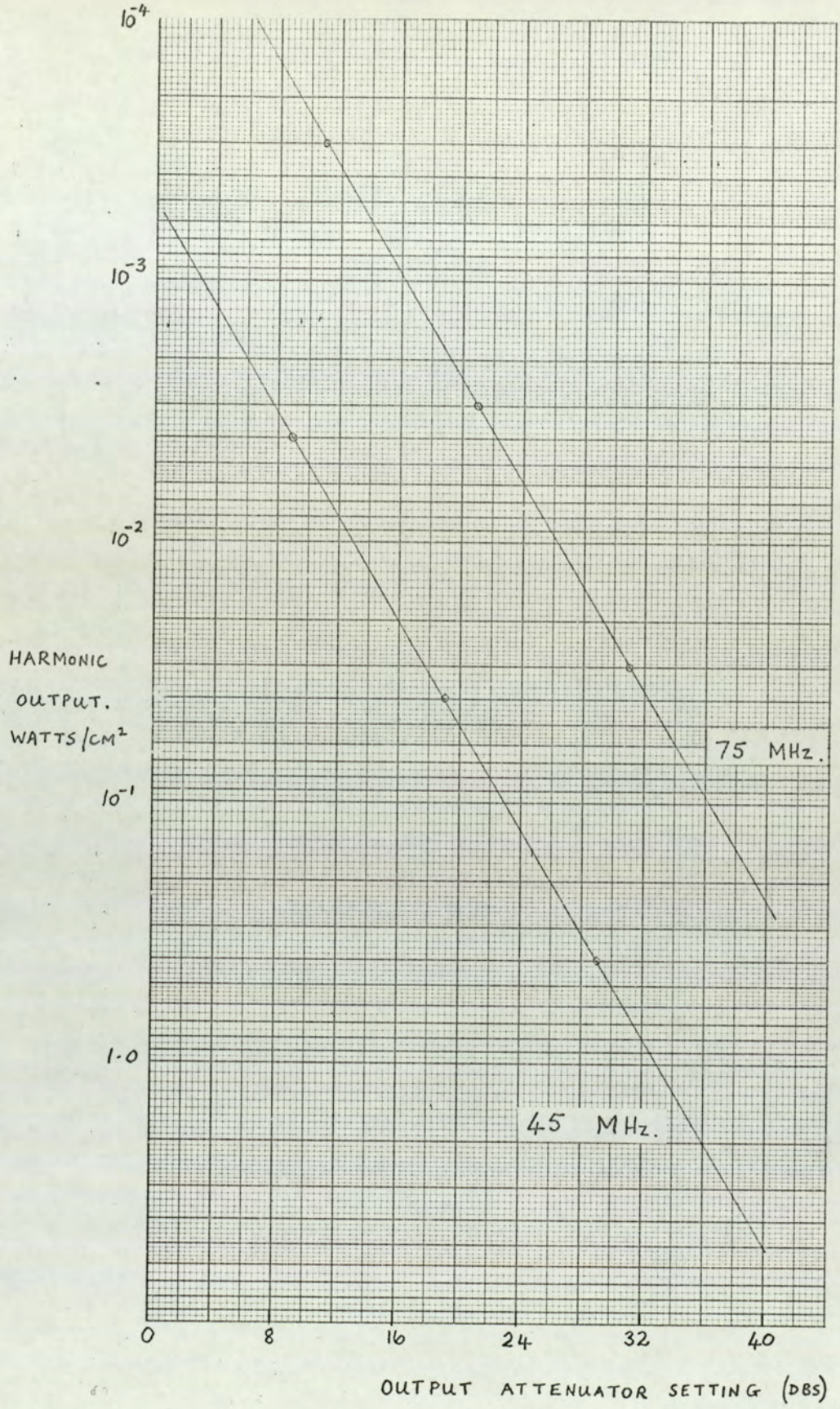

FIG. 79. HARMONIC OUTPUT ACOUSTIC INTENSITY VERSUS OUTPUT ATTENUATOR SETTING.

takes this error into account.

The primary objective was to assess the contribution to the measured acoustoelectric voltage due to each harmonic generated. The theory given in section 2.4. indicates the predicted acoustoelectric voltage under amplifying conditions to be given by:

$$V_{ae} = -\frac{R_m}{K E_{th}} Q_o \left(1 - e^{-2\alpha w}\right) e^{+2\alpha L} \quad - - - - - (5.6)$$

where Q_o is the input acoustic intensity. The problem here is that the harmonics are generated within the crystal, and therefore the parameter Q_o cannot be measured. However, if it is assumed that each harmonic originates at the input face of the crystal with an unknown Q_o then the factor $Q_o e^{+2\alpha L}$ indicates the acoustic intensity at the output face of the crystal. Thus this factor may be replaced in equation (5.6) by the experimentally determined Q_L. The predicted acoustoelectric voltage then becomes

$$V_{ae} = -\frac{R_m}{K E_{th}} Q_L \left(1 - e^{-2\alpha w}\right) \quad - - - - - (5.7)$$

Reference to figure 44(a) indicates the factor appearing in equation (5.7) to tend to unity for high values of amplification coefficient. Thus the predicted acoustoelectric voltage due to an acoustic signal of output intensity Q_L which has undergone high amplification during a single transit of the crystal is given by:

$$V_{ae} = -\frac{R_m}{K E_{th}} Q_L \quad - - - - - - - (5.8)$$

It will be made apparent shortly that the assessed values of harmonic amplification under the applied conditions relevant to this harmonic investigation are not sufficiently high to merit the use of equation (5.8). The acoustoelectric voltage due to the input 15 MHz signal and the third and fifth harmonics generated was therefore calculated using equation (5.7). The acoustoelectric voltage due to the second and fourth harmonics which unfortunately

could not be detected, since the output transducer only operated at odd harmonics of the fundamental frequency were then estimated in a manner to be described shortly. The total predicted acoustoelectric voltage due to the fundamental input signal and the harmonics up to the fifth harmonic was then obtained, and this was compared with the measured acoustoelectric voltage.

The crystal conductivity throughout the investigation was chosen to be 25.0 10^{-6} (ohm cm.)$^{-1}$ and for each input acoustic intensity, the d.c. voltage applied to the crystal was that known to result in an amplification of the 15 MHz. input signal of 6 dbs/L. As shown in figure 75 this ranged from 650 volts to 900 volts. Although the 15 MHz. output signal was not monitored during the harmonic investigation, except for the occasional check, the acoustoelectric voltage was checked to agree at each input intensity, with that measured during normal operation and reported in figure 75.

Figure 80 gives the output acoustic intensity of the detected third and fifth harmonics as a function of the input acoustic intensity of the 15 MHz. input signal. The 15 MHz. output intensity is also shown. As previously explained, output intensity in this context denotes the acoustic intensity immediately prior to transduction that is, the acoustic intensity at the output crystal face. The ratio of input intensity to output intensity of the 15 MHz. signal indicates 6 dbs. amplification.

In order to determine, as accurately as possible, the acoustoelectric voltage due to the harmonics, it was necessary to attempt an assessment of the amplification of the harmonic signals as they propagated through the crystal. To illustrate the manner in which this was accomplished, consider the harmonic output intensity shown in figure 80, for an input acoustic intensity of 0.18 watt/sq.cm. The output intensity of the 45 MHz. harmonic is seen to be approximately 0.065 watts/sq.cm. and of the 75 MHz. harmonic,

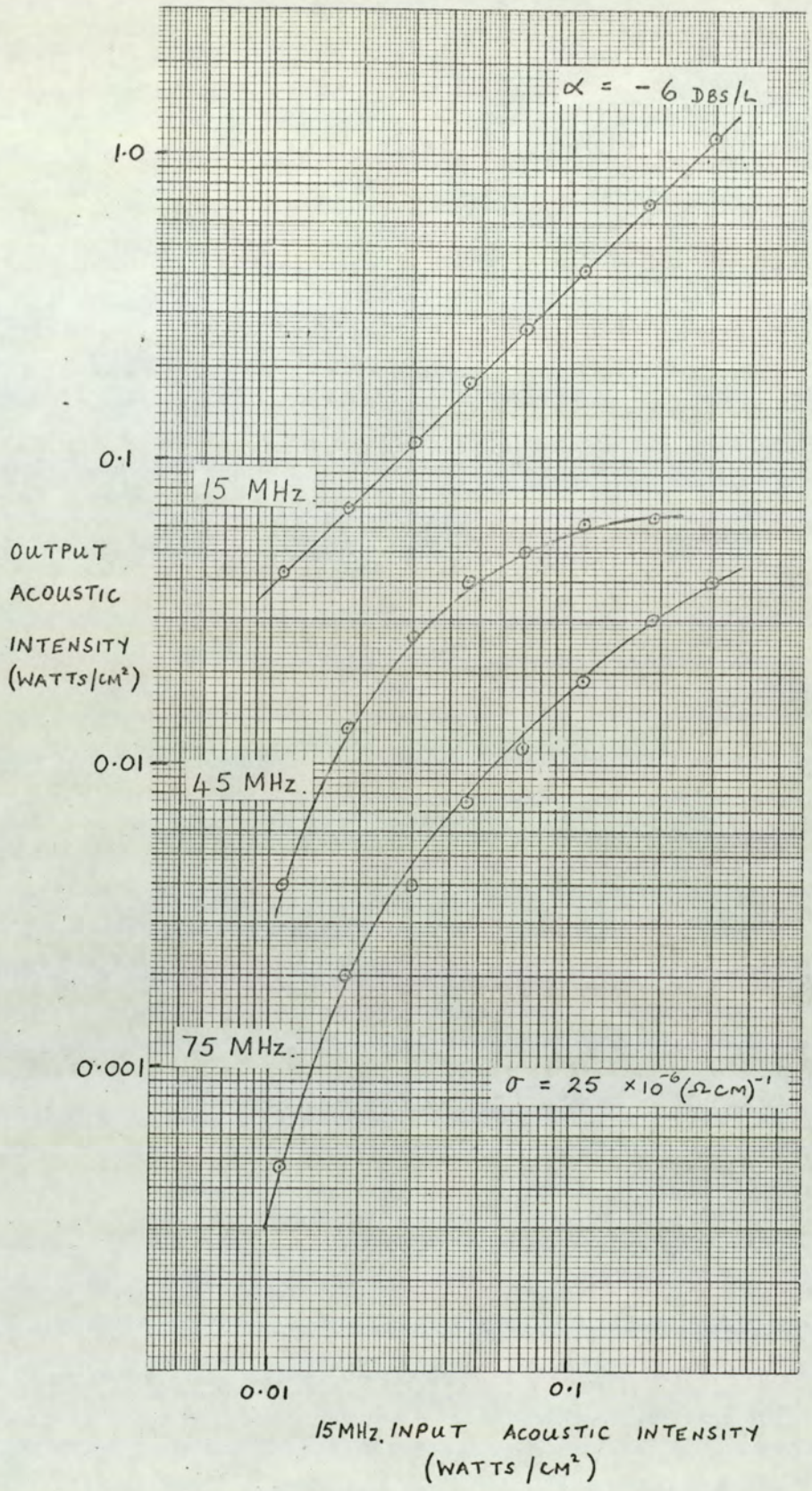

FIG. 80. HARMONIC OUTPUT VERSUS

15 MHz. INPUT ACOUSTIC INTENSITY

6 DBS/L AMPLIFICATION OF INPUT SIGNAL

$\sigma = 25 . 10^{-6}\ (\Omega CM)^{-1}$

0.03 watts/sq.cm. Reference to figure 34 indicates than an acoustic intensity of 0.065 watts/sq.cm. at 45 MHz. would be input to the crystal under normal calibrated operation if the db. setting of the input attenuator were 15.5 dbs. However, the question being asked here essentially, is what input intensity at 45 MHz. would result in an output intensity of 0.065 watts/sq.cm. if the crystal conductivity is 25 10^{-6} $(\text{ohm cm})^{-1}$ and the applied d.c. voltage is 800 volts. This applied voltage was that noted to result in an amplification of 6 dbs/L for this particular input acoustic intensity of the fundamental, as shown by figure 55.

Since the input-output characteristics at 45 MHz were not measured for a crystal conductivity of 25 10^{-6} $(\text{ohm cm})^{-1}$, recourse was necessary to the most relevant available input-output characteristics at this acoustic frequency to enable this question to be answered. These are given in figure 64, and were determined for a crystal conductivity of 17.5 10^{-6} $(\text{ohm cm})^{-1}$. Figure 84(a) indicates that, for applied voltages between 650 and 900 volts, the linear amplification of a 45 MHz acoustic signal is some 3 dbs/L greater at 25.0 10^{-6} $(\text{ohm.cm})^{-1}$ than that at 17.5 10^{-6} $(\text{ohm.cm})^{-1}$. It was therefore assumed that the input-output characteristics at 25.0 10^{-6} $(\text{ohm.cm})^{-1}$ were similar to those given in figure 64, but that under small signal conditions the amplification was 3 dbs/L greater. Figure 64 indicates that for an applied d.c. voltage of 800 volts, an input signal corresponding to a 40 dbs setting of the input attenuator is amplified by 24.5 dbs, and thus has an output intensity equal to the observed harmonic intensity. Using figure 34 it may be concluded that the effective input acoustic intensity of the harmonic is approximately 0.00027 watts/sq.cm.

Figure 44(a) indicates that the factor $\left(1-e^{-2\alpha w}\right)$, for α = 24.5 dbs/L, has a value of 0.75 and thus the acoustoelectric voltage due to the 45 MHz. harmonic generated by a fundamental signal of input intensity, 0.18 watts/sq.cm., may be calculated using

either equation (5.6) or (5.7).

A similar argument may be applied to the 75 MHz. harmonic. As previously noted, a 15 MHz. input signal of 0.18 watt/sq.cm. with 800 volts d.c. applied to the crystal of conductivity 25. 10^{-6}(ohm cm)$^{-1}$, results in a 75 MHz. harmonic output intensity of 0.03 watts/sq.cm. Figure 35 shows that under normal calibrated operation at 75 MHz. such an acoustic intensity would be input to the crystal if the db. setting of the input attenuator were about 10 dbs. However a 6 db correction is necessary to this value to account for the previously referred to error in the insertion loss measurement at this frequency. Thus the db. setting which results in a "true" input acoustic intensity of 0.03 watts/sq.cm. is not 10 dbs, but 16 dbs. Reference to figure 72 indicates than an input acoustic signal corresponding to 43 dbs in the input attenuator is amplified 27 dbs under these applied conditions and thus has an output intensity of 0.03 watts/sq.cm. The effective input intensity of the 75 MHz signal corresponding to an input attenuator setting of 43 dbs is seen to be 0.00006 watts/sq.cm. after suitable correction of figure 35. From figure 44(a) the factor $\left(1 - e^{-2\alpha w}\right)$ for 27 dbs amplification is 0.78.

Using the information thus derived it is possible to estimate what fraction of this particular fundamental input acoustic intensity is converted to each of the odd harmonics at the input face of the crystal in order that the measured harmonic output results. This will be shown to be necessary to enable a determination of the acoustoelectric voltage generated by the even harmonics.

It has been shown that with 800 volts d.c. applied to the crystal of conductivity 25.0 10^{6} (ohm cm.)$^{-1}$, a 15 MHz. input acoustic intensity of 0.18 watts/sq.cm. generates a detected 45 MHz. output intensity of 0.065 watts/sq.cm. Normal operation of the amplifier under these conditions shows that this output intensity would result from a 45 MHz. input acoustic signal of intensity 0.00027 watts /sq. cm. This is 0.15 % of

the 15 MHz. input intensity which resulted in the detected harmonic output. Similarly, a 75 MHz. input intensity of only 0.00006 watts/sq.cm would, under normal operation, result in an output intensity signal equal to the observed 75 MHz. output harmonic intensity and this is estimated to be 0.033% of the 15 MHz. input intensity producing this harmonic output.

Column 2 of Table 2 indicates the applied d.c. voltage required to amplify each 15 MHz. input by 6 dbs/L. The amplification coefficient of the resulting 45 MHz. and 75 MHz. harmonics was determined in each case from the input-output characteristics as explained. The example illustrating this determination was chosen because, in this particular case, 800 volts were applied to the crystal, and input-output plots were available at each frequency for this applied voltage. This was considered to facilitate appreciation of the argument. At other input intensities however, interpolation of the available input-output plots was necessary to enable an accurate assessment of the harmonic amplification. The results obtained are given in columns 4 and 6 of Table 2.

In order to obtain a realistic evaluation of the sum acoustoelectric voltage due to all the harmonics up to, and including, the 75 MHz. harmonic it is necessary to determine the contribution due to the 30 MHz. and 60 MHz. harmonics also.

Since the 15 MHz. fundamental transducers used in the fabrication of the amplifier operated only at odd harmonics of the fundamental frequency, all conclusions regarding these even harmonics had to be drawn from available information obtained from the investigation of the odd harmonics. The output acoustic intensity of the even harmonics may not be measured, and thus calculation of the acoustoelectric voltage due to these harmonics demands a knowledge of the amplification coefficient and also their effective input acoustic intensity. The amplification coefficient of the 60 MHz

TABLE 2

15 MHz.Input Acoustic Intensity Watts/Sq.Cm	Applied DC Voltage	Amplification Coefficient (Dbs/L)				
		15 MHz	30 MHz	45 MHz	60 MHz	75 MHz
0.011	650	6	15	25	25	25
0.018	680	6	20	31	31	31
0.030	700	6	22	30	29	27
0.045	720	6	23	30	29	27
0.070	740	6	24	30	29	27
0.110	770	6	24	28	28	27
0.180	800	6	24	25	26	27
0.300	900	6	22	20	22	23

TABLE 3

15 MHz.Input Acoustic Intensity Watts/Sq.Cm	% Input Intensity Conversion to Harmonics of Frequency (MHz)			
	30	45	60	75
0.011	0.28	0.10	0.036	0.013
0.018	0.14	0.08	0.037	0.022
0.030	0.16	0.09	0.049	0.027
0.045	0.15	0.09	0.052	0.031
0.070	0.15	0.09	0.056	0.035
0.110	0.17	0.10	0.060	0.036
0.180	0.32	0.15	0.070	0.033
0.300	0.66	0.30	0.154	0.070

harmonic, reported in column 5 of Table 2, was estimated by considering the values determined for the 45 MHz and 75 MHz harmonics, and the results reported in column 3 of this Table for the 30 MHz harmonic were obtained by interpolating between the appropriate small signal amplification at 15 MHz. described in figure 83, and the 45 MHz. harmonic amplification coefficients given in column 4 of Table 2.

The input acoustic intensity of the even harmonics was determined as follows. In the manner already indicated it was possible to calculate what fraction of each 15 MHz input acoustic intensity was converted to the 45 MHz and 75 MHz harmonics at the input face of the crystal in order that after appropriate amplification, as indicated in Table 2, the detected harmonic output resulted. The results thus calculated are given in Table 3, and it will be noted that the percentage conversion to 45 MHz. is greater than the percentage conversion to 75 MHz. for any given fundamental input. It was thus assumed that the percentage conversion of the fundamental input acoustic intensity to 60 MHz. harmonic was greater than to 75 MHz., but less than to 45 MHz., which was in turn less than the percentage conversion to 30 MHz. harmonic. A geometrical relationship between that converted at each frequency was considered more acceptable than an arithmetical relationship. Thus, for a given 15 MHz. input, the percentage intensity conversion to a 45 MHz. signal to that converted to a 60 MHz. signal was taken to be equal to the ratio of 60 MHz. conversion to 75 MHz. conversion. This assumption allowed the calculation of the percentage conversion to 60 MHz. given in column 4 of Table 3. Considering the geometrical progression of intensity conversion to apply to the second harmonic also, column 2 of Table 3 was calculated by extrapolation. It was therefore possible now to calculate the input acoustic intensity of the 30 MHz. and 60 MHz. harmonic signals for each value of 15 MHz. input intensity.

A knowledge of the input acoustic intensity, and the subsequent amplification during propagation through the crystal allowed the calculation of the acoustoelectric voltage due to the even harmonics using equation (5.6). Table 4 gives the acoustoelectric voltage calculated for each harmonic over the acoustic intensity range investigated and the last column of this Table indicates the total contribution due to all the harmonics. This is plotted against the 15 MHz. input acoustic intensity in figure 81. Also shown in this figure is the measured acoustoelectric voltage which has been taken from figure 75.

The results of this experiment, and the assumptions made to enable the calculation of the sum acoustoelectric voltage will be discussed in the following chapter.

It will be noted that figure 80 indicates the 45 MHz. harmonic output to saturate as the input intensity of the fundamental is increased. To investigate this further, the 45 MHz. harmonic output was plotted as a function of input acoustic intensity of the fundamental acoustic signal, under different applied conditions. Figure 82(a) shows this for an applied d.c. voltage of 800 volts for a crystal conductivity of 16.0 10^{-6} (ohm cm.)$^{-1}$. It may be seen that for small input acoustic intensities the harmonic output varies as the cube of the input intensity. As the input acoustic intensity of the fundamental is increased however, the harmonic output is seen to saturate. Deviation from the small signal slope occurs for an input attenuator setting of 44 dbs. Reference to figure 53, which presents the appropriate input-output characteristics of the fundamental, indicates that with 800 volts d.c. applied to the crystal, the fundamental also starts to deviate from linearity at approximately this input attenuator setting.

Similar results have been reported by Tell[75], who has proposed a theory of harmonic generation. The piezoelectric field

TABLE 4

15 MHz Input Acoustic Intensity Watts/Sq.Cm	Estimated Acoustoelectric Voltage(mV) Frequency (MHz)					Total V_{ae}
	15	30	45	60	75	
0.011	3.2	0.1(5)	0.7	0.2	0.10	4.3
0.018	5.2	0.4	3.7	1.7	1.0	12.0
0.030	9.0	1.5	6.3	3.5	2.0	22.3
0.045	13.5	2.5	9.5	5.3	1.5	32.3
0.070	21.0	5.4	15.0	9.3	2.5	53.2
0.110	32.0	9.5	15.5	16.0	4.3	77.3
0.180	52.0	30.0	17.5	17.5	6.7	123.7
0.300	90.0	62.0	17.4	15.5	6.5	191.4

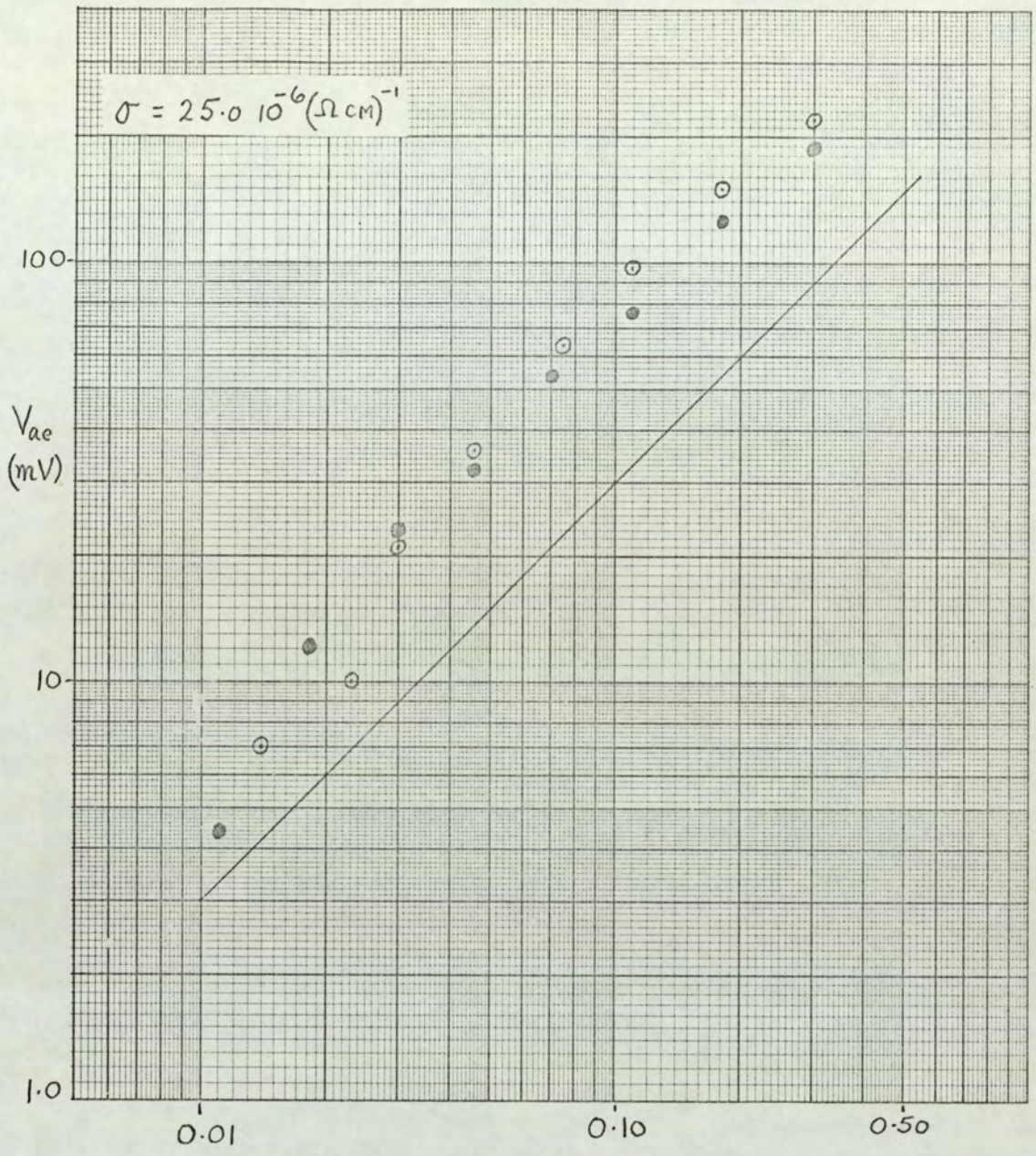

——— ACOUSTOELECTRIC VOLTAGE PREDICTED FOR 6 DBS/L GAIN OF THE 15 MHz. INPUT.

⊙ ⊙ MEASURED ACOUSTOELECTRIC VOLTAGE.

● ● ESTIMATED TOTAL ACOUSTOELECTRIC VOLTAGE DUE TO HARMONICS AND THE FUNDAMENTAL.

FIG. 81. THE ACOUSTOELECTRIC VOLTAGE ARISING FROM THE GENERATION OF HARMONICS

and the strain were expressed as a Fourier series, and the second harmonic was assumed to be small compared to the fundamental. Higher harmonics were considered negligible. Although second harmonic generation has been observed by several workers as indicated in chapter 1, experimental work concerning higher harmonics does not appear to have been reported in the literature.

Figure 82(b) presents the change in harmonic output measured for a higher crystal conductivity, but lower applied voltage than that of figure 82(a). Note that here the slope of the curve is not quite 3 as expected from theory [75]. Saturation of the harmonic output is seen to occur at about the same measured output intensity as in figure 82(a). Similar experiments to measure the harmonic output at 75 MHz. as a function of input acoustic intensity of the fundamental showed the harmonic output to vary as the fifth power of the input intensity at very small inputs only. As the input intensity was increased the harmonic output did not increase at the expected rate. The variation of the 75 MHz. harmonic output shown in figure 80 does indicate an increase according to theory smallest input intensities.

The acoustoelectric origin of the harmonics was established by noting the disappearance of any detectable harmonic when the crystal was returned to its insulating state by removing the illumination. The variation in amplitude of the second harmonic as a function of the electron density in the absence of an applied d.c. field has been reported by Kroger [73]. This showed the harmonic output to increase to a maximum and then to decrease to almost nothing as the electron density was increased. Similar results were noted for the higher harmonics with the crystal used in this research. Since a comprehensive experimental investigation of harmonic generation would constitute a separate study, no further work concerning harmonic generation will be reported. However some general suggestions relating to such a study are given in chapter 7.

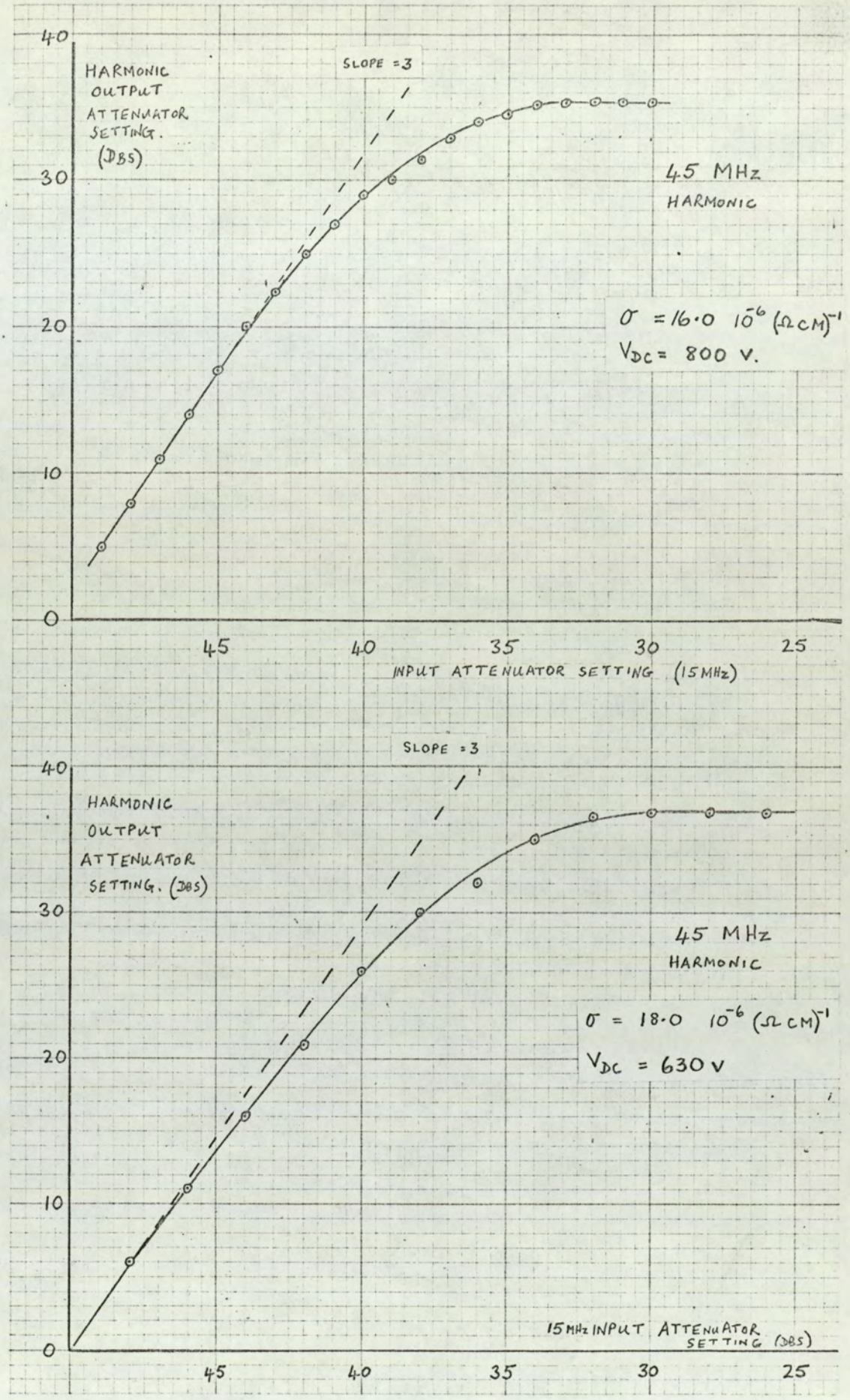

FIG. 82. 45 MHz HARMONIC OUTPUT VERSUS 15 MHz INPUT INTENSITY. APPLIED DC VOLTAGE AND CRYSTAL CONDUCTIVITY CONSTANT. TWO CASES

5.3.4 The effect of carrier trapping on the Weinreich relationship

An account of the effect of carrier trapping on both acoustic propagation and the acoustoelectric field has been given in chapter 1. The impetus to consider carrier trapping came from the experimental work of Wang [36] who showed that the acoustic and acoustoelectric crossover occurred at different applied voltages. Greebe [40,41] suggested that the trapped space charge would not be in phase with the mobile space charge and Uchida et al [45,46] modified White's theory accordingly. The theory of Uchida has been described in more detail in chapter 2. Southgate and Spector [47] have considered the effect of carrier trapping on the acoustoelectric field in a similar manner, and derived a modified Weinreich relationship. This work is also described in chapter 2 in more detail.

After this discussion of the prominent theories associated with the effects of trapping on acoustoelectric effects an analysis was presented which allowed the trapping parameters to be determined from experiment. The relevant equations are given below:

$$f_r = \left[P + \left(\frac{\omega}{\omega_D}\right)\frac{1}{X} \right]^{-1} \qquad (5.9)$$

$$f_i = \left\{ X \left[P + \left(\frac{\omega}{\omega_D}\right)\frac{1}{X} \right] \right\}^{-1} \qquad (5.10)$$

$$\omega\tau = \left[X\,(P-1) + \left(\frac{\omega}{\omega_D}\right) \right]^{-1} \qquad (5.11)$$

$$X = \left[\frac{4A}{(1-A)^2} \right]^{\frac{1}{2}}$$

$$A = \left| \left(\frac{\alpha_{MAX}}{\alpha_{MIN.}} \right) \right| \qquad (5.12)$$

$$P = \left. \frac{v_d}{v_s} \right)_{\alpha = 0}$$

It was argued that the parameters A and P could be determined quite easily and after determining f_v, f_j and $\omega\tau$ the effect of trapping on the acoustoelectric field could be calculated using the theory of Southgate and Spector, and the results compared with experiment. Such an experimental test of these theories has not been reported previously.

The experimental work presented in section 5.3 of this chapter indicates that the applied voltage necessary for acoustic crossover increases substantially as the input acoustic intensity is increased. In order to investigate trapping effects it is therefore necessary to ensure that such power effects are absent, by obtaining experimental results with a small acoustic intensity input signal. Since the measured acoustoelectric voltage is proportional to input acoustic intensity this has meant that a valid experimental test of the trapping theories can be carried out only for small acoustoelectric voltages. This provides further justification for determining the trapping parameters from experimental data obtained by observing the acoustic crossover and attenuation and not the acoustoelectric voltage.

Figure 83 presents the observed variation of attenuation coefficient with applied voltage of a very small 15 MHz input acoustic signal, at various crystal conductivities. The polarity of the applied d.c. voltage was reversed in the manner described in chapter 4, and the observed attenuation variation for a positive going applied voltage is also given. Figure 84(a) presents the same information obtained for a 45 MHz. input signal and figure 84(b) for a 75 MHz. acoustic input.

Strong anomalous behaviour was observed in the attenuating region at 45 MHz. as indicated. A small increase in crossover voltage was noted at 45 MHz. for low crystal conductivities, but at higher crystal conductivities the crossover voltage of the acoustic signal was determined to be a constant. The amplification

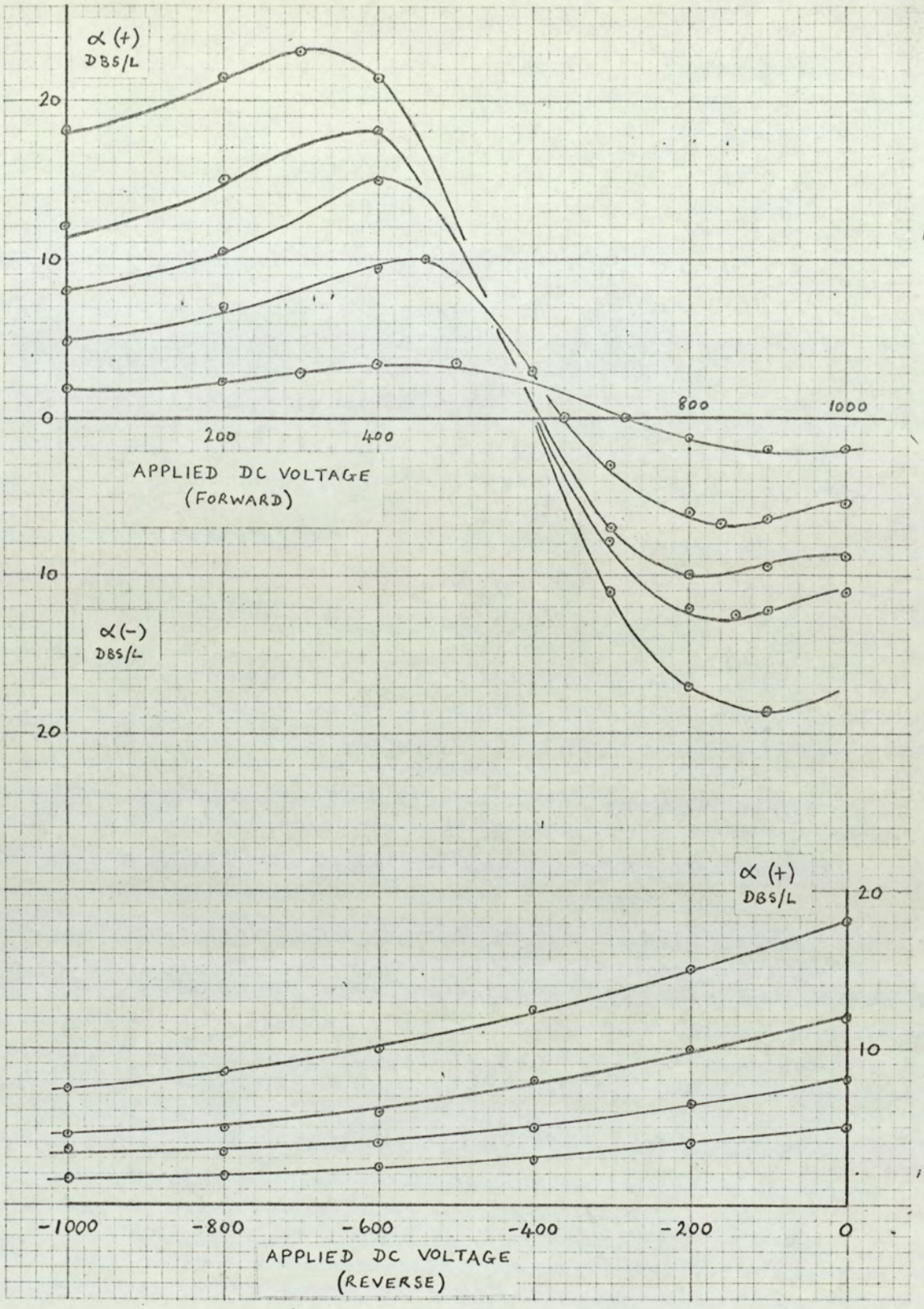

FIG. 83. VARIATION OF ATTENUATION (α +) COEFFICIENT WITH APPLIED D.C. VOLTAGE 15 MHz. VARIOUS CONDUCTIVITIES.

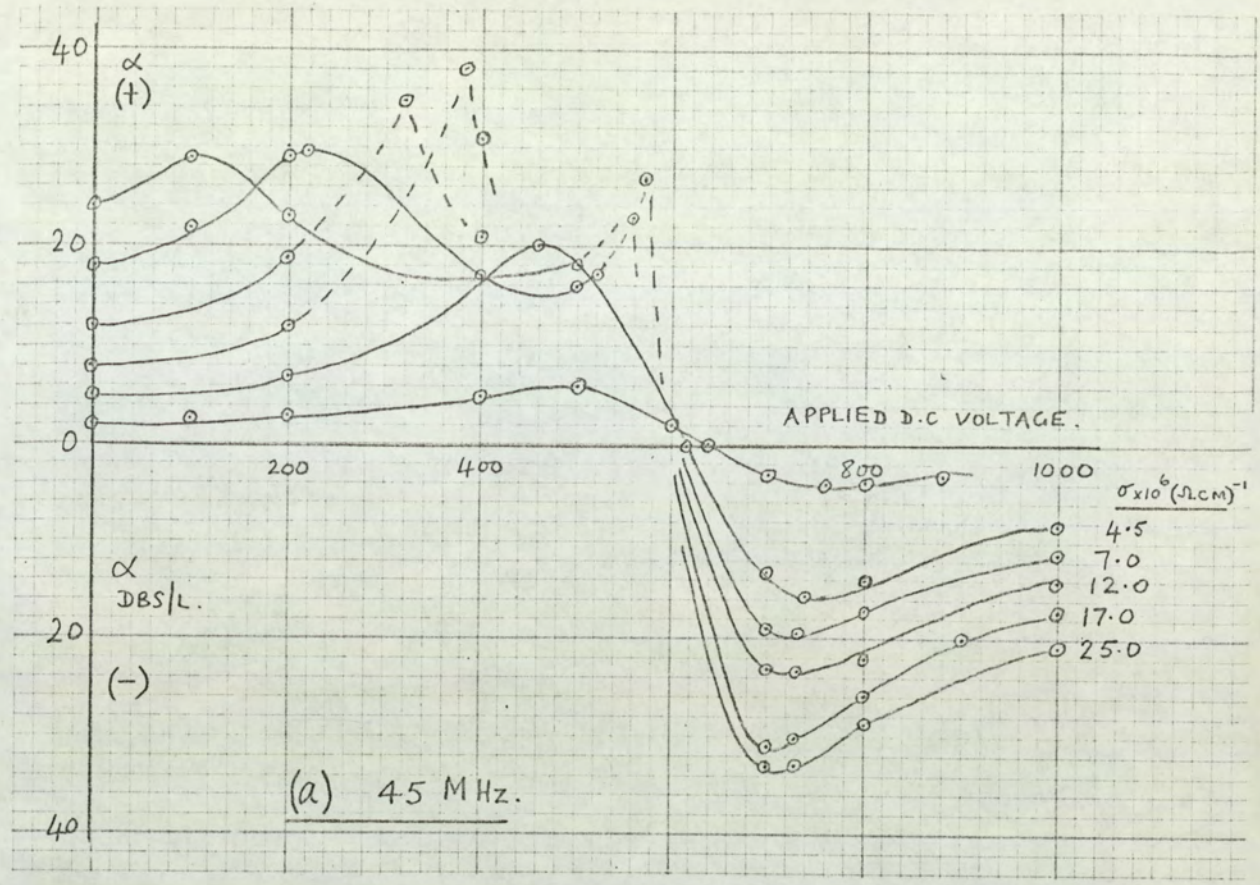

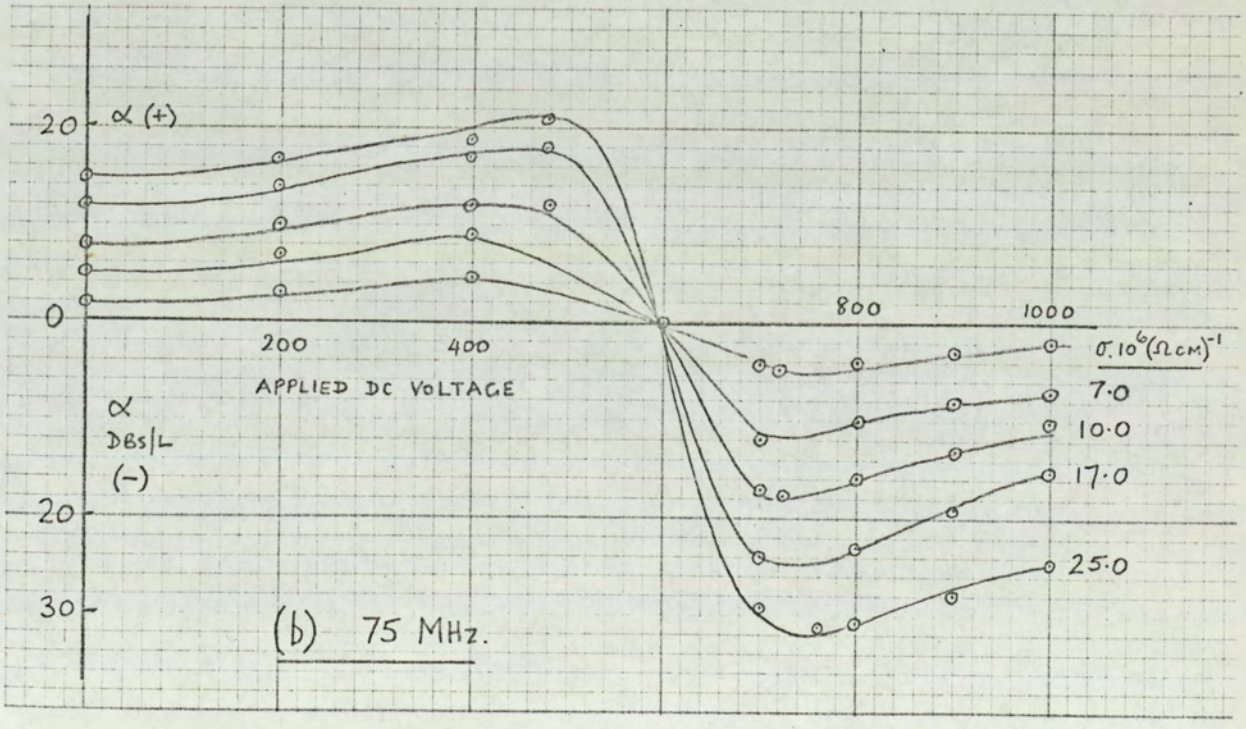

FIG 84. VARIATION OF ATTENUATION COEFFICIENT WITH APPLIED VOLTAGE. AT (a) 45 MHz. (b) 75 MHz.

characteristics at 45 MHz. are seen to be well behaved, with large recorded gains at high crystal conductivities. A brief discussion of the anomalous attenuating behaviour observed at 45 MHz. will be given in chapter 6.

The attenuation - d.c. voltage characteristics measured at 75 MHz. indicate no change in acoustic crossover though the maximum gain exceeds the maximum loss under a given set of conditions.

The observed characteristics at 15 MHz., reported in figure 83 do allow the calculation of the trapping parameters, and table 5 presents the ratio of maximum attenuation to maximum gain, $\left(\frac{\alpha_{MAX}}{\alpha_{MIN}}\right)$, at each conductivity and also records the acoustic crossover voltage expressed as a ratio of electron drift velocity to acoustic velocity. This experimental data allows the calculation of the trapping parameters f_r , f_j , and $\omega\tau$, using equations (5.9) to (5.12). These are also given in table 5. Southgate and Spector note that the applied voltage resulting in acoustoelectric field crossover, expressed as the ratio of electron drift velocity to acoustic velocity is given by

$$\left.\frac{v_d}{v_s}\right)_{E_{ae}=0} = \frac{f_r}{(f_r^2 + f_j^2)} \quad - - - - - \quad (5.13)$$

Using the calculated values of f_r and f_j appearing in table 5 this ratio may be determined at each crystal conductivity. This is given in table 6, column 4, as an applied voltage. Column 3 of table 6 gives the observed d.c. voltage producing acoustoelectric voltage crossover at each crystal conductivity. Agreement between the predicted values and those observed is reasonable.

The observed asymmetry of the attenuation - d.c. voltage characteristics observed at 15 MHz. appear to be consistent with the observed acoustic and acoustoelectric crossover voltages, as described by the trapping theories. The asymmetry at 45 MHz. is not due to carrier trapping and demands alternative explanation.

TABLE 5

$\sigma \times 10^6$ (OHM CM)$^{-1}$	MAX. ATTEN / MAX. GAIN (A)	$\left(\frac{v_d}{v_s}\right)_{\alpha=0}$	f_r	f_j	$\omega\tau$
2.2	1.71	1.20	0.84	0.270	1.32
6.0	1.52	1.07	0.94	0.200	2.9
9.5	1.52	1.03	0.97	0.196	5.5
16.0	1.43	1.02	0.98	0.176	8.8
25.0	1.25	1.00	1.00	0.112	52.0

TABLE 6

$\sigma \times 10^6$ (OHM CM)$^{-1}$	$V_{DC.}$ ($\alpha=0$) OBSERVED	$V_{DC.}$ ($E_{ae}=0$) OBSERVED	$V_{DC.}$ ($E_{ae}=0$) CALCULATED
2.2	720	650	660
6.0	640	610	615
9.5	610	600	605
16.0	605	600	600
25.0	600	600	600

5.3.5 Current saturation

A brief account was given in chapter 1 of the work which has been reported in the literature relating to the amplification of broadband acoustic flux, and the resulting current saturation. Strong acoustic flux build up was observed during the course of the experimental work and this section describes some typical measurements carried out. These measurements indicate to what extent the total crystal current departs from an ohmic value due to the acoustoelectric current accompanying the acoustic flux build up, under various conditions of applied voltage and crystal conductivity. The effect of the acoustic flux amplification on the amplification of an input acoustic signal is also noted.

Figure 85 clearly shows the current saturation to be closely related to acoustic flux amplification. Figure 85(a) shows the simultaneously monitored applied voltage (bottom trace) and crystal current (top trace). Figure 85(b) indicates the voltage to be applied some 40 μ secs after an acoustic signal is input to the crystal. The detected echo train is shown at the far left of the photograph. Figure 85(c) shows acoustic flux build up to be substantial when the crystal conductivity is increased, and the final photograph shows the resulting current saturation.

Figure 86 demonstrates the usefulness of a differential display in the measurement of the acoustoelectric voltage due to the flux amplification. Figure 86(a) shows the acoustic display and the simultaneously displayed applied voltage. Fig 86(b) shows the differential amplifier display when the variable resistor R_m referred to in section 4.4. is made equal to the crystal resistance. Figure 86(c) shows the effect of increasing the applied voltage. The acoustic display shows the amplified acoustic flux, and the resultant acoustoelectric voltage is displayed with great sensitivity in figure 86(d). Such a display allows the measurement of the

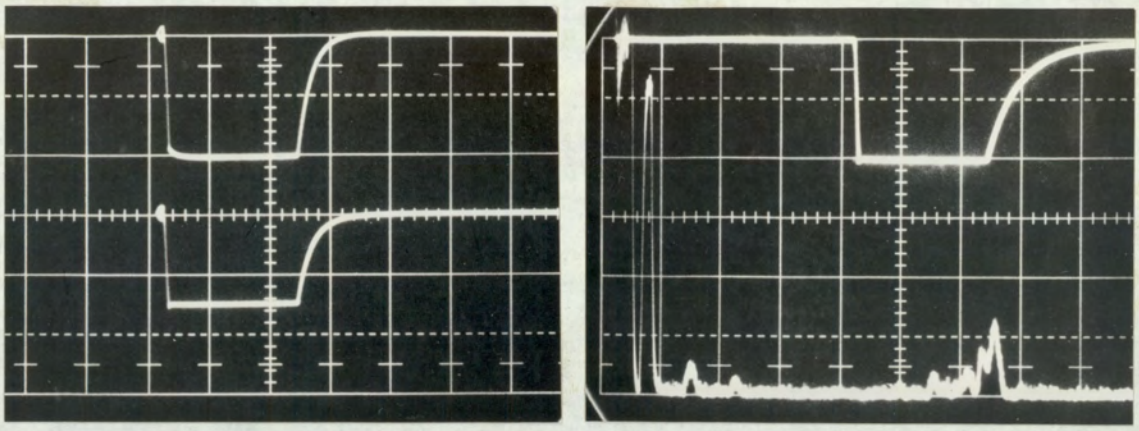

(a) (b)

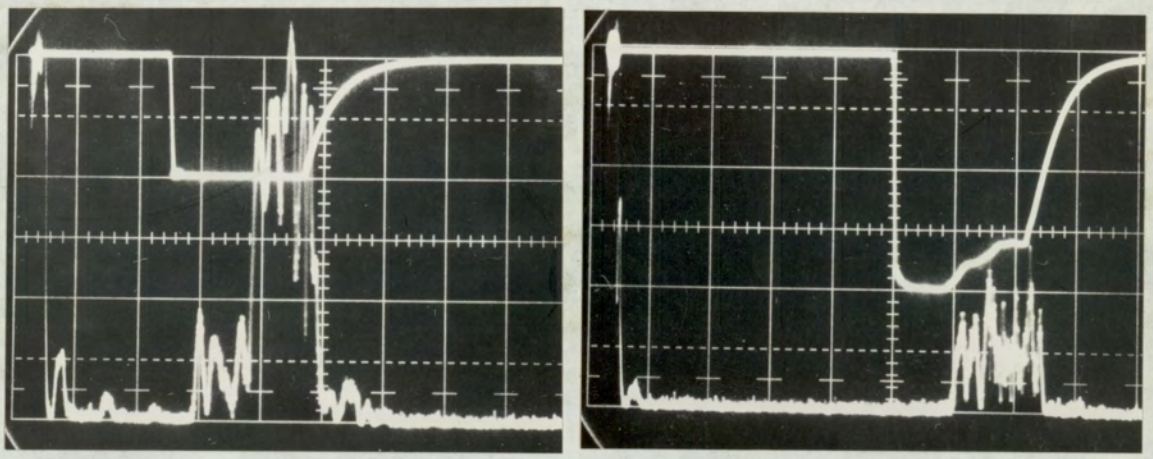

(c) (d)

PHOTOGRAPH

SCALES	
CURRENT	10 MA | SQ.
VOLTAGE	400 V | SQ

(a) TOP TRACE : CURRENT
BOTTOM TRACE : APPLIED DC VOLTS.
ATTENUATING VOLTAGE
NO CURRENT DECAY.

(b) TOP TRACE : DC VOLTAGE
BOTTOM TRACE : ACOUSTIC DISPLAY
FLUX BUILD UP STARTING.

σ FOR (a) AND (b) $8.8\ 10^{-5}\ (\Omega\ \text{CM.})^{-1}$

(c) σ INCREASED TO $1.1\ 10^{-4}\ (\Omega\ \text{CM.})^{-1}$

(d) CORRESPONDING CURRENT DECAY.

FIG 85. CURRENT DECAY DUE TO ACOUSTIC FLUX AMPLIFICATION.

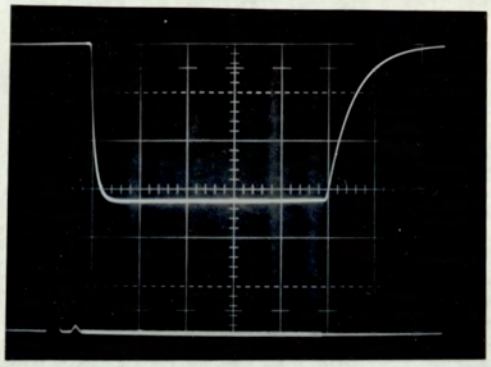

(a)

TOP TRACE D.C. VOLTAGE
SCALE : 200 V/SQUARE
BOTTOM TRACE ACOUSTIC DISPLAY
TIME SCALE 10 μSEC/SQUARE

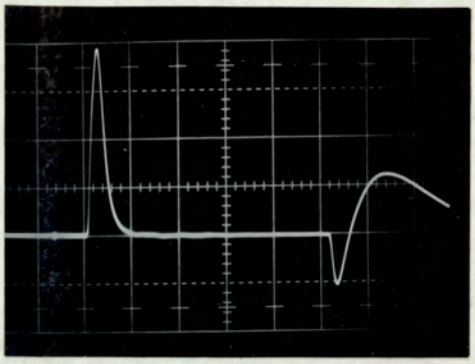

(b)

DIFFERENTIAL
AMPLIFIER DISPLAY.

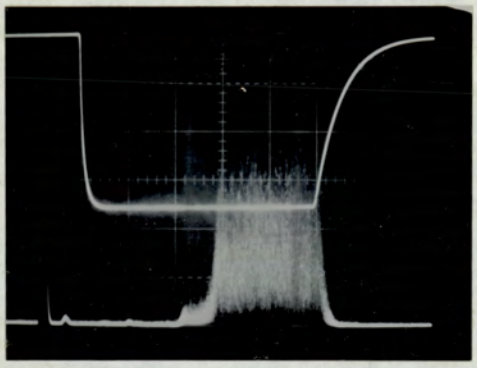

(c)

VOLTAGE INCREASED
FLUX BUILD UP.

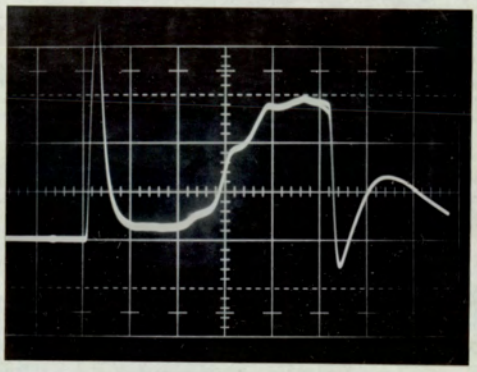

(d)

DIFFERENTIAL
AMPLIFIER DISPLAY
SCALE 50 MV/SQUARE

FIG. 86. DIFFERENTIAL AMPLIFIER

DISPLAY OF ACOUSTOELECTRIC
VOLTAGE ACCOMPANYING FLUX
AMPLIFICATION

ohmic current, and the reduced current at any chosen time after the application of the applied voltage.

For a given crystal conductivity the displayed acoustic flux was observed to grow as the applied voltage was increased from the crossover value of 600v. For an applied voltage of about 800 volts however the acoustic flux was observed to become attenuated, with correspondingly less reduction of the total crystal current. This is shown in figure 87 where the crystal current has been measured over a wide range of applied voltage for six crystal conductivities. No acoustic flux amplification was observed for applied voltages less than 600 volts, which was also generally recorded as being the crossover voltage for the onset of acoustic amplification of a small intensity input acoustic signal. For voltages greater than 600 volts acoustic flux amplification resulted in current reduction and two measurements of current were made. The ohmic value was measured shortly after the application of the applied voltage and before flux amplification occurred. The reduced current measurement was made 50μsecs after voltage application.

In figure 87 the crystal conductivity is expressed in terms of the voltage appearing across R_m , the small resistance in series with the crystal. The ordinate of figure 87 expresses the crystal current in terms of $V_{\ell m}$, the voltage measured across R_m . In order to obtain the crystal current it is necessary to divide this voltage by the value of R_m , namely 520 ohms.

McFee [31] has shown that the presence of acoustic flux substantially reduces the possible amplification of an input acoustic signal. Figure 88 presents a typical example of this. Figure 88(a) shows the detected single transit acoustic signal which has been amplified during transit in the absence of significant acoustic flux. Flux amplification is seen to become significant after 25μsecs however. Figure 88(b) shows a reduction in the amplification of

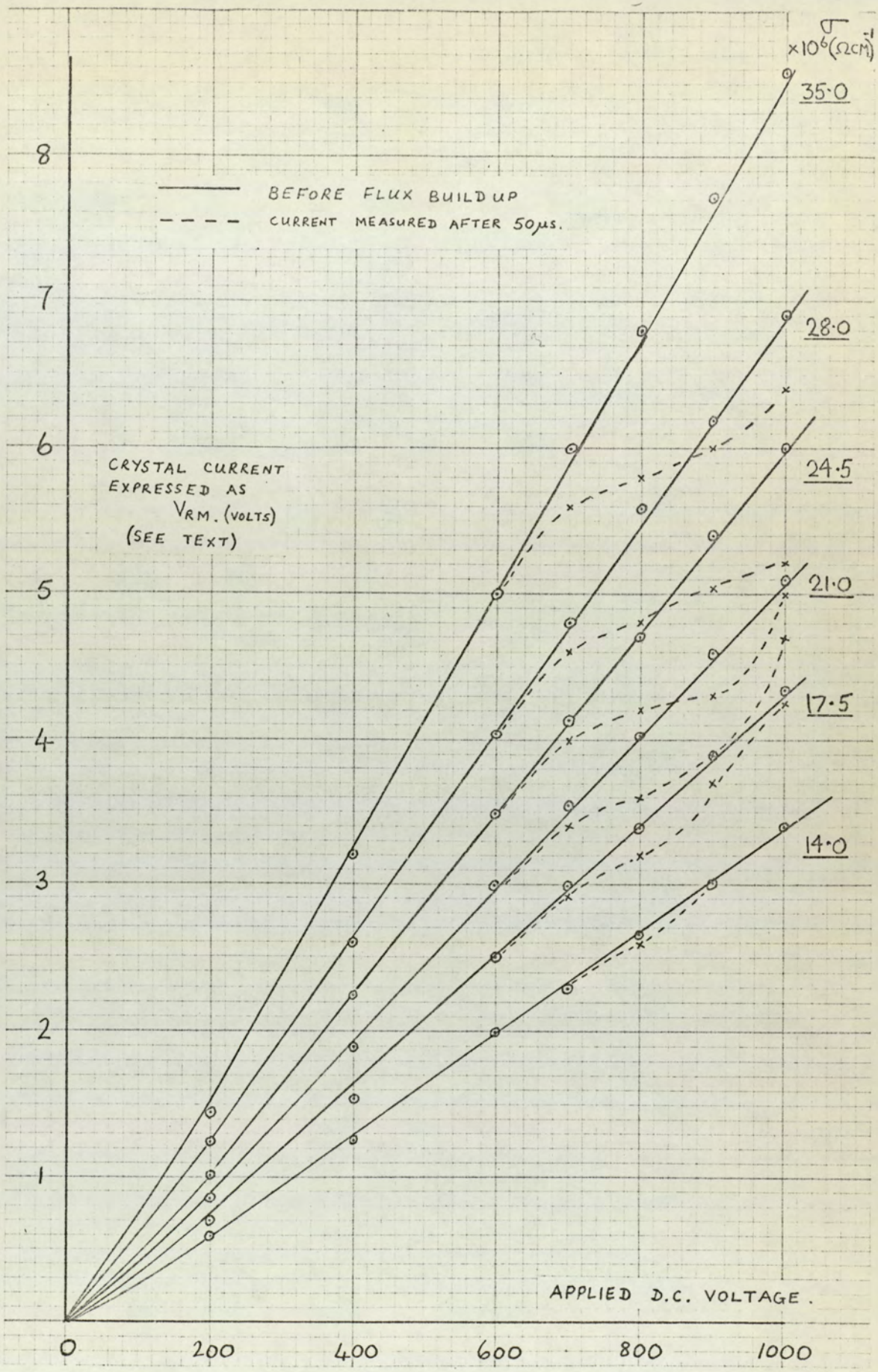

FIG. 87. CURRENT - VOLTAGE CHARACTERISTICS

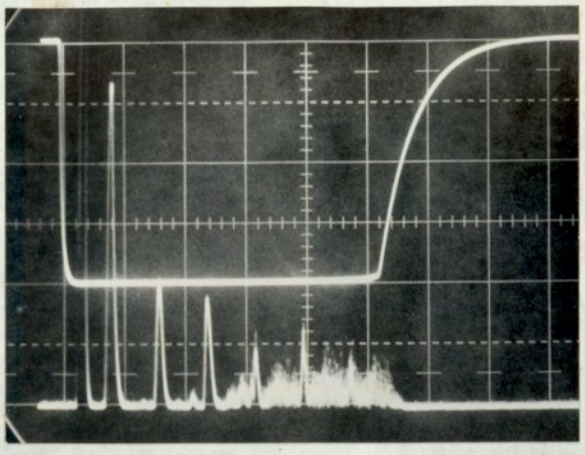

(a)

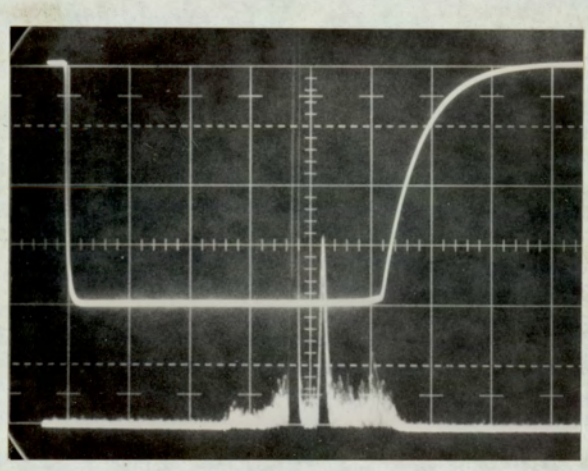

(b)

GENERAL : 45 MHz OPERATION

UPPER TRACE : APPLIED D.C. VOLTAGE

LOWER TRACE : ACOUSTIC ECHO TRAIN.

HORIZONTAL 10 μSEC. / SQUARE

VERTICAL 200 VOLTS / SQUARE:

PHOTOGRAPH (a) ~ SHOWING FLUX BUILD-UP AFTER 30 μSECS.

(b) ACOUSTIC INPUT DELAYED ~ REDUCTION OF GAIN OF FIRST TRANSIT SIGNAL

FIG 88. EFFECT OF FLUX GROWTH ON ACOUSTIC TRANSMISSION

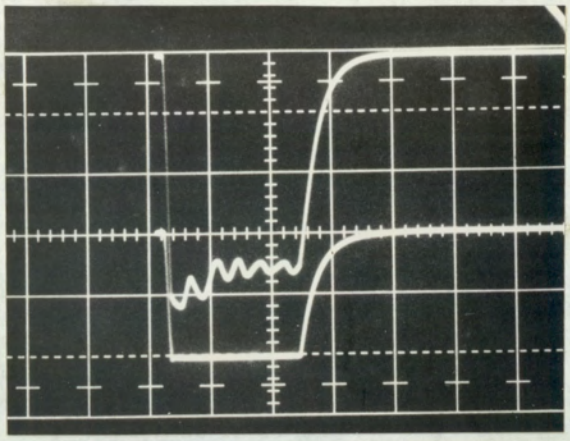

(a)

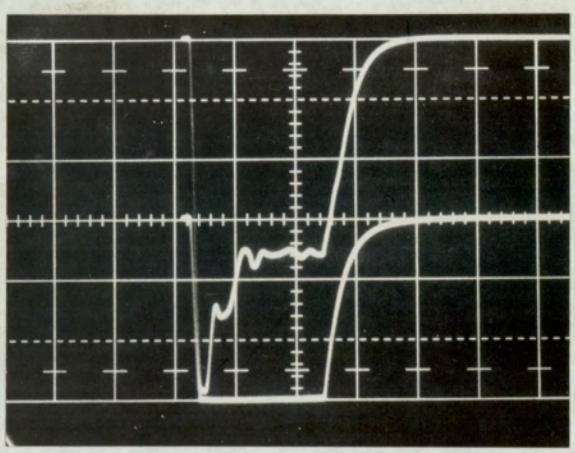

(b)

$\sigma = 1.1 \; 10^{-4} \; (\Omega \text{ CM.})^{-1}$

HORIZONTAL : 20 μSECS / SQUARE.

TOP TRACE : CRYSTAL CURRENT

SCALE 10 M.A. / SQUARE

BOTTOM TRACE : APPLIED DC VOLTAGE.

SCALE 400 VOLTS / SQUARE

FIG. 89 CURRENT OSCILLATION PRODUCED BY ACOUSTIC FLUX.

the input signal, when input to the crystal in the presence of the amplified flux. The reduction of gain is substantial and thus the amplification of broadband acoustic flux is a serious drawback to any commercial application of the acoustoelectric amplifier as an amplifying device.

Figure 86(d) shows the acoustoelectric voltage due to the flux build up to be "stepped". McFee [31] has identified maxima in the display of acoustic flux with minima in the corresponding current saturation, and has argued that this is associated with the acoustic flux propagating to and fro in the crystal. Under certain circumstances the effect of the flux is to produce current oscillation. Much experimental work has been carried out on current oscillation, and reported in the literature. Figure 89 shows an example of current oscillation due to the flux amplification. The operating details appear under the photographs.

Although an investigation into current oscillation is outside the scope of this thesis, a review of some of the published work was given in chapter 1 since such oscillation is inherently attributable to an acoustoelectric voltage resulting from flux amplification.

CHAPTER 6

Discussion of the results

6.1 The results obtained with no drift voltage applied to the crystal

6.1.1 The variation of attenuation coefficient with crystal conductivity

The variation of attenuation coefficient with crystal conductivity, measured at four acoustic frequencies, in the absence of an applied d.c. voltage, is given in figures 27 to 39. Summarily, these indicate that although the crystal is suitably acoustoelectrically active, anomalies in attenuation, particularly at the higher frequencies, result in an unimpressive comparison between experiment and theory The measured variation of attenuation for small conductivities is seen to be linear at each frequency as predicted by White's theory, and the slope of this linear variation was used to determine the square of the electromechanical coupling factor (K^2) in each case. These were given in Table 1.

Henrich and Weinreich [42] have given an indication of the range (0.034 - 0.039) of experimentally determined values of K^2 reported in the literature for shear wave coupling in cadmium sulphide. Wilson [95] has reported that an initial value of only 0.005 for K^2 was related to the surface etch pit density of the (0001) face. A decrease in etch pit density due to annealing, correlated with an increase in K^2. As a result of this spread in the reported values of the electromechanical coupling factor it is common practice to choose a value of K^2 which best fits the experimental data. Such an approach is considered to be well justified, and the values reported in Table 1 were obtained

in this manner. Thus for small crystal conductivities the experimental and theoretical variation of attenuation coefficient with crystal conductivity is seen to agree in figures 37 to 39.

At 15 MHz the observed variation of attenuation over the entire conductivity range investigated is seen to be in reasonable agreement with that predicted by White's theory, using the determined value of K^2. Theory predicts that the attenuation should peak when the ratio $\frac{\omega_c}{\omega}$ is unity and such a peak occurs experimentally. The observed magnitude of maximum photosensitive attenuation is, however, slightly less than that predicted, using a value of 0.043 for K^2. Although it would appear from figure 37(b) that this value of K^2 is appropriate at low crystal conductivities, the subsequent disagreement between theory and experiment indicated in figure 37(a) would seem to indicate a lower value of K^2 to be more appropriate. Exact agreement between theory and experiment at the peak value ($\frac{\omega_c}{\omega} = 1$) is obtained for $K^2 = 0.035$, which lies within the range of published values, given by Henrich and Weinreich, whilst the value $K^2 = 0.043$ lies outside this range. Figure 90 compares the measured variation of attenuation coefficient at 15 MHz with that predicted by White's theory for $K^2 = 0.035$. The overall agreement is seen to be improved considerably.

The results obtained at 45 MHz and reported in figure 38 are puzzling. For small crystal conductivities the observed attenuation coefficient suggests the high value of 0.047 for K^2. The measured variation of attenuation with crystal conductivity is seen to be linear until $\frac{\omega_c}{\omega}$ exceeds 0.1, whereupon the attenuation coefficient decreases slightly and then remains insensitive to conductivity increase. Such behaviour requires more intensive study before a satisfactory explanation may be given. All the experimental results presented at 45 MHz with no drift voltage applied

to the crystal have been obtained with $\frac{\omega_c}{\omega}$ less than 0.1.

The values of K^2 determined from the small conductivity, zero voltage, attenuation variation observed at 75 MHz and 105 MHz both lie within the range 0.033 to 0.038. The observed attenuation at each frequency soon becomes independent of crystal conductivity however, as shown in figures 39(a) and (b) respectively.

With the exception of those results obtained at 15 MHz., reported in figure 37 and reconsidered in figure 90, the observed photosensitive attenuation variation is not well described by White's theory. Although the observed variation is linearly related to the crystal conductivity for small conductivities as predicted, the higher conductivity variation suggests an attenuation anomaly which is not understood. It was stressed in the introduction of chapter 5 that it has not been the intention to compare the observed acoustic behaviour with that predicted by White's theory. Consequently an explanation of the observed zero-voltage attenuation variation with crystal conductivity was not specifically sought.

6.1.2. The acoustoelectric voltage during acoustic transit

The analysis of the Weinreich relationship presented in chapter 2 resulted in a theoretical description of the acoustoelectric voltage which was consistent with the measurement technique adopted. This technique received a full explanation in chapter 4. A number of equations were derived which enabled a calculation of the acoustoelectric voltage, as an acoustic signal of known input intensity and duration propagated through the crystal with a known attenuation coefficient.

It was necessary to consider the propagation of the input acoustic signal in three stages. The first considered the introduction of a finite width acoustic signal into the crystal. The second stage of the analysis, initiated when the acoustic signal

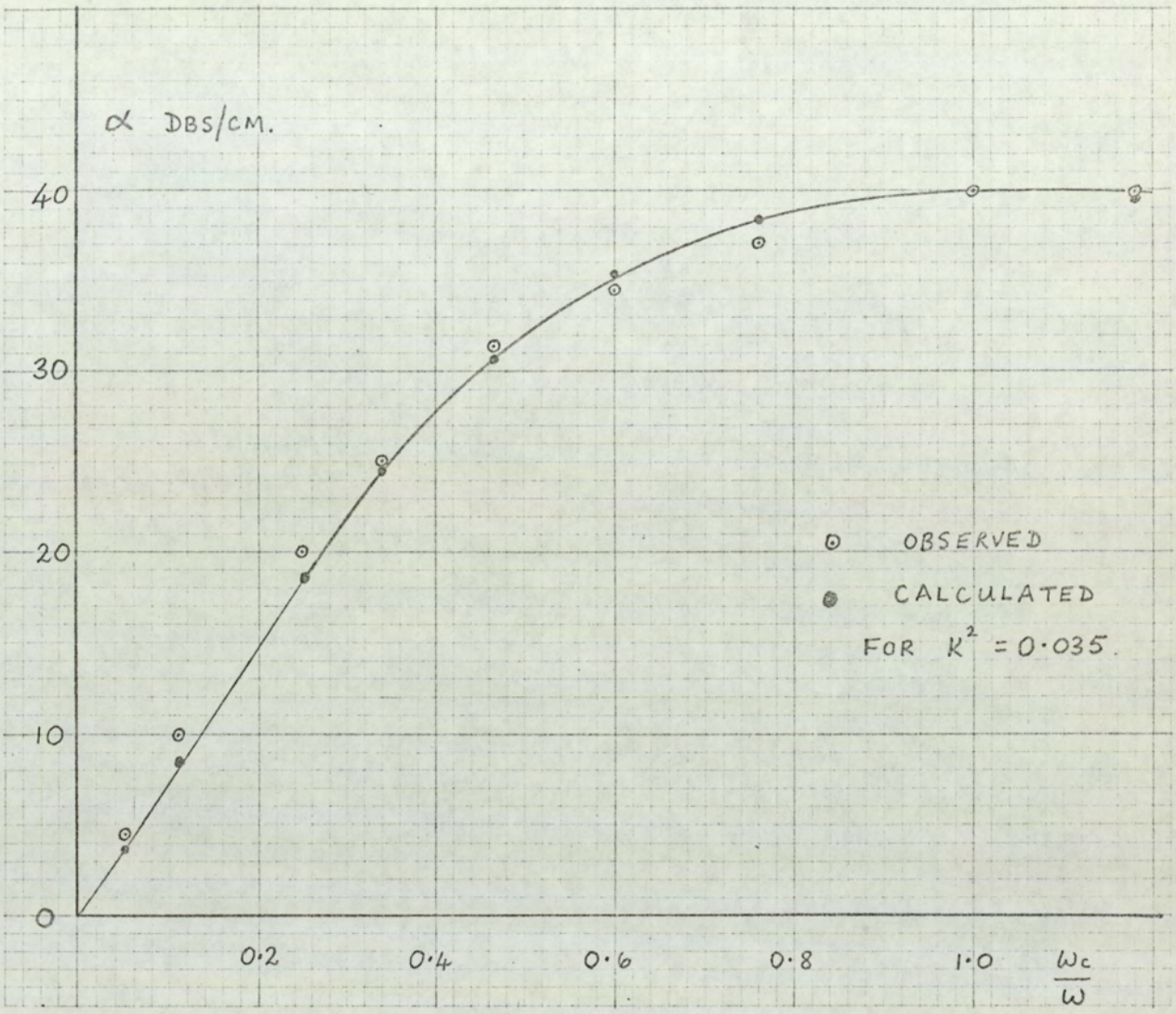

FIG. 90. THE VARIATION OF ATTENUATION WITH CRYSTAL CONDUCTIVITY AT 15 MHz. – A COMPARISON BETWEEN THEORY AND EXPERIMENT WITH $K^2 = 0.035$.

was wholly within the crystal, considered the subsequent propagation of the acoustic signal until its leading edge reached the output face of the crystal. The final stage then considered the ensuing period of acoustic reflection.

Figure 41 shows a comparison between theory and experiment of the variation of acoustoelectric voltage during a time period corresponding to a single acoustic transit, and reflection, of an input acoustic signal of 1 μ sec half height width. The experimental variation displayed in figure 41 was obtained at 45 MHz. Although the quantitative agreement between theory and experiment at other acoustic frequencies is less impressive, as indicated by figures 43 to 46, the observed change in the shape of the acoustoelectric voltage display, as the crystal conductivity was increased was observed to be similar at all frequencies. In this respect, the two examples shown in figure 41, and the trace obtained for a high attenuation coefficient given in figure 42 are quite typical.

Since the quantitative agreement between theory and experiment at 45 MHz is so impressive, it is interesting to examine the steps necessary to obtain a calculated value of the acoustoelectric voltage under a given set of applied conditions, in order to determine whether such good agreement is justified.

Consider the equation which predicts the maximum acoustoelectric voltage under attenuating conditions. This corresponds to the input acoustic signal just within the crystal.

$$V_{ae} = \frac{R_m}{KE_{th}} Q_o \left(1 - e^{-2\alpha w}\right) \quad \text{------(6.1)}$$

The symbols are defined in chapter 2.

In order to obtain a calculated value of acoustoelectric voltage using this equation, or for that matter, any of the other equations derived in chapter 2, it is first necessary to determine

R_m, K, E_{th} Q_o, α and W, and the accuracy with which these parameters are determined obviously influence the accuracy of acoustoelectric voltage calculation.

An assessment of the experimental errors associated with determining these parameters was carried out, and the overall error in calculating the acoustoelectric voltage from the Weinreich relationship was estimated to be no more than $\pm$ 15%. This figure does not include the consequences of an error in the input acoustic intensity since there would seem to be no effective means of assessing such an error. The measurement of input acoustic intensity has received some discussion in section 5.3. The experimental errors assessed for each of the other parameters were estimated by taking into account the method used for their determination and the accuracy with which they were measured. The good agreement between theory and experiment noted at 45 MHz would appear therefore to be well justified, and not particularly a result of cancelling errors.

Figures 40 and 41 indicate the variation of acoustoelectric voltage with time, as the acoustic signal propagates through the crystal. It will be noted that the maximum of the displayed variation occurs when the acoustic packet is just within the crystal. During all other experimental work under attenuating conditions the maxima of the displayed traces were noted only, and therefore the calculated acoustoelectric voltages were determined from equation (6.1).

Similarly under amplifying conditions, the maxima of the acoustoelectric voltage displays occurred when the leading edge of the acoustic packet had just completed a single transit of the crystal. Accordingly, calculated values of acoustoelectric voltage were obtained using equation (6.2)

$$V_{ae} = \frac{-R_m}{K E_{th}} Q_o \left(1 - e^{-2\alpha W}\right) e^{+2\alpha L} \quad ---(6.2)$$

Because of the limited time period available for this research it was not possible to exploit all the features of the theoretical analysis of the Weinreich relationship presented in chapter 2. There are, however, two in particular which merit a short discussion here.

The predicted acoustoelectric voltage during the first reflection of the acoustic signal was determined to be given by the following equation:

$$V_{ae} = \frac{R_m}{KE_{th}} Q_o e^{-2\alpha L} \left[\left(e^{2\alpha x_3} - 1 \right) - R \left(1 - e^{-2\alpha (w - x_3)} \right) \right] \quad --(6.3)$$

x_3 is the width of the acoustic signal travelling in the forward direction during reflection, and R is the reflection coefficient of the output face of the crystal. The variation of x_3 during reflection is considered to be from w to zero.

If the crystal is considered to be attenuating then the predicted acoustoelectric voltage when reflection ceases, that is, when x_3 is zero, is given by:-

$$V_{ae} = \frac{R_m}{KE_{th}} Q_o e^{-2\alpha L} \left[- R \left(1 - e^{-2\alpha w} \right) \right] \quad ----(6.4)$$

After reflection, the entire acoustic signal then propagates back through the crystal. Equation (6.4) thus indicates the maximum acoustoelectric voltage after reflection. The ratio of the maximum acoustoelectric voltage in the forward direction, $(V_{ae})_F$ given by equation (6.1), to the maximum after reflection, $(V_{ae})_B$ given by equation (6.4) is therefore

$$\left| \frac{(V_{ae})_F}{(V_{ae})_B} \right| = \frac{1}{R\, e^{-2\alpha L}} \quad ----(6.5)$$

Thus the reflection coefficient of the output face of the crystal is

given by $$R = \left| \frac{(V_{ae})_B}{(V_{ae})_F} \right| e^{+2\alpha L} \quad - - - - \quad (6.6)$$

This would seem to allow a simple experimental means of determining the acoustic intensity reflection coefficient of the boundary.

The calculated acoustoelectric voltage variation during reflection, given in figures 40(a) and (b) were obtained by assuming R to be unity. A smaller value of R indicates some transmission of acoustic energy through the crystal boundary, resulting in a smaller acoustoelectric voltage generated by the reflected portion of the acoustic signal. Effectively, this subtracts from the conventionally positive acoustoelectric voltage generated by the forward going portion, and a decrease in R therefore results in a more positive predicted net acoustoelectric voltage during reflection. The maximum negative acoustoelectric voltage corresponding to the completion of reflection, is reduced, and the time taken for the net acoustoelectric voltage to become zero is increased. The satisfactory agreement between theory and experiment during reflection, illustrated by figure 40, demonstrates however, that the choice of R is not critical.

Information relating particularly to attenuation variation within the crystal may also be obtained by studying the acoustoelectric effect. Stage two of the analysis considered the subsequent propagation of the acoustic signal through the crystal, after its introduction into the crystal. The observed variation of the acoustoelectric voltage during this stage of acoustic propagation can be examined and if gross inhomogeneity were present the observed variation would not be exponential as predicted. A best fit could then be attempted and conclusions regarding the extent and nature of the conductivity inhomogeneity drawn. The advantage of this method is that the attenuation variation within the crystal is investigated independently of bond losses, transducer efficiencies, and reflection coefficients. The close agreement between theory and experiment demonstrated by figure 40 indicates that conductivity homogeneity in the crystal

used does not affect the results to any serious extent.

McFee [39] has used the acoustoelectric crossover to indicate conductivity inhomogeneity. Attenuating and amplifying regions in the crystal may be identified by the sign of any acoustoelectric voltage displayed. This method of inhomogeniety recognition, though useful in a broad sense, lacks definition. Henrich and Weinreich [42] have studied the acoustoelectric effect to obtain information on trapping and attenuation. Both the electronic attenuation and lattice attenuation were determined from information derived from the exponential decay of the displayed acoustoelectric voltage, at different crystal conductivities. They also investigated the magnitude of the acoustoelectric voltage displayed and obtained information relating to trap depths and densities. Their method of analysis was presented in outline only and this was noted to involve substantial computation.

Summarising, the experimental results presented in section 5.2.2. indicate convincingly that the analysis of the Weinreich relationship given in chapter 2 allows a quantitative test of this relationship. The good agreement between theory and experiment shown in figures 40 and 41 justifies the conclusion that under linear conditions the Weinreich relationship is quantitatively valid. The next section discusses the results obtained at frequencies between 15 MHz and 105 MHz. The less impressive quantitative agreement at frequencies other than 45 MHz would seem to indicate an error in the determination of input acoustic intensity at these frequencies. Prior discussion given in section 5.2.5. suggests that the disagreement may not be entirely attributed to such an error however. Qualitatively similar acoustoelectric voltage displays investigated as a function of input acoustic intensity, acoustic pulse width, and crystal conductivity were observed at all frequencies.

6.1.3. Variation of the acoustoelectric voltage as a function of input acoustic intensity.

The linear variation of the acoustoelectric voltage with input acoustic intensity, for a constant attenuation coefficient has received more experimental attention than any other aspect of the Weinreich relationship. It was first noted by Wang [36] and has subsequently been verified by many others.

The results given in figures 45 to 48 of this thesis were obtained over a wide range of crystal conductivity and input acoustic intensity at four acoustic frequencies. With the exception of those results reported in figure 46 for 45 MHz operation, the comparison between theory and experiment is not always close. Figure 45 presents the observed variation of acoustoelectric voltage with input acoustic intensity at 15 MHz for six values of attenuation as indicated in the table below the graph. The acoustoelectric voltage has been predicted for the four largest attenuation coefficients. The ratio of predicted to observed acoustoelectric voltage in each case lies between 3.0 and 3.5. Thus the noted disagreement between theory and experiment at this acoustic frequency would seem to be independent of crystal conductivity, and would possibly suggest an error in the determination of the input acoustic intensity. However the results obtained under amplifying conditions at 15 MHz do not substantiate this conclusion.

The comparison between theory and experiment at 45 MHz shown in figure 46 is excellent at low crystal conductivities. As the attenuation coefficient becomes large however, the observed acoustoelectric voltage is seen to be slightly less than that calculated. In the preliminary discussion of these results given in chapter 5 it was noted that for a small attenuation coefficient the good agreement between theory and experiment was maintained even when the attenuation coefficient was observed to be power dependent,

providing the reduction in attenuation coefficient was taken into account when determining the predicted acoustoelectric voltage. It may therefore be concluded that the Weinreich relationship is valid under certain non-linear conditions, with a reservation on the degree of non-linearity. The strong non-linearity observed under amplifying conditions will allow the opportunity to discuss this conclusion in more detail shortly.

The variation of acoustoelectric voltage with input acoustic intensity observed at 75 MHz and 105 MHz as shown in figures 47 and 48 has already been discussed at some length in chapter 5. At 75 MHz the measured acoustoelectric voltage is between 3.0 and 4.2 times larger than that calculated, and, at 105 MHz the ratio ranges from 4.2 to 5.0. The possible sources of this discrepancy were examined in section 5.2.5 and it was concluded that an error in acoustic intensity determination was responsible, although a thorough check of this determination proved inconclusive.

6.1.4. The variation of acoustoelectric voltage with input acoustic pulse width

The predicted dependence of the acoustoelectric voltage on the acoustic signal width, given by equation (6.1), was consequent of the assumption of an input acoustic signal of constant amplitude, with zero rise time and fall time, whereas experimentally, the half height width was measured.

A comparison between theory and experiment of the variation of the acoustoelectric voltage with acoustic signal width is presented in figure 49 for various crystal conductivities at 45 MHz. At low conductivities the agreement is good over the entire, indicated, range of W.

At high crystal conductivities however, an input acoustic signal of duration less than about 1.5 μ sec results in an observed

acoustoelectric voltage which is smaller than that predicted, whilst an input acoustic signal of greater duration results in the predicted acoustoelectric voltage being greater than that observed. This disagreement between theory and experiment is never more than 10% however, which is less than the experimental error estimated in section 6.1.2 , to be associated with acoustoelectric voltage calculation. Thus the results given in figure 49 would seem to validate equation (6.1) and endorse the assumption of an idealised acoustic signal.

This investigation was repeated at 15 MHz and qualitatively similar results were obtained, although as previously indicated, the quantitative agreement between theory and experiment at 15 MHz is not so good. It was noted however, that this disagreement was not affected by pulse width, which strongly suggests that it is not a result of conductivity inhomogeneity near the input transducer.

6.2. Experimental results with a drift voltage applied to the crystal.

6.2.1. The input-output characteristics

The most noticeable aspect of these is the marked reduction of acoustic amplification which occurs as the input acoustic intensity is increased. To a lesser extent this is also true of the observed attenuation. As an example consider figure 51 with 700 volts d.c. applied to the crystal the amplification of a very small acoustic input is seen to be 7 dbs/L. As the input acoustic intensity is increased, the measured amplification remains a constant until input attenuator setting of about 40 dbs. is reached whereupon the acoustoelectric interaction becomes non-linear. The acoustic amplification becomes power dependent, and is reduced as the input acoustic intensity is increased further. The plotted variation of acoustic output against acoustic input is then no longer parallel to the dark level plot. Continued increase of input acoustic

intensity finally results in no observed amplification and the input-output curve crosses the dark level line. Thereafter, for larger acoustic inputs, the crystal is observed to attenuate the input signal. For small acoustic inputs the applied d.c. voltage resulting in acoustic crossover is independent of the input acoustic intensity. In the power dependent region however, the acoustic crossover voltage increases with increasing acoustic intensity, for a given crystal conductivity. This is an important feature of the observed non-linear acoustic behaviour.

Figures 51, 53 and 55 together show the effect on the input - output characteristics at 15 MHz of increasing the crystal conductivity. Acoustic amplification and attenuation is seen to increase, in qualitative agreement with White's theory. The non-linearity is a little more pronounced at the highest conductivity considered (figure 55), however the general pattern of acoustic behaviour is seen to be little affected by crystal conductivity at 15 MHz.

Figures 62 and 64 present typical input-output characteristics observed at 45 MHz. With a low crystal conductivity figure 62 indicates the non-linear region to be similar to that observed at 15 MHz. However, at a high crystal conductivity, figure 64 indicates the non-linear behaviour of the crystal to be more marked. The deviation from linearity, observed under amplifying conditions occurs at a considerably smaller acoustic input intensity than previously observed at 15 MHz. The observed amplification and attenuation at 45 MHz is also noted to be greater than that observed under similar applied conditions at 15 MHz. This is also expected from White's theoretical description of the attenuation coefficient. Figure 64 describes a variation of amplification coefficient which has not previously been described in the literature. With 700 volts applied to the crystal, for example, the variation

of observed amplification with input acoustic intensity indicates the output acoustic intensity to remain a constant over quite a wide range of input acoustic intensity. For input signals larger than that observed to result in acoustic crossover, the input - output characteristic indicates the output to decrease even though the input signal is being increased. This situation does not occur over a wide range of input intensity however, and for the highest input intensities employed, the observed net attenuation is observed to remain constant.

Any explanation of the non-linear attenuating region of the input - output characteristic is complicated by the observation of significant distortion of the output acoustic signal, which was displayed using an oscilloscope in the manner described in chapter 4. The acoustic echo was observed to become wider, and the top of the detected echo was seen to split into two and sometimes three, distinct peaks. This distortion was generally observed to occur over that region of the input-output curve corresponding to a net reduction in acoustic output with increasing acoustic input. Further increase of the input acoustic intensity resulted in one of these peaks suddenly increasing in amplitude, and the subsequent growth of this very narrow peak with increasing input intensity allowed the input-output characteristic to be completed. Similar anomalous behaviour has been observed in this laboratory using a different cadmium sulphide crystal [96].

Figures 69 and 72 present a description of the attenuation variation for two crystal conductivities at 75 MHz. The general pattern of behaviour in the amplifying region is similar to that observed at the lower acoustic frequencies.

The saturation of gain as the input acoustic intensity is increased has been previously noted by Ishiguro et al [45], Hanlon [33] and Hickernell [29], and is generally considered to occur when the

density of bunched electrons n_{so}, approaches the density of electrons in the conduction band, n_o. White's theory predicts the bunched electron density to be

$$n_{so} = \frac{\sigma e S_o}{q v_s \varepsilon} \left[\gamma^2 + \left(\frac{\omega_c}{\omega} + \frac{\omega}{\omega_D} \right)^2 \right]^{-\frac{1}{2}} \quad ----(6.7)$$

where S_o is the strain amplitude and the other symbols have been previously defined. The average electron density in the conduction band is given by

$$n_o = \frac{\sigma}{q\mu}$$

Thus, $$\left(\frac{n_{so}}{n_o}\right) = \frac{e S_o \mu}{\varepsilon v_s} \left[\gamma^2 + \left(\frac{\omega_c}{\omega} + \frac{\omega}{\omega_D} \right)^2 \right]^{-\frac{1}{2}} \quad ----(6.8)$$

The strain amplitude S_o, may be determined from the acoustic intensity Q since

$$Q = \frac{1}{2} c v_s S_o^2 \quad ----- (6.9)$$

Therefore the ratio $\left(\frac{n_{so}}{n_o}\right)$, as predicted by White may be numerically calculated for a given set of applied conditions.

A discussion of White's theory was presented in chapter 2 and it was noted that in order to maintain a linear solution of the wave equation it was necessary to ignore the non-linear term, $\tilde{n}_s q \mu \tilde{E}_1$.

It was also shown that this was justified if n_{so} was small compared to n_o.

White's expression for the attenuation coefficient is given below.

$$\alpha = \frac{K^2}{2 v_s} \omega_c \frac{\gamma}{\gamma^2 + \left(\frac{\omega_c}{\omega} + \frac{\omega}{\omega_D} \right)^2} \quad ---(6.10)$$

where α is in nepers/cm.

Table 7 compares the amplification predicted using equation (6.10), with the observed amplification in the linear region under different conditions at 15, 45 and 75 MHz. At 15 MHz the ratio of calculated to observed amplification is seen to vary between about 4: 1 to 2: 1. Agreement is better at 45 MHz. where, for two different crystal conductivities, the ratio lies between 2: 1 and 1: 1. At 75 MHz the agreement between theory and experiment is within 1·5 : 1. Without exception, for a given crystal conductivity and acoustic frequency the disagreement between theory and experiment of the results considered is poorest where the applied conditions lead to near - maximum gain. This is generally realised with an applied voltage of about 700 volts, and agreement is better at higher applied voltages.

Since the equations derived by White are valid under linear conditions only, there is little justification in using equation (6.8) to determine the ratio $\frac{n_{so}}{n_o}$ under the strong non-linear conditions reported. There is some justification however, in using this equation to determine the electron density ratio when non-linearity in amplification first occurs. The following values were used to calculate $\frac{n_{so}}{n_o}$.

$$q = 1.60 \times 10^{-19} \text{ coulombs}$$
$$v_s = 1.75 \times 10^{3} \text{ M sec}^{-1}$$
$$\varepsilon = 8.0 \times 10^{-11} \text{ F.M}^{-1}$$
$$\omega_D = 4.8 \times 10^{9} \text{ sec}^{-1}$$
$$C = 1.49 \times 10^{10} \text{ N.M}^{-2}$$

The strain amplitude, S_o , was determined using equation (6.7). The elastic constant c was obtained from the literature [42] and the expression for the electromechanical coupling factor

$$K^2 = \frac{e^2}{\varepsilon c}$$

TABLE 7

Figure No.	Acoustic Freq.(MHz)	$\sigma \times 10^6$ (ohm cm.)$^{-1}$	Applied Voltage	Amplification Coefficient		$\frac{\alpha_c}{\alpha_o}$
				Observed α_o DBS/L	Calculated α_c	
53	15	16.0	700	7.0	29.0	4.2
			800	12.0	30.0	2.4
			900	12.0	24.0	2.0
62	45	5.0	700	13.0	25.6	2.1
			800	13.0	14.9	0.97
			1000	8.0	7.8	1.00
64	45	17.0	700	31.0	64.0	2.06
			800	26.0	45.6	1.75
			900	20.0	32.7	1.63
			1000	16.0	25.5	1.60
69	75	12.0	700	23.0	36.6	1.60
			800	22.0	25.4	1.15
			900	17.0	18.0	1.05
			1000	14.0	14.0	1.00

was used to calculate the piezoelectric constant e at each acoustic frequency. This was determined to be 0.22 $\pm$ 0.01 coulombs M^{-2}.

Table 8 presents the values of n_{so} to n_o so calculated. Column 5 indicates the input attenuator setting which resulted in the onset of amplification reduction observed under the applied conditions specified in columns 2 to 4. The source of the data is indicated in column 1. Column 6 of Table 8 gives the observed amplification in dbs/L for this acoustic input and column 7 indicates the acoustic intensity at the output face of the crystal, determined from the relevant value of input acoustic intensity given by figures 33 to 37, and taking into account the observed amplification due to a single acoustic transit. The values of acoustic intensity given in column 7 have been used in equation (6.9) to determine the strain at the output face of the crystal, and hence $\frac{n_{so}}{n_o}$ using equation (6.8).

Prior to discussing these results relating to the onset of non-linearity it is useful to reconsider the relevance to the amplification process of the bunched space charge. A full discussion of the linear theory of acoustic amplification has been given in chapter 2, and it was shown that the amplification coefficient could be expressed as follows:

$$\alpha = \frac{\frac{1}{2}\,\tilde{J}.\tilde{E}_1}{Q} = \frac{\frac{1}{2}\,q v_s n_{so} E_{1o} \cos\theta}{Q} \qquad --(6.11)$$

where n_{so} is the density of bunched electrons, E_{1o} is the piezoelectric field, θ, the phase angle between $\tilde{n}_s$ and $\tilde{E}_1$ and Q the local acoustic intensity. The linear theory also predicts that both n_{so} and E_{1o} are linearly related to the strain. Since the local acoustic intensity Q is proportional to the square of the strain, the linear amplification coefficient is seen to be independent of strain. A reduction in gain due to an increase in strain must

therefore be attributed to either non-linearity between the piezoelectric field and the strain, or the bunched carrier density and the strain. The greatest recorded acoustic intensity leading to the start of gain non-linearity is, from column 7 of table 8, 0.16 watts. cm^{-2}. This corresponds to a strain of 1.1 10^{-5}. Hutson and White [24] have argued that the assumption $n_{so} << n_o$ requires the strain amplitude to be less than $\frac{\varepsilon v_s}{\mu e}$, the value of which is $3. 10^{-5}$. Thus the maximum experimental strain resulting in the onset of non-linearity is of the same order as the limiting strain given by Hutson and White. This strain is considered small enough to ensure that Hooke's law is obeyed, and that the crystal behaves as an elastic medium.

Hanlon [33] has shown that the onset of gain reduction occurs when $\frac{n_{so}}{n_o}$ is about 0.5, and complete saturation is reached for $\frac{n_{so}}{n_o}$ a little less than two. At first glance the calculated values of $\frac{n_{so}}{n_o}$ given in column 8 of Table 8 suggest that gain reduction occurs when $\frac{n_{so}}{n_o}$ lies between 0.2 and 0.6 in agreement with Hanlon's value of 0.5. Confidence in the numerical accuracy of the values of $\frac{n_{so}}{n_o}$ presented is, however, limited by the assessed difference between the predicted and observed values of amplification using White's theory (Table 7) and also the experimental errors associated with determining the critical strain leading to the gain reduction. Thus, although the results of Table 8 do enable several conclusions to be drawn regarding gain reduction, these will relate to the qualitative, rather than quantitative, nature of the results. For reasons of brevity the values of $\frac{n_{so}}{n_o}$ calculated for the onset of gain reduction will be hereafter referred to as the critical value, and will be denoted $\left(\frac{n_{so}}{n_o}\right)_{CRIT.}$. For a given acoustic frequency and crystal conductivity $\left(\frac{n_{so}}{n_o}\right)_{CRIT}$ would appear to be independent of applied d.c. voltage, although the critical strain, given in column 7 of Table 8 is observed to increase with applied voltage. This leads to the important conclusion that gain reduction does not occur when the

TABLE 8

Figure No.	Frequency MHz	$\sigma \times 10^6$ (ohm cm)$^{-1}$	Vdc volts	Input Attenuator Setting	α Dbs/L	Q_L Watts/Sq.Cm	$\left(\frac{n_{so}}{n_o}\right)_{CRIT.}$
62	45	5.0	700	44	13	0.002	0.25
			800	38	13	0.008	0.26
			1000	27	8	0.030	0.26
51	15	9.5	700	43	7	0.011	0.29
			800	43	10	0.023	0.29
69	75	12.0	700	47	23	0.001	0.17
			800	40	22	0.005	0.20
			900	31	17	0.012	0.21
			1000	27	14	0.016	0.25
53	15	16.0	700	40	7	0.022	0.48
			800	40	12	0.047	0.49
			900	35	11	0.140	0.52
64	45	17.0	600	25	-	0.006	0.56
			700	54	31	0.013	0.51
			800	43	26	0.050	0.58
			900	34	20	0.100	0.57
			1000	28	16	0.160	0.56
55	15	25.0	600	32	-	0.030	0.58
			700	40	11	0.055	0.60
			800	42	15	0.090	0.63
72	75	25.0	700	48	29	0.007	0.31
			800	47	31	0.009	0.30

strain within the crystal reaches a particular value. In fact, the results indicate that non-linearity initiates over a wide range of strains. The conclusion that the critical strain increases as the applied voltage is increased; all else maintained constant - provides evidence to support the use of White's linear theory to calculate $\frac{n_{so}}{n_o}$ at the onset of non-linearity. Equation (6.8) indicates that as the applied voltage, or γ, is increased n_{so} is reduced. Figure 8(a), shows that maximum bunching for a given set of applied conditions occurs when the electron drift velocity is equal to the acoustic velocity. If non-linearity initiates when $\left(\frac{n_{so}}{n_o}\right)_{CRIT}$ reaches a certain value then it becomes clear that in order to maintain this critical value as γ is increased it becomes necessary to compensate for the decrease in n_{so} due to the increase in γ by increasing the strain.

Temporary exclusion of the results of Table 8 relating to 75 MHz operation reveals a distinct correlation between the calculated values $\left(\frac{n_{so}}{n_o}\right)_{CRIT.}$ and the crystal conductivity for 15 MHz and 45 MHz operation. The average value of $\left(\frac{n_{so}}{n_o}\right)_{CRIT}$ increases as the crystal conductivity is increased. Unfortunately, the values calculated for 75 MHz operation would not appear to substantiate this conclusion. It might be remembered however that a comparison between the calculated and observed acoustoelectric voltage under a wide range of conditions in the absence of an applied drift field was presented in section 5.2.3. and that this comparison indicated the experimental results to be some four times greater than those predicted by the Weinreich relationship. A discussion of this discrepancy was given in section 5.2.5. and after a careful investigation into the possible causes of the discrepancy it was concluded that the input acoustic intensity determination at 75 MHz was in error by a factor of four. The observation that $\left(\frac{n_{so}}{n_o}\right)_{CRIT.}$ generally increases with crystal conductivity would seem to affirm

this conclusion, since such an error in acoustic intensity measurement at 75 MHz would result in $\left(\frac{n_{so}}{n_o}\right)_{CRIT.}$ being calculated as two times too small. If the values of $\left(\frac{n_{so}}{n_o}\right)_{CRIT}$ given in Table 8 for 75 MHz operation are thus multiplied by two, then the results so obtained support the conclusion that $\left(\frac{n_{so}}{n_o}\right)_{CRIT.}$ increases with crystal conductivity. As further evidence to justify this correction it may be noted that $\left(\frac{n_{so}}{n_o}\right)_{CRIT.}$ has been calculated for a conductivity of 25.10^{-6} $(ohm.cm)^{-1}$ at both 15 MHz and 75 MHz, and after correcting the 75 MHz values as indicated, this is seen to be 0.62 in each case.

Figure 91 presents the determined variation of $\left(\frac{n_{so}}{n_o}\right)_{CRIT.}$ with crystal conductivity. The graph shows that for low crystal conductivities non-linearity will not be observed until $\left(\frac{n_{so}}{n_o}\right)_{CRIT}$ approaches a lower limit of about 0.2. If the applied conditions are such that this never reaches 0.2, then it may be concluded that non-linearity will not be observed. As the crystal conductivity is increased, the onset of non-linearity occurs at greater values of $\left(\frac{n_{so}}{n_o}\right)_{CRIT}$. Thus for a conductivity of $15.\ 10^{-6}$ $(ohm\ cm)^{-1}$ non-linearity will not be observed until $\left(\frac{n_{so}}{n_o}\right)_{CRIT.}$ becomes about 0.5. At very high crystal conductivities the graph indicates an upper limit of $\left(\frac{n_{so}}{n_o}\right)_{CRIT}$ equal to about 0.7. The variation of $\left(\frac{n_{so}}{n_o}\right)_{CRIT}$ with crystal conductivity given in figure 91 is independent of acoustic frequency as is demonstrated by the position of the points on the plot determined at each of the three frequencies.

6.2.2. The variation of acoustoelectric voltage

The input-output characteristics presented in chapter 5, and discussed in section 6.2.1 describe the variation of acoustic attenuation over a wide range of applied conditions. Each attenuation measurement was complemented by a measurement of the simultaneously generated acoustoelectric voltage, and the variation of acoustoelectric voltage corresponding to each input - output characteristic is also presented in chapter 5.

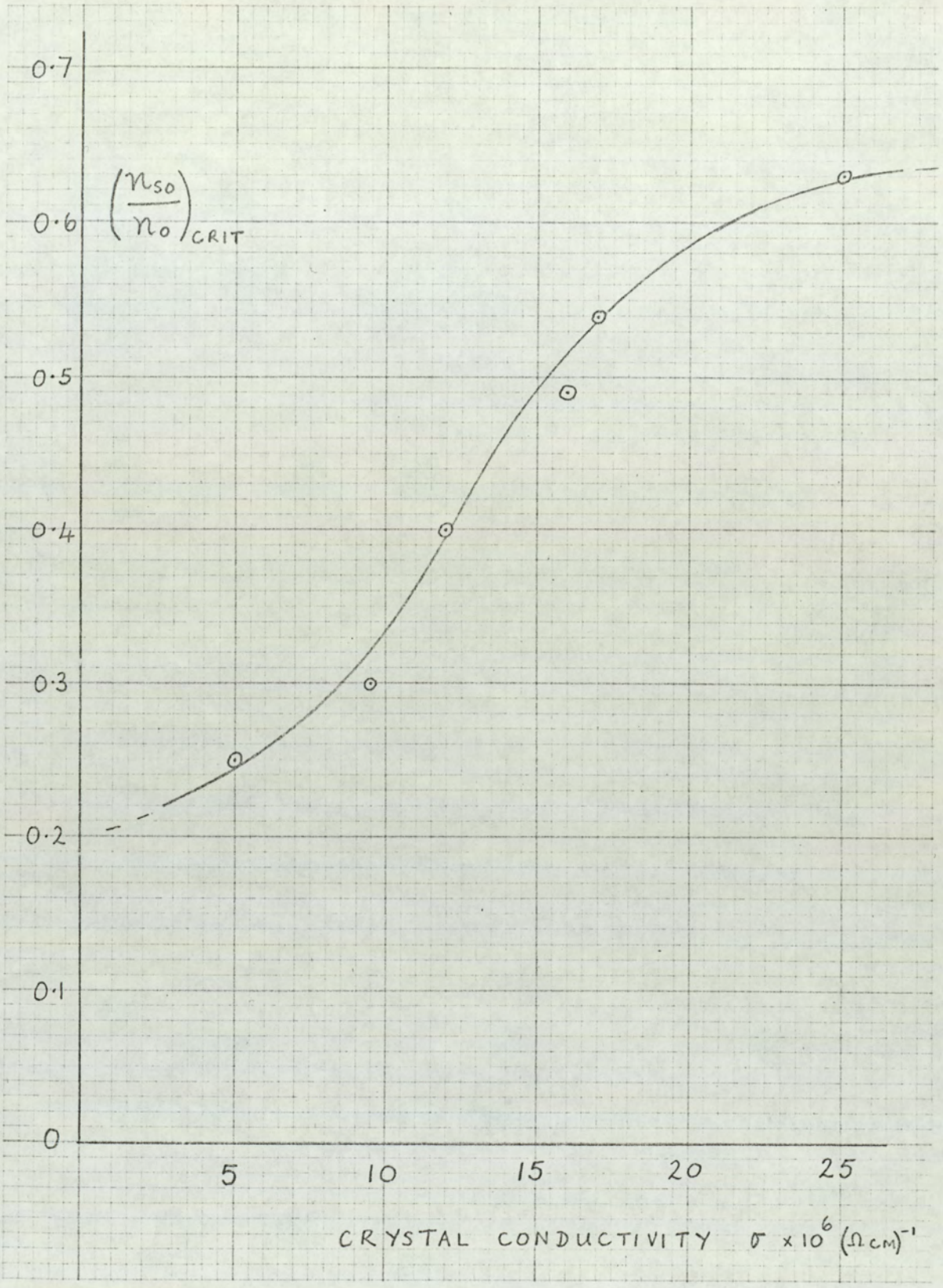

FIG. 91. THE VARIATION OF $\left(\frac{n_{so}}{n_o}\right)_{CRIT}$ WITH CRYSTAL CONDUCTIVITY

The onset of non-linearity, recognised by the onset of gain reduction, is seen from the input - output characteristics to occur generally at small input acoustic intensities. The Weinreich relationship indicates the acoustoelectric voltage to be directly proportional to the input acoustic intensity. Using the data presented in Table 8, and assuming the Weinreich relationship to be valid under linear conditions, the acoustoelectric voltage generated at the onset of non-linearity has been calculated for each case described in Table 8. The results, given in Table 9, indicate that the acoustoelectric voltage thus calculated is small. Most of the acoustoelectric voltage measurements reported have therefore been made under non-linear conditions.

Before examining in detail the effect of non-linearity on the validity of the Weinreich relationship, some general observations regarding the measured variation of acoustoelectric voltage under different applied conditions may be noted. In each case, the acoustoelectric voltage variation has been plotted against the input attenuator setting, to enable an immediate comparison with the corresponding input-output characteristics. As predicted, the magnitude of the acoustoelectric voltage generated under attenuating conditions is seen to be much smaller than that generated under amplifying conditions. This illustrates the difficulty in investigating the Weinreich relationship for small signal attenuation, and attention will be mainly concentrated on the experimental results obtained under amplifying conditions.

The observed amplification variation for a given crystal conductivity and acoustic frequency, with different applied d.c. voltages, as the input acoustic intensity is increased, generally shows a marked correlation with the corresponding acoustoelectric voltage variation. Figure 51, 53 and 55 for example, show that the plotted amplification curves in the non-linear region rarely

TABLE 9

For applied conditions see Table 8

α dbs/L	Q_L Watts/sq.cm	V_{ae} (mV) Calculated
13	0.002	0.27
13	0.008	1.08
8	0.030	2.80
7	0.011	0.91
10	0.023	2.50
23	0.001	0.19
22	0.005	0.93
17	0.012	1.90
14	0.016	2.30
7	0.022	1.82
12	0.047	6.10
11	0.140	16.80
-	0.006	-
31	0.013	2.80
26	0.050	10.20
20	0.100	17.60
16	0.160	25.00
-	0.030	-
11	0.055	6.50
15	0.090	13.20
29	0.007	1.47
31	0.009	1.90

intersect, and figures 52, 54 and 56 show this to be true of the corresponding acoustoelectric voltage curves also. The amplification variation described by figures 62, 64 and 69 on the other hand, indicate the plotted curves to cross one another in several places, and the corresponding observed variation in acoustoelectric voltage given in figures 63, 65 and 70 are seen similarly to intersect. Without exception, where two applied d.c. voltages were noted to result in the same measured amplification for a particular crystal conductivity and acoustic frequency, the corresponding acoustoelectric voltage curves were also observed to cross. It was noted, however, that the acoustoelectric voltage intersection generally occurred at a higher input acoustic intensity than that resulting in amplification curve intersection. An attempt to correlate the magnitude of this difference with the applied conditions resulting in the difference proved fruitless, and few conclusions could be drawn from the information thus derived. Consequently, a detailed analysis of several specific examples was undertaken and the following discusses the analysis carried out for one such example; namely, the intersection of the 800 volt and 900 volt input-output plots of figure 64 and the corresponding acoustoelectric voltage plots of figure 65. These figures show the input attenuator setting resulting in curve intersection to be 28 dbs and 22 dbs respectively.

Using the data given in Table 8 relevant to the example considered it was concluded that with 800 volts applied to the crystal the leading edge of an input acoustic signal corresponding to an input attenuator setting of 28 dbs would be linearly amplified over 11/26 of the crystal length before the onset of non-linearity. With 900 volts applied, linear amplification was determined to occur over the first 7/10 of acoustic transit. The subsequent non-linear amplification of the propagating acoustic signal was noted to be

6 dbs at 800 volts and 3 dbs at 900 volts.

In sections 5.3.3 and 5.3.4 experimental results were presented indicating harmonic generation to occur under non-linear amplifying conditions and it was shown that the acoustoelectric voltage generated by the harmonics could contribute substantially towards the measured acoustoelectric voltage. If it is assumed that harmonic generation occurs at the onset of amplification non-linearity then the foregoing analysis indicates for the example considered that the acoustoelectric voltage generated by harmonics may be expected to be significant with 800 volts applied to the crystal since approximately one half of the crystal is available for the generation and subsequent amplification of the harmonics. However with 900 volts applied, the non-linearity is less marked, and does not occur until the input acoustic signal is much nearer the output face. Indeed, when the leading edge of the acoustic signal has reached the output face, the lagging edge is only just being amplified non-linearly. The harmonic generation at 900 volts may therefore be considered weak, and since only a small fraction of the crystal is available for the subsequent amplification of the harmonics, the acoustoelectric voltage generated by these harmonics will not be very significant.

Figure 65 shows that with 800 volts d.c. applied to the crystal an input attenuator setting of 28 dbs results in a measured acoustoelectric voltage which is greater than that measured with 900 volts applied. An analysis of the non-linear behaviour of the crystal indicates that harmonic generation is more significant with 800 volts applied, and it is suggested that if the acoustoelectric voltage generated by the harmonics were to be quantitatively determined, in each case, and subtracted from the corresponding measured acoustoelectric voltage, the resulting values would be equal, and consistent with the measured amplification. The acoustoelectric voltage curves would then intersect at the same

input attenuator setting as that noted to result in the intersection of the corresponding input-output curves given in figure 64.

The example chosen to illustrate the contention that harmonic generation is responsible for the observed difference in input attenuator setting as described, is fairly typical, and the conclusions drawn from the analysis presented are considered to be generally applicable to such a case. It should be noted however, that a more rigorous approach is really required to determine whether this explanation is valid when the input-output curves are noted to intersect at an input attenuator setting which results in marked non-linear behaviour at each of the applied voltages being considered. Strong harmonic generation will occur in each case, and the acoustoelectric voltage due to the harmonics will depend on their subsequent amplification.

In general however, the observed difference in the measured acoustoelectric voltage, under applied conditions which indicate an equal net amplification, and thus, according to the Weinreich relationship, an equal acoustoelectric voltage, for a given input attenuator setting at two applied voltages, is consistent with the relative degree of non-linear behaviour noted. Figures 51 to 56 indicate that at 15 MHz curve intersection is not common. The input-output curves at this frequency show that non-linearity in amplification is not very marked, and the lack of intersection of the corresponding acoustoelectric voltage curves suggests that the difference in the degree of non-linearity observed with various d.c. voltages applied to the crystal at a given input attenuator setting is not sufficient to result in a very different harmonic - generated, acoustoelectric voltage contribution to the measured acoustoelectric voltage.

The consequences of harmonic generation at 15 MHz have been quantitatively assessed in section 5.3.4. and this work is

discussed in section 6.2.4. The following section considers more rigorously the general validity of the Weinreich relationship under non-linear conditions.

6.2.3. The validity of the Weinreich relationship under non-linear conditions.

The input - output characteristics and the corresponding variation in acoustoelectric voltage have been discussed in general terms in section 5.3.1. , and in the preceding two sections of this chapter.

The non-linear acoustoelectric effects may be more rigorously appraised by comparing the measured acoustoelectric voltage with that predicted by the Weinreich relationship for the simultaneously measured acoustic attenuation, over the input acoustic intensity range resulting in non-linearity. As explained in chapter 5, a two-fold comparison is possible since the attenuation, or amplification, consistent with the measured acoustoelectric voltage may also be calculated and compared with the measured attenuation, or amplification.

At 15 MHz attention has been directed to some of the results given in figures 53 and 54. The experimental and theoretical values of attenuation and acoustoelectric voltage for an applied d.c. voltage of 200 and 400 volts are given in figures 58 and 59 respectively. In both cases the measured acoustoelectric voltage, indicated by the solid line in the bottom graph, is seen to be less than that predicted. The large difference indicated between the observed and the predicted attenuation emphasises the fact that the acoustoelectric voltage is only weakly dependent on the attenuation coefficient under attenuating conditions.

The results obtained with no drift voltage applied to the crystal at 15 MHz., have been described in section 5.2.3. The observed acoustoelectric voltage was determined to be about three times smaller than that predicted, and this disagreement was noted

to be independent of input acoustic intensity. It would therefore appear reasonable to question the accuracy of the input acoustic intensity determination at 15 MHz. A comparison of experiment with theory under amplifying conditions at 15 MHz., and subsequent experimental work concerning harmonic generation does however suggest a satisfactory acoustic intensity determination.

Garshka et al [44] have measured the variation of acoustoelectric voltage with acoustic intensity under the same conditions at 15 MHz and 45 MHz. Although they only specify the relative acoustic intensity, their results also indicate the acoustoelectric voltage generated at 15 MHz for a given acoustic intensity to be some three times smaller than that generated under identical conditions at 45 MHz. In view of this it would be useful to repeat the investigation with a number of crystals and thus determine more conclusively whether the disagreement is due to an error in input acoustic intensity or not. If the disagreement were noted to be of the order of three or four for each crystal, then further work could be carried out to identify the cause of the disagreement. An error in acoustic intensity determination would result in a wider range of disagreement, since the error would most probably be different in each case.

Under attenuating conditions the acoustoelectric voltage has been measured when the acoustic signal is just within the crystal. This has been shown to correspond to the maximum of the acoustoelectric voltage generated during a single acoustic transit. On the other hand the attenuation coefficient used to calculate the predicted acoustoelectric voltage is determined from an acoustic transit of the entire crystal. Therefore, if the portion of the crystal near the input transducer was markedly inhomogeneous, then the acoustoelectric voltage measured under attenuating conditions would not be consistent with the average attenuation coefficient of the crystal. If this

were the case however, the results at 45 MHz would also be affected, and no such effect has been noted. The possibility that this disagreement between theory and experiment at 15 MHz is due to the effects of carrier trapping will be discussed in section 6.2.5.

Apart from the work of Garshka et al little other published data is available concerning the variation of acoustoelectric voltage with acoustic intensity at different acoustic frequencies, and this apparent violation of the Weinreich relationship at 15 MHz remains unexplained.

Figures 60 and 61 present a similar comparison between experiment and theory under amplifying conditions at 15 MHz. Figure 60 describes the results obtained with 700 volts applied to the crystal and figure 61 those results for 800 volts applied. The measured acoustoelectric voltage is seen in both cases, to be greater than that predicted from the observed amplification. Furthermore, the acoustoelectric voltage becomes larger as the input acoustic intensity is increased, despite the fact that the observed amplification is reduced and acoustic attenuation is recorded at the greatest input intensities. Both figures 60 and 61 indicate good agreement between theory and experiment for small input acoustic intensities, thus discouraging the suggestion of an error in input acoustic intensity determination.

At 45 MHz., agreement between theory and experiment is seen to be much better under attenuating conditions than that indicated by the results obtained at 15 MHz. The results given by figure 66 for a d.c. voltage of 100 volts applied to the crystal, at 45 MHz show that the Weinreich relationship is valid until the observed non-linearity results in a reduction in attenuation of more than three dbs. The same was found to be true in the absence of an applied d.c. field. A reduction in attenuation was noted as the input intensity was increased, and good agreement between theory and

experiment was maintained by taking this reduction into account (see section 5.2.3.)

Figures 67 and 68 show that quantitative agreement between experiment and theory for small signal amplification at 45 MHz is very good. Further evidence of the quantitative validity of the Weinreich relationship is given in figure 73, which will be discussed shortly. Figure 68, describing the non-linearity observed at 45 MHz with 1000 volts d.c. applied, shows that the Weinreich relationship is quantitatively valid until non-linearity in amplification is observed. As the amplification is reduced the observed acoustoelectric voltage continues to increase. The predicted acoustoelectric voltage also continues to increase until an input attenuator setting of 20 dbs is reached. Further increase in input acoustic intensity results in further reduction in amplification, and the increase in the predicted acoustoelectric voltage due to increasing the input acoustic intensity is not sufficient to compensate for the decrease in observed amplification. Thus the predicted acoustoelectric voltage starts to decrease and for very large acoustic inputs is seen to become positive, as the acoustic signal is observed to be attenuated. When acoustic crossover is observed, and acoustoelectric voltage crossover accordingly predicted, the observed acoustoelectric voltage is seen to be some 300 mV. The predicted amplification of the input acoustic signal consistent with the observed acoustoelectric voltage is however only 7 dbs/L. This serves to emphasise that under amplifying conditions the acoustoelectric voltage is strongly dependent on the amplification coefficient, whereas under attenuating conditions a large change in attenuation only results in a small change in acoustoelectric voltage. This is well illustrated by figure 57.

Figure 71 presents a comparison of theory with experiment at 75 MHz for a crystal conductivity of $12.0 \cdot 10^{-6}$ $(\text{ohm cm})^{-1}$ and

with 700 volts d.c. applied to the crystal. The results obtained with no volts applied to the crystal at this frequency, (figure 47), indicated that the measured acoustoelectric voltage was about four times greater than that calculated by the Weinreich relationship. An analysis of the possible sources of this discrepancy was given in section 5.2.5. and it was concluded that an error in input intensity determination was responsible. This conclusion received support when a study, described in section 6.2.1., was made of the circumstances resulting in the onset of non- linearity. Better agreement between theory and experiment is obtained at 75 MHz when this correction is taken into account.

The onset of amplification non-linearity was shown, in section 6.2.1. to occur when the strain at the output end of the crystal resulted in a certain ratio of bunched electron density to free electron density. This critical ratio was seen to be dependent on the crystal conductivity. As the input acoustic intensity is increased for a given crystal conductivity, the critical electron density ratio is attained at earlier stages of acoustic propagation until the input acoustic intensity is sufficiently large to result in non-linearity at the input end of the crystal. Thereafter, an increase in input acoustic intensity leads to more pronounced non-linearity over the entire crystal length. Although net amplification is still recorded when the entire crystal behaves non-linearly, this is much reduced and eventually a certain input acoustic intensity is noted to result in no net amplification of the input signal. This acoustic intensity will henceforth be denoted the crossover intensity. Further increase in input acoustic intensity is then observed to result in net attenuation of the input signal.

Throughout the experimental work the net amplification or attenuation measured for a given set of applied conditions was

determined by comparing the acoustic output with that noted for the same input intensity with zero d.c. voltage applied to the unilluminated crystal. These reference conditions ensured no acoustoelectric interaction and any change in amplitude of the acoustic signal as it propagated through the crystal under these conditions was due entirely to non-electronic loss, which was considered to be very small. When an acoustic signal of crossover intensity is input to the crystal however, it is quite unrealistic to consider the acoustic signal to propagate through the crystal with no change in amplitude. It is much more realistic to consider the acoustic signal to be amplified as a result of the albeit, non-linear acoustoelectric interaction and, at the same time, to lose energy to the lattice as a result of the strong non-linear conditions present.

It was shown in section 5.3.3 that the generation of harmonics, and their subsequent amplification resulted in a large contribution to the total measured acoustoelectric voltage. It was also shown that the acoustic intensity of the fundamental acoustic signal was little affected by harmonic generation. These results will be discussed in section 6.2.4. It should be noted however, that throughout the harmonic investigation the applied d.c. voltage was adjusted at each input attenuator setting to ensure a measured net amplification of 6 dbs/L. The harmonic output was not assessed for input powers which were too great to enable 6 dbs amplification to be recorded for applied d.c. voltages up to a maximum of 1000 volts. The successful explanation of the noted disagreement between the measured and predicted acoustoelectric voltage given in section 5.3.3. in terms of the acoustoelectric voltage contribution of the generated harmonics is therefore only known to be valid for input acoustic intensities much less than the crossover intensity. This would suggest that the increase in non-electronic loss does not become significant until the input acoustic intensity approaches the

crossover intensity for a given set of applied conditions. For input acoustic intensities greater than the crossover intensity, the non-electronic loss becomes greater than the acoustoelectric amplification, which approaches zero as the non-linearity becomes more marked, and the measured acoustic output indicates net attenuation.

A cautionary note might well be sounded here. The predicted variation of acoustoelectric voltage given for comparison with that measured in the non-linear region has been calculated by assuming the measured amplification to be a constant throughout the crystal, and that the amplitude of the propagating acoustic wave changes exponentially with distance. Under non-linear conditions however, the acoustoelectric amplification may only be considered linear until $\left(\frac{n_{so}}{n_o}\right)_{CRIT.}$ is reached. When the whole crystal behaves non-linearly the gain per radian of the acoustic wave becomes increasingly smaller towards the output end of the crystal. No attempt has been made to take this reduction in amplification coefficient within the crystal into account in calculating the acoustoelectric voltage under non-linear conditions. It should be emphasised however, that only under strong non-linear conditions will this be significant.

A noticeable feature of the observed non-linearity in amplification over a wide range of applied conditions was the increase in acoustic crossover voltage with input acoustic intensity. Although a detailed study of the applied d.c. voltage required for acoustoelectric voltage crossover for different input acoustic intensities was not undertaken, it was generally noted that under non-linear conditions a larger applied voltage was required to result in acoustic crossover than that required for the corresponding acoustoelectric voltage crossover. It is important not to confuse this difference in acoustic and acoustoelectric voltage crossover

with that observed when carrier trapping is significant, and care is needed to ensure that any investigation of carrier trapping is carried out under linear conditions. The experimental results of Wang [36] showing the applied d.c. voltage leading to acoustic crossover to be greater than that resulting in acoustoelectric voltage crossover were subsequently interpreted to be due to carrier trapping; the difference may, however, have been consequent of non-linearity.

A satisfactory interpretation of the non-linear variation in amplification and simultaneously observed acoustoelectric voltage is not possible until the strong non-linear behaviour observed over a wide range of applied conditions, as described in figures 51 to 72 is better understood. Unquestionably, the contribution to the measured acoustoelectric voltage due to harmonic generation becomes more significant as the non-linearity becomes more marked. The results concerning harmonic generation, described in section 5.3.3 demonstrate this significance. The behaviour of an acoustic signal of input intensity in excess of the crossover intensity for a given set of applied conditions, lacks sufficient experimental investigation to enable a wholly acceptable explanation. A non-linear loss mechanism has been tentatively postulated to explain the observed attenuation of such large acoustic inputs under applied conditions which are noted to lead to substantial amplification of small acoustic inputs. This suggestion is only inspired by the results described plus the knowledge that distortion of the output acoustic signal does occur under conditions of strong non-linearity.

The comparison between theory and experiment under amplifying conditions at each acoustic frequency considered, for small acoustic inputs indicates the Weinreich relationship to be quantitatively valid under linear, and slightly non-linear conditions. The difficulty in measuring the acoustoelectric voltage for small acoustic inputs has been explained in section 5.3.1. Figure 73

describes the results of a careful investigation of small signal amplification and acoustoelectric voltage variation carried out at 45 MHz for three different crystal conductivities. The upper graph describes the observed variation in amplification with applied d.c. voltage and the solid curves in the lower graph describe the corresponding variation in the simultaneously measured acoustoelectric voltage. The dashed lines indicate the acoustoelectric voltage variation predicted by the Weinreich relationship, and good agreement with experiment is noted. To further demonstrate the validity of the Weinreich relationship under small signal conditions, two values of amplification coefficient were chosen and it was shown that the measured acoustoelectric voltage corresponding to the chosen values of amplification was sensibly constant and independent of applied d.c. voltage or crystal conductivity.

The following section discusses the experiments described in sections 5.3.2. and 5.3.3. concerning harmonic generation and the validity of the Weinreich relationship for each harmonic.

6.2.4. Harmonic generation

The variation of acoustoelectric voltage with input acoustic intensity described in section 5.3.1. and discussed in the preceding few sections of this chapter, was measured under both attenuating and amplifying conditions, over a wide range of crystal conductivity at three acoustic frequencies. In every case, a constant d.c. voltage, within the range zero to 1000 volts, was applied to the crystal. As the input acoustic intensity was increased under amplifying conditions, the acoustoelectric behaviour of the crystal became increasingly non-linear and the amplification was reduced. The corresponding measured acoustoelectric voltage variation was then affected by the increase in input acoustic intensity, the decrease in amplification, and also further consequences of the observed non-linear behaviour. Interpretation of the noted disagreement between theory

and experiment was complicated by the increasing non-linearity in amplification. This complication was overcome by adjusting the applied d.c. voltage at each input acoustic intensity to maintain constant the net measured attenuation (or amplification) of the crystal. Comparison of experiment with theory is thus facilitated since the acoustoelectric voltage is then predicted to be directly proportional to the input acoustic intensity.

Figures 74 to 77 describe the results thus obtained. Included in each figure is a table specifying the applied d.c. voltage range required to maintain the chosen value of attenuation for each crystal conductivity, over the acoustic intensity range of measurement.

The acoustoelectric voltage variation measured under attenuating conditions at 15 MHz and 45 MHz is described in figures 74 and 76 respectively. Agreement with theory is quantitatively good at 45 MHz, and qualitatively good at 15 MHz. Similar agreement under such conditions at these acoustic frequencies has been described and discussed in previous sections of this thesis. It may be generally concluded that little non-linearity occurs under attenuating conditions and accordingly only a small change in applied voltage is necessary in order to maintain the attenuation coefficients specified in the figures. The results also show, in agreement with theory, that providing the net attenuation is maintained constant, the measured acoustoelectric voltage variation is independent of crystal conductivity.

Figures 75 and 77 describe the results obtained under amplifying conditions at 15 MHz and 45 MHz respectively. Those described in figure 75 for a chosen amplification coefficient of 6 dbs/L, convincingly demonstrate that as the input acoustic intensity is increased, the measured acoustoelectric voltage cannot be wholly attributed to the input acoustic signal. This observation received

additional confirmation when the same experiment was repeated at 45 MHz for the same amplification coefficient, with similar results as described by figure 77. In each case, the disagreement between theory and experiment is noted to become greater as the acoustic intensity is increased, and furthermore, the disagreement increases with crystal conductivity. Good agreement between theory and experiment is noted for small acoustic inputs.

The observed variation of acoustoelectric voltage with input acoustic intensity for a constant amplification coefficient of 16 dbs/L is also described in figure 77. It was not possible to maintain this amplification coefficient for input acoustic intensities in excess of 0.01 watt cm^{-2} even though the applied d.c. voltage was increased to over 1000 volts. Although there is some indication of disagreement with theory for input acoustic intensities greater than 0.003 watt cm^{-2}, this is not too marked.

As a possible explanation of the observed disagreement between theory and experiment under non-linear conditions - a disagreement which was noted to increase with increasing input acoustic intensity and crystal conductivity, and to be significant only under amplifying conditions - an acoustoelectric voltage contribution arising from the generation and subsequent amplification of harmonics was postulated.

Section 5.3.3 describes in detail the work carried out to verify this suggestion quantitatively.

Visual evidence of harmonic generation was first obtained by monitoring the harmonic output resulting from the non-linear amplification of a 15 MHz input acoustic signal. The Y-cut quartz transducers of the acoustoelectric amplifier allowed odd harmonic detection only, and figure 78 presents a typical oscilloscope display of a 15 MHz input acoustic signal, and also typical displays of the third, fifth and seventh harmonic output. The experimental techniques

adopted to enable harmonic display have been described in section 5.3.3.

The difficulties associated with the display and subsequent measurement of acoustic signals of frequency greater than 100 MHz recommended a fundamental frequency of 15 MHz, since this enabled accurate measurement of the third and fifth harmonics to be accomplished. Furthermore, the observed variation of acoustoelectric voltage with input acoustic intensity at this frequency, given in figure 75, shows the greatest disagreement between theory and experiment, for a crystal conductivity of 26. 10^{-6} (ohm cm)$^{-1}$. The harmonic investigation was therefore carried out under those applied conditions which resulted in the observed acoustoelectric voltage variation described by figure 75 for this particular crystal conductivity.

In order that the acoustoelectric voltage generated by the harmonics under these applied conditions could be determined quantitatively, the variation of the 45 MHz. and 75 MHz. harmonic output was noted in terms of the output attenuator setting necessary to result in a standard display height of the detected harmonic signals for each value of the input acoustic intensity of the 15 MHz. fundamental as this was increased in steps from 0.01 to 0.3 watts/sq.cm. The d.c. voltage was increased as shown in Table 2, in order to maintain a net measured amplification of 6 dbs/L of the fundamental input. The higher limit of the acoustic intensity range of the fundamental indicates the maximum input which could be amplified by 6 dbs/L, and the lower limit indicates the smallest input acoustic intensity to result in a measurable acoustoelectric voltage.

The determination of the acoustic intensity of the third and fifth harmonics within the crystal, immediately prior to transduction and subsequent detection - hereafter referred to as the output acoustic intensity of the harmonics - was achieved by taking

into account the insertion loss of the particular transformer assembly being used on the output side of the crystal, and performing a similar calculation to that detailed in appendix 4. A calibration graph giving the output acoustic intensity of the detected harmonics in terms of the noted output attenuator setting was presented as figure 79, and the measured harmonic output intensity variation as a function of the input intensity of the fundamental was described in figure 80. A correction was made to the calculated output acoustic intensity of the 75 MHz. harmonic to account for an error in the determination of the insertion loss of the 75 MHz. transformer assembly as indicated by prior experimental work at this frequency, and the results given in figures 79 and 80 for the 75 MHz. harmonic incorporated this correction.

The calculation of the acoustoelectric voltage generated by the harmonics was consequent of certain assumptions which will be discussed shortly. Basically, the harmonics were considered to originate at the input face of the crystal, at the expense of the input 15 MHz. acoustic signal, and then to be linearly amplified throughout crystal transit. This amplification was dependent on the applied conditions which, it must be stressed, were varied each time the fundamental input acoustic intensity was increased

In the case of the 45 MHz. and 75 MHz. harmonics, knowledge of the output acoustic intensity of the harmonics generated by each fundamental input, enabled a determination of their effective input acoustic intensity and subsequent amplification as described in section 5.3.3 using the most relevant input-output characteristics available at these two frequencies. Account was taken of the variation in applied d.c. voltage as the input acoustic intensity of the fundamental was increased, in order to ensure that the results obtained were as accurate as possible. The amplification coefficient of the even harmonics was estimated from the values

determined for the odd harmonics, and Table 2 presents the estimated amplification coefficient of all the harmonics up to 75 MHz., generated by each input acoustic intensity of the fundamental, under the applied conditions noted to result in a 6 dbs/L amplification of the fundamental.

The effective input acoustic intensity of the 45 MHz. and 75 MHz. harmonics was expressed in Table 3 as a percentage of the fundamental input acoustic intensity. The percentage conversion to the 30 MHz. and 60 MHz. harmonics was then determined by assuming a geometrical progression of acoustic intensity conversion, and computing the geometrical ratio from the values calculated for the 45 MHz. and 75 MHz. harmonics. The results, given in Table 3, enabled the effective input acoustic intensity of all the harmonics being considered, to be calculated for each input acoustic intensity of the fundamental. This, and a knowledge of the amplification of these harmonics during crystal transit as given in Table 2, enabled the acoustoelectric voltage generated by each of the harmonics to be calculated using equation (5.6). The results obtained were given in Table 4, together with the acoustoelectric voltage predicted for a 6 dbs/L amplification of each 15 MHz. input acoustic signal. The predicted total acoustoelectric voltage due to the fundamental and the harmonics was shown in figure 81 to be in good agreement with that measured, over the fundamental input acoustic intensity range of interest.

The assumption that the detected harmonic output may be attributed to the linear amplification of a harmonic signal originating at the input face of the crystal would appear, at first, to be a gross approximation, since under non-linear conditions, the fundamental acoustic signal will continuously generate harmonics as it propagates through the crystal. It should be emphasised however, that this assumption was made to enable the calculation of the acoustoelectric

voltage due to the harmonics, and it can be argued that the harmonic intensity generated during propagation through the crystal of the fundamental was taken into account to some extent by determining a value for the effective input intensity of the harmonic signal which resulted in the measured harmonic output after appropriate amplification. Whether or not this assumption may be considered reasonable will now be considered.

The growth of the harmonic wave as it propagates through the crystal may be attributed to acoustoelectric amplification and continuous harmonic generation by the propagating fundamental acoustic signal. The acoustoelectric amplification of the harmonic signal may be determined for a given set of applied conditions by noting the resulting amplification of an input signal of the harmonic frequency under normal operation; that is, acoustic generation and detection at the same acoustic frequency. This will be referred to as the normal amplification coefficient. The growth of the propagating harmonic signal resulting from the continuous non-linear generation of harmonics by the fundamental will depend largely on the degree of non-linearity. Under strong non-linear conditions the contribution of the non-linearly generated harmonics to the propagating harmonic signal becomes increasingly significant. On the other hand if non-linearity is less marked the detected harmonic output intensity will be more dependent on the acoustoelectric amplification of the harmonic signal as it propagates through the crystal, and the growth of the harmonic wave may be considered to be approximately exponential, with an amplification coefficient which strictly should be taken to be a little larger than the normal amplification coefficient in order to account for the small but continuous non-linear harmonic generation arising from the fundamental. Since there is no way of determining this co rrection the linear amplification of the harmonics was assumed to be as determined for normal operation.

The limits of the input acoustic intensity range over which the harmonic investigation was carried out are seen from figure 33 to correspond to input attenuator settings of 37 to 22 dbs. Figure 55 describing the input-output characteristics of the fundamental relevant to the harmonic investigation suggests that within this range of input attenuator setting, the non-linearity associated with 6 dbs amplification is not very marked, and thus the assumption of an exponentially growing harmonic wave, for the purpose of acoustoelectric voltage calculation, is not considered unreasonable for this particular investigation. The slight disagreement between theory and experiment shown in figure 81 particularly at the higher 15 MHz. input intensities is perhaps indicative of the increasing significance of the harmonics generated within the crystal as non-linearity becomes more marked.

The assumption that harmonic generation occurs at the input crystal face may be shown to be justified for a fundamental input acoustic intensity greater than 0.03 watts/sq.cm. For input acoustic intensities less than this, non-linearity initiates within the crystal after some linear amplification has taken place and the assumption that harmonic amplification occurs throughout crystal transit is thus not very appropriate. However, even at the smallest 15 MHz. input acoustic intensity considered, non-linearity occurs within the first half of the crystal, and the reasonable agreement between theory and experiment indicated in figure 81 for these particular fundamental inputs would seem to verify a point made earlier. This was that the harmonic intensity generated during the transit of the fundamental signal through the crystal was taken into account by determining a value for the effective input intensity of the harmonic signal which resulted in the measured harmonic output after appropriate amplification.

The correction to the acoustic intensity determination of

the 75 MHz. harmonics indicated necessary from previous experimental work would appear to be well justified and the good agreement between theory and experiment consequent of this correction substantiates the conclusion that the Weinreich relationship is quantitatively valid at 75 MHz. It may also be concluded that the Weinreich relationship may be applied to each harmonic, as suggested by Butcher and Ogg [76,77] and independently by Tien [71].

6.2.5. The effect of carrier trapping on the Weinreich relationship

An analysis was presented in chapter 2 which enabled the trapping parameters f_r , f_J , and $\omega\tau$ to be determined from experimental data accruing from a study of attenuation variation with applied d.c. voltage.

This was measured at 15, 45 and 75 MHz. for various crystal conductivities and was reported in figures 83, 84(a) and 84(b) respectively. The necessity of avoiding power effects by studying the attenuation of small input acoustic intensities has been emphasised previously. As shown in figure 84(a), strong anomalous behaviour was noted under attenuating conditions at 45 MHz. which prohibited any investigation of trapping at this acoustic frequency. Anomalous attenuating behaviour was also observed at 45 MHz. with no drift voltage applied to the crystal. The attenuation, measured as a function of crystal conductivity, was shown in figure 38 to increase linearly as expected at low conductivites, but then to level off and show no further change with increasing conductivity. Similar behaviour has been noted by Southgate and Spector [47] who have suggested that a piezoelectrically inactive shear mode polarised perpendicular to the piezoelectrically active mode was responsible for the observed attenuation variation. They considered the levelling off of the observed attenuation to result when the active mode became smaller than the inactive mode. They also observed

non-linearity in attenuation at low power levels with various d.c. voltages applied to the crystal, and tentatively postulated coupling between the active and inactive modes to be responsible. No attempt was made to study the anomalous behaviour reported in this thesis, and the carrier density was maintained sufficiently low at 45 MHz. to avoid such compliciation.

The observed variation of attenuation coefficient with applied d.c. voltage at 15 MHz. described in figure 83, illustrates the essential consequences of carrier trapping - reduced amplification, and an increase in cross-over voltage at low conductivities - and the relevant information derived from figure 83 required to calculate the trapping parameters, using equations (5.9) to (5.12), was given in Table 5. The values of f_γ and f_j so determined, also given in Table 5, were substituted into equation (2.6 1) which indirectly predicts the applied d.c. voltage resulting in acoustoelectric voltage cross-over. The cross-over voltages determined experimentally at each crystal conductivity were seen in Table 6 to compare favourably with those predicted. Thus it would appear that the observed asymmetry in the attenuation - d.c. voltage curves at 15 MHz. and the noted increase in the applied d.c. voltage necessary for acoustic and acoustoelectric voltage crossover are consistently described by the trapping theories of Uchida et al [45] and Southgate and Spector [47].

It should be noted that the values of f_γ and f_j given in Table 5 are moduli and that equation (2.5 6) indicates f_j to be negative. Note also that as the crystal conductivity is increased the effects of carrier trapping become less significant. The values of $\omega\tau$ given in Table 5 indicated the trapping time to vary from 1.4×10^{-8} sec. to 5.6×10^{-7} sec as the crystal conductivity was increased. This range of values is in agreement with values reported by Uchida et al [45,46].

It was suggested in section 6.2.3 that the disagreement

between the measured and predicted acoustoelectric voltage noted at 15 MHz under small signal conditions was perhaps due to carrier trapping. The measured acoustoelectric voltage was seen to be about three times smaller than that predicted. Substitution of the determined trapping parameters given in Table 5 into equation (2.5 9)shows however that carrier trapping cannot account for such a large disagreement. Moreover, results given in section 5.2.3. indicated the disagreement to be independent of crystal conductivity whereas the trapping parameters are seen to be very dependent on crystal conductivity. Consequently if carrier trapping were responsible for the noted disagreement, then this should have become smaller as the crystal conductivity was increased.

6.2.6. Current saturation

The results described in section 5.3.5. were included largely out of interest, and no attempt was made to comprehensively investigate the consequences of acoustic flux amplification. Throughout the experimental work described previously, the duration of the applied d.c. voltage pulse was always maintained sufficiently short to ensure negligible acoustic flux build-up. A few remarks of a general nature will be given here to supplement the description of the results given in section 5.3.5.

The amplification of broadband acoustic flux was noted to be strongly sensitive to crystal conductivity as shown in figure 85, and also applied d.c. voltage, as shown in figure 86. Figure 85(d) convincingly indicates that the acoustic flux amplification results in an acoustoelectric current which opposes the ohmic current, and the use of the differential amplifier to determine more accurately the magnitude of the acoustoelectric current was demonstrated in figure 86. Figure 86(d) shows a typical display which allowed the effect of crystal conductivity and applied d.c. voltage on the growth of acoustic flux to be determined by noting the ohmic current

a few microseconds after the application of the applied d.c. voltage puse, and the reduced current after 50 microseconds. The resulting current-voltage characteristics were given in figure 87.

Acoustic flux amplification, and hence current reduction, was not observed at any crystal conductivity for applied d.c. voltages less than 600 volts, which was the value noted previously to be the threshold voltage for the onset of acoustic amplification. Acoustic flux growth was also noted to be insignificant for crystal conductivities less than about $15.0\ 10^{-6}$ $(\text{ohm cm.})^{-1}$. It may be noted from figure 87 that for a given crystal conductivity, the acoustoelectric current opposing the ohmic current at first increases as the applied d.c. voltage is increased from 600 volts and then decreases. This correlated with the observed variation in acoustic flux amplification as the applied voltage was increased. Blotekjaer and Quate[50] have studied the acoustic flux spectrum in CdS over the frequency range of 90 - 1000 MHz. They concluded that the peak frequency was 250 MHz. and they were unable to detect flux components above 450 MHz. McFee[31] has also observed flux components over a frequency range from 15 to 400 MHz. It should be mentioned that only flux components of frequency equal to the odd harmonics of the 15 MHz transducers may be detected. White's theory predicts that the applied d.c. field for maximum amplification of an acoustic wave of frequency ω is given by

$$\gamma = -\left(\frac{\omega_c}{\omega} + \frac{\omega}{\omega_D}\right)$$

Thus the observation that an increasingly larger applied voltage is necessary to result in the maximum detected flux output as the crystal conductivity is increased may possibly be due to higher frequency components becoming more dominant. An alternative explanation is that this may be attributed to the increasing flux intensity. Experiments with an input acoustic signal show that

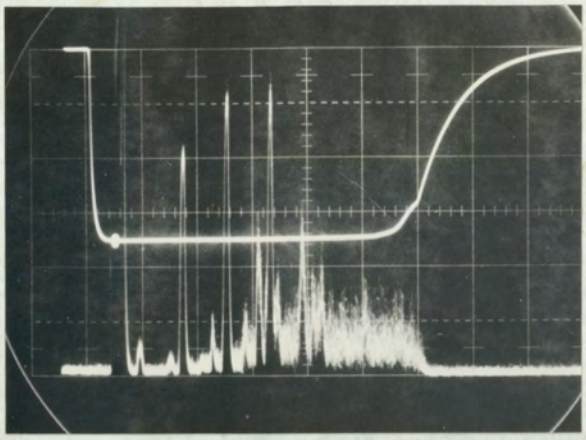

(a) INPUT SIGNAL FREQUENCY 15 MHz.
OUTPUT FREQUENCY 45 MHz.
TOP TRACE : APPLIED VOLTAGE
SCALE : 200 VOLTS/SQUARE
BOTTOM TRACE : ROUND TRIP
GAIN OF HARMONIC.
HORIZONTAL SCALE : 10 μs/SQ.

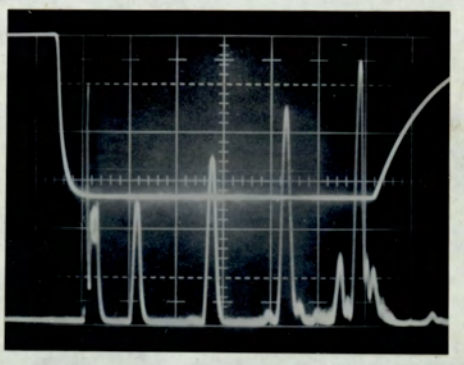

TOP TRACE : APPLIED VOLTAGE
SCALE 200 v/SQ.

(b) BOTTOM TRACE : ROUND TRIP
GAIN OF 75 MHz SIGNAL.
HORIZONTAL SCALE : 5 μs/SQ.

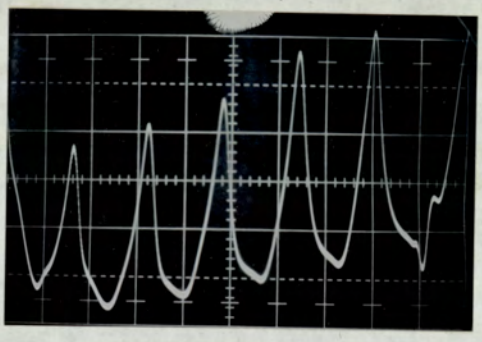

ROUND TRIP GAIN INDICATED
BY ACOUSTOELECTRIC
VOLTAGE, DISPLAY

(c) INPUT SIGNAL FREQUENCY
15 MHz.
DC VOLTS 800
HORIZONTAL SCALE : 5 μs/SQ
VERTICAL SCALE : 20 mv/SQ.

FIG. 92. TYPICAL ROUND TRIP GAIN OF ACOUSTIC AND ACOUSTOELECTRIC SIGNALS.

an increase in input intensity results in maximum amplification occurring at greater applied voltages.

Figure 85(b) shows that the applied conditions resulting in that particular display only result in significant flux build up after the d.c. voltage has been applied to the crystal for 25μ secs. This suggests that the round trip gain of the flux components under these conditions is not very great. When the round trip gain becomes appreciable the resulting accustoelectric current may lead to current oscillation, as shown by figure 89. The oscillatory nature of the acoustoelectric current is shown more clearly in figure 92(c). Figures 92(a) and (b) present examples of acoustic round trip gain. Note that in figure 92(a) the growth of acoustic flux suppresses the round trip gain. A similar example of the effect of acoustic flux on the acoustic amplification of an input acoustic signal was shown in figure 88.

As indicated in chapter 1, many papers have been published concerning current saturation and oscillation and no attempt has been made to comprehensively discuss the observations described in section 5.3.5 relating to this aspect of the acoustoelectric interaction.

CHAPTER 7

CONCLUSIONS AND SUGGESTIONS FOR FURTHER WORK

7.1 General conclusions

A review of the published work concerning the acoustoelectric interaction showed that the acoustoelectric effect had been largely ignored, and that a comprehensive experimental investigation of the Weinreich relationship was lacking. Measurement of the acoustoelectric voltage affords a most direct means of studying the acoustoelectric interaction, as indicated by the results presented in this thesis. The object of this work has been to investigate to what extent the measured acoustoelectric voltage and the simultaneously measured acoustic attenuation coefficient are related, by determining quantitatively, the validity of the Weinreich relationship over a wide range of experimental conditions.

During the course of the work, strong non-linear acoustoelectric behaviour was observed and the Weinreich relationship has been studied under both linear and non-linear conditions. The following subsections present a summary of the conclusions reached in each case.

7.1.1. Linear acoustoelectric behaviour

Although this was noted under both amplifying and attenuating conditions, the observed variation of amplification coefficient with input acoustic intensity, at each acoustic frequency, showed non-linearity to occur within the crystal at quite small input intensities. This emphasised the need for a stringent limitation of the input acoustic intensity under amplifying conditions if non-linear effects were to be avoided. Unfortunately, the acoustoelectric voltage generated under linearly amplifying conditions was then too small in most cases to allow accurate

measurement. Sufficient experimental evidence was presented however, showing the Weinreich relationship to be quantitatively valid under linearly amplifying conditions. Under attenuating conditions the observed acoustoelectric behaviour was largely linear. As predicted, the acoustoelectric voltage was noted to be much smaller than that generated under amplifying conditions and accurate measurement of the acoustoelectric voltage under attenuating conditions, over a wide range of input acoustic intensity, was achieved only in the absence of an applied d.c. voltage.

Comparison between theory and experiment of the acoustoelectric voltage variation with input acoustic intensity, acoustic pulse width, and as the acoustic signal propagated through the crystal, measured with no applied d.c. voltage, over a wide range of crystal conductivity at 45 MHz was particularly impressive, and left no doubt as to the quantitative validity of the Weinreich relationship under linear conditions. In general, the results obtained at 45 MHz. and 75 MHz. for linear operation of the amplifier under both amplifying and attenuating conditions indicated the Weinreich relationship to be quantitatively valid.

Under attenuating conditions at 15 MHz. the measured acoustoelectric voltage was seen to be some three times smaller than that predicted, although qualitative agreement with theory was noted. This disagreement was investigated and it was concluded that neither crystal inhomogeneity nor carrier trapping effects were responsible. Agreement was noted to be better under amplifying conditions at this acoustic frequency and this suggested that an error in input acoustic intensity determination was not responsible for the observed disagreement under attenuating conditions either. This conclusion received support when harmonic generation was investigated.

At 75 MHz. the measured acoustoelectric voltage was noted to be some four times larger than that predicted. However subsequent experimental work under non-linear conditions indicated that this disagreement was attributable to an error in input acoustic intensity determination, and quantitative agreement between theory and experiment was noted for a large number of experiments when this error was taken into account.

7.1.2. Non-linear acoustoelectric behaviour

This was mainly observed under amplifying conditions and was noted to become more marked as the crystal conductivity was increased. The onset of non-linearity was studied over a wide range of amplifying conditions, and it was shown that this related to a limitation of electron bunching . Several features of the results obtained from this study were explained by White's linear theory of acoustic amplification.

Under moderately non-linear conditions the noted disagreement between the predicted and observed acoustoelectric voltage was attributed to the generation of harmonics and experimental work carried out to investigate this suggestion showed the Weinreich relationship to be quantitatively valid for each harmonic. It was also concluded that energy conversion to harmonics was not very great under these conditions, although it was suggested that this could become significant under strong non-linear conditions. A net attenuation of large acoustic inputs was noted under those applied conditions which resulted in a high amplification of a small input acoustic signal, and it was tentatively suggested that an increase in non-electronic loss may have been partly responsible.

The observed variation of the d.c. voltage required for the onset of amplification as the input acoustic intensity was increased emphasised the need to restrict the input acoustic intensity to that known to result in linear acoustoelectric behaviour in order that

the effects of carrier trapping could be identified and investigated. This investigation was carried out at 15 MHz. only, since the observed variation of acoustic attenuation with applied d.c. voltage at 45 MHz. and 75 MHz. indicated anomalies which prevented such an investigation. It was shown that the prominent trapping theories described consistently the variation in acoustic and acoustoelectric voltage crossover with crystal conductivity.

The experimental results reported in this thesis indicate the importance of measuring both the acoustoelectric voltage and the acoustic attenuation coefficient if a better understanding of the acoustoelectric interaction is to be obtained. The Weinreich relationship has been shown to be quantitatively valid under linear conditions and thus provides a useful means of investigating non-linear effects.

7.2. Suggestions for further work

The acoustic amplifier used in this research comprised two quartz transducers bonded with indium onto opposite faces of a piece of single crystal cadmium sulphide. Although this is simple in design, great difficulty was experienced in effecting the bonds without transducer breakage, whilst ensuring that the transducers remained correctly oriented with respect to the crystal axes so that the propagation of piezoelectrically active shear waves could be studied. The method used to achieve this was described in chapter 3. Although this proved quite satisfactory it is felt that the advantages accruing from a simple, reliable means of accurately fabricating such an amplifier would make worthwhile its development.

The experimental arrangement may also be improved. The accurate measurement of small acoustoelectric voltages in the presence of an applied d.c. voltage was complicated by small changes occurring in the illumination of the crystal. Although this was not sufficient to cause any variation in the acoustoelectric voltage

it prevented the use of the most sensitive ranges of the differential amplifier. Some variation in illumination intensity undoubtedly arises from the intrinsic inability of the tungsten lamps to maintain a constant illumination output even under the most rigorous control. However, small variations in the lamp supply voltage was also considered to be partly responsible for the noted illumination variation, despite the use of a voltage stabiliser, and therefore some improvement might be obtained if a battery is used for the lamp supply.

The error in input acoustic intensity determination at 75 MHz. discussed in chapters 5 and 6 suggests the need for an investigation into the problems of matching the amplifier into a fifty ohm line.

The insertion loss of each matching transformer and associated transducer was shown to be more accurately determined by noting any difference in the acoustoelectric voltage generated by a given acoustic signal input to one end of the crystal and then the other. This exploitation of the acoustoelectric effect in the absence of an applied d.c. voltage, to determine relative acoustic input suggests a possible device potential - a means of determining, absolutely, very small acoustic intensities. The validity of the Weinreich relationship under linear conditions would enable a calibration graph of input acoustic intensity versus acoustoelectric voltage to be prepared for a given crystal given a knowledge of the attenuation coefficient of the input acoustic signal whose acoustic intensity was to be determined. Prior measurement of the attenuation coefficient of small input intensity acoustic signals over a given acoustic frequency range, whilst maintaining the crystal conductivity a constant would allow a reasonably accurate determination of the attenuation of an acoustic signal of intermediate frequency by interpolation. Thus the crystal, having evaporated

d.c. contacts to enable acoustoelectric voltage measurement, could be bonded to the source, or effective source, of the acoustic signal of unknown intensity using salol or vacuum grease, and in the case of shear waves, rotated to obtain maximum acoustoelectric voltage. The illumination of the crystal could be adjusted so that the calibration graphs were valid, and the acoustic intensity determined from a measure of the acoustoelectric voltage. If the acoustic signal were longitudinal then a crystal having d.c. contacts in a plane perpendicular to the c - axis would be required. This would appear to offer a useful means of accurately determining very small acoustic intensities, and a feasibility study would seem worthwhile.

The investigation of harmonics reported in this thesis showed that harmonics higher than the second can be detected and measured. Previous reported experimental work has only considered the second harmonic. In order to investigate the generation of even, as well as odd, harmonics of a given fundamental, it would be necessary to either change the detecting transducer, or to bond two or even three transducers of the appropriate fundamental frequencies onto the output crystal face. If such a study were carried out then the use of indium as a bonding material would be ill-advised, and something less permanent is recommended. The use of salol or vacuum grease - both known to allow good acoustic transmission - would also enable a study of spurious mode propagation. Southgate and Spector [47] have suggested that attenuation anomalies as reported in this thesis are due to the propagation of a piezoelectrically inactive shear wave polarised perpendicular to the active wave. This could be investigated if the output transducer were able to be rotated.

APPENDIX 1

The piezoelectric equations of state

The basic equations of state for a piezoelectric crystal relate the elastic and electrical properties of the material.

Arbitrarily, the stress T_{ij} and the piezoelectric field E_i may be considered as independent variables. The strain S_{ij} and the electric displacement D_i may then be considered as dependent variables and may be expressed in differential form as follows:

$$dS_{ij} = \left(\frac{\partial S_{ij}}{\partial T_{kl}}\right)_E dT_{kl} + \left(\frac{\partial S_{ij}}{\partial E_k}\right)_T dE_k \quad \text{------(A1.1)}$$

$$dD_i = \left(\frac{\partial D_i}{\partial T_{jk}}\right)_E dT_{jk} + \left(\frac{\partial D_i}{\partial E_j}\right)_T dE_j \quad \text{-----(A1.2)}$$

Each of the bracketted differential coefficients describes a particular physical effect. In equation (A.1.1) $\left(\frac{\partial S_{ij}}{\partial T_{kl}}\right)_E$ describes the differential change in strain produced by a change in stress, at constant electric field. This differential coefficient describes the elastic compliance s_{ijkl} . The second differential coefficient $\left(\frac{\partial S_{ij}}{\partial E_k}\right)_T$ of equation (A.1.1) describes the differential change in strain produced by the piezoelectric field, at constant stress. This describes the converse piezoelectric effect, and the coefficient may be expressed as the piezoelectric moduli d_{kij} . Equation (A.1.1) may therefore be written, in integrated form, as

$$S_{ij} = s_{ijkl} T_{kl} + d_{kij} E_k \quad \text{-------(A1.3)}$$

The differential coefficient $\left(\frac{\partial D_i}{\partial T_{jk}}\right)_E$ of equation (A.1.2) describes the change in electric displacement due to a change in

electric displacement due to a change in applied stress, at constant electric field. This effect is known as the direct piezoelectric effect and the coefficients are the piezoelectric modul d . The coefficients for the direct and converse piezoelectric effects are numerically equal. The change in electric displacement due to a change in electric field, at constant stress, described by the coefficients $\left(\frac{\partial D_i}{\partial E_j}\right)_T$ of equation (A.1.2) defines the permittivity $\varepsilon_{ij}^{\ T}$. Equation (A.1.2) may also be expressed in integrated form.

$$D_i = d_{ijk}\, T_{jk} + \varepsilon_{ij}^{\ T} E_j \quad \text{(A1.4)}$$

The direct piezoelectric effect may be written in differential form as follows:

$$\partial P_i = d_{ijk}\, \partial T_{jk} \quad \text{(A1.5)}$$

where ∂P_i is the change in polarisation produced by an applied stress. The electric displacement for an anistropic crystal may be written ,

$$D_i = \varepsilon_o E_i + P_i \quad \text{(A1.6)}$$

where ε_o is the permittivity of vacuo, and in differential form this may be written

$$\partial P_i = \partial D_i - \varepsilon_o\, \partial E_i \quad \text{(A1.7)}$$

If the electric field is held constant equation (A.1.7) indicates that

$$\partial P_i = \partial D_i$$

Thus the direct piezoelectric effect, given by equation (A.1.5) may also be expressed by the following equation.

$$\partial D_i = d_{ijk}\, \partial T_{jk} \quad (E \text{ constant.})$$

$$\text{(A1.8)}$$

Under isothermal conditions it may be shown that

$$\varepsilon^S - \varepsilon^T = - d_{ikl}\, d_{jmn}\, c^E_{klmn} \qquad \text{(A1.9)}$$

ε^S is the permittivity at constant strain, and this condition may be satisfied by imagining the crystal to be firmly surrounded by a medium with infinite elastic stiffness. If the crystal were so mounted as to allow strains to take place as freely as possible then the permittivity would be that at constant stress ε^T.

The dimensionless ratio $\left(\frac{\varepsilon^S - \varepsilon^T}{\varepsilon^T}\right)^{\frac{1}{2}}$ is known as the electromechanical coupling factor and is designated K. This expresses the electrical energy to the total energy of the crystal and is a measure of piezoelectric activity.

Consideration of the relevant partial derivatives yields the following relationships.

$$\begin{aligned} d_{ijk} &= e_{ilm}\, s^E_{lmjk} \\ e_{ijk} &= d_{ilm}\, c^E_{lmjk} \end{aligned} \qquad \text{(A1.10)}$$

where e_{ijk} are piezoelectric constants and give a measure of the differential change in electric displacement with strain at constant electric field.

Equation (A.1.3) may be rearranged to give

$$T_{ij} = c_{ijkl}\, S_{kl} - d_{kij}\, c_{ijkl}\, E_k \qquad \text{(A1.11)}$$

Using the relationships of equation (A.1.10) and omitting the tensor notation this may be written

$$T = cS - eE \qquad \text{(A1.12)}$$

Substituting T_{ij} from equation (A.1.11) into equation (A.1.4) and again dropping the tensor notation, yields

$$D = dcS - d^2cE + \varepsilon^T E$$

Thus $$D = dcS + E\left(\varepsilon^T - d^2c\right)$$

Using the relationships of equation (A.1.10) this becomes

$$D = dcS + \varepsilon^T E\left(1 - \frac{e^2}{\varepsilon^T c}\right)$$

But $$\varepsilon^T\left(1 - \frac{e^2}{\varepsilon^T c}\right) = \varepsilon^S$$

from equations (A.1.9) and (A.1.10) .

Therefore,

$$D = eS + \varepsilon^S E \qquad \text{---------(A 1.13)}$$

This is the other piezoelectric equation of state.

The piezoelectric equations of state are thus

$$D = eS + \varepsilon^S E$$

and $$T = cS - eE \,.$$

APPENDIX 2

The phase relationship equations from Whites theory

The following twelve equations describe comprehensively the phase relationships between the piezoelectric field $\tilde{E}_1$, the bunched space charge $\tilde{n}_s$, and the strain $\tilde{S}$. The phase angles between $\tilde{E}_1$ and $\tilde{S}$, and $\tilde{n}_s$ and $\tilde{S}$ are ψ and ϕ respectively, and the phase angle between $\tilde{n}_s$ and $\tilde{E}_1$ is θ. These equations were used to obtain figures 4 to 8.

$$\tan \psi = \frac{-\left(\frac{\omega_c}{\omega}\right)\gamma}{\left[\gamma^2 + \left(\frac{\omega}{\omega_D}\right)\left(\frac{\omega_c}{\omega} + \frac{\omega}{\omega_D}\right)\right]} \quad ----(A\,2.1)$$

$$\sin \psi = \left[\frac{\left(\frac{e}{\varepsilon}\right)\left(\frac{\omega_c}{\omega}\right)\gamma}{\gamma^2 + \left(\frac{\omega_c}{\omega} + \frac{\omega}{\omega_D}\right)^2}\right]\frac{S_o}{E_{1o}} \quad ---(A.2.2)$$

$$\cos \psi = -\left(\frac{e}{\varepsilon}\right)\left[\frac{\gamma^2 + \left(\frac{\omega}{\omega_D}\right)\left(\frac{\omega_c}{\omega} + \frac{\omega}{\omega_D}\right)}{\gamma^2 + \left(\frac{\omega_c}{\omega} + \frac{\omega}{\omega_D}\right)^2}\right]\frac{S_o}{E_{1o}} \quad --(A\,2.3)$$

$$|E_{1o}| = \left(\frac{e}{\varepsilon}\right)\left|\left[\frac{\gamma^2 + \left(\frac{\omega}{\omega_D}\right)^2}{\gamma^2 + \left(\frac{\omega_c}{\omega} + \frac{\omega}{\omega_D}\right)^2}\right]^{-\frac{1}{2}}\right| S_o \quad --(A.24$$

$$\tan \phi = -\frac{\left(\frac{\omega_c}{\omega} + \frac{\omega}{\omega_D}\right)}{\gamma} \quad ----(A\,2.5)$$

$$\sin\phi = -\left(\frac{\omega_c e}{q v_s}\right)\left[\frac{\left(\frac{\omega_c}{\omega}+\frac{\omega}{\omega_D}\right)}{\gamma^2+\left(\frac{\omega_c}{\omega}+\frac{\omega}{\omega_D}\right)^2}\right]\frac{S_o}{n_{so}} \quad \text{---(A 2.6)}$$

$$\cos\phi = \left(\frac{\omega_c e}{q v_s}\right)\left[\frac{\gamma}{\gamma^2+\left(\frac{\omega_c}{\omega}+\frac{\omega}{\omega_D}\right)^2}\right]\frac{S_o}{n_{so}} \quad \text{--(A 2.7)}$$

$$|n_{so}| = \left(\frac{e\omega_c}{q v_s}\right)\left|\left[\frac{1}{\gamma^2+\left(\frac{\omega_c}{\omega}+\frac{\omega}{\omega_D}\right)^2}\right]^{\frac{1}{2}}\right| S_o \quad \text{--(A 2.8)}$$

$$\tan\theta = \frac{-\left(\frac{\omega}{\omega_D}\right)}{\gamma} \quad \text{------(A 2.9)}$$

$$\sin\theta = \left(\frac{\sigma}{q v_s}\right)\left[\frac{(\omega/\omega_D)}{\gamma^2+\left(\frac{\omega}{\omega_D}\right)^2}\right]\frac{E_{10}}{n_{so}} \quad \text{--(A 2.10)}$$

$$\cos\theta = -\left(\frac{\sigma}{q v_s}\right)\left[\frac{\gamma}{\gamma^2+\left(\frac{\omega}{\omega_D}\right)^2}\right]\frac{E_{10}}{n_{so}} \quad \text{(A 2.11.)}$$

$$|n_{so}| = \left(\frac{\sigma}{q v_s}\right)\left|\left[\frac{1}{\gamma^2+\left(\frac{\omega}{\omega_D}\right)^2}\right]^{\frac{1}{2}}\right| E_{10} \quad \text{---(A.2.12)}$$

APPENDIX 3

The determination of the insertion loss correction term arising from acoustoelectric voltage comparison

Let the insertion loss of the transformer matching assembly and associated transducer on the input side of the crystal (henceforth denoted T_1) be L_1 , and suppose that on the output side to be L_2 . The total insertion loss (L_o) is then given by

$$L_o = L_1 + L_2 \qquad \text{- - - - - - - - (A.3.1)}$$

If Q_o is the effective r.f. power input to T_1 and Q_1 is the acoustic power input to the crystal then

$$L_1 = 10 \log_{10}\left(\frac{Q_1}{Q_o}\right) \qquad \text{- - - - - - (A.3.2)}$$

and

$$(V_{ae})_1 = C Q_1 \qquad \text{- - - - - - (A.3.3)}$$

where C is a constant and $(V_{ae})_1$ is the observed acoustoelectric voltage generated with the crystal very weakly illuminated (i.e. sufficient to result in a measurable acoustoelectric voltage, but not sufficient to result in more than 0.5 db increase in the insertion loss of the crystal.)

If the same r.f. signal is now input to T_2 then

$$L_2 = 10 \log_{10}\left(\frac{Q_2}{Q_o}\right) \qquad \text{- - - - - - (A.3.4)}$$

and

$$(V_{ae})_2 = C Q_2 \qquad \text{- - - - - - (A.3.5)}$$

where Q_2 is the acoustic power input to the crystal, C is the same constant as before and $(V_{ae})_2$ is the acoustoelectric voltage so resulting. Using equations (A.3.2) to (A.3.5) gives

$$L_1 - L_2 = 10 \log_{10}\left(\frac{Q_1}{Q_2}\right) = 10 \log_{10}\left(\frac{V_{ae\,1}}{V_{ae\,2}}\right)$$

Substituting for L_2 from equation (A.31) gives

$$L_1 = \frac{1}{2}\left\{ L_0 + 10 \log_{10}\left(\frac{V_{ae_1}}{V_{ae_2}}\right)\right\}$$

This allows an accurate determination of L_1 if $(V_{ae})_1$ and $(V_{ae})_2$ are not equal. It should be noted that L_0 is measured with the crystal in the dark.

APPENDIX 4

The determination of input acoustic intensity

Consider the peak to peak amplitude of the r.f. signal input to the matching transformer assembly and associated transducer, T_1, to be V_{pp}, and suppose this to be measured across a load of R ohms. The power delivered to the load, Q_o, is then $\left(\frac{V_{pp}}{2\sqrt{2}}\right)^2 \frac{1}{R}$ watts, where $\left(\frac{V_{pp}}{2\sqrt{2}}\right)$ is the root mean square value of the peak to peak amplitude. If the insertion loss of T_1 is L_1 dbs, then the power delivered to the crystal is L_1 dbs down on Q_o. This power is delivered to the active region of the transducer of area A sq.cms. Thus the acoustic intensity input to the crystal is L_1 dbs down on $\left(\frac{V_{pp}}{2\sqrt{2}}\right)^2 \frac{1}{RA}$ watts/sq.cm. During the experimental work L_1 was determined as indicated in appendix 3, R was 50 ohms, and A was obtained from the transducer specification (see figure 11).

REFERENCES

1) R.H. Parmenter — Phys.Rev. 89.990 (1953)

2) L. Brillouin — Proc.natn.Acad.Sci(U.S.) 41.401 (1955)

3) A. Van Den Beukel — Appl.scient.Res.B5.459 (1956)

4) N. Mikoshiba — J. phys.Soc.Japan 14. 22 (1959)

5) G. Weinreich — Phys.Rev. 104. 321 (1956)

6) T. Holstein — Westinghouse Research Memo 60-94698-3-M15 (Unpublished)

7) J. Bardeen and W. Shockley — Phys. Rev. 80. 72 (1950)

8) G. Weinreich and H.G. White — Phys. Rev. 106. 1104 (1957)

9) F.J. Blatt — Phys. Rev. 105. 1118 (1957)

10) G. Weinreich, T.M. Sanders, and H.G. White — Phys. Rev. 114. 33 (1959)

11) N. Mikoshiba — J. Phys. Soc. Japan 15. 982 (1960)

12) W. Sasaki and E. Yoshida — J. Phys. Soc. Japan 12. 979 (1957)

13) R. H. Parmenter — Phys. Rev. 113. 102 (1959)

14) E. I. Blount — Phys. Rev. 114. 418 (1959)

15) N. Mikoshiba — J. phys. Soc. Japan 14. 1691 (1959)

16) See reference 11 of reference 10

17) G. Weinreich — Phys. Rev. 107. 317 (1957)

18) A.R. Hutson — J. Phys. Chem. Solids 8 467 (1959)

19) A.R. Hutson — J. appl. Phys. 32 (Supplmt) 2287 (1961)

20) H.D. Nine — Phys. Rev. Lett. 4. 359 (1960)

21) A.R. Hutson — Phys. Rev. Lett 4. 505 (1960)

22) H.D. Nine and R. Truell — Phys. Rev. 123. 799 (1961)

23) J.J. Kyame — J. acoust. Soc. Am. 26. 990 (1954)

24) A.R. Hutson and D.L. White — J. appl. Phys. 33. 40 (1962)

25) E.P. Warekois et al — J. appl. Phys. 33. 690 (1962)

26) P.C. Waterman — J. appl. Phys. 29. 1190 (1958)

27) D.L. White — J. appl. Phys. 33. 2547 (1962)

28) A.R. Hutson, J.H. McFee, and D.L. White — Phys. Rev. Lett. 7. 237 (1961)

29) F.S. Hickernell and N.G. Sakiotis — Proc. IEEE 52. 194 (1964)

30) R.M. White — IEEE Trans. Sonics and Ultra Sonics Su-13 69 (1966)

31) J.H. McFee — J. appl. Phys. 34. 1548 (1963)

32) W.C. Wang and J. Pua — Proc. IEEE 51. 1235 (1963)

33) J.T. Hanlon — Proc IEEE 55. 1128 (1967)

34) D.L. White, E.T. Handelman and J.T. Hanlon — Proc. IEEE. 53. 2157 (1965)

35) J.E. May — Proc. IEEE. 53. 1465 (1965)

36) W.C. Wang — Phys. Rev. Lett. 9. 443 (1962)

37) H.N. Spector — J. appl. Phys. 34. 3628 (1963)

38) S.G. Eckstein — J. appl. Phys. 35. 2702 (1964)

39) J.H. McFee — Physical Acoustics - Vol. lV.Pt A. Academic Press. London (1966) Ed. - W.P. Mason

40) C.A.A.J. Greebe — Phys. Lett. 4 45 (1963)

41) C.A.A.J. Greebe — Solid St. Commun. 3. 227 (1965)

42) V.E. Henrich and G. Weinreich — Phys Rev. 178 1204 (1969)

43) P.S. Karla and E.P. Garshka — Soviet Phys.solid St. 10. 852 (1968)

44) E.P. Garshka et al — Soviet Phys solid St. 10 480 (1968)

45) I. Uchida and T. Ishiguro et al — J. phys Soc Japan 19. 674 (1964)

46) T. Ishiguro, I. Uchida and T. Suzuki — IEEE Int.Conf.Record 12. 93 (1964)

47) P.D. Southgate and H. Spector — J. appl Phys. 36 3728 (1965)

48) A.R. Moore and R.W. Smith — Phys. Rev. 138 1250A (1965)

49) A. Rannestad — Internal Rep. E - 90. Contract No. AF 61(052) - 958 Norwegian Defence Research Establishment. Kjeller. Norway

50) K. Blotekjaer and C.F. Quate — Proc.IEEE 52.360 (1964)

51) R.W. Smith — Phys. Rev Lett 9.87 (1962)

52) L. Esaki — Phys. Rev. Lett 8. 4 (1962)

53) A.R. Hutson — Phys. Rev. Lett 9 297 (1962)

54) A.R. Moore — Phys. Rev. Lett. 12. 47 (1964)

55) J. Zucker and S. Zemon — Appl. Phys. Lett. 9. 398 (1966)

56) A.R. Moore — Appl. Phys. Lett. 13. 126 (1968)

57) R. Klein — Phys. Lett. 28A. 428 (1968)

58) I.W. Stanley — Appl. Phys. Lett 10. 76 (1967)

59) W.H. Haydl — Rev. scient. Instrum 36. 681 (1965)

60) W.H Haydl — M.L. Report 1183 Microwave Lab. Stanford Univ. California

61) H. Kroger et al — Phys. Rev. Lett 12. 555 (1964)

62) W.H. Haydl and C.F. Quate — Appl.Phys. Lett. 7. 45 (1965)

63) W.H. Haydl — Appl. Phys. Lett. 10. 36 (1967)

64) J.D. Maines — Appl. Phys. Lett 8 67 (1966)

65) H.J. Fossum — Internal Rep. E - 93. Contract No. AF 61(052) - 958 Norwegian Defence Research Establishment. Kjeller. Norway

66) J.H. McFee and P.K. Tien — J.appl.Phys. 38. 1721 (1967)

67) J.H. McFee, P.K. Tien and H.L. Hodges — J.appl.Phys. 38. 1721 (1967)

68) W.H. Haydl, K. Harker and C.F. Quate — J. appl. Phys. 38. 4295 (1967)

69) B.K. Ridley — Proc. phys. Soc (London)

70) J.D. Maines and E.G.S. Paige — Phys.Lett. 7 45 (1965)

71) P.K. Tien — Phys. Rev. 171. 970 (1968)

72) A.E. Lord and B.B. Chick — J. acoust Soc. Am. 40 1473 (1966)

73) H. Kroger — Appl. Phys. Lett. 4. 190 (1964)

74) C. Elbaum and R. Truell — Appl. Phys. Lett. 4. 212 (1964)

75) B. Tell — Phys. Rev. 136. A772 (1964)

76) P.N. Butcher and N. Ogg — Brit. J. Appl Phys. (J.Phys.D) 1. 1271 (1968)

77) P.N. Butcher and N. Ogg — Brit. J. Appl.Phys.(J.Phys.D) 2. 333 (1969)

78)	A. Many and I. Balberg	Phys. Lett 24A.705 (1967)
79)	J.D. Maines and E.G.S.Paige	Electronics Lett. 4. 196 (1968)
80)	A.K. Ganguly and E.M. Conwell	Phys. Lett. 29A.221(1969)
81)	D.J. Larner	Appl. Phys. Lett 15.20 (1969)
82)	M. Kent Parsons	IEEE trans sonics and ultrasonics SU 14. 142 (1967)
83)	W.H. Haydl	Rev. scient Instrum. 36. 681 (1965)
84)	CdS crystals from	Eagle Picher Co.Ltd. (Note: Grade B refers to resistivity range not quality)
85)	W.L. Bond	J. scient. Instrum. 38. 63 (1961)
86)	G.W. Fynn and W.J.A. Powell	Research and Dev. April/May (1965)
87)	R.W. Smith	Phys. Rev. 97. 1525 (1955)
88)	L.E. Kinsler and A.R. Frey	Fundamentals of Acoustics Wiley. N.Y. 1950.
89)	Quartz transducers from:	Valpey Corporation
90)	R.D. Brew	U.S. Patent 2671746
91)	D.L. Arenberg	U.S. Patent 2754238
92)	E.A. Davis and R.E. Drews	J. appl. Phys. 38. 2663 (1967)
93)	See for example:	Fundamentals of Ultrasonics P. 52 Butterworths (1963)
94)	J.H. McFee, T.B. Bateman	J. appl. Phys. 39. 4471 (1968)
95)	R.B. Wilson	J. appl. Phys. 37. 1932 (1966)
96)	R.M. Rollason	Private communication

ACKNOWLEDGEMENTS.

This research was carried out at the University of Aston in Birmingham during the tenure of a Research Assistantship.

I am very grateful to Dr. R.W. Cotterhill for his encouragement and unfailing advice throughout the research, and for his excellent supervision of the work.

I would also like to thank Professor S.E. Hunt, Head of the Department of Physics, for so readily giving his help whenever it was requested.

Special thanks are also due to Dr. R.M. Rollason for his stimulating companionship.

Many members of the Physics Department, Technical and Academic Staff, have contributed in some way or other to this work, and I would like to record my appreciation of this. Particular credit belongs to Mr. J. S. Sidwell for his enthusiastic help in overcoming some of the problems encountered in developing the measurement techniques employed.

Finally, my thanks to Mrs. R. Finch for typing the thesis so well.